THERMAL DEVELOPMENT AND REJUVENATION OF THE MARGINAL PLATEAUS ALONG THE TRANSTENSIONAL VOLCANIC MARGINS OF THE NORWEGIAN-GREENLAND SEA

by

NİLGÜN OKAY

A dissertation submitted to the Graduate Faculty in Earth and Environmental Sciences in partial fulfillment of the requirement for the degree of Doctor of Philosophy, The City University of New York

1995

This manuscript has been read and accepted for the Graduate Faculty in Earth and Environmental Sciences in satisfaction of the dissertation requirement for the degree of Doctor of Philosophy.

May 8, 1995
Date

Professor Kathleen Crane
Chair of Examining Committee

6/1/95
Date

Professor Frederick C. Shaw
Executive Officer

Professor Kathleen Crane

Professor Somdev Bhattacharji

Professor Millard F. Coffin

Supervisory Committee

THE CITY UNIVERSITY OF NEW YORK

Abstract

THERMAL DEVELOPMENT AND REJUVENATION
OF MARGINAL PLATEAUS ALONG
THE TRANSTENSIONAL VOLCANIC MARGINS
OF THE EASTERN NORWEGIAN-GREENLAND SEA

by

Nilgün Okay

Adviser: Professor Kathleen Crane

The predominance of large-scale paleo-shear zones in the Norwegian-Greenland Sea is thought to be the major cause of asymmetric seafloor spreading in this region. Plate reconstructions suggest that nascent mid-ocean ridges propagated into these obliquely oriented shear zones causing transtension to occur. The asymmetric evolution of the northern Norwegian-Greenland Sea is evident from both the morphology of the seafloor as well as its geophysical characteristics. The eastern passive margins of the northern Norwegian-Greenland Sea are punctuated by volcanic plateaus which have significantly higher heat flow than the western passive margins. It is hypothesized that marginal volcanic plateaus formed originally in response to

deviatoric stress developed at nascent mid-ocean ridge/shear zone intersections along transtensional margins causing lava to pond upwards on the eastern flank of the intersections. In addition, not only did paleo-shear zones serve as loci for the extrusion of seafloor basalts, but the distal limbs of these shear zones appear to be present-day sites for the emanation of heat from the seafloor thus thermally rejuvenating the eastern margins in the process. Heat flow analyses suggest that the thermal interactions between the Aegir and paleo-Mohns Ridges with the Eastern Jan Mayen Fracture Zone System created the Vøring Plateau and rejuvenated the adjacent continental crust (to a thermal age of 16 my). The subsequent northward propagation of the paleo-Mohns Ridge into/and along the paleo-Senja Shear Zone, probably underplated the Svalbard Platform, and thus caused a broad thermal swell in the region. Multiple intrusions from this northward propagating asthenosphere probably occurred along deep-seated faults in and adjacent to the Svalbard Platform and the northern Svalbard-Nordaustlandet margin. Thermal modeling results also reveal that a secondary detachment fault system cuts the southern Yermak Plateau and intersects the Spitsbergen Shear Zone and could have acted as a conduit for the upward propagation of the Knipovich Ridge-related asthenosphere. Recent northward propagation of the Knipovich Ridge caused rejuvenation of the southern Yermak Plateau (35-11 mybp). SeaMARC-II, and geophysical data also suggest diffuse intrusion and thermal rejuvenation along the northern Svalbard-Nordaustlandet margin creating the Yermak Seamount, Mosby Peak and the Nordaustlandet Volcanic Terrain (20-37 mybp) in the process.

PREFACE

"Everything can be found at sea according to the sprit of your quest."
Joseph Conrad

The world's ocean is an important part of the global environment; because of its size and shape. It interacts with the earth's atmosphere and land masses so that it is vital to man's existence. The world's ocean resources have created a tremendous interest in recent years. This interest has accelerated the growth of the earth sciences and oceanography. New sea-floor mapping techniques and shipboard geophysical sensors have greatly improved the study of the world oceans in the last thirty years. Indeed, the first detailed seafloor maps are only thirty-five years old.

The early scientists, aboard H. M. S. Challenger, accomplished the first ocean wide survey. This famous expedition (1872-1876) opened the era of ocean exploration. The Challenger, with its crew and seven scientists, crossed the Atlantic, Pacific, and Antarctic Oceans to observe weather, currents, water chemistry, temperature, bottom topography, sediments, and marine life on a global scale. These measurements have provided the factual foundation for the science of oceanography.

The Norwegian North Polar Expedition into the Arctic Ice which took place a century ago aboard the Fram, and was lead by the Norwegian explorer Fridtjof Nansen between the years 1893-1896. The first detailed knowledge of the Arctic Ocean's oceanography was obtained during this expedition. Nansen (1904) defined

the bathymetry of the Fram Strait as a deep passage for exchange of the deepest water masses between the Arctic Ocean and Norwegian-Greenland Sea. He also postulated the existence of a 1500 m-deep sill; the so called Nansen Sill at 80°-81°N.

The first results from this systematic survey were published by Louise Boyd in 1948. Bathymetric data has continued to accumulate since then by such investigators as Stocks (1950), Litvin (1964), and Johnson and Eckhoff (1966). Johnson and Heezen (1967) described the evolution of the region in the context of seafloor spreading. Vine and Matthews (1963) introduced the relationship of marine magnetic lineations to seafloor spreading, and Pitman and Heirtzler (1966) established the first magnetic time scale for the region.

Depth measurements have appeared on maps as early as 1504. Magellan made the first deep-sea sounding in the Pacific Ocean in possibly 1521. He used the technique of tossing the lead, used to this day. An electronic sounding device, called an echo sounder or sonic depth finder, was developed in the 1920's. The SS Velekari under the leadership of Louise Boyd made the first systematic echo-sounding profiles of the Nordic Seas in 1937-1938 (Boyd, 1948).

Development of the echo-sounder has resulted in improvements including high resolution digital imagery and accurate bathymetry across swaths of ensonified sea-floor: the side-scanning sonar. It constantly scans the seafloor beneath and to the sides of the research vessel. Sea mapping and remote characterization, carried out by the SeaMARC-II, sonar system combines the best abilities of the long-range side-

looking sonar, GLORIA, and SeaBeam, the multibeam hull-mounted echo-sounding systems.

More than 30 years ago, shortly after the first transpolar voyage under the ice by the USS Nautilus, nuclear-powered submarines were first recognized as unique platforms for conducting Arctic Ocean research. Since the legendary Alexander the Great descended (in 310 b.c) into the sea in a glass berry-like bell (Thurman, 1991), the use of manned submersibles such as ALVIN has contributed significantly to new discoveries in the world oceans. However, adequate surveys on the Arctic Ocean seafloor have not happened, and I propose that only multi-national submarines operating under the ice in a systematic manner can collect the quality of data required to fill in the large data gaps.

ACKNOWLEDGMENTS

I believe this thesis will prove to be a significant contribution to the scientific community especially during the Nansen Arctic Centennial Anniversary. This is the first dissertation on marine geophysics in the City University of New York.

I would like to thank my research adviser Prof. *Kathleen Crane* for introducing me to this study and counseling in my work. I thank my committee members, Prof. *Somdev Bhattacharji* and the geology professors of Brooklyn College of the City University of New York, and Dr. *Milliard Coffin* of Texas University of Austin, whose contributions were vital.

I am indebted to those institutions and individuals that permitted me to use their data. I would like to thank Prof. *Eirik Sundvor* of the University of Bergen, Norway, for the use of heat flow and seismic data sets; and to Prof. *Brian J. Mitchell* of Saint Louis University for use of the earthquake data set. Thanks to Dr. *Norman S. Cherkis* of the Navy Research Lab for the Bathymetric Chart of the Norwegian-Greenland Sea and Arctic Ocean, Dr. *Lisa Gahagan* for the fracture zones data of University of Texas. Individual credits are given in the captions of tables and figures. I like to thank Dr. *Roger W. Buck* from Lamont-Doherty Earth Observatory of Columbia University, and Dr. *Fernando Martinez* of the Institute of Geophysics of Hawaii University, for their assistance with the numerical models.

I also wish to thank Dr. *Keith Clark* for reviewing the maps, Dr. *Andrew Sounders* of Edinburgh University, and Prof. Dr. *Aral İ. Okay* of İstanbul Technical

University for helpful discussions. I also thank Prof. Dr. *Kazım Ergin* of Istanbul Technical University, who was recently honored with the TUBİTAK Geosciences Award for giving me great inspiration from the beginning of my academic carrier.

I would like to thank the captain, officers and crew of the R/V "*Håkon Mosby*" who helped to collect these data during miserable weather, at all hours. I also acknowledge the technical and scientific assistance of the Hawaii Group, who assisted in the collection of the first set of SeaMARC-II data. The excellent cooperation between the ship's crew and the scientific personal was a main factor in the success of this cruise.

The SeaMARC-II side-looking sonar imagery and bathymetric data were processed in the Naval Research Lab. My responsibility was mapping the northern Svalbard and Nordaustlandet continental margins. I used various computer software to produce the geological and geophysical maps in the Spatial Analysis and Remote Sensing Laboratory (*SPARS*) of Hunter College of the City University of New York. I have been fortunate to have enjoyed the professional environment, during my computer modeling studies, afforded to me at Lamont-Doherty Earth Observatory of Columbia University. I thank my adviser for providing me this opportunity. Special thanks goes to Geology Department of Istanbul Technical University.

I acknowledge financial support from the Educational Ministry of the Government of Turkey, US Office of Naval Research, City University of New York Teaching Fellowship and The Helena Rubinstein Foundation during my master and doctoral research studies. Journalist, Mr. *Doğan Ulug* of Hürriyet Gazetesi and TV

Producer, Ms. *Aliye Ak* of the Voice of Anatolia, New York showed great interest in my research in the Arctic Ocean.

I am grateful to my parents *Ayten and Sadık Okay* and my sisters Assoc. Prof. *Nesrin Okay* and *Esin Okay* for their faith, continued encouragement, and support during my studies in New York City.

Nilgün Okay

TABLE OF CONTENTS

page

LIST OF TABLES

LIST OF ILLUSTRATIONS

FIGURES

PLATES

INTRODUCTION

Substantial topographic and volcanic asymmetries evolve during the development of some passive margin pairs. This asymmetric development is reflected in the passive margin-morphology (for example, deeply subsided margins vs. marginal plateaus), structure (generally narrower continental-oceanic transition zone with a structural high vs. a broad continental-oceanic transition zone), and thermal evolution (rapid uplift, magnetic smooth zones, high sedimentation rate, and unusually high heat flow vs. subsidence, well developed magnetic anomalies, low sedimentation rates and normal heat flow) of the passive margin (Lister *et al.*, 1986, 1991; Steckler, 1989; Myhre and Eldholm, 1987; Etheridge *et al.*, 1990; Keen *et al.*, 1990; Okay and Crane, 1993; Okay, 1994). Those margins that are characterized by broad volcanic plateaus are often referred to as volcanic margins.

Detailed studies suggest that not all of the volcanic passive margins have "obvious connections to hotspots during the continental thinning and extension phases (Coffin and Eldholm, 1994)". For example, parts of the US and Canadian east coast (Sheridan *et al.*, 1993), the western Svalbard-Barents Sea margin (Myhre *et al.*, 1982), and the northwestern Australian Cuvier-Exmouth margins (Hopper *et al.*, 1992) have no spatial relation to "known hotspots" (Figure 1). In these cases, volcanic passive margins may form at the oblique intersection of a pre-existing fracture zone (or paleo-shear zone) with a propagating mid-ocean ridge because asymmetric stress fields about the intersection create asymmetric thermal structures

Figure 1. Transform faults, associated with seaward-dipping reflectors and large igneous provinces along some passive margins. Modified from the work by Coffin and Eldholm (1994) and Gahagan *et al.* (1992) with additional data from Austin and Uchupi (1982), Bonatti and Crane (1982), Bonatti (1985), Mutter *et al.* (1989), Keen and Beumont (1990), Etheridge *et al.* (1990). North Atlantic-Norwegian-Greenland Sea: 1-Spitsbergen Shear Zone and Yermak Plateau (Y) along the northern Svalbard-Nordaustlandet Margin; Morris Jesup Rise (MR); 2-Senja Fracture Zone (FZ) and Senja-Vestbanken (SJ) volcanic margin; 4-Greenland FZ, Northeast Greenland margin (NEG); 4-Jan Mayen FZ, and Vøring Plateau (Vø) along the Norwegian volcanic margin and Lofoten margin (L), Møre margin (Mø), Jan Mayen Ridge (JM), North Atlantic Volcanic Province (NAVP), Hatton Bank (H), the eastern Greenland margin (EG). Atlantic Ocean: 5-Labrador FZ, Southeast Greenland margin (SEG), Southwest Greenland margin (SWG), 6-Bight FZ, 7-Charlie Gibbs FZ, the New Foundland Margin (NF); 8-Pico FZ, 9-E Azores FZ, Azores (AZ), New England Seamounts (NW), Baltimore Canyon Trough (BL), Carolina Trough (C), Sohm Abyssal Plain (SO), 10-Oceanographer FZ, 11-Hayes FZ, 12-Atlantis FZ, Canary Islands (CAN), 13-Kane FZ; 14-Fifteen-Twenty FZ, Cape Verde Rise (CAP); 15-Vema FZ; 16-Sierra Leone FZ, Sierra Leone Rise (SIE), Ceara Rise (CE); 17-St. Paul FZ, 18-Romanche FZ, 19-Ascension FZ, Gulf of Guinea (GF); 20-Bode Verde FZ, Angola Plain (AN); 21-St. Helene; 22-Hotspur FZ; 23-Martin Vaz FZ, Abutment Plateau (AU), ; 24-Rio de Janeiro FZ, Brazilian margin (B), 25-Rio FZ, Rio Grande Rise (RIO), Argentine margin (A); 26-Tristan da Cunha FZ, Walvis Ridge (WAL), Cape Basin (CA); 27-Falkland-Agulhas FZ, Agulhas Ridge (AG), Falkland Plateau (FL), Meteor Rise (MET), Georgia Rise (GE), Mozambique Basin (MO); 28-Conrad FZ; 29-South Sandwich FZ; 30-Islas Orcadas FZ, Islas Orcadas Rise (IS). Indian Ocean: 31-Shaka FZ, 32-Dutoit FZ, Maud Rise (MAU); 33-Astrid FZ, Astrid Ridge (AST); 34-Discovery FZ, Conrad Rise (CON), 35-Melville FZ, 36-Vema FZ, 37-Owen FZ, Kutch Basin (KUTC); Ninetyeast Ridge (N); Seychelles Bank (S); Kerala Basin (KE); Mascarene Plateau (MAS); 38-Red Sea FZ system, Yemen plateau basalts (YEM), Ethiopian Plateau basalts (ET); 39- Kerguelen FZ, Kerguelen Plateau (KERG); 40-Amsterdam FZ; 41-Soma FZ; 42-Investigator FZ; 43-Surya FZ; 44-George FZ; 45-Tasman FZ; Broken Ridge (BR), Cuvier Plateau (CU), Scott Plateau (SC), Naturaliste Plateau (NA); Eyre Terrace (EY); Lord Howe Rise Seamounts (LR); Wilkes Land (W); Gunnerus Ridge (GUN); Maud Rise (MAU); Explora Wedge (EXP).

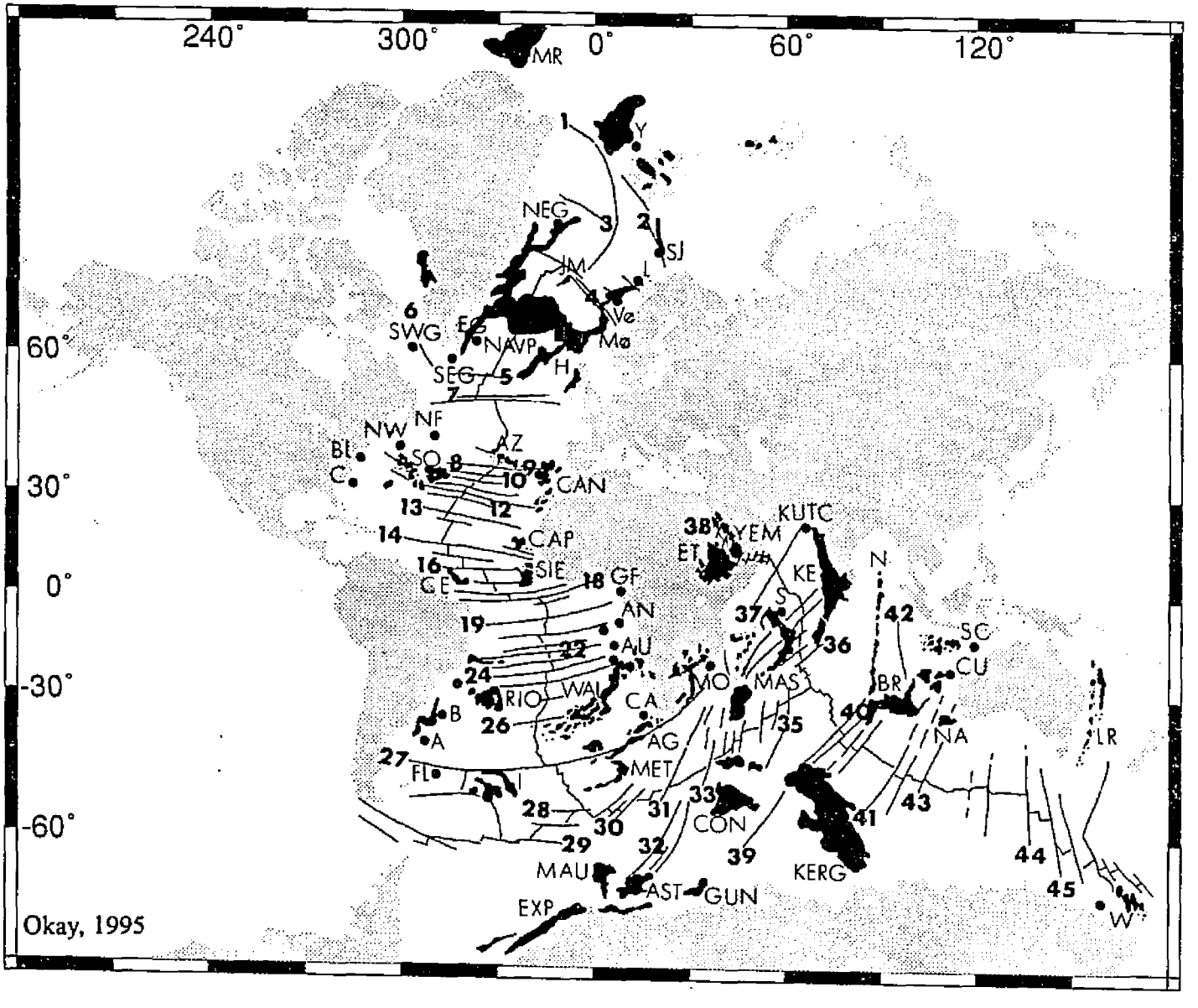
240°
300°
0°
60°
120°
60°
30°
0°
-30°
-60°
MR
Y
NEG
SJ
JM
L
Ve
Mø
SWG
NAVP
H
SEG
NW
NF
AZ
BL
C
SO
CAN
CAP
SIE
GE
GF
AN
AU
RIO
WAI
CA
MO
MAS
B
A
AG
MET
FL
CON
MAU
AST
GUN
EXP
KERG
KUTC
YEM
ET
KE
S
N
SC
CU
BR
NA
LR
W
Okay, 1995

and local plate kinematics (Figure 2, Bonatti and Crane, 1982; Crane *et al.*, 1988, 1991; Okay and Crane, 1993; Okay *et al.*, 1993; Okay, 1994). This type of volcanic margin is classified as "transtensional" or transform margin (a combination of shearing and extension, Myhre *et al.*, 1982; Max and Ohta, 1988; Mutter *et al.*, 1989; Etheridge *et al.*, 1990; Crane *et al.*, 1991; Lister *et al.*, 1991; Okay and Crane, 1993; Keen *et al.*, 1993; Okay, 1994).

Transtensional margins, although they are globally significant, have been largely neglected in the literature. Transtensional passive margins can be found in almost every ocean basin (Figure 1). Their importance is related to the effects of changes in relative plate motion, complex- and multiple-stage shear movements, and the degree to which a propagating mid-ocean ridge enters into a pre-existing shear zone. All of these events contribute to at least one or several episodes of extensive volcanic activity. Some transtensional margins are also characterized by thickening of basaltic crust associated with seaward-dipping volcanic sequences along the line of continental breakup (Keen and deVoogd, 1988; Myhre *et al.*, 1988; Etheridge *et al.*, 1990; Lister *et al.*, 1991; Lorenzo *et al.*, 1991; Keen *et al.*, 1993; Okay and Crane, 1993).

The term transtensional margin is generally used to describe a continental margin that is aligned parallel to the direction of relative motion at the time of continental rifting. Strike-slip motion occurs along such a margin during early ocean formation, first between adjacent continental blocks and later between continent and ocean, giving a distinctive thermal evolution (Keen *et al.*, 1990).

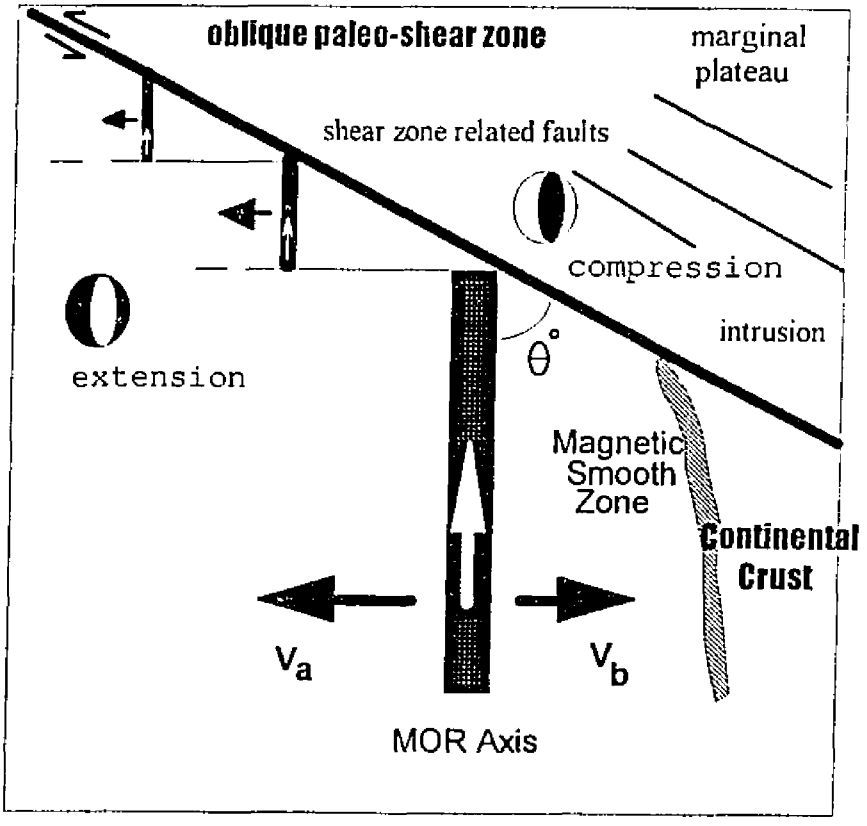

Figure 2. Oblique impact of propagating ridge with paleo-shear zone. Plan view model shows a mid-ocean ridge (MOR) propagating obliquely into a paleo-shear zone. An impact occurs at an oblique angle ($0° < \theta° < 90°$) forming a transtensional volcanic margin. Spreading rate on the extensional side (V_a) is greater than spreading rate on the compressional side (V_b). Due to asymmetric deviatoric stress, the mid-ocean ridge axis deflects along the paleo-shear zone. As the system matures, small pull-apart spreading centers and new oceanic crust form on the extensional side (Crane and Bonatti, 1987). Magma tends to pond vertically at the continent-oceanic crustal transition (on the compressional side), creating a marginal plateau in the process (Okay and Crane, 1993).

Another example of transtensional passive margin development can be seen today in the northern Red Sea where the propagating Red Sea spreading center is impinging obliquely upon series of parallel multiple-fault zones (the Dead Sea, Brothers, Shagara, and Hamish Fracture Zones in Figure 3). It has been suggested that these shear zones are actively breaking up into small pull-apart basins (Courtillot, 1982; Bonatti and Crane, 1982, 1984; Crane and Bonatti, 1987). At the present, the western margin of the northern Red Sea is undergoing compression and the eastern margin is undergoing extension. The compressive side of this impact is characterized by underplating of the continental crust by ultramafic assemblages (Bonatti *et al.*, 1984, 1986). Crane and Bonatti (1987) suggested that the compressional front at the tip of the obliquely propagating ridge could have uplifted the (underplated) continental crust creating ultramafic islands (Zabargad Island) in the process.

Oblique paleo-shear zones and propagating ridges are also very common in the eastern Norwegian-Greenland Sea created by the separation of Norway-Svalbard and Greenland. These offer a unique opportunity to investigate the development of transtensional volcanic margins. The asymmetric uplift, high heat flow and volcanism bordering the eastern margin is well known and has been cited as evidence for rifting and spreading across a throughgoing lithospheric detachment which dips eastwards underneath Svalbard (Crane *et al.*, 1991; Okay and Crane, 1993).

A number of detailed studies and surveys have been carried out in the Norwegian-Greenland Sea and provided a great deal of new geological and geophysical data (e.g., Vogt *et al.*, 1981; Myhre *et al.*, 1982; Mutter *et al.*, 1982,

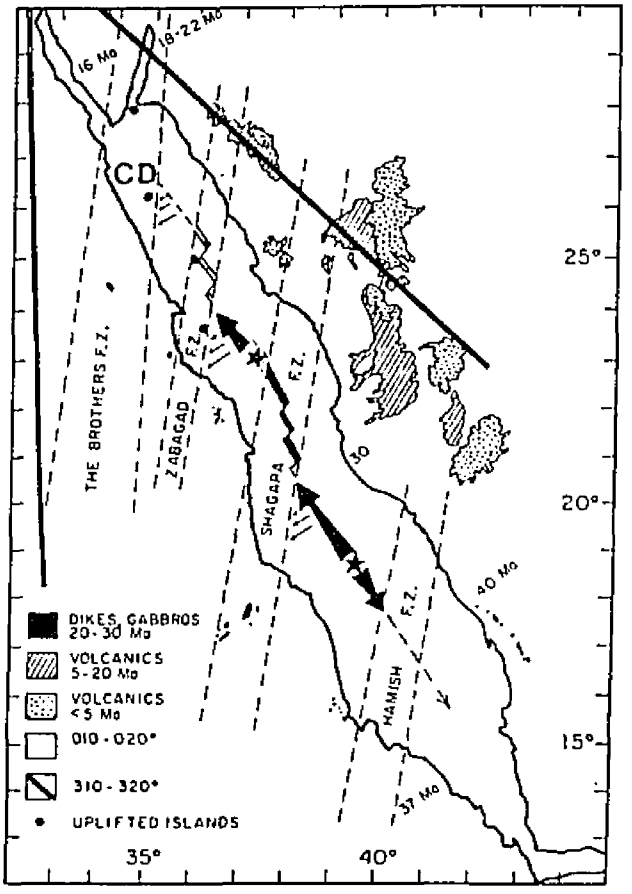

Figure 3. Location of the present-day active transtensional passive margin development in the northern Red Sea (Bonatti and Crane, 1982). CD: Conrad Deep. The propagation occurs when the rift obliquely impacts against the paleo-shear zones: Hamish, Shagara, Zabargad and the Brothers Fracture Zones. Uplifted islands (e.g., Zabargad Island) are evidence that western margin may be under compression due to the asymmetric stress field.

1984; Crane *et al.*, 1982, 1988; Jackson *et al.*, 1984; Vogt, 1986; Eldholm *et al.*, 1987, 1989; Vorren *et al.*, 1989; Mitchell *et al.*, 1990; Sundvor and Austegård, 1990; Zehnder *et al.*, 1990; Thiede *et al.*, 1990; Faleide *et al.*, 1991; Okay *et al.*, 1991, 1993; Sundvor *et al.*, 1991; Doss *et al.*, 1991; Vogt *et al.*, 1991, 1993; Crane and Solheim, 1995). The purpose of this dissertation is to use the new data (bathymetry, SeaMARC-II side-looking sonar, seismic, magnetics, earthquake-seismicity, gravity, and the results of the Deep Sea Drilling Project and Ocean Drilling Program) to constrain thermo-mechanical models for the evolution of the Eastern Norwegian-Greenland Sea and adjacent Eastern Arctic Ocean margins, and to better understand the development of transtensional volcanic margins and marginal plateaus.

The study is based on heat flow tied to geological and geophysical data. These data from seven transtensional margin transects are tested against various lithospheric-extension models. In this work, I only speculate on the mechanical causes for asymmetric ocean basin development, but the kinematic opening models can give some insight into how the interaction of a propagating rift/ridge with a paleo-shear zone affects the development of a rift/ridge and passive margin system and related asthenospheric underplating of adjacent continental crust.

The dissertation consists of seven chapters. Chapter 1 introduces characteristics of volcanic passive margins based on the evidence for thick basaltic crust determined from various geophysical parameters. Chapter 2 discusses the unique role that paleo-shear zones play on the thermal mechanisms of the rifting, modes of the lithospheric extension, and development of passive margins. Chapter 3

contains a brief summary of plate boundary evolution and overall geology and geophysics, including the morphological characteristics, seismic data, sedimentation history and variations of heat flow, earthquake seismicity, magnetics and gravity data along the plate boundaries and margins of the Eastern Norwegian-Greenland Sea.

New observations from the SeaMARC-II (side-looking sonar) Surveys allow for new interpretations of morpho-tectonic/volcanic events along the Svalbard-Nordaustlandet Margin and are presented in Chapter 4. These allow us to test models for the evolution of the northern margin. Chapter 5 presents the modeling of heat flow data from marginal plateaus and margins of the Eastern Norwegian-Greenland Sea. Chapter 6 discusses the development of the region controlled by the interactions of obliquely propagating ridges and paleo-shear zones. In addition, the concept of rift/ridge related "asthenospheric corridors" which may underplate broad regions of continental crust adjacent to transtensional volcanic margins, creating large-scale thermal rejuvenation is introduced. Chapter 7 summarizes the development of transtensional volcanic margins and surroundings interacting with paleo-shear zones and related pre-existing continental weakness zones.

Chapter 1

CHARACTERISTICS OF VOLCANIC PASSIVE MARGINS

A. MAGMATISM ALONG VOLCANIC PASSIVE MARGINS

1. THICK BASALTIC CRUST

The recognition of thick, seaward-dipping volcanic sequences in some passive margins has recently led to reconsideration of passive margin development (e.g., Hinz and Weber, 1976; Mutter *et al.*, 1982, 1984, 1988; Coffin and Eldholm, 1991). These margins are distinct from margins where magmatic activity is limited (or absent) prior to the development of oceanic crust (Figure 1-1, Mutter *et al.*, 1988). For example, volcanic passive margins have thick seaward-dipping volcanic sequences (Hinz and Weber, 1976; Hinz, 1981; Myhre *et al.*, 1982; Mutter *et al.*, 1982, 1984, 1989; Skogseid and Eldholm, 1987; Larsen and Jakobsdóttir, 1988; Keen *et al.*, 1988; Coffin and Eldholm, 1994) which may also form marginal plateaus (Eldholm *et al.*, 1989; Mutter *et al.*, 1989; Lister *et al.*, 1986, 1991; Lorenzo *et al.*, 1990; Okay and Crane, 1993) whereas non-volcanic margins are characterized by rapid initial subsidence, prominent block-faulting, and little- or no-volcanism during continental breakup (e.g., LePichon and Sibuet, 1981; Austin and Uchupi, 1982; Dunbar and Sawyer, 1989). In addition, non-volcanic passive margins generally have

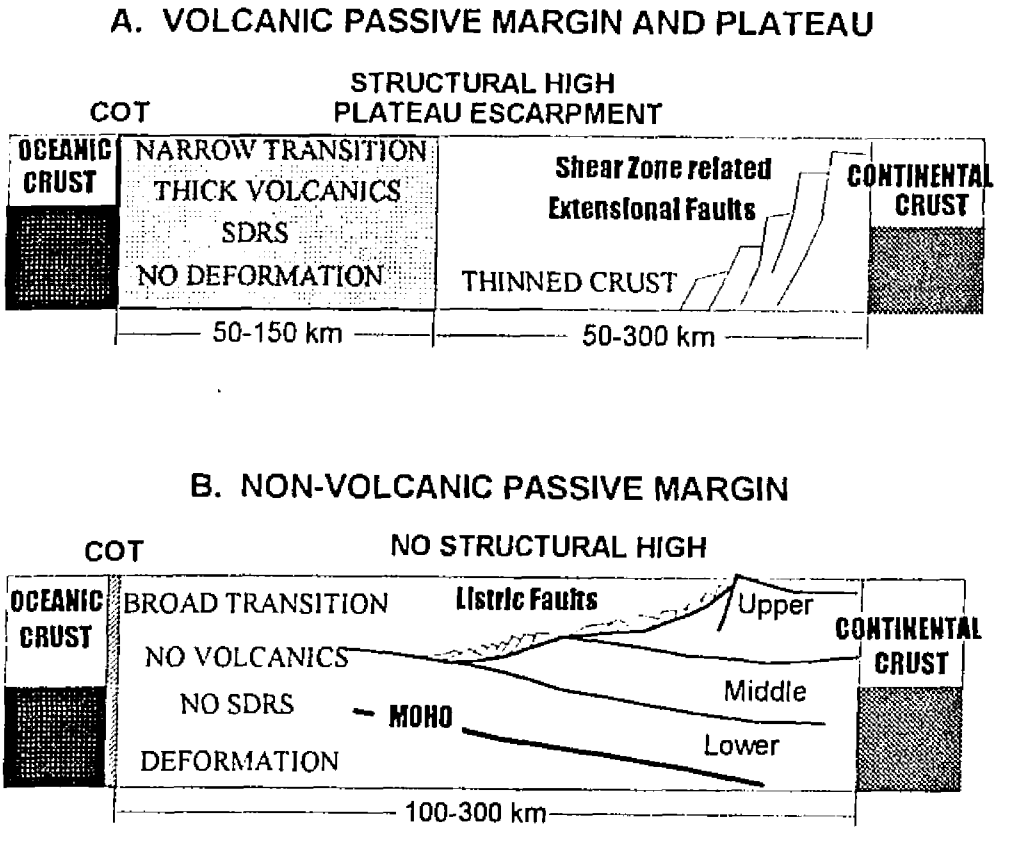

Figure 1-1. Passive margin classification. A diagrammatic summary of observations from passive margin structures compares the structural elements of (a) a volcanic passive margin, (b) a non-volcanic passive margin. An abrupt continent-oceanic crustal transition (COT) is illustrated by volcanic margin with seaward-dipping reflector sequences (SDRS), and plateau formation. The non-volcanic margin exhibits commonly a broader COT and no-structural high. The figure is modified from Mutter *et al.* (1988).

a broader continent-oceanic crustal transition zone than the volcanic ones.

Even though this classification has led to a better understanding of the variability of continental margins, each margin has some special characteristics that make it almost unique (Mutter, 1993). There are some individual margins which may lie along a continuum between the two groups: volcanic and non-volcanic (Figure 1-1). For example, Mutter *et al.* (1988) described the seaward-dipping reflectors from the Wilkes Land margin, off Antarctica, as intermediate in the type between volcanic and non-volcanic "end-members". Another example is the broad passive margin of the US east coast which has been considered as a non-volcanic margin (Mutter, 1993). However, recently seismic studies along this margin have revealed seaward-dipping reflectors and a high velocity deep layer casting doubt on the nature of its origin (Mutter, 1993). Also, a non-volcanic passive margin may not be necessarily broad (Figure 1-1). In contrast, parts of the SE Australian margins are quite narrow (Lister *et al.*, 1986, 1991; Etheridge *et al.*, 1990). Therefore, a wide range of data (including deep seismic-reflection profiles, seismic-refraction profiles, gravity, heat flow, uplift/subsidence histories) is necessary for the complete reconstruction of a passive margin.

Previous studies have already pointed out that thick igneous units formed in the immediate vicinity of the continent-ocean transition along the Norwegian-Greenland Sea (Hinz, 1981; Mutter *et al.*, 1988; Coffin and Eldholm, 1994; Eldholm and Grue, 1994). In this location, volcanism is generally observed as (but not limited to) seaward-dipping reflector sequences that volumetrically exceed the volcanism in

most continental rifts. In addition to the Norwegian-Greenland Sea, Hinz (1981) noted their presence off Argentina and Antarctica, Austin and Uchupi (1982) documented their presence off southwest Africa, and Mutter *et al.* (1989), Lister *et al.* (1986, 1991), and Lorenzo *et al.* (1990) proposed their presence off NW Australia. Similar features are also known in the NE Atlantic off the Hatton Margin (Roberts *et al.*, 1984; Roberts and Ginzburg, 1984) and in its conjugate margin off Eastern Greenland (Larsen and Jakobsdóttir, 1988; Zehnder, 1990).

Mutter and Zehnder (1988) showed that very thick oceanic crust at the continent-oceanic crustal transition (large thicknesses of intrusive and extrusive magmatic rocks) is associated with seaward-dipping reflectors (Figure 1-2). Hinz (1981) suggested that seaward-dipping reflector series (volcanic units) resulted from seaward tilting and foundering of an intra-continental rift system that had been strongly affected by magmatic activity, placing the seaward-dipping units on continental crust. Mutter *et al.* (1982, 1988), Eldholm *et al.* (1989), and Eldholm and Grue (1994) suggested that these units formed during a period of seafloor spreading in the first few million years of opening, whereby, in the initial stage the oceanic crust was very thick thining to its normal thickness 10-15 Ma after the initiation of seafloor spreading.

Evidence for early Tertiary magmatism in the Northern Atlantic Ocean is well documented in the form of extensive exposed flood basalts, buried volcanic sequences on the inner continental margin and unusually thick igneous crustal sections

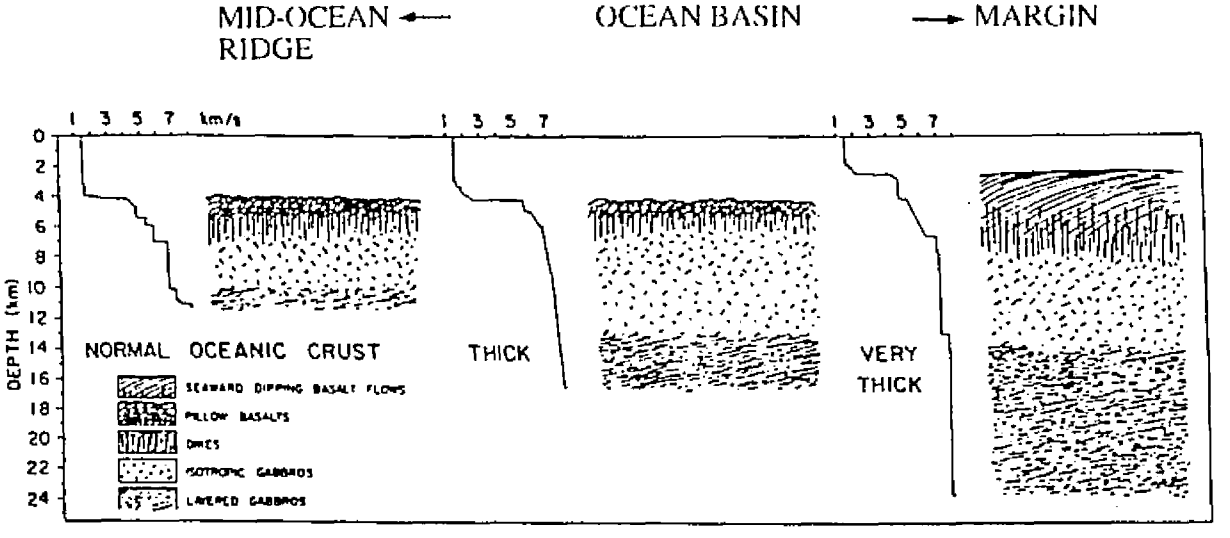

Figure 1-2. Variations in the thickness of oceanic crust during its evolution based on seismic data (after Mutter and Zehnder, 1988). In the initial stage the oceanic crust is very thick and returns to the normal thickness 10-15 Ma after the initiation of seafloor spreading. Thinning of oceanic crust occurs primarily by the reduction in thickness of the intrusive and plutonic components and secondarily by a reduction in thickness of extrusive sequences.

at the continent-oceanic crustal transition which includes, as its' uppermost unit, an extrusive sequence that is recognized as distinctive seaward dipping reflectors in seismic reflector profiles (Larsen *et al.*, 1989). In addition, Larsen and Jakobsdóttir (1988) suggested that the Eastern Greenland Margin is characterized by distinctive seaward-dipping reflectors which indicate thick basaltic crust at the continent-oceanic crustal transition. Observations also show that the formation of the continental margins of Norway and eastern Greenland was characterized by early Tertiary breakup accompanied by intense magmatism, continuing to the present as the Icelandic hotspot (Talwani and Eldholm, 1977; Eldholm *et al.*, 1989; Larsen *et al.*, 1989; Eldholm and Grue, 1994). The primary physical evidence for such magmatism is the eruption of massive volumes of basaltic lavas over an area of several thousand square kilometers. Well-focused hotspot magmatism at the axis of seafloor spreading clearly influences processes of crustal accretion in Iceland even today (Roberts *et al.*, 1984; Larsen and Jakobsdóttir, 1988; White and McKenzie, 1989). However, it is not fully understood to what extent this mantle-upwelling has influenced the more distant volcanic margins within the northeastern Atlantic and the northern Norwegian-Greenland Sea during the initiation of seafloor spreading.

Three models to account for the magmatism and thick basaltic crust along volcanic passive margins have been proposed: "active (mantle-activated rifting)" and "passive (lithosphere-activated rifting)" mantle plume models, and a third "secondary convection" model, in which asthenospheric mantle convectively overturns close to the conjugate trailing edges of pre-existing thick and cold lithosphere (Storey *et al.*,

1991; Kent *et al.*, 1992). The active and passive mantle plume models are mutually exclusive, but secondary convection could contribute additional magmatism to either (White and McKenzie, 1989).

White and McKenzie (1989) suggested that the development of a volcanic passive margin is a result of a "timely" interaction between an evolving active-mantle plume (hotspot) and an intra-continental rift. They also suggest that the voluminous magmatism results from decompressional melting of the mantle in the presence of elevated mantle temperatures associated with the hotspot. The enchanced melt volume is derived from increased mantle temperatures reflecting thermal upwelling from deep in the mantle (perhaps even the mantle-core boundary). White and McKenzie (1989) proposed that hotter mantle begins to melt at a greater depth in the Earth than cooler mantle would, thus resulting in a greater volume of melt. In this case, mantle-induced convective melting (focused in a narrow zone) produces a uniform pure-shear extension (McKenzie, 1978) across the region that characterizes the evolution of a symmetric rifted volcanic margin (McKenzie, 1985; White and McKenzie, 1989).

For the lithosphere-activated rifting model, Mutter *et al.* (1988) suggested that large horizontal-temperature gradients resulted from rapid lithospheric extension and asthenospheric upwelling at a nascent spreading center. They proposed that small-scale convection could account for the excess-melt production during the earliest phase of seafloor spreading, and the convection increases the melt production by circulating a greater volume of mantle through the solidus. Buck (1986) and Keen (1987) have evaluated extensional models which incorporate small-scale convection,

and showed that the convective thinning (from below) could become the dominant process in the continental breakup, and could provide stretching to create the necessary conditions to trigger the flow. They suggested that it is not necessary to invoke the active involvement of high-temperature convective mantle plumes impinging at the base of the lithosphere (Şengör and Burke, 1978; Bonatti, 1987), although lithospheric doming above a mantle plume could result in extension and provide the link between active- and passive-rifting mechanisms (Houseman and England, 1986).

Zehnder *et al.* (1990) suggested, based on seismic and geochemical studies (Mutter and Zehnder, 1988; Klein and Langmuir, 1989) that the emplacement of thick basaltic crust at the passive margin is caused by moderate partial melting through rift-induced small-scale convection (Keen and deVoogd, 1988). After the initiation of seafloor spreading, the convection cells will become broader and the rate of material circulation should be much less. Mutter and Zehnder (1988) and Zehnder *et al.* (1990) suggested that after seafloor spreading commences, convection slows, and crustal thickness is expected to diminish, however, the amount of partial melting of the source does not change dramatically. As the plate boundary moves further from the continental crust, the horizontal-temperature gradients will decrease and the convection will abate. As the spreading continues the volcanic margin will subside and the continent-oceanic crustal transition will remain shallow (Mutter *et al.*, 1988). Buck (1986) and Steckler (1985) have also shown how this phenomenon can account for anomalous uplift of rift flanks (for example, the Gulf of Suez).

2. MAGMATIC UNDERPLATING AND MARGINAL PLATEAUS

Volcanic rocks associated with large igneous provinces, flood basalts, seaward dipping reflector sequences, and multiple intrusion zones (within adjacent continental crust) probably represent only a small part of the total melt production along the passive margin (Mutter *et al.*, 1982, 1984; Eldholm, 1989). A large percentage of the melt generated on passive margins is probably underplated in the lower crust adjacent to continental crust where it can be identified by its high seismic velocity, thermal swell uplift and thermal rejuvenation (McKenzie, 1985; McKenzie and Bickle, 1988; McNutt, 1984; Mutter and Zehnder, 1988; Okay, 1994). Magmatism may lead to the underplating of the adjacent continental crust by asthenospheric mafic melts (e.g., Yoder, 1976; Michael and Bonatti, 1985; White *et al.*, 1987; Okay, 1994). Keen and deVoogd (1988) noted that the process of magmatic underplating, which creates a pile of mafic (and ultramafic ?) rocks whose thickness approaches that of oceanic crust, may have produced "oceanic" layers, and these "oceanic" rocks may in some cases strongly resemble ophiolite suites.

White *et al.* (1987) and Keen (1987) suggested that partial melting in the mantle generates deep-seated magmatic injections creating thick basaltic crust along the volcanic passive margins (for example, margins of the Northeastern Atlantic Ocean and Norwegian-Greenland Sea). However, they did not explain why thick basaltic marginal plateaus occur where they do. Mutter *et al.* (1989), Lorenzo *et al.* (1991), and Okay and Crane (1993) proposed that the development of the volcanic

marginal plateaus (for example, Exmouth Plateau, southern Yermak Plateau) is governed by simple-shear lithospheric extension mechanisms along a major detachment fault. Okay and Crane (1993) recently proposed that mid-ocean ridge related magmatic injections may propagate within/along paleo-shear zones contributing to the vertical ponding of basalts on the compressional side of the propagating mid-ocean ridge and paleo-shear zone intersection (Figure 2). In this manner, over time, a marginal plateau may be created. The thermal effects from this preferential magmatic intrusion should be observed at considerable distance from the mid-ocean ridge, but only in regions cut by pre-existing fault zones. In addition, asymmetric simple-shear lithospheric extension across a shear zone may be responsible for emplacement of thick basaltic crust, plateau formation along the continent-oceanic crustal transition of the passive margin (Okay and Crane, 1993) and underplating the adjacent continental crust (Okay, 1994, 1995).

B. GEOPHYSICAL CHARACTERISTICS OF TRANSTENSIONAL VOLCANIC MARGINS

1. SEISMIC REFLECTION AND REFRACTION

In the past fifteen years studies of passive margin structure that use mostly multichannel seismic-reflection and -refraction data have yielded important new observations, which considerably advanced our understanding of events during the

early rifting and divergent phases of passive margin formation (DGP Report, 1991; Mutter, 1993; Coffin and Eldholm, 1994). Eldholm and Grue (1994) compiled multichannel seismic reflection, wide-angle reflection, and refraction profiles to show that the offshore igneous rocks emplaced during the transient breakup event of the Norwegian-Greenland Sea were voluminous extrusive complexes creating thick initial oceanic crust, commonly with a lower crustal high-velocity (7.2-7.7 km/s) body beneath the extrusives, and intrusives within pre-Eocene continental crust (along the margins of eastern Greenland and off Norway).

Reflection profiles at many passive margins exhibit sequences of reflectors that roughly describe a wedge-shaped pattern with upwardly curved (seaward-dipping) shapes (Hinz, 1981). These seaward-dipping reflectors were first recognized in marine geophysical surveys of the Vøring Plateau off Norway (Figure 1-3, Hinz and Weber, 1976; Hinz, 1981). The magmatic origin proposed for the seaward-dipping reflectors was verified during the Deep Sea Drilling Project-Leg 38 (Talwani *et al.*, 1976) and the Ocean Drilling Program-Leg 104 of the Vøring Plateau (Eldholm *et al.*, 1987). In this location, the top of the extrusives, a smooth, opaque acoustic basement-horizon, develops above intra-basement reflectors of variable character. In some areas, the basement is seismically indistinct and unstructured; in other areas, it comprises thick wedges of seaward dipping reflectors. Eldholm and Grue (1994) also observed features typical for the continent-oceanic crustal transition on the Norwegian volcanic margin where the upper crust consists of extrusive (sub-aerial ?) basaltic lavas and interbedded sediments of variable thickness.

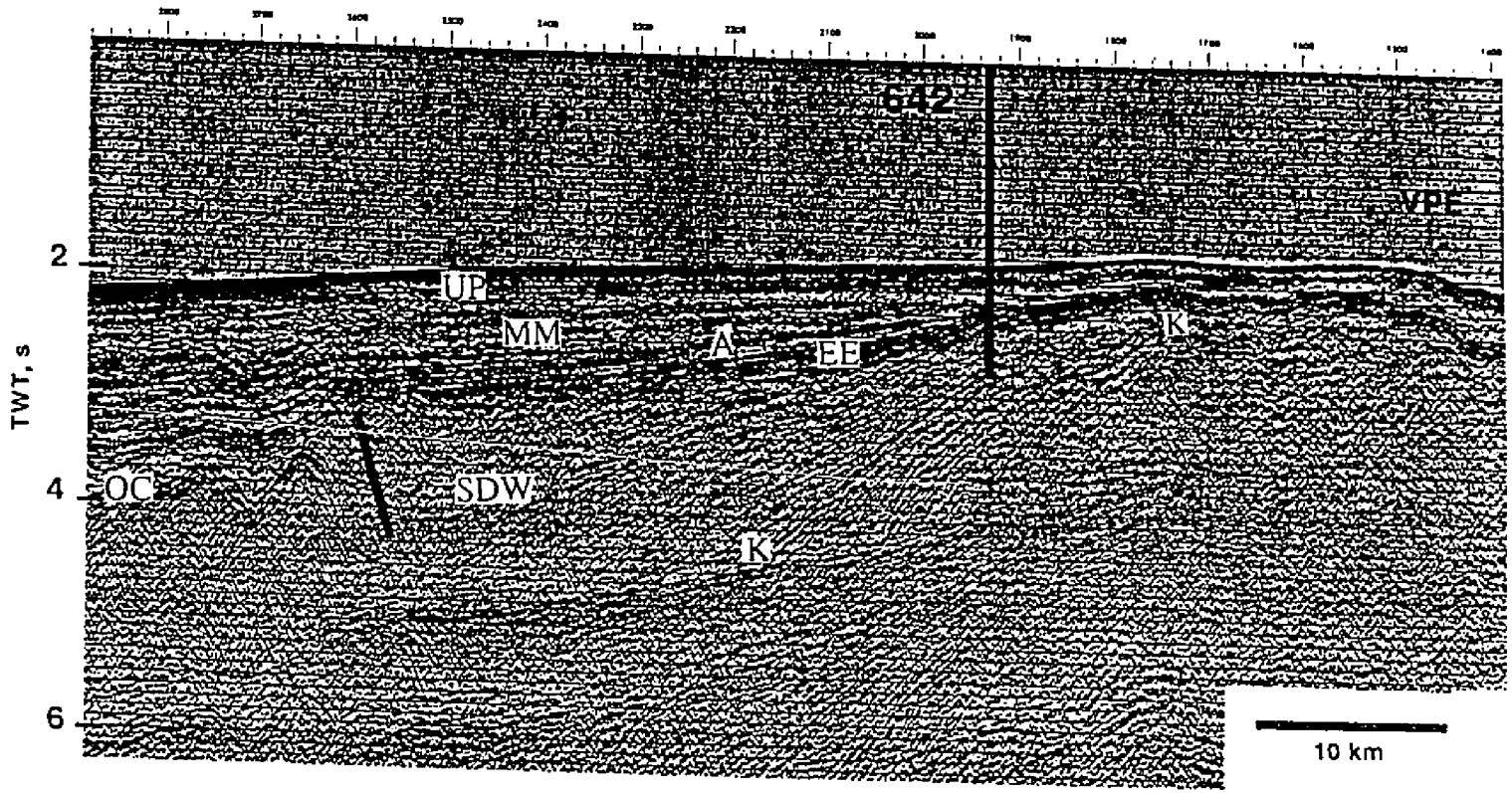

Figure 1-3. Seismic profile across the dipping reflector wedge and ODP Site 642 on the southern Vøring Plateau showing the seaward termination against a basement high (Eldholm, 1990). OC= oceanic crust, SDW= seaward-dipping reflectors, K= basalt/dacite boundary, EE= top lowermost Eocene lava flows, A= lower Miocene, MM= middle Miocene, UP= upper Pliocene, VPE= Vøring Plateau Escarpment.

Some seaward-dipping wedges are approximately 6 km-thick and the velocity increases from 3.5-4 km/s (at the top) to 6-6.5 km/s (in the deepest parts). The maximum velocity-gradient occurs in the uppermost lava unit. Upper crustal velocity-gradients decrease moderately, but distinctly, between the main dipping wedge and its innermost part. Local high-velocity zones also exist below the thick basaltic unit. Eldholm and Grue (1994) interpret these lateral changes as varying crustal properties across the continental-oceanic crustal transition. This transition is underlain by thick lower crustal bodies above an 8+ km/s mantle, which lies within the continental crust and magnetic anomaly 23 (Eldholm *et al.*, 1989). The isovelocity sections show that the deep crustal structure of these margins change dramatically near the margin escarpments (Mutter and Zehnder, 1988); although total crustal thickness remains about the same as that of the continental basins, crustal velocities are significantly lower than either continental or oceanic structures proximal to the marginal escarpment (Figure 1-2).

Along the Newfoundland margin it was found that seaward-dipping reflectors show the seaward rise of Moho toward the continental-oceanic crustal transition associated with a shear zone (cutting the crust and mantle) along which lithospheric extension was accommodated (Keen and deVoogd, 1988). The location of the shear zone inferred from the seismic data between the edge of the shelf and the oceanic crust is shown in Figure 1-4. This shear zone was probably formed during the continent-continent shearing and transtensional opening of Africa and North America. In this case, motion along the shear zone probably proceeded to the point

Figure 1-4. Deep structure of the Newfoundland margin (Keen and deVoogd, 1988). (a) Location of the transtensional margin indicated by the heavy bar in the inset. Major sedimentary basins in the region are stippled. NS: Nova Scotia, NFLD: Newfoundland. Dense stippling shows sediment, and open stippling shows inferred extent of pre-existing continental crust.
(b) Upper: Free-air gravity and magnetic anomaly profiles along line 87-5. Lower: Interpreted line drawing. Solid lines are shown for Moho and basement. The reflectors come from a westward dipping shear zone that may be part of a major detachment along which extension was accommodated during rifting (Lister et al., 1986; Keen et al., 1988), in a manner similar to that proposed by Wernicke (1985). The line drawing interpretation of the seismic reflection data is in general agreement with the reflection, gravity and magnetic observations. The location of a crustal shear zone between the edge of the shelf and oceanic crust is inferred from the seismic data. Continental crustal velocities of about 6.3 km/s were measured out to the COB (Keen et al., 1990). This is related to transform motion along the margin. The shear zone extends seaward to the COB, where shearing must have occurred also during the migration of the mid-ocean ridge along the margin. This boundary may have formed along one of the faults which was created during the earlier phase of transpression. Volcanism has also been active, and a buried seamount (large open circles) lies just seaward of the COB.

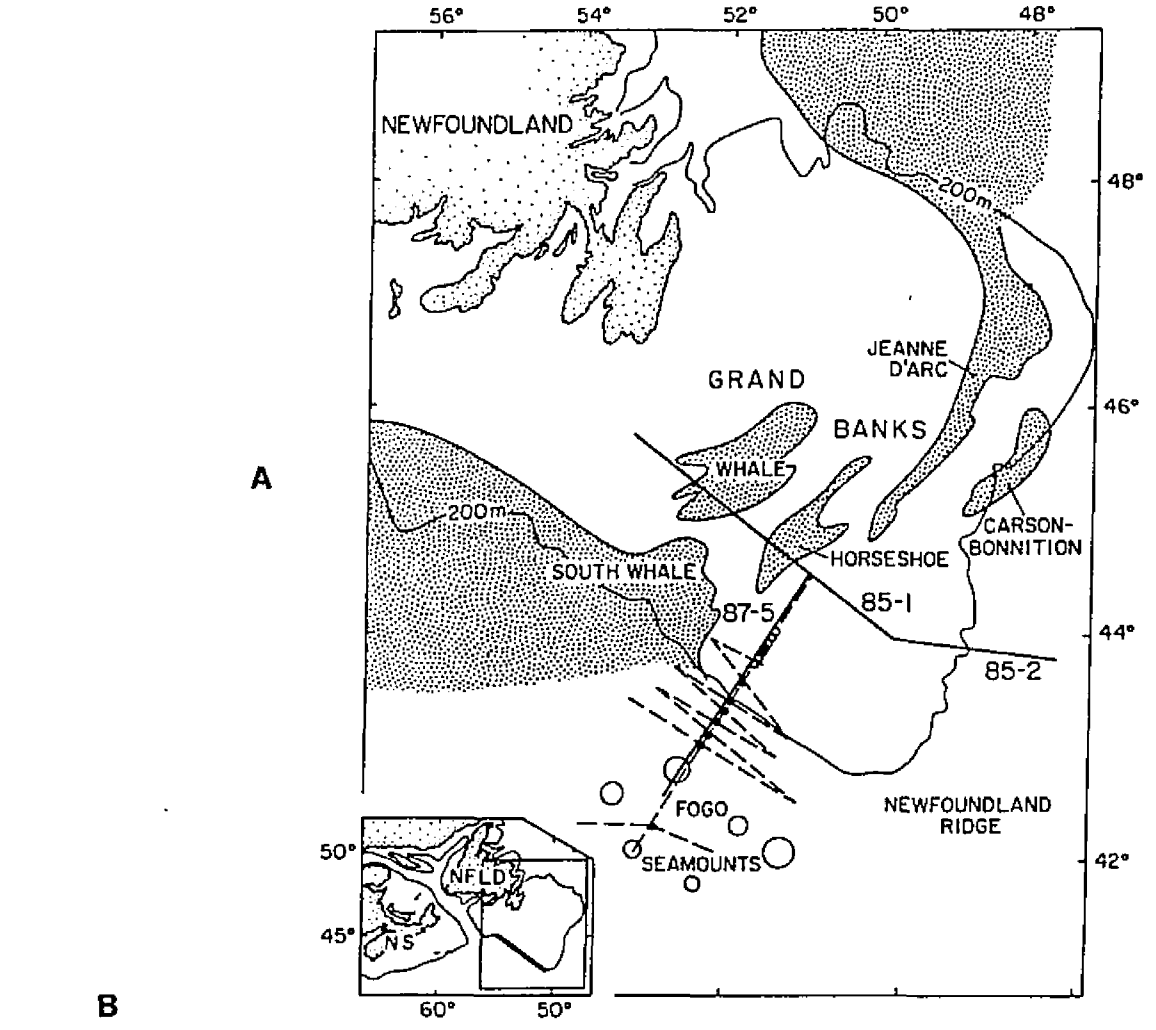
A
56°
54°
52°
50°
48°
NEWFOUNDLAND
200m
48°
JEANNE D'ARC
GRAND
BANKS
46°
WHALE
200m
CARSON-
BONNITION
SOUTH WHALE
HORSESHOE
87-5
85-1
44°
85-2
FOGO
NEWFOUNDLAND
RIDGE
SEAMOUNTS
42°
50°
NFLD
45°
NS
60°
50°
B
SW
NE
MAGNETICS (nT)
250
0
-250
GRAVITY (mGal)
50
0
-50
GRAVITY
ANOMALY
MAGNETIC
ANOMALY
0
50
DISTANCE (km)
COB
DEPTH (km)
0
20
40
K
L
M
N
O
J
I
H
A
B
F
G
D
C
E
CONTINENTAL
SHEAR ZONE

where upper mantle became exposed. Seismic refraction results also show that the crustal transition from continental to oceanic occurs across a narrow zone probably a paleo-transform fault (about 50 km-wide under the outer continental shelf and slope; Keen and Roest, 1990). Keen (1987) reported that the oceanic crust in this region has a velocity of 7.4 km/s; and the oceanic crust adjacent to the transform fault is anomalous in that no oceanic layer 3 is present, yet the total thickness of oceanic crust is within normal limits (7-9 km).

Seismic refraction measurements give estimates of the velocity structure of the deep crust in regions that are typically difficult to image by reflection. Seismic refraction studies along the Norwegian-Greenland-Barents Sea margins indicate a heterogeneous crustal structure (Talwani and Eldholm, 1973). The seismic refraction velocities from the crust strongly show the existence of high-density crustal bodies at the ocean-continent transition zone. Beneath the dipping wedges, the distinct layer is often found with a seismic velocity of around 7.2 km/s (not present in either the adjacent continental or the oceanic crust (Figure 1-2).

The velocity of the lower crustal body is not characteristic of normal oceanic or continental crust, although it occurs in some other continental settings (Meissner, 1986) and in thickened crust on volcanic margins (Coffin and Eldholm, 1992). Mutter and Zehnder (1988) interpreted these high-velocity (5-7 km/s) layers to be igneous rocks that intruded (and/or underplated) the cold, old continental crust adjacent to the passive margin. Similar velocities are also found under actively rifting

areas such as Afar in East Africa where they are usually interpreted as hot, low velocity mantle.

Some lower crustal bodies have been explained as ponding or magmatic underplating by accumulation of mantle-derived material (mafic magma) at the base of the continental crust (McNutt, 1984; LASE Study Group, 1986; White *et al.*, 1987; Coffin and Eldholm, 1994; Okay, 1994). The low velocity crust might represent serpentinized mafic intrusive rocks incorporating continental fragments at depth, overlain by sediments and basalts nearer the surface. Mafic magma ponded or underplated at the base of continental crust depends on the density contrast between the old crust and the melt (Furlong and Fountain, 1986). Decompressional melting of hot asthenospheric mantle would produce 7.1 to 7.2 km/s velocities in ponded basaltic melt because of increasing MgO content (White and McKenzie, 1989). It is also questionable whether magmatic underplating takes place when the continental crust is highly attenuated (e.g., during the late rift stage) because crustal strength rapidly becomes negligible due to conductive heat transfer whereas massive mafic upwelling reaches the brittle crust (Dixon *et al.*, 1989).

Thus underplating should only occur beneath continental crust (Eldholm and Grue, 1994), off the US East Coast (LASE Study Group, 1986), and the Cape Verde Rise-West Coast of Africa (McNutt, 1988), and the southern Yermak Plateau and northern Svalbard margin (Bonatti and Michael, 1989; Okay and Crane, 1993). Drilling at site 642 of ODP Leg-104 (the Vøring Plateau off Norway; Eldholm *et al.*, 1986) and site 918 of the Ocean Drilling Project Leg-152 (the eastern Greenland

margin; Larsen *et al.*, 1994) revealed that extrusive flows formed the seaward-dipping events. The thinning of oceanic crust away from the margin is thought to reflect a diminishing magma budget (Figure 1-2; Mutter and Zehnder, 1988).

The Cuvier margin, part of the western Australia, occurs on the outer flank of the Exmouth sub-basin's bounding structural high, where the development of seaward-dipping reflectors are observed (Figure 1-5, Mutter *et al.*, 1988). The western Australian margin is assumed to be the boundary between upper- and lower-crustal velocities (between approximately 6.0 and 7.2 km/s from Talwani *et al.*, 1979). The Cuvier margin can thus be interpreted as a truncated equivalent of the extremely broad Exmouth Plateau margin to the north, where no dipping units are present (Mutter *et al.*, 1988).

2. GRAVITY

In some places gravity anomalies occur on the continental shelf edge (in the much younger ocean basins) or within the continent-oceanic crustal transition where lower (mafic) crustal bodies coexist with the continental crust. This transition is sometimes associated with a depth discontinuity (Cochran, 1982) and with a steep gravity gradient (Talwani and Eldholm, 1973; Rabinowitz and LaBrecque, 1977). These marginal isostatic gravity highs may indicate oceanic crust injected during the initial spreading between continents (Rabinowitz and LaBrecque, 1977). They imply that as the ocean basin matures, the elevated crust which is preserved as partly

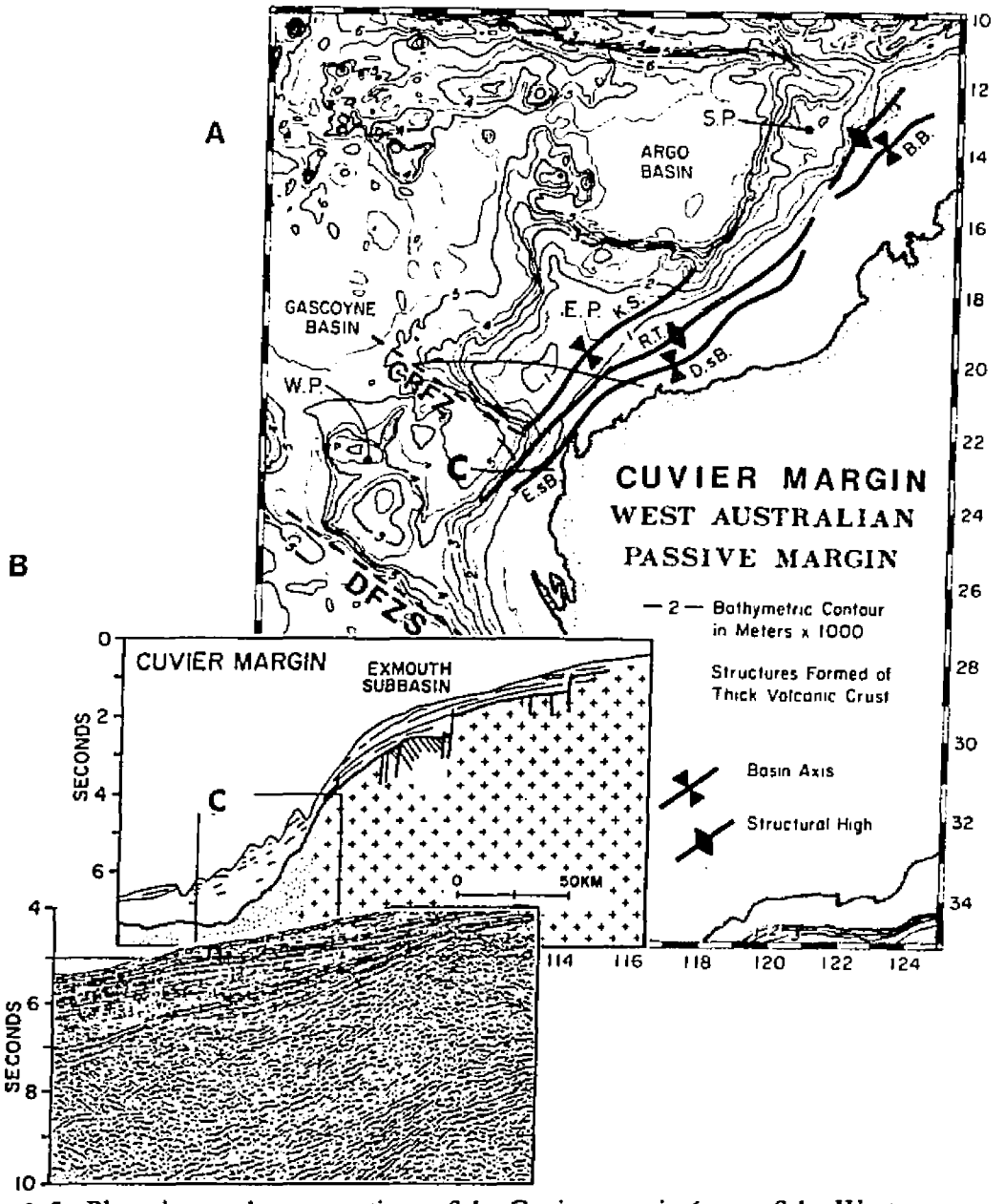

Figure 1-5. Plan view and cross sections of the Cuvier margin (part of the West Australian passive margin) where the branches of the Diamantina Fracture Zone system (dashed lines, DFZS) presumably cuts the passive margin (after Mutter *et al.*, 1988). (a) Major structural elements in the passive margin off Western Australia. Abbreviations are SP: Scott Plateau, EP: Exmouth Plateau, WP: Wallaby Plateau, NP: Naturaliste Plateau, KS: Kangaroo Syncline, RT: Rankin Trend, EsB: Exmouth sub-basin, DsB: Dampier sub-basin, BB: Browse Basin. (b) The Cuvier margin shows evidence for the development of seaward-dipping reflectors that are shown in an example reflection profile in box-C. Dense stipple shows oceanic crust, and crosses show inferred extent of pre-existing continental crust.

uncompensated basement highs, causes gravity maxima. In most cases, such as over the Grand Banks, Newfoundland (Figure 1-4) the anomalies are strongly positive, with maxima of 40-60 mGal, while over the oceanic region the anomalies are generally negative (because of the edge effect created by the continental margin).

In the young northern Red Sea (Figure 1-6), the central rift of the nascent spreading center is characterized by both a gravity minimum and a heat flow high. In contrast, over the flanks of the spreading center (the continental margins of the Red Sea) the gravity anomalies are a maximum (Pout *et al.*, 1986; Cochran *et al.*, 1986, 1991; Martinez and Cochran, 1988, 1989).

3. MAGNETICS

Although some continental margins exhibit prominent magnetic anomalies near continent-oceanic crustal transitions, they are often characterized by a "magnetic smooth zone" with extremely low-amplitude (or moderate) magnetic anomalies. The crust beneath the magnetic smooth zone has been interpreted as a unique "inhomogeneous amalgamation of different crustal types" or "rift-zone crust" (Talwani *et al.*, 1979).

Along the southern Australian margin (Eyre Terrace and western Tasmanian margin, Figure 1-7) a broad (150 km-wide) magnetic smooth zone is cut by two main half-grabens and associated smaller fault blocks which comprise the Eyre sub-basin (Lister *et al.*, 1991). The basin consists of rotational normal faults that trend

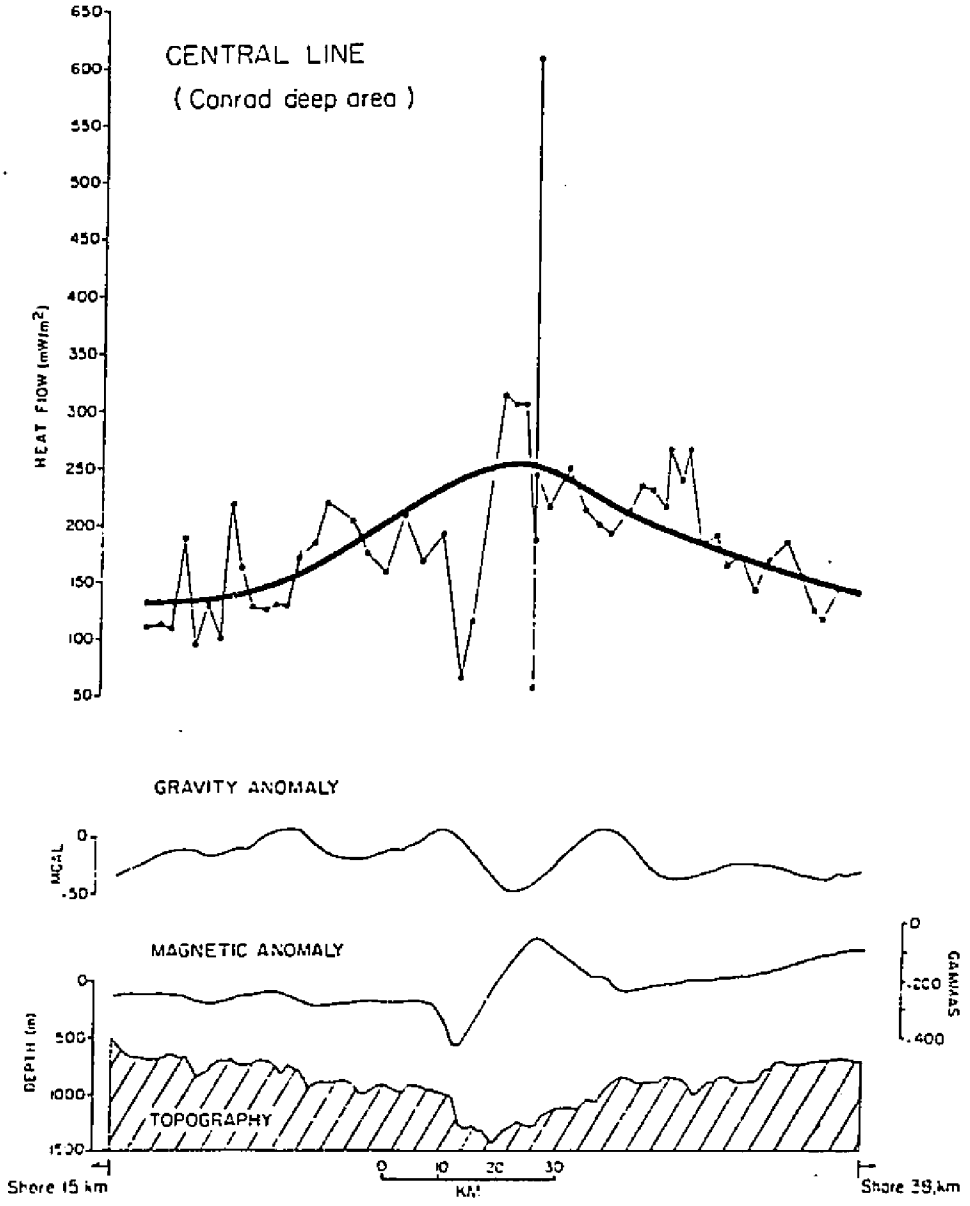

Figure 1-6. Geophysical profiles along the line in the northern Red Sea (Conrad Deep; Cochran, 1982). Well developed central depression characterized by high heat flow values and large gravity minimum. Also, gravity highs over seaward edges of topographic blocks in marginal areas.

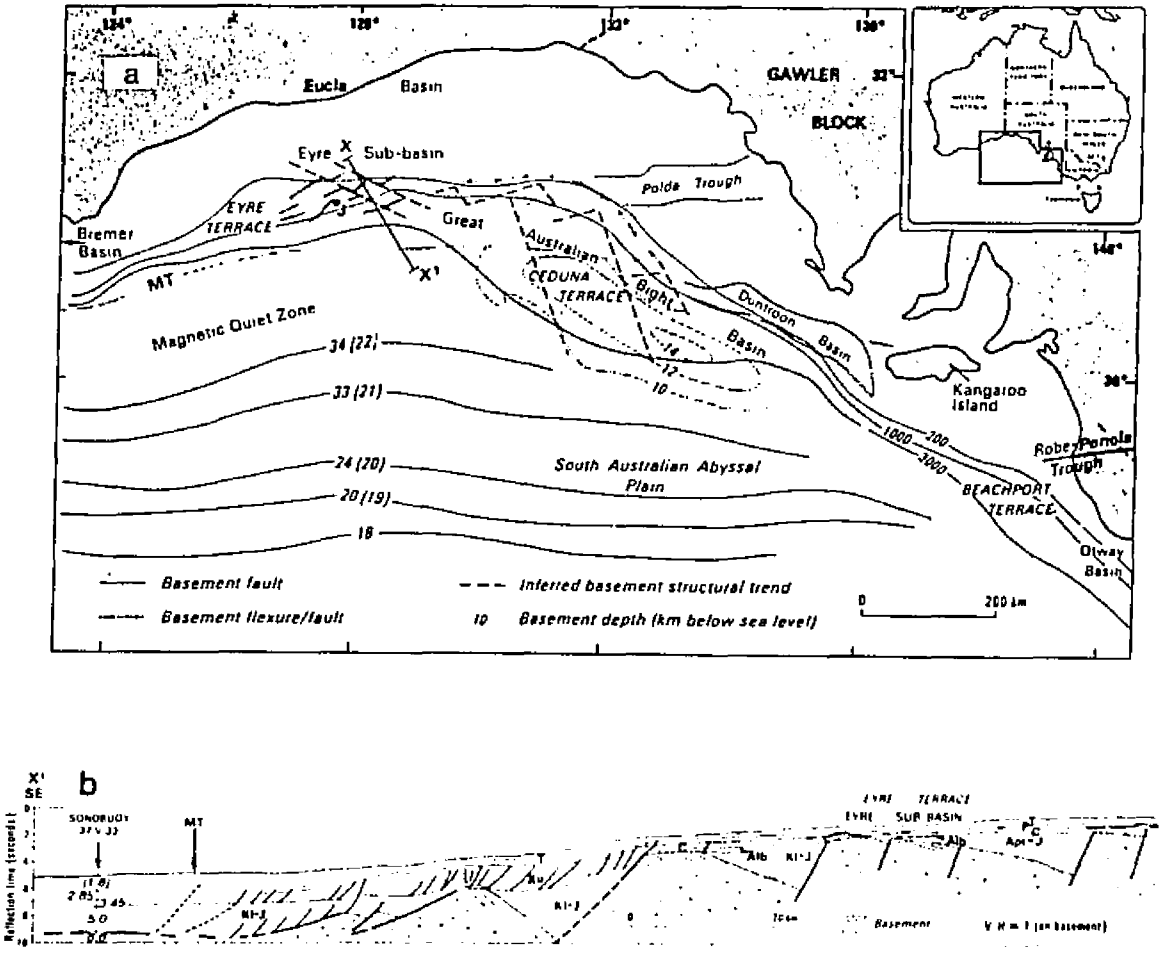

Figure 1-7. Eyre Sub-basin of the southern Australia. (a) Map of the southern margin of Australia (Lister *et al.*, 1991). Location of seismic profile X-X' interpreted in (b); MT is the axis of the magnetic trough which defines the landward edge of the magnetic smooth zone. Numbered lines on the oceanward side of the magnetic smooth zone are magnetic anomaly traces interpreted by Cande and Mutter (1982), and previous interpretation by Weissel and Hayes (1972) are shown in parentheses. (b) Line drawing from seismic-reflection profile X-X' across the Eyre Terrace and out onto the continental rise of the southern Australian margin showing the ages of sequences.

east-northeast and transfer faults that trend northwest. The outer (seaward) boundary of the magnetic smooth zone coincides with this anomalously shallow, complex basement structure, and represents the sharp boundary with anomalously shallow basement topography with obvious oceanic crust produced at the southeast Indian Ridge (Lister *et al.*, 1991).

Another example is the northern Red Sea region where the magnetic field is very flat (Cochran, 1982). The magnetic anomalies in this region are characterized by smooth low-amplitude (less than 100 γ) anomalies. Many of the magnetic anomalies are associated with gravity anomalies suggesting that they are due to complex basement structure or to intrusion of dense highly magnetic rock (Figure 1-6). The relationship between the gravity and magnetic anomalies in the northern Red Sea is typical for the early development of passive margins and suggests that when continental rifting was initiated by the plate motion of Arabia respect to Africa, the lithosphere was still thick and cold, and thus extension therefore appears to occur diffusely across an area of the order of 100 km-wide rather than at a single "spreading center" (Bonatti and Crane, 1982). However, along transtensional margins, such as in the Norwegian-Greenland Sea, magnetic lineations are unclear or absent (Vogt, 1986).

4. HEAT FLOW

According to Sclater *et al.* (1980) the newly-formed oceanic lithosphere progressively cools as it moves away from the mid-ocean ridge yielding heat flow which falls off at a decreasing rate from the ridge crest towards the oldest oceanic crust near the continental margins where it is often characterized by below average and relatively uniform values (about 40 mW/m^2 for the ages of >50 Ma). However, unusual scatter may occur in the plot of heat flow versus oceanic crustal age, which may be the result of the sedimentation effect or of the thermal structure of the margin (Hutchison, 1985).

Some marginal plateaus are thermally uplifted and reheated. For example, high heat flow from the margins of the Northern Red Sea (Buck *et al.*, 1988; Martínez and Cochran, 1989), along the southern and western margins of Australia (Cull and Denham, 1979), the eastern margins of the Norwegian-Greenland Sea (Langseth and Zielinski, 1974; Crane *et al.*, 1982; 1988; 1991; Okay and Crane, 1993) and eastern Arctic Ocean may suggest a volcanic build-up related to seafloor-spreading, perhaps due to interaction between marginal fracture zones and obliquely propagating mid-ocean ridges. Corresponding changes in a continent-ocean transition, seaward dipping volcanic sequences, oceanic basalt chemistry, positive free-air gravity anomalies as well as a magnetic smooth zone are all characteristic of a volcanic margin.

Chapter 2

THE THERMO-MECHANICAL DEVELOPMENT OF TRANSTENSIONAL VOLCANIC MARGINS

A. SHEAR ZONES AND TRANSTENSIONAL VOLCANIC MARGINS

1. STRUCTURAL DEVELOPMENT OF TRANSTENSIONAL VOLCANIC MARGINS

Lithospheric structures, such as fracture zones can control the rifting process and distribution of volcanism originating in the asthenosphere (Dewey and Şengör, 1979; McNutt, 1984). Newly forming plate boundaries interacting with pre-existing continental fracture (or paleo-shear) zones may control the initial break between continents (Atwater and Macdonald, 1977; Crane and Bonatti, 1987).and the development of passive margins (Courtillot, 1982; Bonatti and Crane, 1984; Bonatti, 1994). According to Courtillot (1982) and Bonatti and Crane (1984) paleo-shear zones can be thought of as "locked zones" that are resistant to opening by propagating ridges. These fractures are caused either by shallow mantle convection controlled by episodic mid-plate stresses or pre-existed in the crust prior to seafloor spreading.

In contrast to most oceanic fracture zones, which evolve at right angles to the direction of the mid-ocean ridge axis, paleo-shear zones tend to maintain their original orientation in the crust millions of years after the initiation of new episodes of seafloor

spreading. As new plate motions evolve, these pale-shear zones tend to remain oriented obliquely to present-day plate movement directions (Menard and Atwater, 1968; Atwater and Macdonald, 1977; Crane and Bonatti, 1987). When a mid-ocean ridge propagates into a paleo-shear zone, the angle of impact (θ°, Figure 1) of the propagating ridge and paleo-shear zone may control the state of stress across the newly forming volcanic margin (Crane, 1976; Kastens *et al.*, 1979; Crane and Bonatti, 1987). Analyses of bathymetry and magnetics suggest that ridges and paleo-shear zones readjust themselves to a nearly right-angled configuration (VanAndel *et al.*, 1969; Crane, 1976; Atwater and Macdonald, 1977). The stress field surrounding a ridge-shear zone oblique intersection (depending on the angle of impact) must be asymmetric creating compression and transtension across the shear zone. In addition, during adjustment of the pre-existing structure to the new stress regime, extensional and compressional stresses must change in magnitude across the paleo-shear zone (VanAndel *et al.*, 1969; Crane, 1976; Kastens *et al.*, 1979; Crane and Bonatti, 1987; Crane *et al.*, 1982). Thus, it is expected that asymmetric crustal structures and volcanism evolve as oceanic crust is created (Crane *et al.*, 1991; Okay *et al.*, 1993; Okay and Crane, 1993).

The asymmetric stress across the ridge-shear zone intersection may create passive margins under compression on the acute angle side of impact (Figure 1). The compressional margin at the intersection should also be the site where magma accumulates vertically and dips seaward (Bonatti and Crane, 1982, 1984; Crane *et al.*, 1988; Okay and Crane, 1993). Through time, due to deviatoric stress around the

ridge-shear zone intersection, forward propagation of the ridge ceases and it is deflected along the paleo-shear zone creating small zones of extension (pull-apart basins) in the process (Figure 2). The "punctiform" style of propagation along the shear zone allows the most rapid adjustment of the ridge and paleo-shear zone to its ideal orthogonal shape (Bonatti and Crane, 1982; Bonatti, 1994). Besides compressional and extensional stresses, there may be combined dynamic effects of forward-push force and lateral-spreading force acting on the newly forming margin.

The paleo-shear zone may be constructed of deep-seated faults that act as strike-slip (shear) planes (Crane *et al.*, 1988), accommodation zones (Rosendahl, 1987), or detachment faults (Figure 2-1; Wernicke, 1985; Lister *et al.*, 1986, 1991; Buck *et al.*, 1988; Etheridge *et al.*, 1990; Crane *et al.*, 1991; Torske and Prestvik, 1991; Okay and Crane, 1993). In the extreme case, rifting along a detachment fault generates asymmetric extension that forces the spreading center to remain on one side of the newly forming ocean basin (Buck *et al.*, 1988; Martínez and Cochran, 1988; Crane *et al.*, 1991; Okay and Crane, 1993). This case will be discussed later in the text.

2. Thermal Evolution of Transtensional Volcanic Margins

Paleo-shear zones may evolve into volcanic passive margins if the temperature-structure at the intersection of a propagating ridge and a paleo-shear zone is characterized by large lateral thermal gradients. Several studies (England,

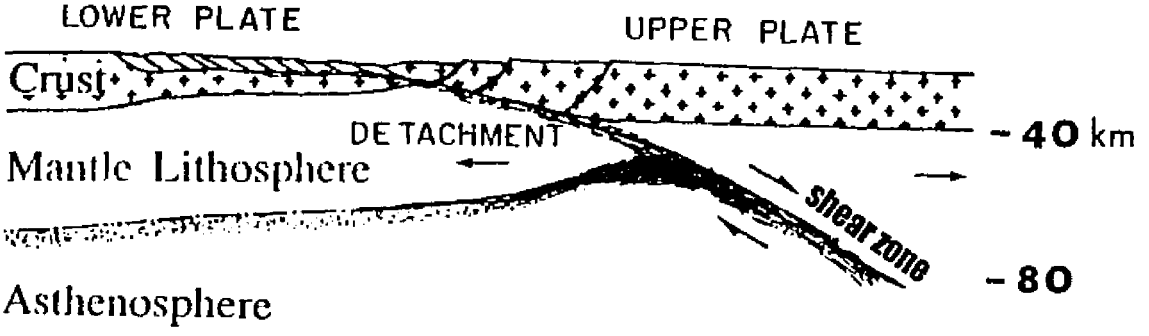

Figure 2-1. Geologic model of the detachment fault. Simple-shear lithospheric extension occurs along a low angle (θ°) detachment fault. The detachment fault divides the lithosphere into an upper plate (hanging-wall) and lower plate (foot-wall). Thinning of the lower lithosphere is offset from the thinning of the upper lithosphere producing an asymmetric lithospheric cross-section along the detachment fault. Throughgoing low-angle shear zone (detachment surface) leads to gross asymmetry and displaces zone of mantle upwelling (thin arrows) from region of major upper crustal extension.

1983; Houseman and England, 1986; Sonder and England, 1989; Buck, 1991) show that lithospheric extension along a newly forming plate boundary can be considered as the deformation of a thin-viscous sheet with a temperature-dependent rheology. According to the thin-sheet model, crustal rheologic variations at the transition zone produce lateral pressure gradients that cause the hot, weak, lower crust to flow (Buck, 1991). The lower-crustal flow produced at the transition zone is analogous to the flow of mantle under a mid-ocean ridge (Buck, 1991). The rate of lower crustal flow also depends on crustal rheologic variations such as crustal viscosity, density, heat flux, thickness, and the rift width. The strain rate dependence of viscosity also plays an important role in the flow rate. For example, high stress decreases the effective viscosity, and increases the lower crustal-flow rate (Buck, 1991).

Along the nascent transtensional volcanic margin, the geometry of the obliquely propagating ridge and paleo-shear zone interaction produces asymmetric deviatoric stress that should increase the rate of the lower crustal-flow. The resulting thermal gradients should cause density instabilities that can induce small-scale convection in the upper mantle creating isotherms which form asymmetrically across the transtensional plate boundary. In this case, mantle material passively upwells to a depth where partial melting occurs (Verhoogen, 1954; Ahern and Turcotte, 1979; Foucher *et al.*, 1982) inducing a great volume of melting (Mutter *et al.*, 1988; Pedersen and Skogseid, 1989; Zehnder *et al.*, 1990; Keen *et al.*, 1994). This type of convection is enhanced by the temperature structure of the lithosphere that in turn

changes the temperature of the lithosphere by thermal expansion and causes a dynamic crustal uplift at the surface (Keen, 1987; Buck, 1986).

Along transtensional volcanic margins, the deviatoric stress fields surrounding the intersection of a propagating ridge and a paleo-shear zone may cause shallow magma bodies to erupt from the shear zone. However, the deeper asthenosphere may continue to propagate in its original direction perhaps in response to far-field state of stress (Okay, 1994). If the paleo-shear zone only cuts through the shallow crust, then its likely that this propagating asthenospheric corridor will proceed underneath the paleo-shear zone intersecting other neighboring deep-seated pre-existing continental faults. These deep-seated faults could act as vertical thermo-mechanical boundaries (conduits) which promote the intrusion by dikes and in some cases the extrusion of magma. In this manner, continental crust is thinned and underplated by mantle material (Bonatti, 1985, 1994), and the uplifting and thermal rejuvenation of the passive margin and adjacent continental crust will follow in the process (Okay and Crane, 1993; Okay, 1994).

Data suggesting asthenospheric underplating of adjacent continental crust might be the following:

1. a broad thermal swell and uplift on the continental crust ahead of the propagating mid-ocean ridge,
2. regions of off-axial high heat flow on and adjacent to the continental margin,
3. apparently younger crust on the compressional side of the ridge and paleo-shear zone intersection,

4. low free-air gravity anomalies and low seismic refraction velocities that are indicative of hot, low-velocity mantle,

5. a magnetic smooth zone,

6. a seismically active region ahead of the propagating ridge tip or on the compressional side of the intersection indicating an asymmetric stress field,

7. large erosion and high sedimentation rates indicating rapid thermal uplift in the neighboring continental crust, and

8. oceanic-type mantle rocks lying at shallow levels on the edge of a transtensional volcanic margin (seaward-dipping igneous sequences), and "multiple zones of intrusions" on the adjacent continental crust suggesting a propagating lateral heat source.

3. The Effects of Rift Width on the Development of Transtensional Volcanic Margin

Observations show that thermal development of some volcanic margins is controlled by asymmetric convection depending on the rift width (of lithospheric extension; Turcotte *et al.*, 1973; England, 1983; Buck, 1986; Mutter *et al.*, 1988; Martínez and Cochran, 1989). For example, a wide rift would take longer to develop than a narrow rift. Melt produced across a wide rift would be distributed over a much greater area than across a narrow rift. As an example, the northern Blake Plateau from the Carolinas to the Canadian Maritime provinces, has a width of transition

which varies but is relatively narrow ranging from 15 to 20 km beneath the Baltimore Canyon Trough (Austin and Uchupi, 1982) to 70 km southeast of Nova Scotia (Keen and Keen, 1974). On the eastern side of the North Atlantic, faulted-thinned continental crust has a sharp contact with oceanic crust off Norway (Talwani and Eldholm, 1973), in the Bay of Biscay, and off northwestern Spain (Boillot *et al.*, 1980). Lake Tanganyika and Lake Malawi (and other) segments of Africa rift system (Rosendahl, 1987), segments of the North Anatolian Fault System (Şengör *et al.*, 1985), and the southern part of the Western Australian margin (Marshall and Lee, 1987) are also characterized by sharp continental transitions.

Buck (1991) recently proposed three extension modes observed in continental lithosphere: the narrow mode, the wide mode, and the core complex mode. Geologic conditions and observable differences of the three modes of extension are illustrated in Figure 2-2.

a. The Narrow Rift Mode:

Localized crustal thinning results in a narrower initial zone of lithospheric extension. Continued crustal thinning leads to narrow rifting. If the lower crustal rheology is weak compared to the mantle rheology, narrow rifting occurs at a high strain rate. In this case, mantle lithosphere controls the weak lower crust to produce a narrow extension (Sawyer, 1985; Buck, 1991). For example in Figure 2-2a

Figure 2-2. Three modes of continental lithospheric extension (after Buck, 1991). Arrows represent directions of strain.
(a) Characteristics of the narrow rift mode: concentrated upper crustal, lower crustal and mantle lithospheric extension. The rate of induced mantle flow will be greater and faster for the narrow margin where more partial melting occurs.
(b) Characteristics of the wide rift mode: uniform upper and lower crustal thinning over a width greater than the lithospheric thickness. The amount of produced melt remains the same but, because of the wide extension zone, convection slows.
(c) Characteristics of the core complex mode: concentrated upper crustal extension with lower crustal thinning over a broad area.

MODES OF LITHOSPHERIC EXTENSION

Narrow Rift Mode

$Q_s = 60\ mW/m^2$

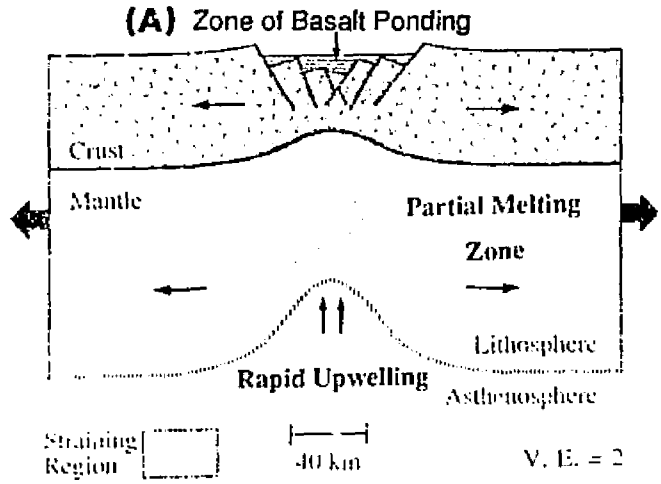

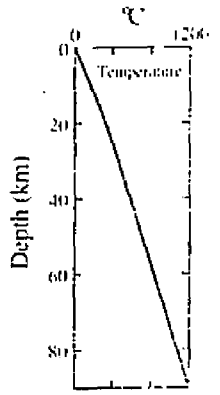

(B) Wide Rift Mode

$Q_s = 80\ mW/m^2$

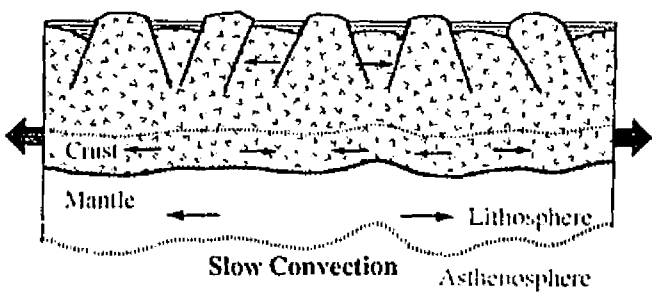

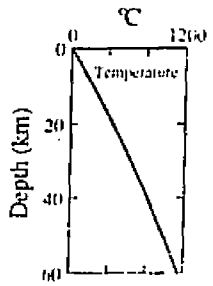

(C) Core Complex Mode

$Q_s = 100\ mW/m^2$

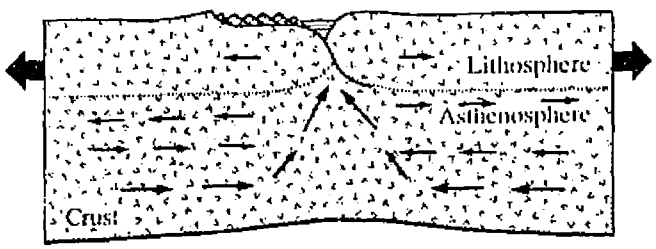

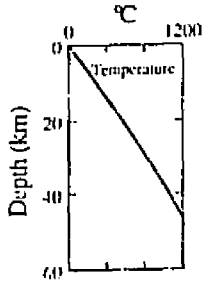

a narrow rift forms with an observed heat flow of around 60 mW/m^2 at the rift valley (of a continental rift), and the estimated crustal thickness at the time of rifting is greater than 80 km (Buck, 1991). Along the passive margin, the extension of the lithosphere continues as a narrow rift until an ocean basin forms and the locus of extension becomes a mid-ocean ridge (Rosendahl, 1987; Buck *et al.*, 1988; Buck, 1991).

b. The Wide Rift Mode:

The wide rift mode occurs when an upper- and lower-crust thins homogeneously over a wide area that is greater than its lithospheric thickness (Figure 2-2b). Examples of this type of rifting are similar to the Basin and Range and Aegean regions. In the Basin and Range the average heat flow is about 90 mW/m^2 (Lachenbruch and Sass, 1978) and the crustal thickness is 25-35 km (Eaton, 1963). The Aegean Sea region extends with an average extension rate of 3-10 cm/yr (McKenzie, 1978), and is without any extrusive volcanic imprints (Dewey and Şengör, 1979). The heat flow in the Aegean region is greater than 90 mW/m^2 (Jongsma, 1974), and crustal thickness is about 30-35 km (Makris, 1982).

c. The Core Complex Mode:

Core complexes are areas where high-grade metamorphic rocks have surfaced from the lower crust (Davis, 1988). Core complexes occur when the upper crust is

extended locally in association with a detachment fault or a shear zone (Wernicke, 1985; Lister *et al.*, 1986; Buck *et al.*, 1988; Block and Royden, 1990; Buck, 1991).

The transtensional volcanic margin geometry may produce a core complex formation if it forms at the intersection of a propagating ridge with a shear zone. In this case, the newly forming crustal transition zone causes crustal differences that produce horizontal-thermal gradients and lower-crustal flow. With increasing deviatoric stress the lower-crustal flow causes the lithosphere to be hotter or thinner than normal. This crustal rheology could produce core complexes at a region, where broad underplating occurs identifiable by a thermal swell and uplifting of the continental crust.

The lower crustal flow has the effect of thinning the crust over a broad area (Figure 2-2c, less than 100 km; Buck, 1991). When the lower crust cannot flow fast enough then the mode of extension depends on the lithospheric strength. For example, the Northern Red Sea (a narrow rift) and the Basin and Range (a wide rift) have experienced and are presently experiencing similar extension rates (Buck, 1991). This indicates that these regions were subjected to different initial thermal parameters depending on their crustal rheologies. A narrow rift forms when the lower-crustal rheology is weak or the lithospheric rheology is strong (if the lithosphere is initially cold). A wide rift forms when the crustal rheology is strong or lithospheric strength is weak (if the lithosphere is initially warm). A core complex forms when the lithosphere is hotter or thinner than normal. Then the lower-crust can flow rapidly to

form core complexes. This may be produced by a broad underplating of cold lithosphere and lateral heating.

Heat flow versus crustal thicknesses for all three modes from several locations are compared in Figure 2-3. The crust is considered to be thick at the time of core complex extension in the Altiplano, in the Andes, and the Tibetan Plateau (Hamilton, 1987). Both the Altiplano and Tibetan Plateau have a crustal thickness of around 60 km and their heat flow values average 90 mW/m^2 (Henry and Pollack, 1988). It is thought that a good example of a core complex formation is found in the Basin and Range Province (Buck, 1988, 1991). Buck (1991) suggests that the southern Basin and Range passed through all three modes of extension. Rifting started with the core complex formation followed by a wide rift mode, which is characterized by high angle normal faults and distributed upper crustal extension. He suggests that the last phase has now begun with the propagation of narrow rifting in the western and eastern sides of the region.

B. MECHANICAL MODES OF LITHOSPHERIC EXTENSION

Extension thins the continental crust and heats the lithosphere by upwelling or propagation of asthenospheric material. The role of lithospheric extension models: pure-shear and simple-shear on the development of various types of continental margins are described in the following sections. Model formulations and parameters for various types of lithospheric extension models are presented in Appendix A-3.

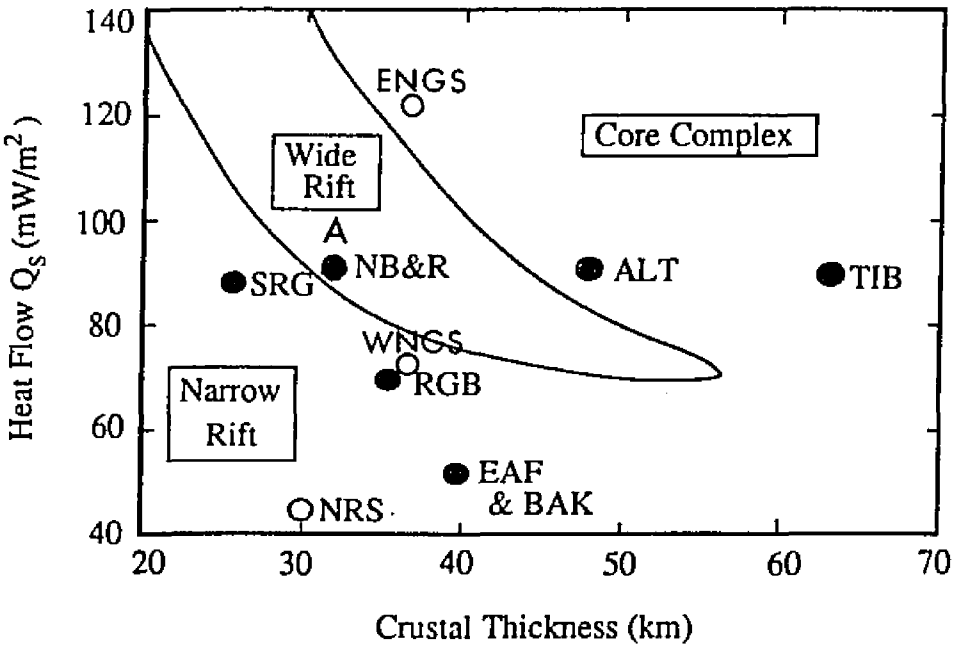

Figure 2-3. Lithospheric extension modes from several regions. Modes are plotted as a function of heat flow and crustal thickness (after Buck, 1991). Hollow circles indicate oceanic areas and dark circles indicate continental areas. A: Aegean Sea, ALT: Altiplano, BAK: Baikal, EAF: East African Rift, NBR: Northern Basin and Range, NRS: Northern Red Sea, SRB: Southern Rhinegraben, SRG: Southern Rio Grande, TIB: Tibet (references are cited in text); and ENGS: Eastern Norwegian-Greenland Sea and WNGS: Western Norwegian-Greenland Sea (this study).

1. Pure-Shear Lithospheric Extension Model

a. Symmetric Pure-Shear Lithospheric Extension Model:

Pure-shear lithospheric extension can be produced by mantle-activated rifting that is a result of upwelling asthenosphere or a vertically rising mantle plume from the core-mantle boundary (LePichon and Sibuet, 1981; White and McKenzie, 1989; Latin and White, 1990; Kent *et al.*, 1992). In this case, rifting extends upper crust over uniformly thinned lower crust (McKenzie, 1978). This type of extension mechanism thins the upper-brittle crust above the lower-ductile crust (Figure 2-4). The depth to Moho moves symmetrically into the region where the maximum thinning occurs. Melting is centered under the region of maximum crustal thinning. Upwelling of asthenospheric material produces a rapid symmetric extension and uplifting. The extension and melt production depend on the changing width of the extension over time. More partial melt can be produced with a large extension rate or with a narrow width of extension (Buck *et al.*, 1988). Slow extension rates (<1 cm/yr) or zones of wider extension cannot produce the conditions approaching the mantle solidus anywhere in the lithosphere (Buck *et al.*, 1988; Martínez and Cochran, 1989).

The amount of uplift depends on the amount of heat transported by convection and the anisotropy of viscosities in the lithosphere (Artyushkov, 1973; Bhattacharji and Koide, 1978; Bott, 1982). Mantle-activated rifting is triggered by the strength of the lithosphere to respond to vertical movement of the anomalously low-density mantle below it. If the plates bounding the region prevent the rifting apart at a rate that forms oceanic crust, then a hotspot will result.

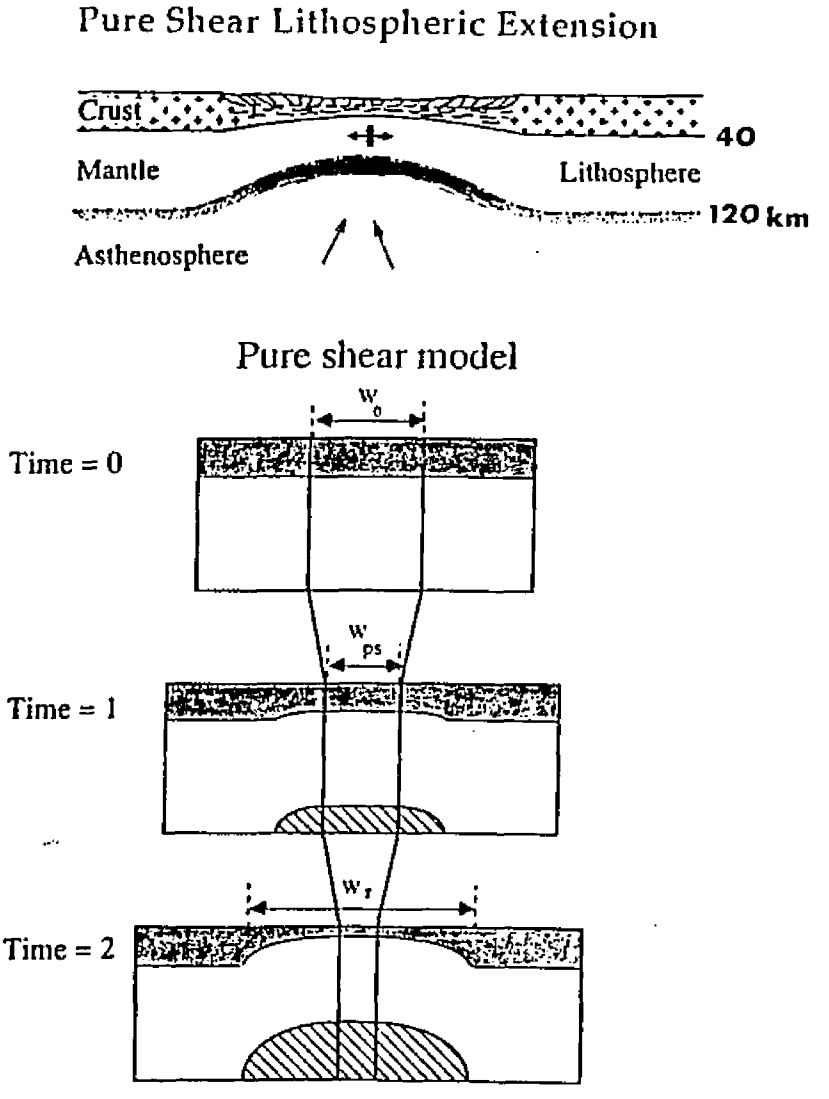

Figure 2-4. Pure-Shear Lithospheric Extension Model. The first diagram is a geologic model of pure-shear lithospheric extension. A series of diagrams illustrates the lithosphere and asthenosphere during the pure-shear lithospheric extension (from time= 0 to time= 2). The model produces melting centered under the region of maximum crustal thinning. W_o, initial width of extending zone; W_{pr}, width of extending zone; W_r, width after extension (Buck *et al.*, 1988).

b. Asymmetric Pure-Shear Lithospheric Extension Model:

The asymmetric pure-shear lithospheric extension model is a migrating pure-shear extension (Figure 2-5). The lithospheric plates on either side of the extension move with different extension rates in opposite directions. Asymmetric extension occurs when one flank of a spreading center extends more than the other flank. Mantle-activated rifting may produce asymmetric pure-shear extension that in turn produces asymmetric topography, heat flow and crustal thickness (Crane *et al.*, 1991; Okay and Crane, 1993). In addition, asymmetric deviatoric stress across the intersection of a propagating rift and shear zone may produce asymmetric pure-shear extension of the lithosphere (Crane *et al.*, 1991). In this model, it is assumed that the horizontal gradient of the horizontal extension is constant across the extending region and is equal to the vertical gradient of vertical extension.

c. Ridge Shift (Jump) Model:

The ridge shift model presents a rifting scenario where one active rift dies and a new rift opens up at some distance from the previous rift. This mechanism is illustrated in Figure 2-5 (Crane *et al.*, 1991). Episodic behaviors of mantle-activated rifting may regenerate or relocate the convective melting and ridge axis. Conjugate aseismic ridges may also develop during this process (LaBrecque and Hayes, 1979; Mutter *et al.*, 1988). There is no direct evidence how this relocation occurs although one hypothesis proposes that the rifting shifts in response to the state of deviatoric stress about the plate boundary.

Figure 2-5. Geologic models of various lithospheric extensions. Schematic diagrams of lithosphere and asthenosphere during and after extension (Crane *et al.*, 1991).
(a) Asymmetric Pure-Shear Lithospheric Extension produces an asymmetric cross-section of the deformed brittle-upper layer of the lithosphere over a ductile-lower layer. Difference in extension velocities (U_{b1} and U_{b2}) produces asymmetry. W_o, initial width of extending zone.
(b) Simple-shear lithospheric extension occurs along a low angle (θ°) detachment fault. The detachment fault divides the lithosphere into an upper plate (hanging-wall) and lower plate (foot-wall). Thinning of the lower lithosphere is offset from the thinning of the upper lithosphere producing an asymmetric lithospheric cross-section along the detachment fault. W_{ss}, width of the extending zone under simple shear.
(c) The ridge jump (shift) model produces a shift in the ridge center. This mechanism results in asymmetric pure-shear lithospheric extension of the continental lithosphere.

LITHOSPHERIC EXTENSION MECHANISMS

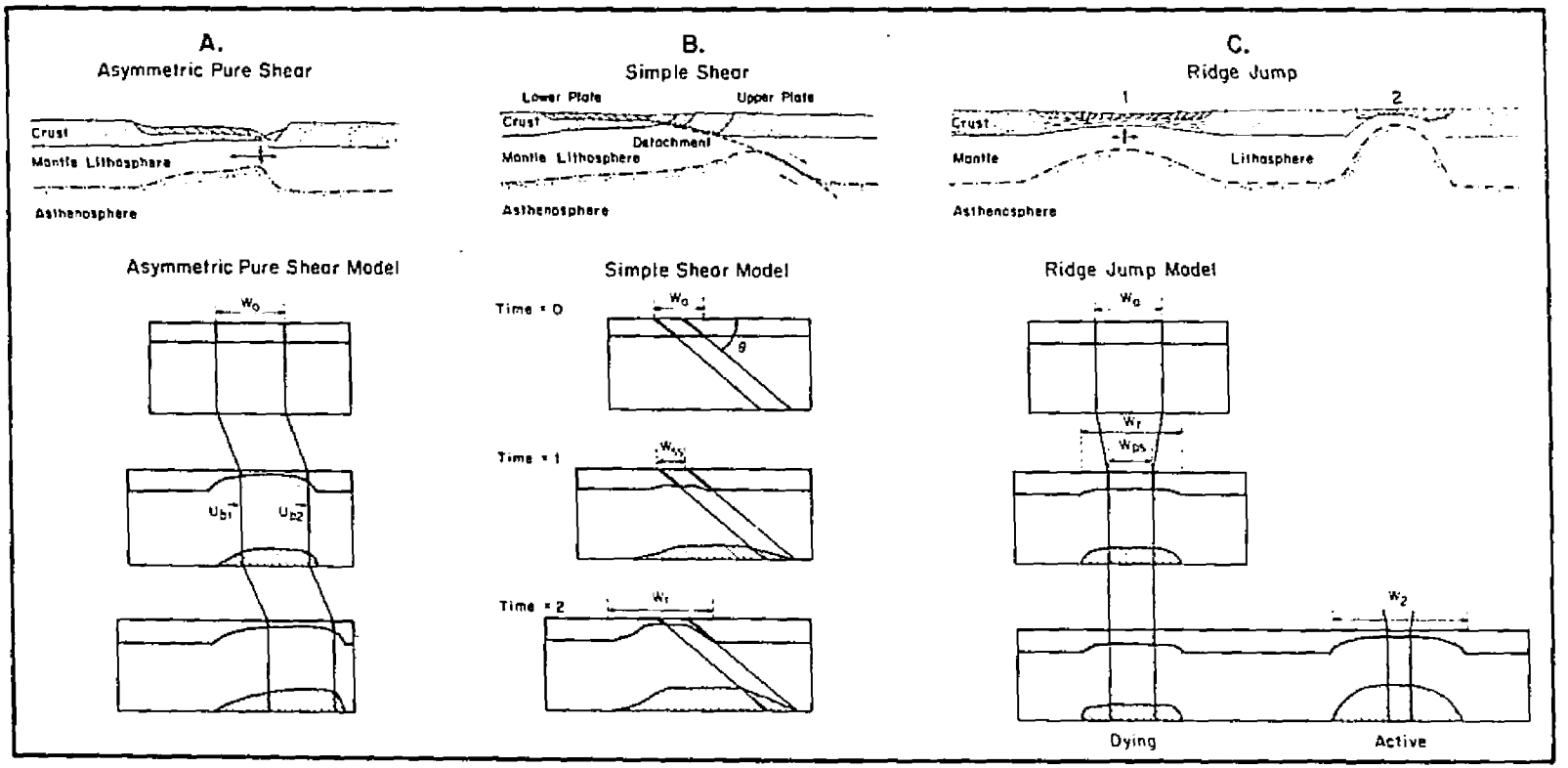

When the ridge-axis shifts into an older region of an oceanic basin, vigorous short-lived convective flow generates a newly forming thick oceanic crust (Mutter *et al.*, 1988). Detailed studies indicate that shifting occurs almost instantaneously (LaBrecque and Hayes, 1979; Cande *et al.*, 1982). During ridge propagation there may be one or more shifts of the ridge axis towards a particular direction. The ridge shift model generates a net strain that is created by at least two episodes of symmetric spreading displaced laterally from one another (Mutter *et al.*, 1988). This type of extension produces asymmetric topography, heat flow and crustal thickness (Figure 2-5; Crane *et al.*, 1991).

d. Examples of Pure-Shear Lithospheric Extension:

Pure-shear extension is thought to be the most common type of extension associated with seafloor spreading. In fact, most of the quantitative extension models depicting the formation of extensional plate boundaries were based upon the concept of pure shear extension (e.g., the Mid-Atlantic Ridge and the East Pacific Rise).

Examples of ridge-shift extension are more commonly found in the Pacific where plate boundaries are thought to be more mobile and have faster spreading rates (>1 cm/yr). Cases such as the Galapagos Rise, and the Mathematicians Seamounts characterize once active extensional plate boundaries that were deactivated and abandoned by ridge shifting during the incremental formation of the presently active East Pacific Rise.

2. Simple-Shear Lithospheric Extension Model

a. Asymmetric Simple-Shear Lithospheric Extension:

Some young continental and oceanic rifts (with slow spreading rates) are thought to open by simple-shear lithospheric extension (produced across a detachment fault or shear zone surface), in an environment where propagating rift-magma enters into the previously fractured crust characterized by obliquely dipping faults (Wernicke, 1985; Lister *et al.*, 1986, 1991; Mutter *et al.*, 1989; Etheridge *et al.*, 1990; Crane *et al.*, 1991). Detachment faults are thought to extend from the upper crust through the Moho and into the lower crust (Figure 2-5). During extension, lower crust and upper mantle lithosphere is thought to be dragged from under the upper crust along the detachment fault surface. The result is the substitution of mantle material for lower crustal rocks and the asymmetric uplift of the continental crust. However, at no point is the advected lithosphere near the mantle solidus (Buck *et al.*, 1988). Since simple shear extrusion is always less effective than pure shear in including partial melting (Buck *et al.*, 1988), a relatively steep detachment is required.

Symmetric pure-shear models assume that the detachment fault represents the brittle-ductile transition and is characterized by rotated tilt blocks, over a more uniformly stretched ductile lower crust. However, Wernicke (1985) suggested that some detachment faults represent low-angle normal-faults that cut through the entire lithosphere (Figure 2-1). An alternative extension geometry may involve delamination of the lithosphere suggested by Lister *et al.* (1986), where the detachment zone runs horizontally below the brittle-ductile transition, steepens, and

then again runs horizontally at the crust-mantle boundary. Lister *et al.* (1986) also emphasize that detachment faults may be merely upper crustal manifestations of major ductile shear zones at depth (Davis *et al.*, 1986). Lister *et al.* (1986) also predicted that there may be two broad classes of passive margins: upper- and lower-plate margins. Upper-plate margins comprise rocks originally above the detachment fault and lower-plate margins comprise the deeper crystalline rocks of the lower plate. Upper-plate and lower-plate margins will differ in their rift-stage structure and their uplift/subsidence characteristics. Their character may suggest the location of: the continent-ocean transition zone, the nature of complex detachment-fault geometries, and the role of transfer faults in the creation of asymmetric margins (Lister *et al.*, 1986, 1991).

Simple-shear lithospheric extension produces asymmetries in crustal thinning, uplift, and heat flow (Buck *et al.*, 1988; Crane *et al.*, 1991; Okay and Crane, 1993). The degree of asymmetry is controlled by the rate of extension, width of the shear zone and dip angle of the detachment fault ($\theta°$ in Figure 2-5), because these have an effect on the lateral heat input from the propagating asthenosphere into the fractured continental lithosphere.

b. Examples of Simple-Shear/Detachment Fault Extension:

Detachment style-lithospheric extension has been suggested for regions in the US Basin and Range Province, the northern Aegean Sea, Western Anatolia, the northern Red Sea, regions along the Mid-Atlantic Ridge, the NW Australian Margin,

and in the Norwegian-Greenland Sea. Also, examples of such rotated high-angle normal faults have been observed from the Bay of Biscay, the Galicia margin, Grand Banks of eastern Canada, and outer continental slope of the Otway Basin off the northwestern Tasmanian margin (Figure 3).

The concept of detachment fault-extension was first applied by Wernicke (1981, 1985) to the Basin and Range Province, a region where lithospheric extension could be accommodated by a zone penetrating the lithosphere along a low-angle normal fault (<30°). This fault is associated with the formation of the metamorphic core complexes and/or (mylonitic) detachment terranes that consist of a brittle upper plate overlying ductilely deformed igneous and metamorphic rocks. The upper plate is truncated at its base by low-angle faults (Lister *et al.*, 1986).

The detachment fault-extension in the Aegean Sea and Western Anatolia are presently characterized by a number of normal faults (listric faults) which have steep dips at the surface in the E-W and N-NE trending grabens (McKenzie, 1978; Dewey and Şengör, 1979). Earthquake fault plane solutions show that the dips decrease with depth (McKenzie, 1978) suggesting that these faults are detachment surfaces. Structural and paleomagnetic data show that large fault rotations (>20°) occurred. Similar listric faults have been proposed for the Rhinegraben (Şengör *et al.*, 1978; Illies, 1979).

In the Red Sea, simple-shear lithospheric extension is thought to produce significant melting depending on the rate of extension and the dip of the detachment fault (Buck *et al.*, 1988). In the northern Red Sea a simple shear-lithospheric

extension model (with an extension rate of 1 cm/yr and a fault dip of 30°) predicts that the asthenosphere moves slowly (or the lower crust flows) into the base of the attenuated lithosphere during the rifting process.

Mutter *et al.* (1989) and Lorenzo *et al.* (1991) proposed that initial deformation of the northwest Australian passive margin was caused by simple-shear extension along low-angle detachment fault planes. As the asymmetric extension continued, partial melting resulted from the decompression of propagating asthenosphere underplating the continental crust in the region. In the process, convective heating induced thermal uplift of the continental crust creating the Naturaliste, Wallaby, Cuvier, Exmouth and Scott Plateaus in the process (Lister *et al.*, 1986, 1991; Mutter *et al.*, 1988, 1989; Etheridge *et al.*, 1990; Lorenzo *et al.*, 1991). Later, simple shear extension passed laterally into pure-shear extension characterized by high-angle normal faults and more volcanism. The region thus became the locus of continental break-up and seafloor spreading (Mutter *et al.*, 1989; Lorenzo *et al.*, 1991).

More recently, Crane *et al.* (1991) and Okay and Crane (1993) proposed detachment fault-extension scenarios for the evolution of the plate boundary in the Norwegian-Greenland Sea. A full description of the evolution of this plate boundary and the eastern margin forming the boundary between the northern Norwegian-Greenland Sea and western Barents Sea are the focus of this thesis.

3. Differentiating Lithospheric Extension Models

Pure- and simple-shear lithospheric extension models have been widely used to explain the morpho-volcano-tectonic variations of passive margins (Lister *et al.*, 1986, 1991; Buck *et al.*, 1988; Mutter *et al.*, 1989; Etheridge *et al.*, 1990; Lorenzo *et al.*, 1991; Crane *et al.*, 1991; Okay and Crane, 1993). For the past 12 years, there has been considerable controversy concerning the nature of lithospheric extension. In 1978, McKenzie proposed the uniform stretching model, which stated that the lithosphere deforms by bulk-pure shear during extension (Figure 2-4). On the basis of field mapping, seismic experiments, and considerations of the asymmetric distribution, magmatism and topography in the Basin and Range Province, Wernicke (1981, 1985) argued that lithospheric extension could be accommodated by slip along a low-angle (10°-30°) normal fault that penetrates the entire lithosphere (Figure 2-5).

In many cases, topographic asymmetries are also observed across conjugate margins. The observations in these regions indicate that normal faults which extend through the lithosphere act as ductile-shear zones, or detachment faults (Wernicke, 1985; Sawyer, 1985; Lister *et al.*, 1986; Buck, 1988), which can not be predicted by symmetric pure shear-lithospheric extension models. In this case, a low-angle detachment fault is thought to form along deep-seated faults rooted orthogonally to the lithosphere, in which all these faults control the development of half-graben complexes (Wernicke, 1985). Lister *et al.* (1986) proposed that, the asymmetry of an evolving ocean-margin is determined by the direction the detachment fault dips:

toward the mid-ocean ridge or away from it. In this case, conjugate passive margins are described as either upper- or lower- plate in character, depending on their particular geometries. However, following McKenzie and Bickle (1988), Latin and White (1990) argued that on the basis of seismological data from areas of active extension, such as the Aegean, Basin and Range, Yunnan (China), East Africa, Suez, and the North Sea, active normal faults do not have dips of <30°. These authors favor a pure shear rather than simple-shear mechanism for magma generation resulting from adiabatic upwelling of the asthenosphere during extension. Like others (Buck *et al.*, 1988), Latin and White (1990) propose that only very small amounts of melt are likely to be produced by simple shear lithospheric extension mechanism.

In contrast, some authors have proposed that detachment faults are thought to control both the structural and thermal development of volcanic passive margins and continental-oceanic crustal transition zones. The investigations of Buck *et al.* (1988), Crane *et al.* (1991), and Okay and Crane (1993) suggest that once intruded by a propagating ridge, new basaltic crust may intrude up along the detachment surface. As extension continues, oceanic crust should develop asymmetrically towards the ocean side of the detachment fault. Mantle lithosphere is then dragged along the detachment fault from the lower crust. If extension continues for a sufficient time, then marginal plateaus and new oceanic crust develops asymmetrically on either side of the detachment surface (Okay and Crane, 1993).

Lister *et al.* (1986) and Okay and Crane (1993) advanced this model further, stating that more than one detachment fault can be involved in continental lithospheric

extension. When a shear zone related detachment fault cuts another detachment fault with opposite dip, movement across one zone deactivates the other, creating low-standing plateaus along the transtensional volcanic passive margin. Entrapment of asthenospheric material may occur within any of the deep-seated faults cutting the detachment surface. If a rift propagates into one or more of these faults, then magma may erupt along the surface of the fault, while the deep-seated asthenosphere may continue to propagate in its original direction. In this way, multiple zones of intrusions could occur as one fault at a time is crossed by moving asthenosphere. The net effect on the surface would be the appearance of multiple zones of extrusion creating a broad-diffuse plate boundary.

Since pure- and simple-shear lithospheric extension mechanisms produce different geological and geophysical patterns within an extending region, volcanic passive margins formed by the pure shear extension process (a rifted volcanic margin) should exhibit:

1. symmetric bathymetry created by the subsidence of cooled continental and oceanic crust.

2. relatively low and uniform heat flow (averaging 40 mW/m^2) predicted by subsidence models for age-dependent cooling of oceanic crust,

3. prominent magnetic anomalies that allow determination of crustal ages along the margin,

4. marginal isostatic gravity highs, indicating oceanic crust injected during the initial spreading between continents.

5. broadly spaced, listric faults interspersed by dipping reflector sequences suggesting the extrusion of ponded lavas through these faults.

In contrast, a volcanic margin formed by simple-shear lithospheric extension (transtensional volcanic margin) should exhibit:

1. a relatively narrow structural transition from continental to oceanic crust dominated by one or a few closely spaced deep-seated faults interspersed with shallow marginal plateaus,

2. asymmetric bathymetry created by compressional and volcanic uplift and marginal plateau formation on one margin vs. low lying broad extensional-type relief on the opposing margin,

3. regions of high heat flow along the margin,

4. large erosion and high sedimentation rates indicative of rapid uplift,

5. a "magnetic smooth zone" indicating a broad intrusion/extension of volcanic material near and overlapping the continent-oceanic crust transition,

6. an asymmetric distribution of earthquakes indicating an asymmetric stress field,

7. oceanic-type mantle rocks at shallow levels on the edge of the margin, and

8. "Seaward-dipping igneous sequences" similar to "core complexes" in the continental lithosphere, and "multiple-zones of intrusions" on the continental crust.

Chapter 3

THE NORWEGIAN-GREENLAND SEAFLOOR

A. CHARACTERISTICS OF THE PLATE BOUNDARIES

1. PRESENT-DAY PLATE BOUNDARIES

The Mid-Atlantic Ridge can be traced as the Knipovich Ridge into the northern Norwegian-Greenland Sea and divides it asymmetrically (Figure 3-1). The ultra-slow spreading Knipovich Ridge (1.5-2.3 mm/yr half rate on the eastern flank and 1.9-3.1 mm/yr on the western flank at 78°N; Crane *et al.*, 1988; 1991) lies close (less than 100 km) to the western Svalbard Margin. The Knipovich Ridge is characterized by a partially buried rift valley covered by sediment (3200-3700 m deep its northern terminus; Crane *et al.*, 1990, 1991). The current spreading half-rates vary from 1.1 cm/yr in the southern Norwegian-Greenland Sea to 0.3 cm/yr in the eastern Eurasia Basin within the Norwegian-Greenland Sea (Eldholm *et al.*, 1987). The present-day structural geometry also supports the hypothesis of complicating ridge propagation (Crane *et al.*, 1991).

Off-axial bathymetric highs trend obliquely away from the Knipovich Ridge (roughly parallel the NW-SE relative plate direction, Crane *et al.*, 1988, 1990, 1991). Close to the intersection with the Molloy Transform the Knipovich Ridge bends

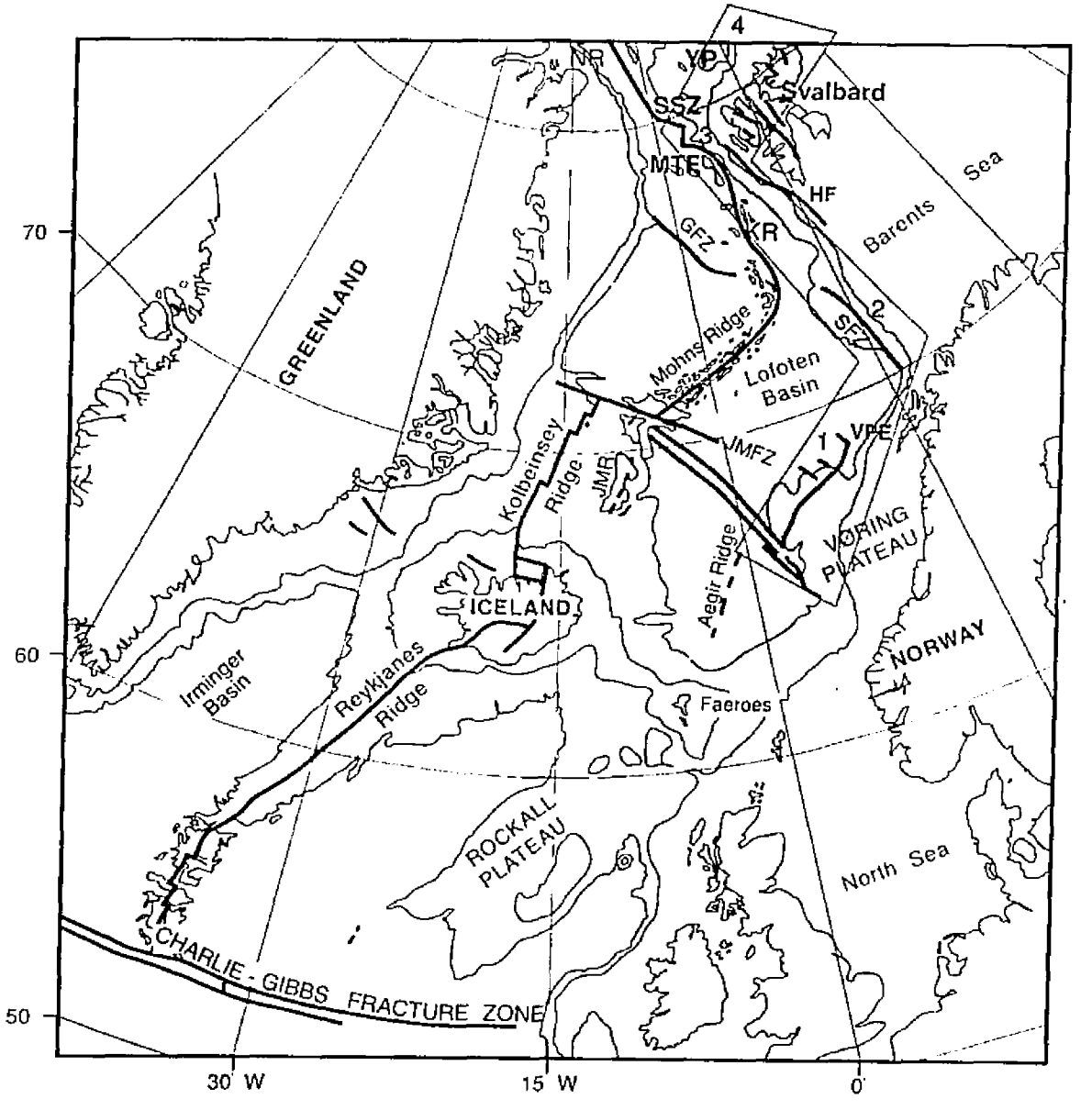

Figure 3-1. Location map of the study area (within the frame) and present plate boundaries in the Norwegian-Greenland Sea and eastern Arctic Ocean. Bathymetry contours every 1 km (Perry *et al.*, 1980). Abbreviations, from south to north: JMFZ: the Jan Mayen Fracture Zone, JMR: the Jan Mayen Ridge, HF: Hornsund fault, VPE: Vøring Plateau escarpment, SFZ: the Senja Fracture Zone, GFZ: the Greenland Fracture Zone, KR: the Knipovich Ridge, MTF: the Molloy Transform Fault, SSZ: the Spitsbergen Shear Zone, YP: the Yermak Plateau, NR: the Nansen Ridge. 1: the Norwegian Margin, 2: the Senja Margin, 3: the Western Svalbard Margin, 4: the Northern Svalbard-Nordaustlandet Margin.

westward (Crane *et al.*, 1990; Okay *et al.*, 1993). The Molloy Ridge and Molloy Transform Fault represent small pull-apart basins which have grown into tiny mid-ocean ridge segments offset by transform faults (Crane *et al.*, 1982, 1991; Okay *et al.*, 1993). A fossil transform fault-ridge (the Hovgård Ridge) is comprised of a seamount-like peak on its eastern part (Crane *et al.*, 1991) and an elongated (fossil) ridge on its western part (Myhre and Eldholm, 1988) in the northern Boreas Basin (78.4°N, 1°E). The Molloy Ridge, a pull-apart basin within the Spitsbergen Fracture Zone is a small section of newly forming oceanic crust (Crane *et al.*, 1982, 1990, 1991). The Molloy Deep (79.2°N, 2.8°E), a nodal basin (exceeding 5000 m) lies at the intersection of the Molloy Ridge with the Molloy Transform (Thiede *et al.*, 1990).

The current plate boundary is believed to continue into the Arctic Ocean along a deep trough that was once called the Spitsbergen Shear or Fracture Zone (Crane *et al.*, 1982, 1991), and its detailed structure is still not well-known (Talwani and Eldholm, 1977; Sundvor *et al.*, 1977; Vogt, 1986; Thiede *et al.*, 1990). Crane *et al.* (1982) suggested that sections of the northern Spitsbergen Shear Zone had been invaded by rift propagation southward from the Nansen Ridge.

The northern terminus of the Spitsbergen Transform Fault continues into the elongate Lena Trough (81°N, 3°W; the most northerly section of the obliquely opening mid-oceanic ridge; Crane *et al.*, 1991). Detailed morphology of the Lena Trough is not available as it lies under year-long ice cover. It is perceived to be a leaky-transtensional zone oriented subparallel to the Knipovich Ridge. Further to the

NW, the Lena Trough intersects with the Nansen Ridge at the northern terminus of the Fram Strait (Thiede *et al.*, 1990).

2. Plate Boundary Evolution

Prior to the Cenozoic, the area between Norway and Greenland was a part of a large epicontinental sea extending into the North Sea and Barents Sea (Birkenmajer, 1981). From Chron 25/24 to 13 the plate boundaries of the North American, Greenland and Eurasian plates met a triple junction, called the North Atlantic Triple Junction (Figure 3-2, Kristoffersen and Talwani, 1978; Srivastava, 1978; Reksnes and Vågnes, 1985).

During several extensional phases in the Mesozoic and the late-Paleocene, the crust between Norway and Greenland was thinned without a crustal break-up (Talwani and Eldholm, 1977). Seafloor spreading was initiated between Chron 25 and 24 (LaBrecque *et al.*, 1979). According to Talwani and Eldholm (1977), Reksnes and Vågnes (1985), Max and Ohta (1988), and Crane *et al.* (1991) since the inception of seafloor spreading, the plate boundaries between Greenland, Norway, and Svalbard have been controlled first by shearing and then transtension (Figure 3-3). Prominent fault lineations and sedimentary basins off Norway and the North Sea resulted from a widespread, nearly synchronous rifting episode during the late Jurassic and early Cretaceous (Ziegler, 1978).

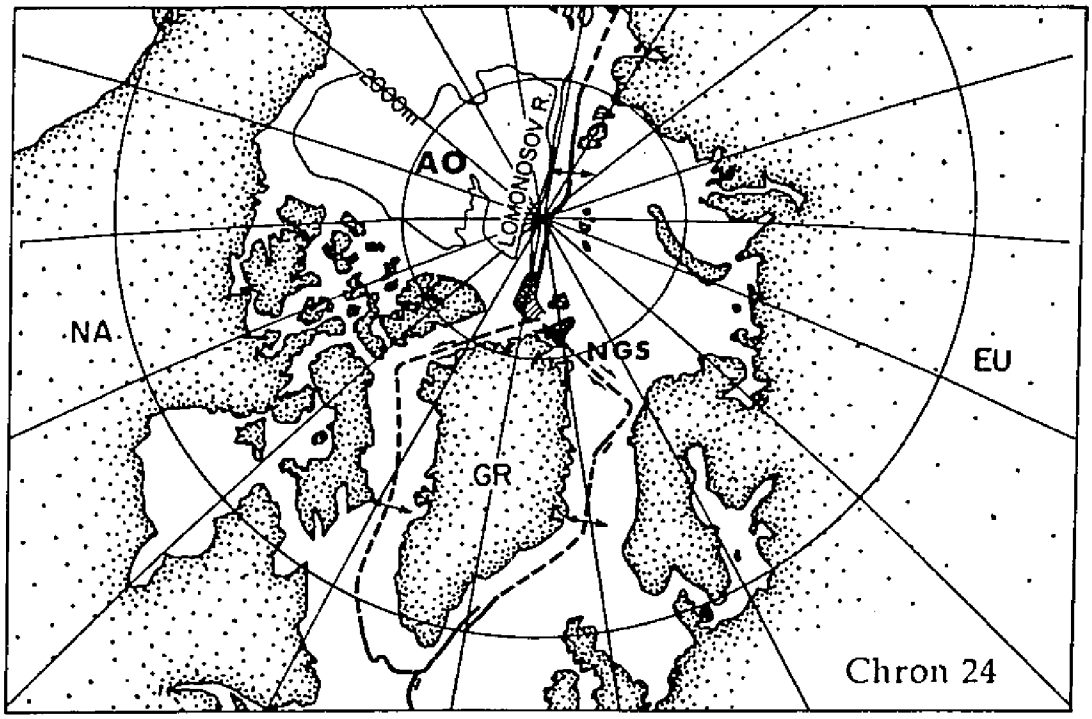

Figure 3-2. Evolution of three plate movements. Simplified model showing the tectonic evolution of the region adjacent to the Norwegian-Greenland Sea (NGS) and Arctic Ocean (AO). The movement of three plates (anomaly 24), GR: Greenland, NA: North America, EU: Eurasian plates. Bathymetry is indicated by 2000 m contour (after Jackson *et al.*, 1984).

Figure 3-3. Initial seafloor opening of the Norwegian-Greenland Sea. Simplified model shows the principal events by Müller and Spielhagen (1990). The motion between Greenland and Eurasia between Chron 33 (80 Ma) and 13 (36 Ma) is calculated by Srivastava and Roest (1989).
(a, b) During Chron 33: In the Lower Paleocene the plate boundary jumped eastward to the Hornsund fault Zone. A drastic counterclockwise change in spreading direction in the Labrador Sea caused between Chrons 25 (59 Ma) and 24 (56 Ma) caused transpression between Greenland and Svalbard.
(c) Strike-slip dominated transpression characterized the period from Chron 24 to 21.
(d) During Chron 23: initial seafloor opening of the Norwegian-Greenland Sea (the Aegir and Mohns Ridges), simplified model by Reksnes and Vågnes (1988). HF: Hornsund Fault, SM: Senja Margin, MR: Mohns Ridge, JMFZ: Jan Mayen Fracture Zone, AR: Aegir Ridge, VP: Vøring Plateau.
(e) During Chron 21: giving rise to 160 km of dextral strike-slip and 15-20 km of shortening determined using finite reconstruction poles for Eurasia relative to Greenland from Srivastava and Roest (1989).

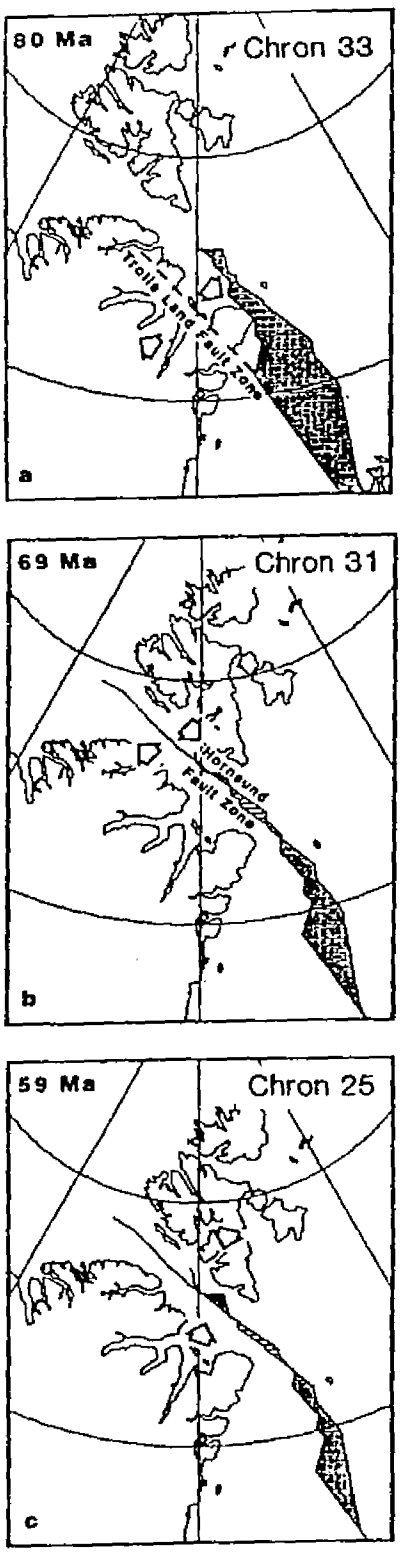
80 Ma
Chron 33
Trolle Land Fault Zone
a
69 Ma
Chron 31
Hornsund Fault Zone
b
59 Ma
Chron 25
c

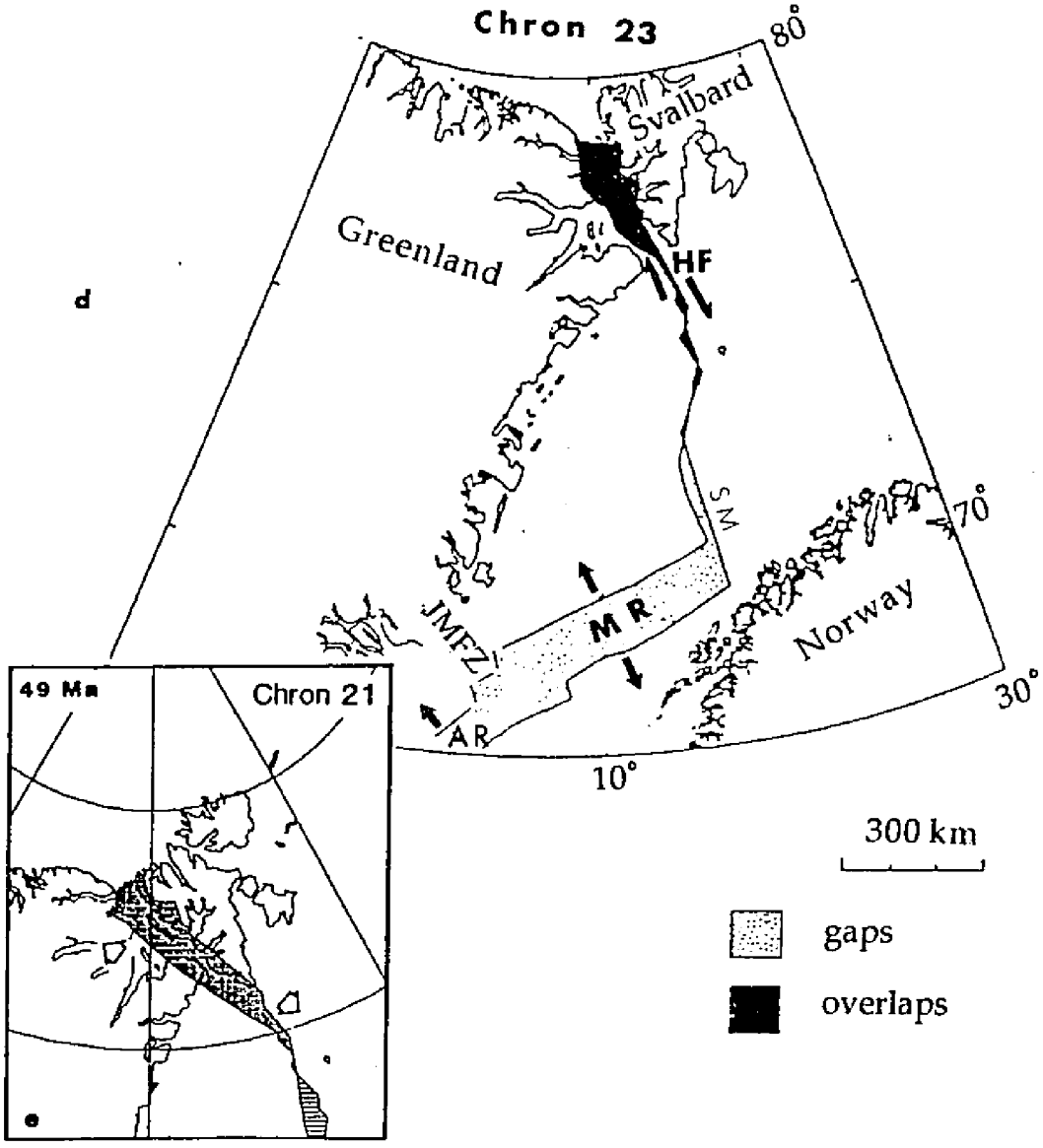
Chron 23
80°
Svalbard
Greenland
HF
d
SM
70°
JMFZ
MR
Norway
AR
30°
10°
300 km
gaps
overlaps
49 Ma
Chron 21
e

The Jan Mayen Fracture Zone System may have originated as a zone of structural weakness in the late Paleozoic and may have been active during the rifting events in the Mesozoic (Bukovics and Ziegler, 1985; Mutter *et al.*, 1984; Skogseid and Eldholm, 1987; Eldholm *et al.*, 1984; Torske and Prestvik, 1991). The paleo-Jan Mayen and Senja-Greenland Fracture Zones were oriented in such a way that the early episode of rifting propagated obliquely into these features (Figure 3-3). The Vøring Plateau was formed, in the region, during the initial opening of the southern Norwegian-Greenland Sea by a voluminous volcanic pulse at the oblique intersection of the Aegir Ridge with the Jan Mayen Fracture Zone (Mutter *et al.*, 1984; Hinz *et al.*, 1987; Skogseid and Eldholm, 1987; Eldholm, 1991; Eldholm and Grue, 1994).

It is generally believed that the Jan Mayen Ridge is of continental origin and that it was separated from Greenland (25 mybp) by the formation of a new spreading center: the Kolbeinsey Ridge (Figure 3-1; Skogseid and Eldholm, 1987). During this separation, the Jan Mayen block was faulted and its configuration of en-echelon rifting was the result of shearing of the Jan Mayen blocks (Nunns, 1982, 1983; Nielsen, 1983). On the eastern side, faults occurred during episodic extension in the Paleocene. Spreading in the new location (between Greenland and the Jan Mayen Ridge) continued until it centralized about the Kolbeinsey Ridge axis during the last 10 mybp (Vogt, 1986). After the spreading axis shifted from the Aegir Ridge to the Kolbeinsey Ridge, the Jan Mayen Ridge was left as a remnant on the seafloor.

The Senja Margin was formed from a megashear zone during the Eocene. Between Chron 25 and 24 the plate boundary was offset between the incipient

Lofoten-Greenland and Eurasia Basins by a regional shear zone probably along the Senja Fracture Zone (Trolle Land Fault Zone) lineament (Figure 3-3). The plate boundary along the Senja Margin propagated to the northeast between Chron 21 and 13. About 50 Ma ago the separating axis shifted to the northwest forming the passive margin between Bjørnøya and 76.5°N creating a deep basin north of the Senja-Greenland Fracture Zone. The early-Paleocene reactivation of the Kimmerian Wrench system along the Senja-Western Svalbard Margin coincides with the dextral shear motion along the Trolle Land Fault Zone (Max and Ohta, 1988).

The northern part of the Senja Margin evolved during the major reorganization of relative plate motion at 36 Ma. During this period, the plate configuration caused transpression between northern Greenland and Svalbard, creating local transpression and transtension across the Tertiary Wrench Regime in the region (Steel *et al.*, 1985; Reksnes and Vågnes, 1985; Müller and Spielhagen, 1990). Along Bjørnøya and the Western Svalbard Margin, pre-existing faults were repeatedly reactivated during the mid-Jurassic and late-Cretaceous (Birkenmajer, 1981). Also, during this time, dextral transpression controlled the wrench movement of the Hornsund Fault Zone (Sundvor and Eldholm, 1979; Vogt, 1986; Max and Ohta, 1988). At Chron 13 the Hornsund Fault Zone became the plate boundary (Figure 3-4). This shift in relative plate motion to the northwest along the paleo-Spitsbergen Shear Zone, caused crustal thinning and later sea-floor spreading in the northern Norwegian-Greenland Sea.

Because of increasing deviatoric stress around and near the Spitsbergen Shear Zone, seafloor spreading could have caused the Mohns Ridge to propagate northward and into the shear around 50 mybp forming the Knipovich Ridge in the process (Figure 3-4). The oblique intersection between the Mohns Ridge and the Spitsbergen Shear Zone could have generated complex regions of extension and compression along and across the former shear zone. Continuing readjustment of the plate boundaries throughout the transtensional shear zone could have resulted in the slivering of the Western Svalbard Margin and the transportation of these slivers to the northwest along the coast of Svalbard. For instance, the Hovgård Fracture Zone is thought to be a remanent piece of continental crust rafted away from the Senja Margin (Myhre *et al.*, 1982).

According to Crane *et al.* (1988, 1991) the latest episode of rift propagation along the Knipovich Ridge occurred between 12 and 16 mybp, and was marked by new episodes of volcanism on Svalbard. As the spreading was slow and confined to a narrow region, magma ponded upwards perhaps creating or thermally rejuvenating pre-existing plateaus in the process (Crane *et al.*, 1991; Okay and Crane, 1993).

One of these, the southern Yermak Plateau was probably thermally reactivated between 16-10 mybp (Crane *et al.*, 1982). During Chron 13 to 7, Birkenmajer (1981) suggests that this region underwent extension as well as shear and compression. The southern plateau could be the result of a thinned and stretched continental crust created as ridge and transform systems migrated across the region. In addition, underplating of Spitsbergen by a propagating asthenospheric front may

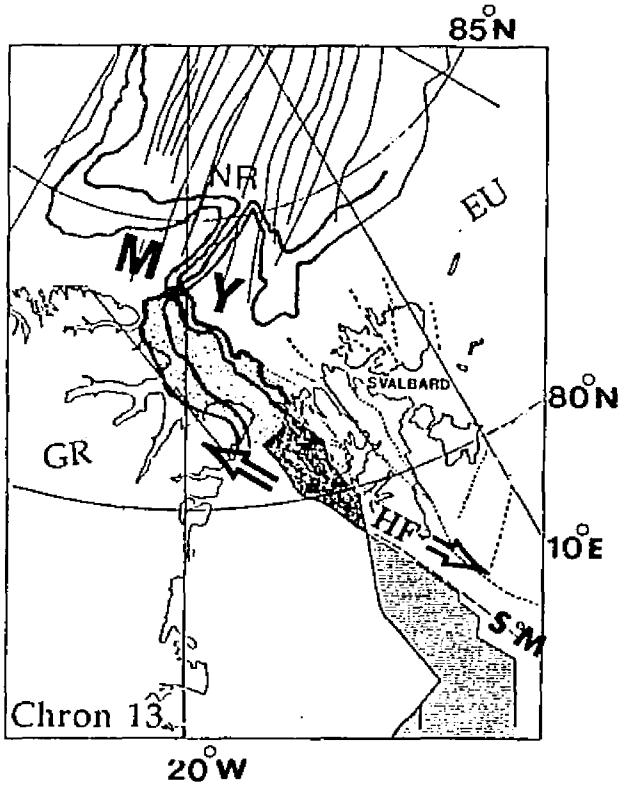

Figure 3-4. The relative motion between Greenland and Svalbard at Chron 13 with the present coordinate grids and the present magnetic anomaly amplitudes (Vogt, 1986). Strike-slip movement dominated the region until 35.9 mybp, subsequently followed by seafloor spreading (Müller and Spielhagen, 1990). Using the pole of rotation for the Eurasian plate (EU) relative to Greenland plate (GR) (after Srivastava and Roest, 1989). Hatched area indicates gaps (dominated by extension) between continental margins (dashed lines are pre-existing continental weaknesses); stippled area indicates overlaps; dark area indicates compression (transpression). The opening of the Norwegian-Greenland Sea (along the Knipovich Ridge) and the Eurasian Basin along the Nansen Ridge (NR) started along the Senja-Western Svalbard Margin, giving rise to an extensional tectonic regime. The location of Svalbard relative to the Yermak Plateau (Y), across the Nansen Ridge is a similar feature, the Morris Jesup Rise (M). NW-SE trending faults are shown in dashed lines; HF: the Hornsund Fault Zone.

have caused injection of basalt into pre-existing shear zone related faults on Svalbard (Okay, 1990; Okay and Crane, 1993; Okay *et al.*, 1991, 1993). The southern section of the Yermak Plateau may have been created in response to a broad and rapid injection of basalt along the continental margin (Okay and Crane, 1993). Thus, the present Spitsbergen Transform should be a post-Chron 5 (ca. 10 Ma) feature, and only a small remnant of the once immense Spitsbergen Shear Zone.

According to Skjelkvåle *et al.* (1989) during Chron 5 either the Yermak Hotspot was regenerated and formed the Quaternary volcanic centers in the area (Prestvik, 1978), or magma erupted in response to the now close proximity of the northward propagating Knipovich Ridge as suggested by Crane *et al.* (1988, 1991). On the other hand, rejuvenated volcanism on the southern Yermak Plateau and Svalbard could have coincided with either increased volcanic activity on the Nansen Ridge or the southern propagation of the Nansen spreading axis into the Spitsbergen Shear Zone as suggested by Feden *et al.* (1979) and Crane *et al.* (1982).

3. Volcanic Events

A major pulse of short-lived voluminous magmatism accompanying early seafloor spreading has been suggested for the formation of the Norwegian-Greenland Sea ocean basin (Eldholm, 1991). Continuous volcanism in the region is marked by the Iceland-Faeroe and the Greenland-Iceland Ridges that lead from the margins to Iceland. The early Tertiary break-up of the North Atlantic Ocean and the Norwegian-

Greenland Sea was associated with short-lived but voluminous magmatic activity in the North Atlantic and eastern Arctic Ocean (Figure 3-5). According to White *et al.* (1987), most igneous accumulations in the North Atlantic and the Norwegian-Greenland Sea are coincident with the early-Tertiary hotspot event centered at the presently active island of Iceland. Composition of the lava on Iceland is typically andesite although more silicic lavas (such as dacite) may be emitted early in an explosive eruption, and later lavas may approach the composition of alkali basalt. This event is documented as the North Atlantic Volcanic Province along the volcanic passive margins and characterized by seaward-dipping seismic reflector sequences (Figure 3-5, Hinz and Weber, 1976; Mutter *et al.*, 1982; Roberts *et al.*, 1984; Skogseid and Eldholm, 1987; Larsen and Jakobsdóttir, 1988; Eldholm *et al.*, 1989a). Vogt (1986) suggested that the frequency of activity or the volume of eruptions (or both) decrease away from Iceland, being generally highest on the Kolbeinsey Ridge and lowest along the Knipovich and Molloy Ridges, where spreading is slow, oblique and the axis is exceptionally deep, or some combination of these.

The Vøring Plateau on the Norwegian Margin to the NE of Iceland, is underlain by volcanic accumulations at the continent-ocean boundary. The drilling results from Leg 104 of the Ocean Drilling Program (Sites 642 and 643 in Figure 3-5) indicate two distinct lava flows of a lower-series of dacitic flows (dated 54 Ma) and an upper-series of subaerial MOR-type tholeiitic flows (dated 57.8 Ma, Eldholm *et al.*, 1989b; Eldholm, 1991).

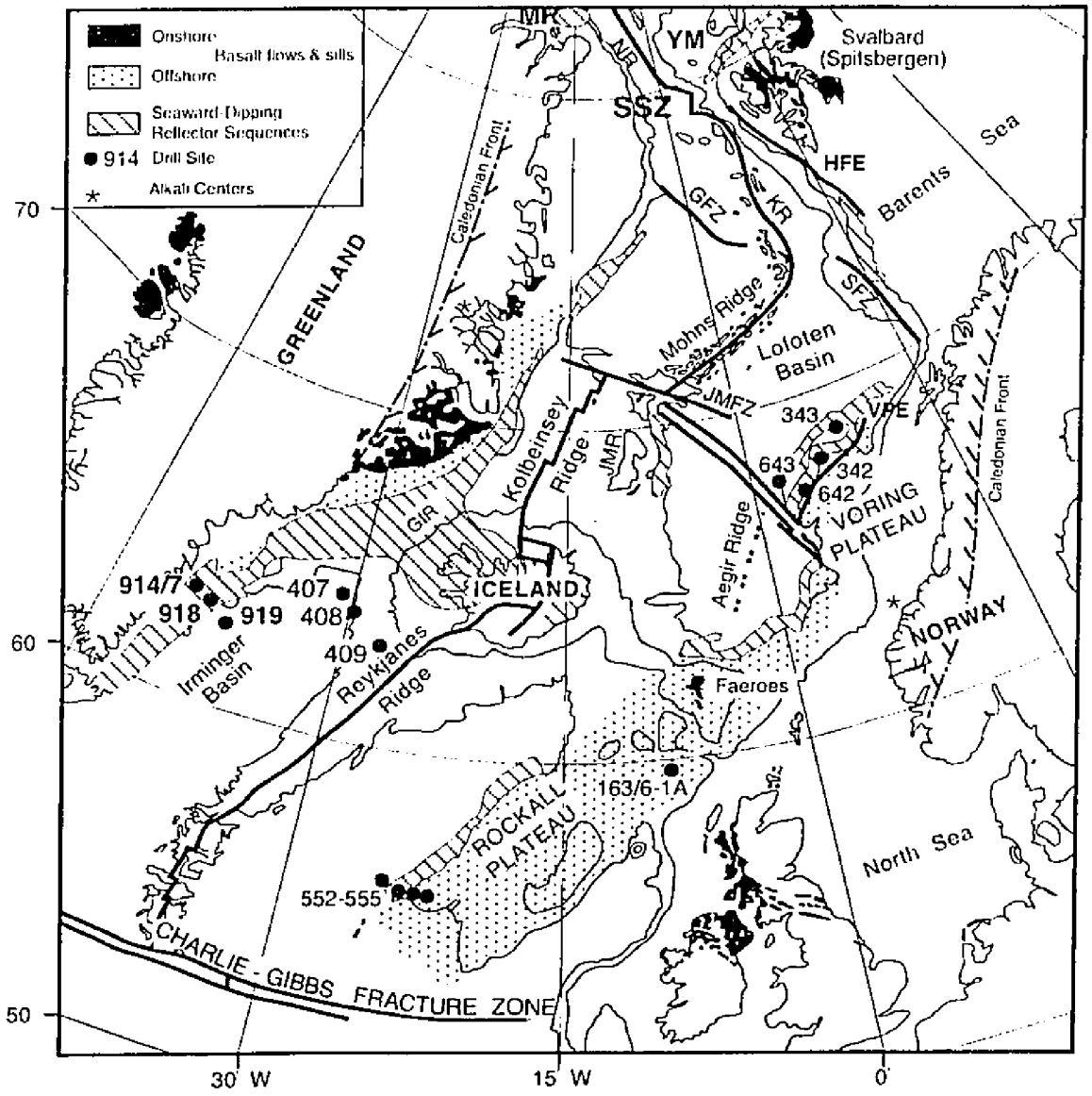

Figure 3-5. Igneous units in the Norwegian-Greenland Sea (modified from Coffin and Eldholm, 1991). The volcanic margins are indicated by seaward dipping reflector wedges (Roberts *et al.*, 1984; Hinz *et al.*, 1987; Skogseid and Eldholm, 1987; Sundvor and Austegård, 1990). Bathymetry is indicated by 1 and 2 km contours. JMFZ: Jan Mayen Fracture Zone, VPE: the Vøring Plateau Escarpment; LFZ: Lofoten, SFZ: Senja, and GFZ: Greenland Fracture Zones, KR: Knipovich Ridge, S: Svalbard, YP: Yermak Plateau, MR: Morris Jesup Rise.

Jan Mayen, an active volcanic island in the southern Norwegian-Greenland Sea, is not located on the present-day plate boundary. Although Jan Mayen was thought to have existed since late middle Tertiary on the basis of glacial morphology or since early Pliocene on the basis of tephra chronology studies performed by Sylvester (1975) on Deep Sea Drilling Project-Leg 38 (Sites 342 and 343 in Figure 3-5), K-Ar dates show that the oldest lavas are only of late Pleistocene in age.

Two occurrences of alkalic volcanic rocks (adjacent to and in the southern Norwegian-Greenland Sea) are situated in continental fault zones along the Kaiser Franz Josephs Fjord in East Greenland and along the paleo-Eastern Jan Mayen Fracture Zone off Norway (Figure 3-5). Torske and Prestvik (1991) suggested that the Greenland rocks are K-Ar dated at 56 Ma and the Norwegian rocks at 55.7 Ma. These volcanics erupted close to the time of initial breakup prior to seafloor spreading.

In north Greenland, along the Arctic coast in northern Peary Land rhyolitic volcanics called Kap Washington Group (83.3°N, 37.45°W) were dated about 63-64 Ma (Feden *et al.*, 1979). This largely subaerial tholeiitic-type volcanic activity associated with the Morris Jesup Rise occurred between Chron 24 and 13 (60-38 Ma, Håkonsson and Schack-Pedersen, 1982). This is in contrast to Svalbard which has been shown to be more recently active (10-12 Ma, Prestvik, 1978).

Some volcanic activity and a few dykes (related to steeply-dipping deep-seated faults trending north-south) occur in the Devonian Graben of Spitsbergen (Max and Ohta, 1988). Amundsen *et al.* (1987) show several Tertiary and Quaternary (60 and

11 Ma) volcanic centers aligned along the northwestern margin of the Tertiary Basin (Hjelle and Lauritzen, 1984). Quaternary volcanic centers: Sverrefjell, Sigurdfjell and Halvdanpiggen (Figure 3-6), are found in the Woodfjørden and Bockfjørden, (Hoel and Holtedahl, 1911; Gjelsvik, 1963; Prestvik, 1978; Skjelvåle *et al.*, 1989). The Sverrefjell stratovolcano consists of interbedded pillow lavas and pahoehoe lava flows (few to several hundreds of meters) containing a wide variety of xenoliths (Skjelvåle *et al.*, 1989). Thermal springs, Jotunkjeldane and Trollkjeldane are located 2 km north and 5 km south respectively of the uneroded Sverrefjell volcanic cone. Sellevoll *et al.* (1991) show that a 3 km thick transitional Moho Zone occurs under the Central Spitsbergen Tertiary Basin that is characteristic of mobilized lower crust or igneous underplating. The northern prolongation of deep-seated faults, in the middle of the Yermak Plateau, is coincident with a positive magnetic anomaly that suggests submarine volcanics. Bonatti and Michael (1989) also suggest that fresh peridotites might be found in this area indicative of oceanic rather than continental mantle material.

Further to the northeast, dolerites and some lavas of Mesozoic ages (145 and 105 Ma, Figure 3-6) occur on both sides of Hinlopenstretet (Johnson and Rich, 1986). Lower Cretaceous doleritic flows (120 Ma) are common on Spitsbergen, Nordaustlandet, Barentsøya, Edgeøya, (Harland, 1971; Prestvik, 1978; Birkenmajer, 1981; Campsie *et al.*, 1988), Kong Karls Land, and in Franz Josef Land, (Campsie *et al.*, 1988). Further east, Siberian plateau basalts are dated as late-Permian/Mesozoic (256 Ma) in Siberia (Green *et al.*, 1984; Johnson and Rich, 1986).

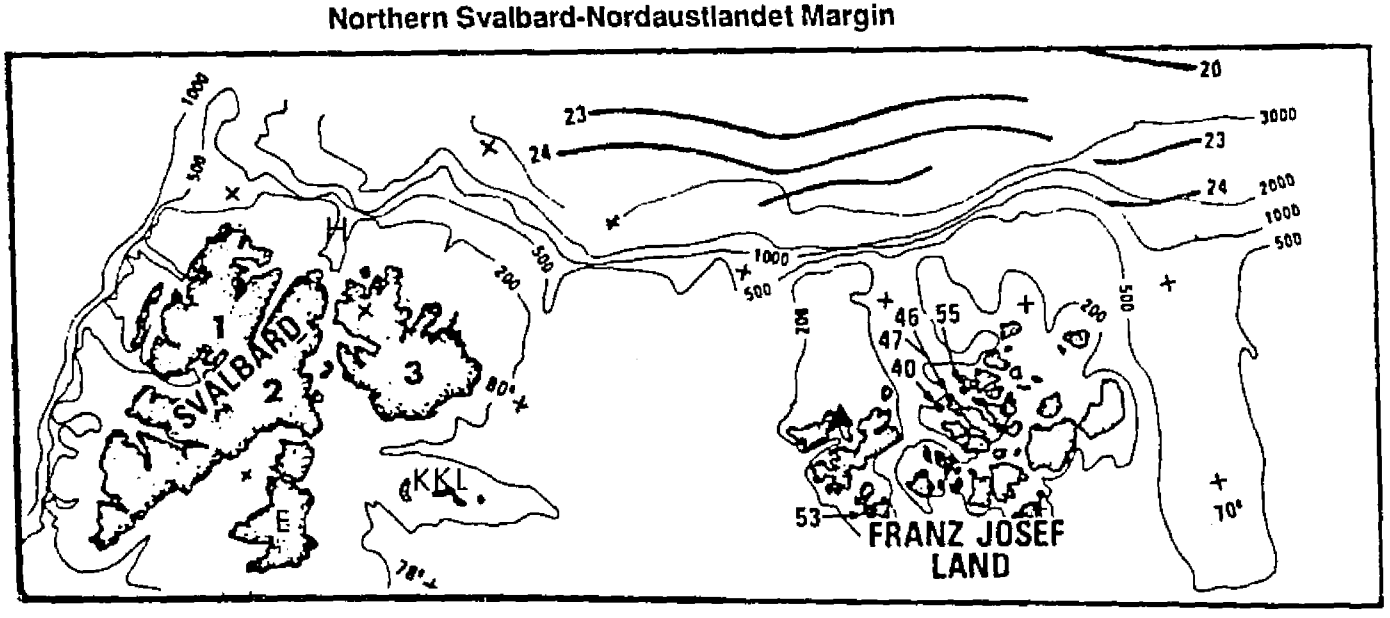

Figure 3-6. Locations of igneous units along the northern Svalbard-Nordaustlandet and eastern Arctic Ocean Margins. Bathymetry contours are in meters. Magnetic anomalies are from Vogt *et al.* (1979). Lower Cretaceous doleritic rocks (120 Ma) from the Franz Josef Land Archipelago (Campsie *et al.*, 1988). 1: Quaternary volcanic centers in Svalbard (11 Ma), 2: Tertiary plateau basalts in Svalbard (60 Ma), 3: Mesozoic rocks (dolerites, 145-105 Ma) from Nordaustlandet, Hinlopenstretet (H), Kong Karls Land (KKL) and Edgeøya (E).

4. HEAT FLOW

In the Norwegian-Greenland Sea, the average heat flow (113 mW/m^2, Langseth and Zielinski, 1974) is higher than in oceans of comparable age (Figure 3-7). However, a relationship exists between decreasing heat flow and increasing age of the oceanic crust or distance from the active spreading axis (Figure 3-8). Heat flow falls off at a decreasing rate from the mid-oceanic ridge towards the oldest oceanic crust at the margins, but this pattern is interrupted by the occurrence of high values on the margins. In general, the Norwegian-Greenland Sea can be subdivided into two main heat flow provinces: (1) active plate boundaries, by high average heat flow, and (2) passive margins characterized by above average and scattered values averaging about 100 mW/m^2. The rough basement topography and thin sediments in the rise axis area (approximately within 100 km of the spreading axis) plus volcanic and structural segmentation of the mid-ocean ridge probably cause spatial variability in the heat flow along and across the mid-ocean ridge (Langseth and Zielinski, 1974; Crane, 1985; Crane *et al.*, 1982, 1988, 1991). In chapter 5, heat flow data will be discussed in detail and thermally derived crustal ages are compared to magnetic ages along the eastern margins of the slow-spreading Norwegian-Greenland Sea.

Heat flow reaches 257 mW/m^2 over the Kolbeinsey Ridge and 75 mW/m^2 over the deactivated Aegir Ridge whereas heat flow on the Mohns Ridge reaches up to 143-268 mW/m^2. Although there are not many data points along the ridges, heat flow values do show a good relationship to age correlated with a well-developed

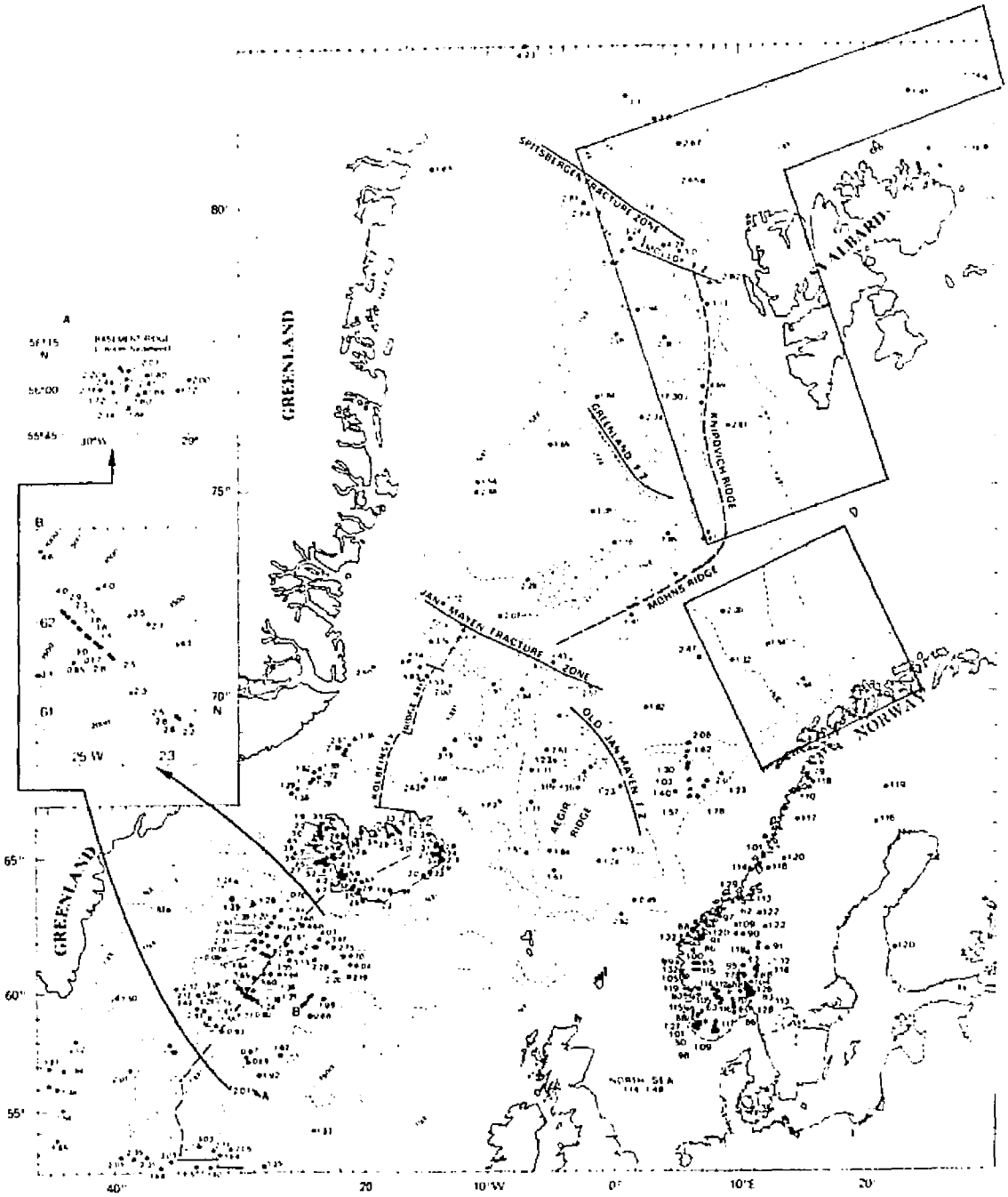

Figure 3-7. Heat flow in the Norwegian-Greenland Sea (1 HFU equals to 41.8 mW/m^2). Additional data near Svalbard are presented later in the text. Stations north of 79°N are from Crane *et al.* (1982) and Jackson *et al.* (1984). This figure is revised from Vogt *et al.* (1981) and Langseth and Zielinski (1974). Boxes indicate where new heat flow data exist. These additional data are discussed in detail in Chapter 5.

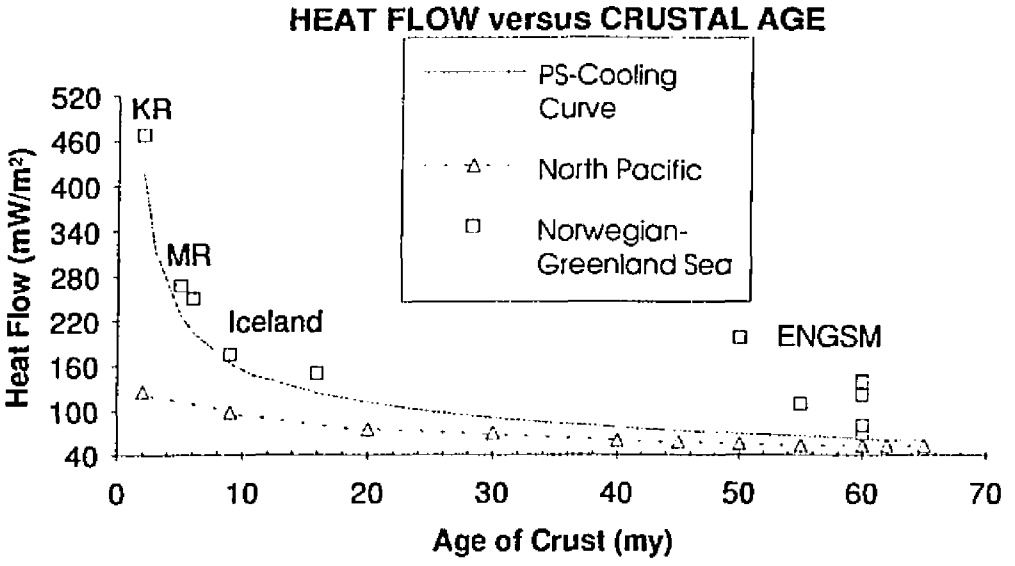

Figure 3-8. Heat flow in relation to crustal age. Summary plot of heat flow values as a function of crustal age where the age of oceanic crust in the Norwegian-Greenland Sea is known from magnetic chronology. Crustal ages are represented in terms of the DNAG Time Scale (Vogt, 1986). This figure is revised from Langseth and Zielinski (1974) and Vogt (1986). Iceland area and the Norwegian-Greenland Sea approximately fit the PS-cooling curve. However, heat flow increases towards the eastern margins (average 124 mW/m^2) of the Norwegian-Greenland Sea. MR: Mohns Ridge, KR: Knipovich Ridge, ENGSM: Eastern Norwegian-Greenland Sea Margin. The dashed line is an interpolation of the mean heat flow-versus-age data of Sclater and Francheteau (1970) for the North Pacific. North Pacific curve is below the PS-cooling curve because of hydrothermal heat lost (Lin and Parmentier, 1989).

magnetic anomaly pattern adjacent to the Mohns and Kolbeinsey Ridges (Langseth and Zielinski, 1974).

Heat flow measurements from the southern Knipovich Ridge is in excess of 461 mW/m^2 and reaches 371 mW/m^2 over the northern section (Crane *et al.*, 1982, 1988, 1991). At the intersection of the northern Knipovich Ridge with the Molloy Transform Fault along the Western Svalbard Margin, heat flow reaches 197 mW/m^2. In this location the plate boundary is often covered by sediment allowing one to gather heat flow data more efficiently at the actual center of spreading (Figure 3-9). At the Molloy Ridge, heat flow reaches 285 mW/m^2 and 229 mW/m^2 near the Lena Trough in the northern Norwegian-Greenland Sea. Exceptionally high heat flow values on the Nansen Ridge (>1164 mW/m^2) were reported by Sundvor and Torp (1987).

5. Seismic Activity

Earthquake seismicity data have been collected by using local networks and individual stations in the Svalbard Archipelago, and the Norwegian-Greenland Sea and eastern Arctic Ocean (Sykes, 1965, 1967; Huseybe *et al.*, 1975; Bungum *et al.*, 1982; Chan *et al.*, 1985; Mitchell *et al.*, 1990). Most epicenters are located in a narrow continuous belt at the center of the mid-ocean ridge axes where earthquake clustering is an expression of the stepwise orientation of the present-day plate boundary in the Norwegian-Greenland Sea (Figure 3-10; Myhre and Eldholm, 1988;

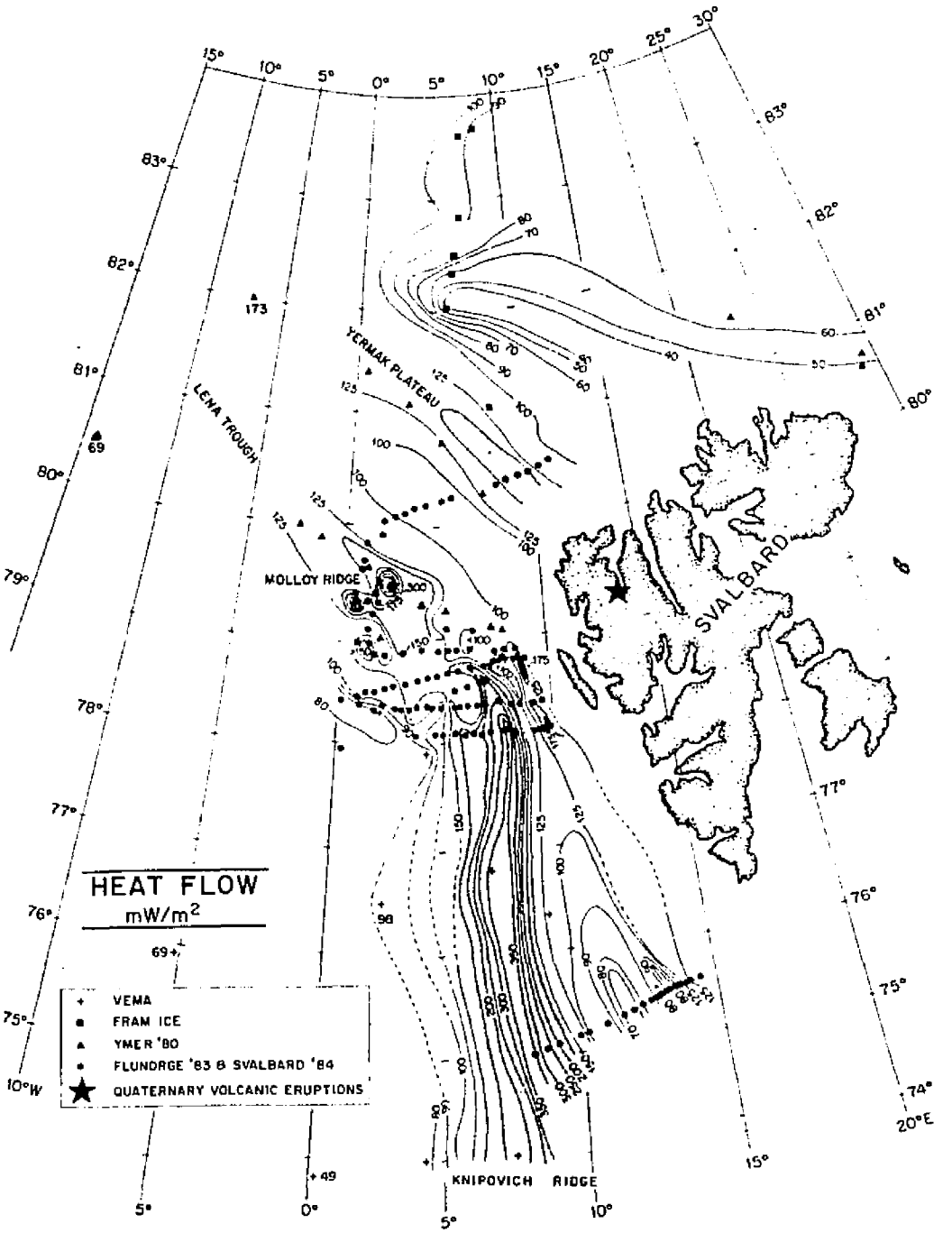

Figure 3-9. Heat flow in the northeastern Norwegian-Greenland Sea. Adjacent to Svalbard, the Knipovich Ridge (418 mW/m^2), the Molloy Ridge and the Yermak Plateau (>138 mW/m^2) are relatively high heat flow provinces (YMER-80; FLUNORGE-83; Sundvor, 1986; Crane *et al.*, 1988, 1991).

Figure 3-10. Distribution of earthquakes in the Norwegian-Greenland Sea. Locations of earthquakes (revised from Vogt, 1986) and large focal spheres indicate fault-plane solutions obtained from Savostin and Karasik (1981) and Mitchell *et al.* (1990). Bathymetric contours (at 400 m and every 1000 m) are from Perry *et al.* (1985). Earthquake epicenters concentrate along the plate boundaries. Seismicity appears concentrated along the shelf edge from south-central Norway and the western Barents Sea to the northern Svalbard and Nordaustlandet Margins.

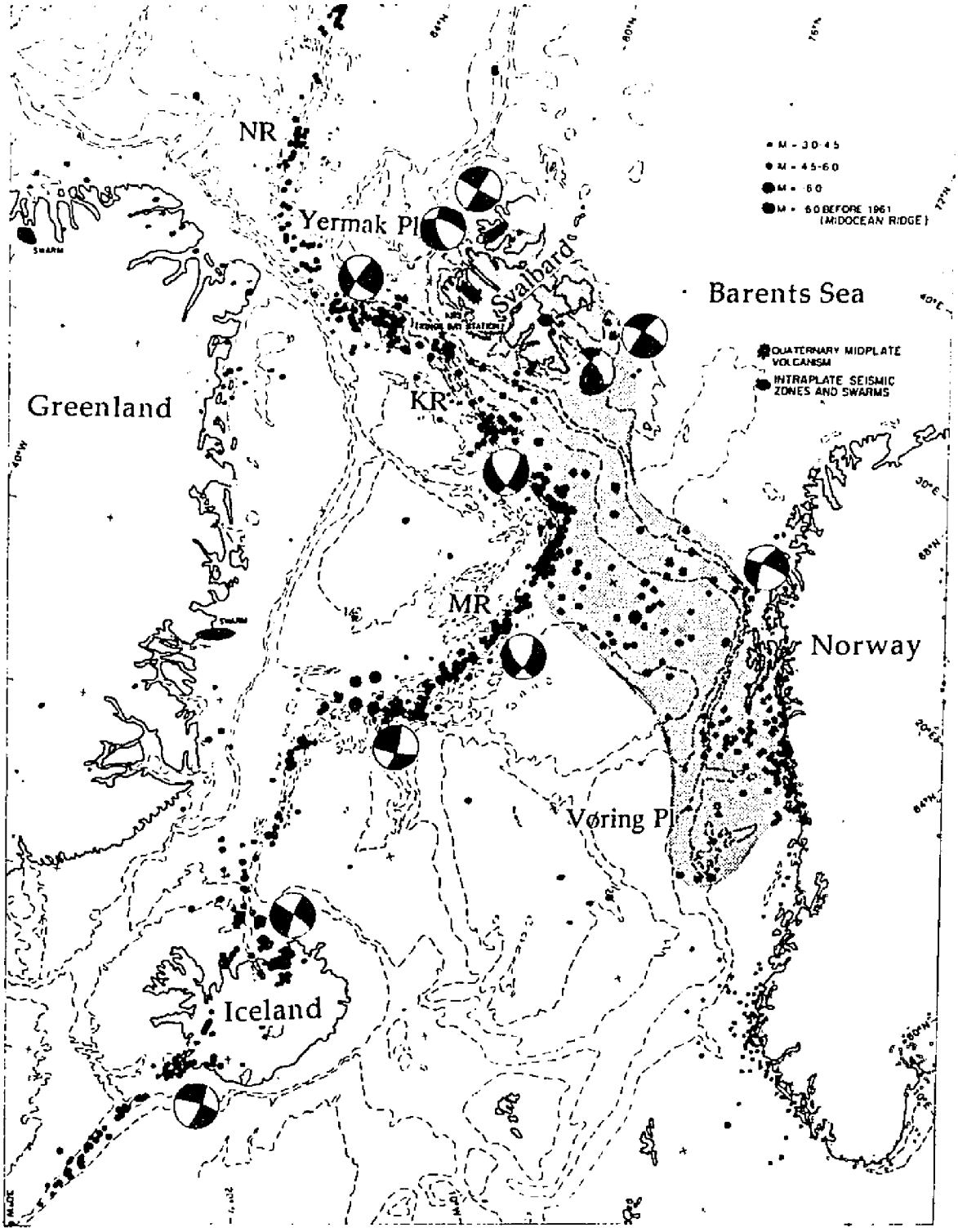
NR
Yermak Pl
Svalbard
Barents Sea
Greenland
KR
MR
Norway
Vøring Pl
Iceland
M - 30-45
M - 45-60
M - 60
M - 60 BEFORE 1961 (MIDOCEAN RIDGE)
QUATERNARY MIDPLATE VOLCANISM
INTRAPLATE SEISMIC ZONES AND SWARMS

Vogt, 1986). The changes from one seismic province to the next are abrupt. Fault plane solutions indicate that the motion along the Mohns, Knipovich, Molloy and Nansen Ridges is normal (Huseybe *et al.*, 1975; Savostin and Karasik, 1981), and along fracture zones (the Jan Mayen and Spitsbergen Fracture Zones) is strike-slip (Sykes, 1967; Savostin and Karasik, 1981). The Mohns Ridge is the most seismically active ridge segment in the Norwegian-Greenland Sea.

Boundaries occur at the Jan Mayen Fracture Zone and the area where the Mohns-Knipovich Ridge system bends. Left-lateral shearing appears in a roughly E-W direction along the Jan Mayen Fracture Zone (Burr and Solomon, 1978). Along the Knipovich Ridge the seismicity has an asymmetric pattern centered over the eastern flanks of the rift valley. Fault plane solutions on the Spitsbergen Shear Zone show right lateral strike-slip movement (Savostin and Karasik, 1981). North of about 77°N, the level of seismic activity decreases on the Knipovich Ridge (Mitchell *et al.*, 1990).

6. Magnetic Anomalies

Magnetic lineations in the Norwegian-Greenland Sea consist of irregularly spaced, low-amplitude anomalies (Figure 3-11). Along some areas of the plate boundaries, as well as volcanic margins, and marginal plateaus magnetic lineations are either not clear or are absent. Several studies (Vogt *et al.*, 1979a, 1979b; Åm, 1975; Phillips *et al.*, 1982; Kovacs and Vogt, 1982; Kovacs *et al.*, 1982) interpreted

Figure 3-11. Magnetic anomalies in the Norwegian-Greenland Sea (from Vogt *et al.*, 1981). Principal anomaly identifications, simplified sediment isopachs (Eldholm and Windisch, 1974) and tectonic features are superimposed. MR: Morris Jesup Rise, YP: Yermak Plateau.

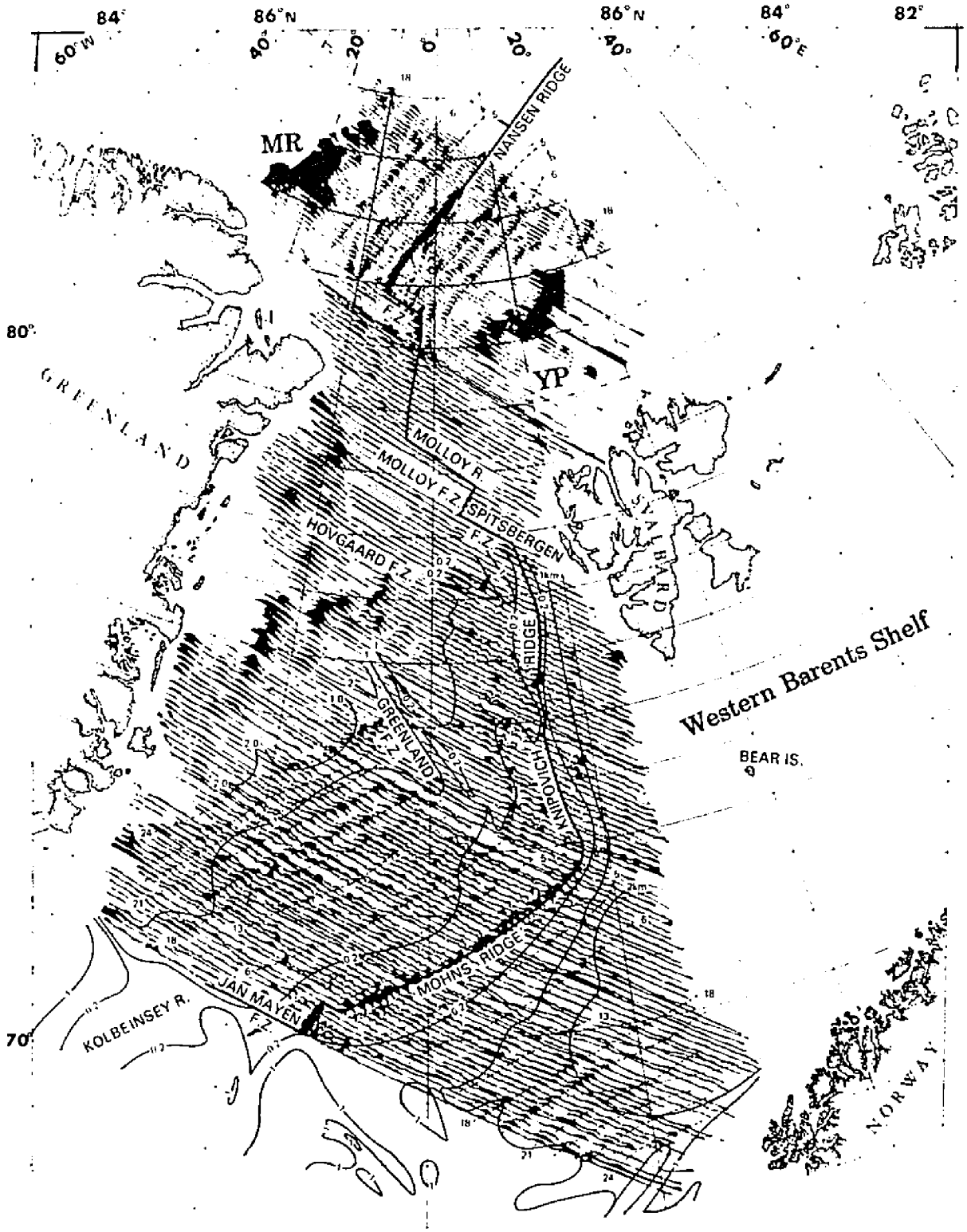
84°
86°N
86°N
84°
82°
60°W
40°
20°
0°
20°
40°
60°E
80°
70°
MR
YP
NANSEN RIDGE
F.Z.
GREENLAND
MOLLOY R.
MOLLOY F.Z.
SPITSBERGEN
F.Z.
HOVGAARD F.Z.
KNIPOVICH RIDGE
GREENLAND F.Z.
Western Barents Shelf
BEAR IS.
MOHNS RIDGE
JAN MAYEN F.Z.
KOLBEINSEY R.
NORWAY

those areas (for example, the northern Vøring Plateau, Senja Margin, northern Knipovich Ridge and southern Yermak Plateau) as "magnetic smooth zones" (Figure 3-12).

Thermal blanketing effect by sediments in the rift valley, slow and oblique spreading, fragmentation due to the shift of the ridge axis, and short lived fracture zones (fossil ridges), are several factors that can modify the nature of magnetic anomalies and make them difficult to interpret. A rapid decrease in depth to the magnetic basement could influence the character of the seafloor spreading-type magnetic anomalies. In general, the depth to magnetic basement is thought to be less than 1 km for the entire Norwegian-Greenland Sea region (Zielinski, 1979; Kovacs and Vogt, 1982). Eldholm *et al.* (1979) suggests that an exceptionally high rate of basalt accumulations (a wider than normal zone of injection) formed either during the initial phase of seafloor spreading or during an abrupt change in the magnetic susceptibility adjacent to the magnetic smooth zone.

The plate boundary around the Spitsbergen Shear Zone is not well-defined because most magnetic anomalies are absent, and the central anomalies are ambiguous. Along the rift valley of the Knipovich Ridge no clear seafloor spreading-type magnetic anomalies are observed (Vogt *et al.*, 1981). They either do not exist (magnetic smooth zones) or have very small amplitudes (Eldholm *et al.*, 1987). However, relatively "punctiform-shaped" high-amplitude magnetic signatures are observed along the Knipovich Ridge presumably associated with major localized volcanic events. Géli *et al.* (1994) observed three high anomaly amplitudes, in excess

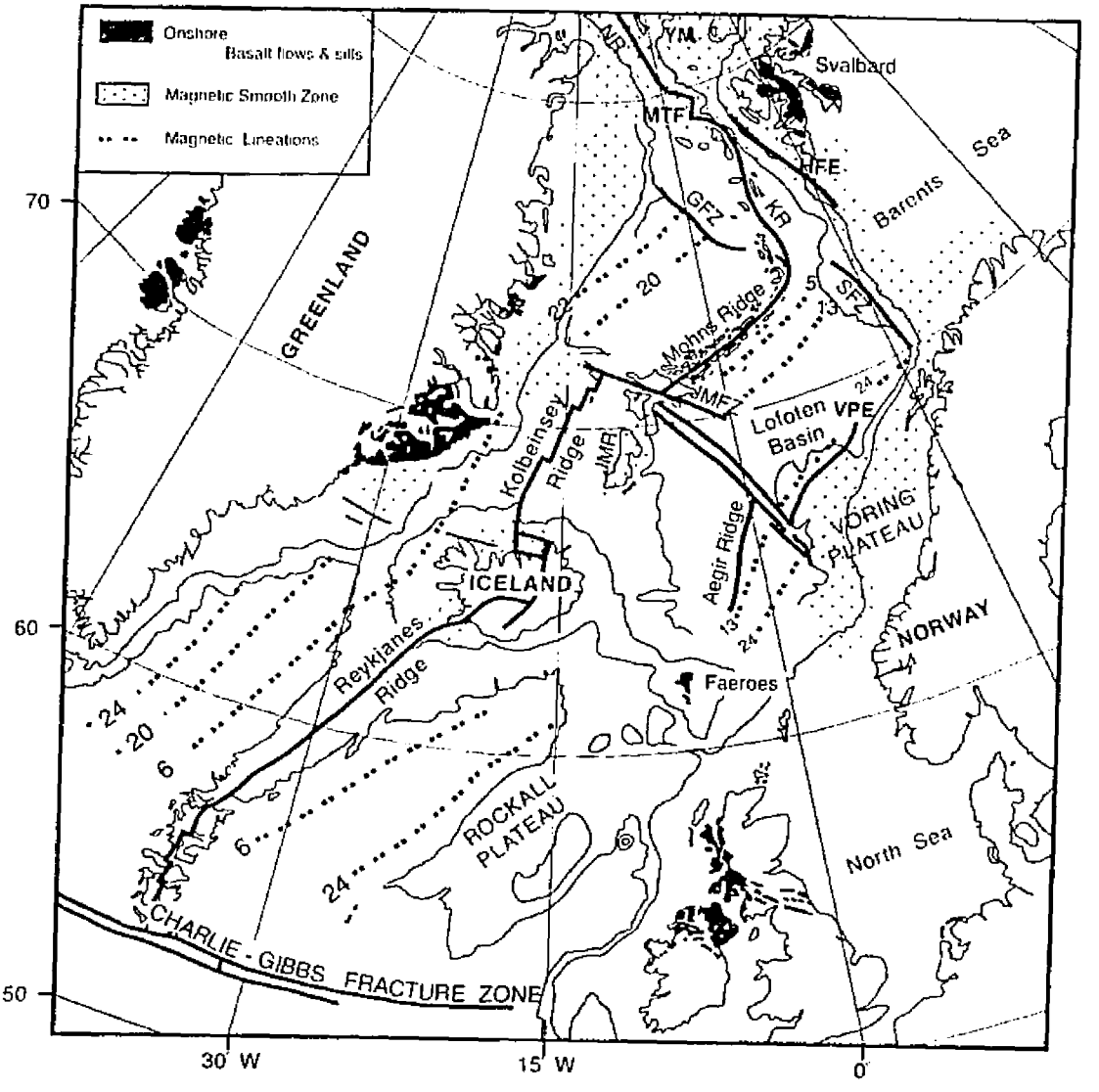

Figure 3-12. Magnetic lineations and smooth zones in the Norwegian-Greenland Sea (from Vogt *et al.*, 1981). FSE: Faeroe-Shetland Escarpment, VPE: Vøring Plateau Escarpment, and GE: Greenland Fracture Escarpment, YP: Yermak Plateau.

of 1200 nT, and interpreted them as lava injection centers. A bathymetric high just to the east of the Hovgård Fracture Zone/Ridge is characterized by a high-amplitude magnetic signature suggesting that the feature is an off-axial volcanic feature.

7. GRAVITY

In general, at a slow-spreading mid-ocean ridge, the free-air gravity anomaly signal is mostly dominated by the variations in the seafloor relief. In addition, over the rift valley inner floor, gravity lows are centered on the bathymetric lows. Figure 3-13 shows the distribution of free-air gravity anomalies in the Norwegian-Greenland Sea. Observations have shown that the Mohns Ridge has a well-defined free-air gravity anomaly pattern characterized along the rift valley by a belt of minimum values. Paralleling the rift valley on both sides, two approximately 80-100 km wide belts of maximum gravity lie in excess of 50 mGal (Talwani and Eldholm, 1977; Grønlie and Talwani, 1982). Outside the rift valley, very high anomaly values are found, up to 110 mGal on the northwestern shoulder, and up to 80 mGal on the southeastern shoulder. Within the ridge axis an en-échelon pattern is present, and the rift valley is defined by the 30 mGal contours (Grønlie and Talwani, 1978, 1982).

The Knipovich Ridge is associated with low gravity anomalies (20 mGal). Grønlie and Talwani (1982) suggest that these low anomalies along the rift valley might be caused by partially melted low density basalts derived from the upper mantle. By contrast, the gravity anomaly on the Hovgård Fracture Zone is broken

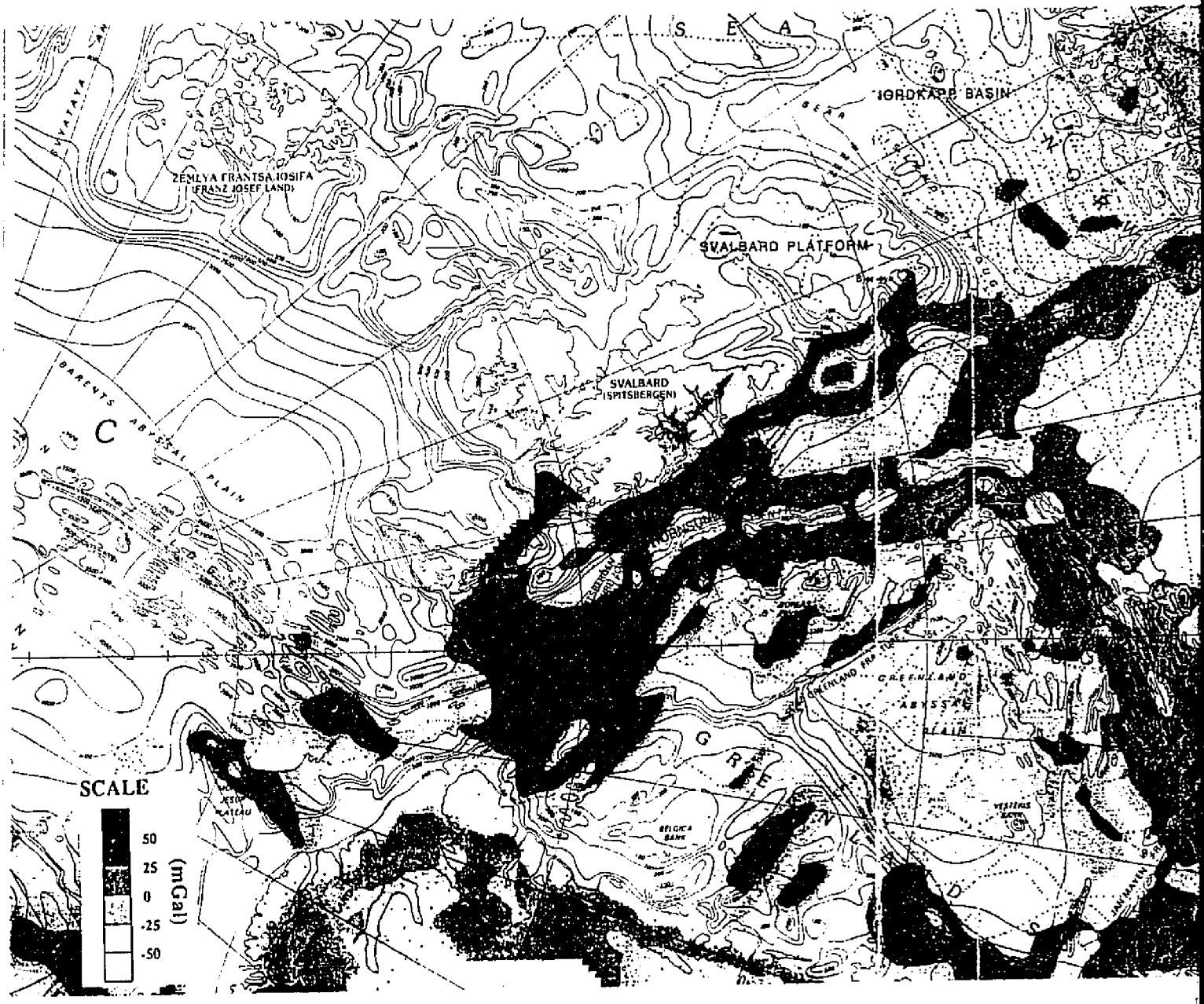

Figure 3-13. Free-air gravity of the Norwegian-Greenland Sea and eastern Arctic Ocean regions (Faleide *et al.*, 1984). Red indicates >100 mGal.

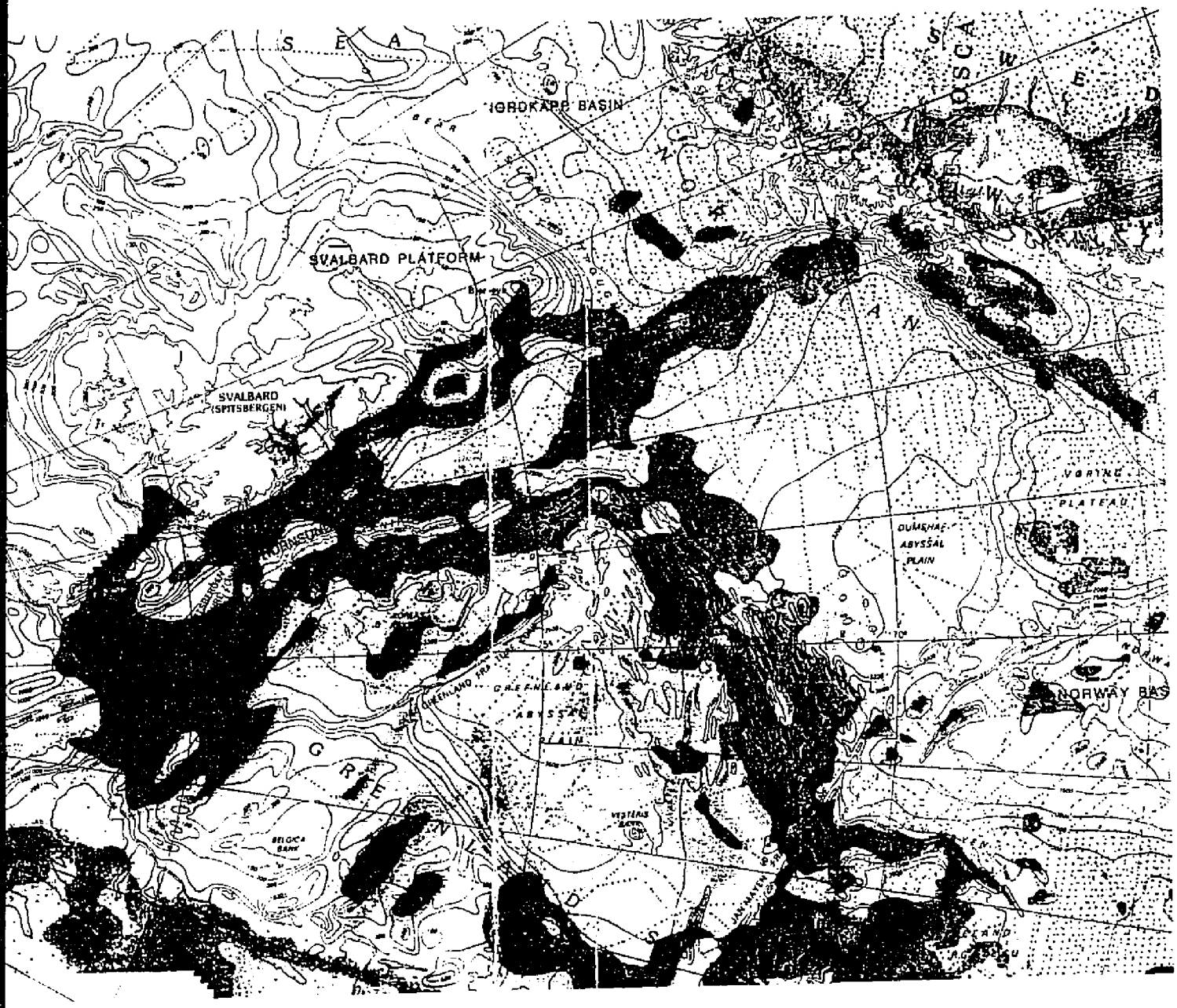

wegian-Greenland Sea and eastern Arctic
ed indicates >100 mGal.

into two isolated peaks of 173 and 131 mGal indicating high density crust beneath it (Myhre and Eldholm, 1988).

B. CHARACTERISTICS OF THE EASTERN MARGINS

1. MORPHO-TECTONIC TRANSECTS OF THE EASTERN MARGINS

The continental shelves and margins bordering the Norwegian-Greenland Sea are deep and morphologically irregular. Glacial valleys stretch from the land, through fjords, onto the continental shelves as evidence of the ice load since the last ice age (Vogt *et al.*, 1981, 1993). The eastern margins of the Norwegian-Greenland Sea can be divided into three morpho-tectonically distinct regions: The Norwegian Margin, the Senja-Western Svalbard Margin, and the northern Svalbard-Nordaustlandet Margin.

a. Norwegian Margin:

The Norwegian Margin is dominated by the Eastern Jan Mayen Fracture Zone System and the Vøring Plateau (Figure 3-14). The Jan Mayen Fracture Zone System (the Western, Eastern and Central Jan Mayen Fracture Zones, and the Norway Basin Fracture Zone) transects the entire southern Norwegian-Greenland Seafloor

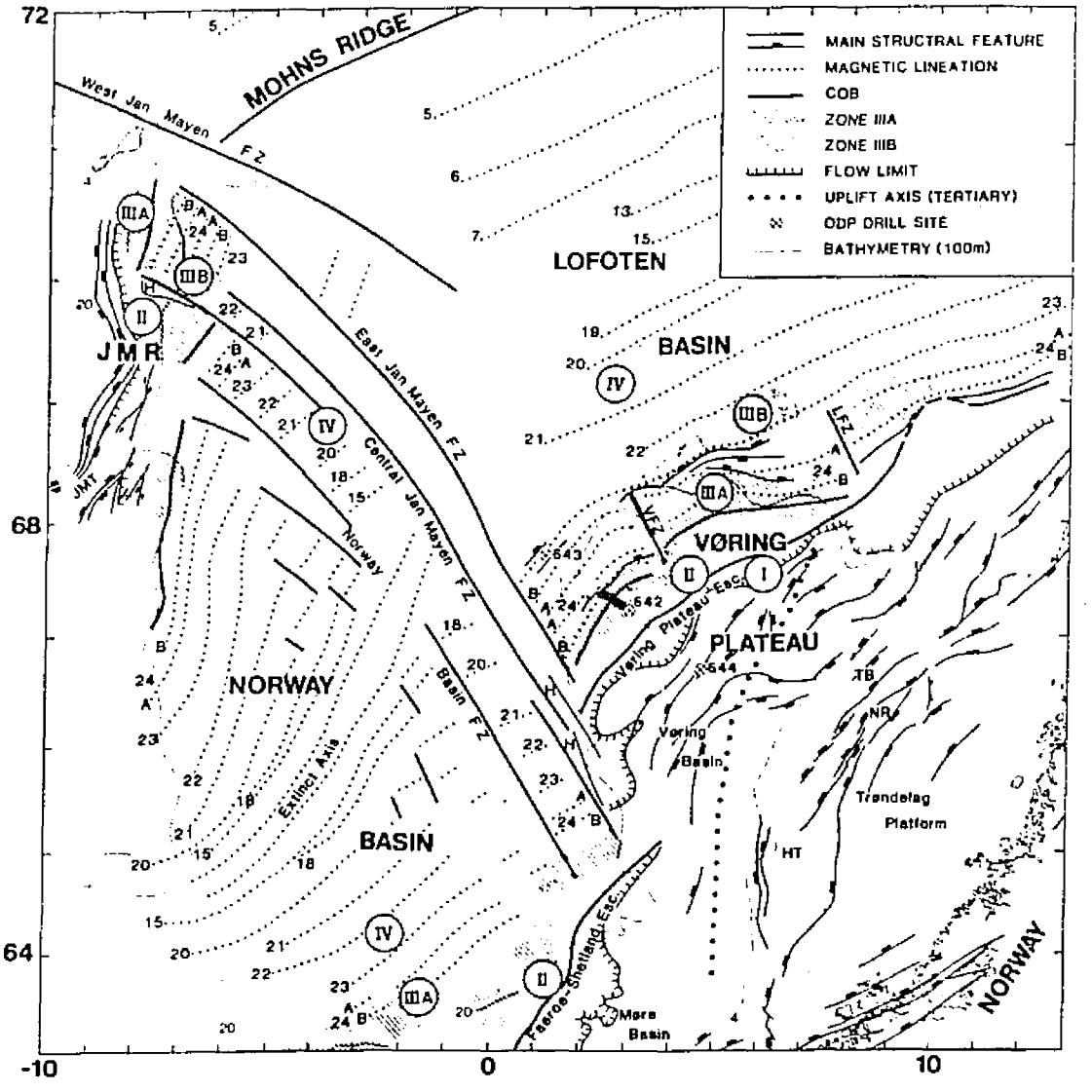

Figure 3-14. Main structural features along the Norwegian Margin: Eastern Jan Mayen Fracture Zone and Vøring Plateau. Part of the Vøring Plateau seaward of the Vøring Plateau Escarpment is the Vøring Outer Ridge. Province-I is underlain by deeply buried Paleocene lava flows and pre-Tertiary sediments and old thinned continental crust. Province-II covers the crest of the Vøring Outer Ridge and has a smooth basement reflector. Province-III is underlain by seaward-dipping basement reflectors. Province-IV is normal oceanic basement with rough seafloor bathymetry (Eldholm, 1991). JMI: Jan Mayen Island.

(Torske and Prestvik, 1991). At its western terminus, numerous seamounts comprise the volcanically-active Jan Mayen Island, which rises to an elevation of 2277 m above sea level (Sylvester, 1975). In contrast, nodal deeps (depressions at ridge-transform intersections) occur at the intersection of the southern terminus of the Mohns Ridge with the West Jan Mayen Fracture Zone (Vogt, 1986).

The eastern continuation of the Jan Mayen Fracture Zone System forms a tectonic boundary between Norway (65.5°N, 6°E) and the Lofoten Basins along the Norwegian Margin. The extinct spreading axis of the Aegir Ridge (65°N, 5°W, a broad 25 km long valley with depths of 4000-4500 m) lies in the southern Norway Basin. The Vøring Plateau, bounded by this extinct ridge and the Eastern Jan Mayen Fracture Zone reaches an average depth of 1450 m adjacent to the Norwegian Margin (Mutter *et al.*, 1984; Eldholm *et al.*, 1989). A continent-oceanic crustal transition defines the Vøring Plateau Escarpment and separates the Vøring Basin from the Lofoten Basin (Talwani and Eldholm, 1972; Eldholm *et al.*, 1989; Skogseid and Eldholm, 1989). The escarpment continues to about 69.3°N defining a region between the Vøring Plateau and the Lofoten Fracture Zone (Torske and Prestvik, 1991).

Large-scale marginal faulting along the coastline of Lofoten and Vesterålen Islands (landward of the Lofoten Fracture Zone) has been suggested by many authors and the over deepened marginal channels are thought by some to reflect actual fault lines (Hotendahl, 1960). However, Talwani and Eldholm (1972) concluded that these marginal channels were probably caused by glacial erosion.

b. Senja Margin:

The Senja Margin, oriented obliquely to the Mohns Ridge, is located between 71°N and Bjørnøya (Bear Island) north of 74°N, and is bounded by the Senja Fracture Zone (south of 73°N, Figure 3-15). To the east of the Senja margin, the continental slope of the southwest Barents Sea contains a submarine fan situated in front of the Bear Island Trough which has accumulated more than 7 km of sediment locally since continental breakup about 55 Ma (Faleide *et al.*, 1984). The Bear Island submarine fan is a depocenter and has a width of 220 km at its proximal part and 400 km at a depth of 2000 m (Vorren *et al.*, 1989; Vogt *et al.*, 1993); it extends over 280 km beyond the shelf break, and is characterized by numerous thin mudflows up to 200 km-long which reach the Mohns Ridge valley (from the SeaMARC-II data, Vogt *et al.*, 1993). On the southern Senja Margin, a large deep-seated salt massif was mapped at a depth of more than 10 km (Myhre *et al.*, 1982).

c. Western Svalbard Margin:

The Western Svalbard Margin extends from Bjørnøya to 80°N adjacent to the Hornsund Fault Zone (Figure 3-15). In this region, the continental shelf is approximately 75 km wide and it narrows to approximately 10 km, near the northwestern tip of Svalbard. The shelf morphology reflects features caused by glacial activity during the last few million years along Svalbard (Vogt *et al.*., 1993). The continent-ocean transition along the Western Svalbard Margin, between 75.5°N

Figure 3-15. Bathymetry and main structural features on the Senja and Western Svalbard Margins, contours every 1000 meters. SF: Senja Fracture Zone, GFZ: Greenland Fracture Zone, WBS: Western Barents Shelf, HF: Hornsund Fault Zone, KR: Knipovich Ridge, HR: Hovgård Ridge, MTF: Molloy Transform Fault, MR: Molloy Ridge, YP: Yermak Plateau. Bathymetry of the northern Svalbard-Nordaustlandet Margin adapted from Cherkis *et al.* (1994).

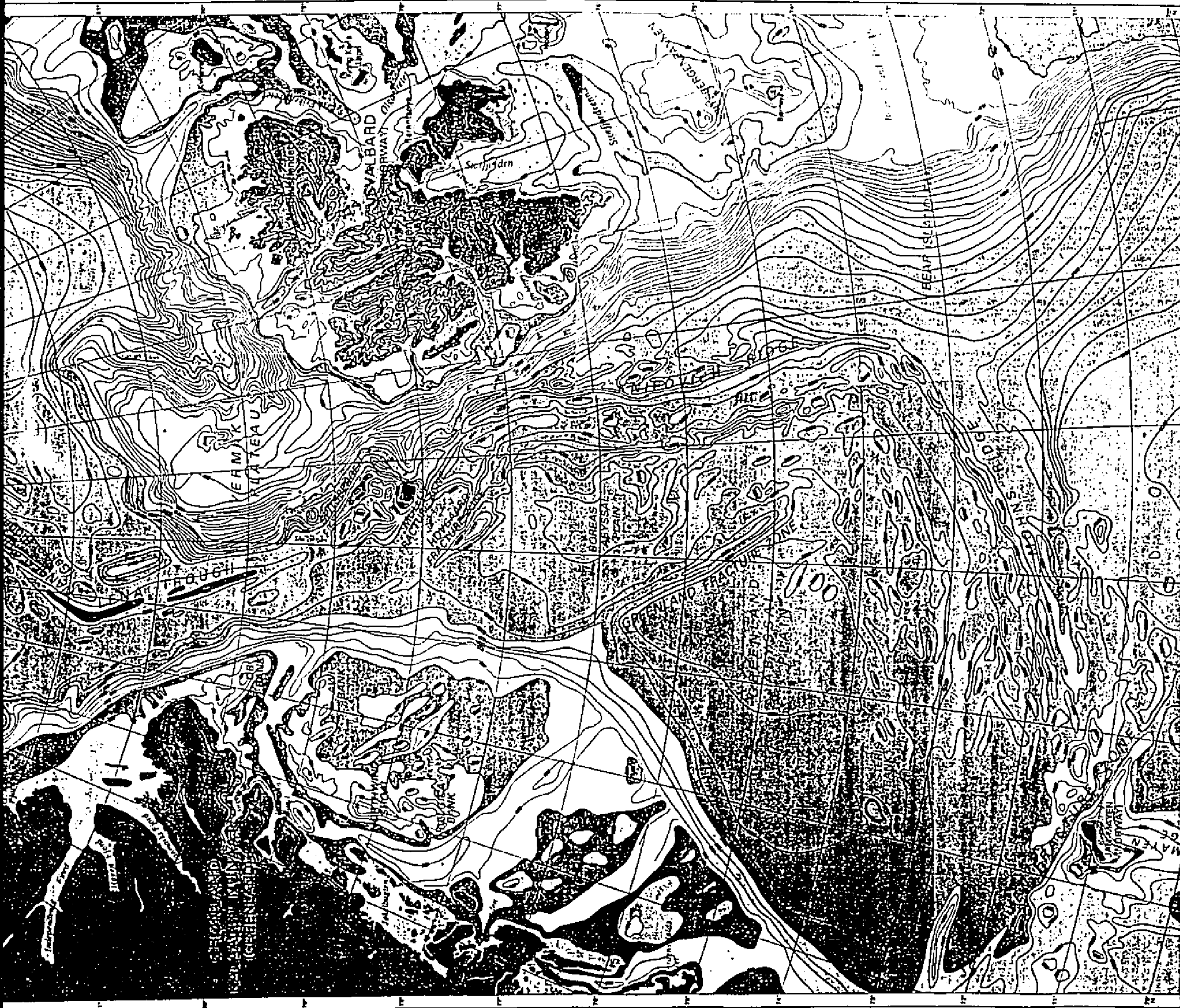
SVALBARD
Storfjorden
BOREAS
GREENLAND FRACTURE ZONE

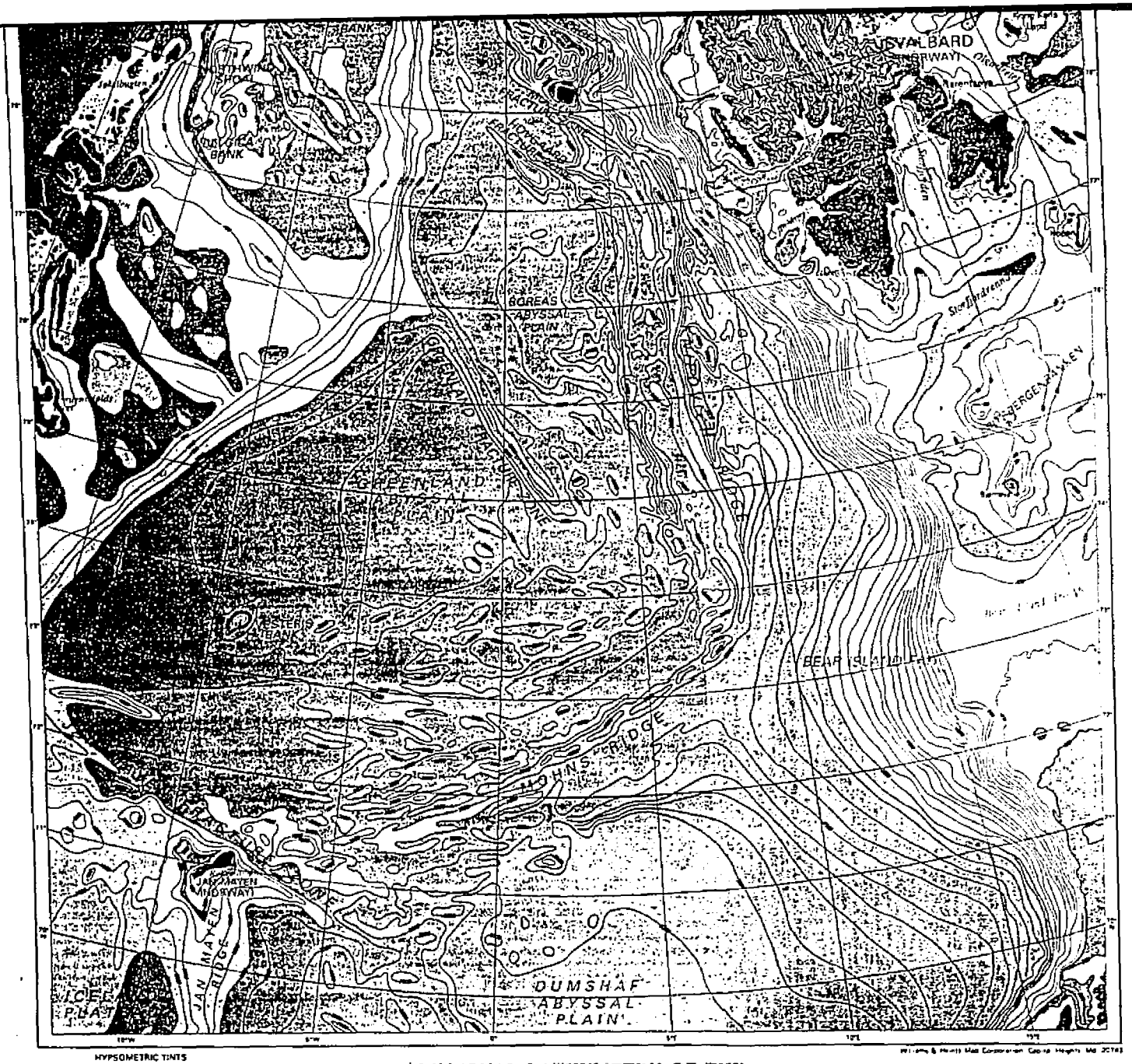

HYPSOMETRIC TINTS

Meters
Land Mass
Sea Level 0
100
200
500
1000
1000
2000
3000
4000
6000

REGIONAL BATHYMETRY OF THE NORTHERN NORWEGIAN – GREENLAND SEA

NAVAL RESEARCH LABORATORY

1994

Compiled by

N. Z. Cherkis and P. R. Vogt
Naval Research Laboratory
Washington, D.C. 20375
U.S.A.

Polar Stereographic Projection

Scale 1:3,000,000
at Latitude 71°N

and 76.5°N, is defined by the Hornsund Fault, with almost a 5-10 km continuous throw (Sundvor and Austegård, 1990). The Hornsund Fault parallels the active Knipovich Ridge, and extends to the southwestern edge of the Yermak Plateau (80°N, Sundvor *et al.*, 1977, 1982a, 1982b; Okay and Crane, 1993).

d. Northern Svalbard-Nordaustlandet Margin:

Three distinct features dominate the northern Svalbard-Nordaustlandet Margin (Figure 3-15): the southern part of the Yermak Plateau, the Hinlopen Strait (Hinlopenstretet, between Spitsbergen and Nordaustlandet Islands) and the Nordaustlandet Margin.

The Yermak Plateau, covered by a thick layer of sediments, extends for 235 km from 80°N to 83°N and its arcuate shape averages 125 km in width (Sundvor *et al.*, 1977, 1978, 1982a). The Yermak Plateau is flat-topped and trends in a northeast-southwest direction, narrowing to the northeast (Sundvor *et al.*, 1982a, 1982b). To the west is a narrow shelf (1 km-wide) bordered by a 300 m high escarpment with a 1:10 gradient (Sundvor and Austegård, 1990). The southwestern flank of the plateau drops to a depth of more than 4000 m merging with the Molloy Deep (Sundvor *et al.*, 1982a). The southern plateau lies at the northeastern edge of the active Eurasian Plate boundary, along the Knipovich Ridge and Molloy Transform Fault.

The northern slope of the Yermak Plateau is bordered by the flank of the Nansen Ridge which extends across the Eurasia Basin where it runs into the Siberian Margin near the outflow of the Lena River into the eastern Arctic Ocean. On the

opposite side of the Fram Strait from the northern Yermak Plateau lies the Morris Jesup Rise (500 to 1000 m deep) adjacent to the northeastern Greenland Margin (Feden *et al.*, 1979; Vogt *et al.*, 1981).

The central and southern Yermak Plateau is topographically irregular and is broken by numerous normal faults (Sundvor *et al.*, 1982b; Okay and Crane, 1993) that are thought to extend into the northern margin of Svalbard where Cenozoic volcanic centers lie aligned along Woodfjørden (Prestvik, 1978; Amundsen *et al.*, 1987; Skjelvåle *et al.*, 1989). A large submarine canyon (the Sofia Canyon, Sundvor *et al.*, 1982a) incises deeply into the eastern flank of the southern Yermak Plateau. It serves as a major conduit for sediment transport for the northern Svalbard Margin.

Further to the east, the Hinlopenstretet divides the island of Spitsbergen from Nordaustlandet. Deep canyons cut the margin north of Hinlopenstretet, west of Kongsfjørden (80°15' N) and off Islefjørden (Ohta, 1972; Pfirman, 1989). The canyon near the Hinlopenstretet forms a channel-like feature crossing the entire margin. This U-shaped depression is about 11-12 km-wide, 400 m-deep and is thought to have been formed by glacial activity (Kristoffersen *et al.*, 1982; Pfirman, 1989).

2. Seismic-Reflection and -Refraction Data

The continental margins of the Norwegian-Greenland Sea and Eastern Arctic Ocean have been studied mostly by multichannel seismic surveys to understand the

lithospheric extension processes (Talwani and Eldholm, 1972; Sundvor *et al.*, 1977, 1978, 1979; Mutter *et al.*, 1982; Kristofferson *et al.*, 1982; Roberts and Ginzburg, 1984; Eldholm *et al.*., 1986; Hinz *et al.*, 1987; Mutter *et al.*, 1988; Larsen and Jakobsdóttir, 1988; Eldholm *et al.*, 1989; Eldholm and Grue, 1994). A large number of multichannel seismic reflection and refraction surveys have been carried out at the Vøring Margin (Eldholm *et al.*, 1979; Mutter *et al.*, 1982, 1984; Hinz *et al.*, 1987; Skogseid and Eldholm, 1989), the Western Svalbard-Barents Margin (Schlüter and Hinz, 1978; Sundvor *et al.*, 1979; Myhre *et al.*, 1982; Eldholm *et al.*, 1987; Myhre and Eldholm, 1988), northern Svalbard and the southern Yermak Plateau (Sundvor *et al.*, 1977, 1978, 1979, 1982a, 1982b; Sundvor and Austegård, 1990; Faleide *et al.*, 1991) and in the Eurasia Basin (Kristoffersen *et al.*, 1982; Jackson *et al.*, 1984). Most of these studies have imaged the sedimentary column and provided only modest constraints on basement structure.

Hinz and Weber (1976), Hinz (1981) and Mutter *et al.* (1988) first noticed the extensive suites of seaward dipping reflectors on the Vøring Plateau from multichannel seismic reflection profiles. These results indicated seaward diverging wedges beneath the smooth acoustic basement of the Outer Vøring Plateau (on the Norwegian Margin, Eldholm *et al.*, 1987) and Faeroe-Shetland Escarpment (on the Møre Margin, Roberts *et al.*, 1984). Based on sonobuoy refraction and a few two-ship refraction measurements, Mutter *et al.* (1982) showed that the crust beneath the seaward dipping units of the Vøring Plateau was at least twice the thickness of normal oceanic crust. Dipping reflectors located immediately seaward of the Faeroe-Shetland

Escarpment are not associated with seafloor spreading magnetic anomaly lineaments (Talwani and Eldholm, 1977).

The Vøring Plateau Escarpment has been mapped to 68.4°N from seismic data (Mutter *et al.*, 1982, 1984; Skogseid and Eldholm, 1987). The escarpment was considered by Talwani and Eldholm (1972, 1977) to be an early Tertiary structure, marking a distinct boundary between continental and oceanic crust. They showed that the acoustic basement of the Outer Vøring Plateau formed a basement high with a smooth and highly reflective summit, quite unlike the rough acoustic signature usually associated with oceanic basement. They also recognized that the oldest marine magnetic isochron-24 occurring in the deep, adjacent Lofoten Basin continued into the region of smooth acoustic basement of the Outer Vøring Plateau. Leg 38 of the Deep Sea Drilling Program drilled into acoustic basement of the Vøring Plateau and confirmed Talwani and Eldholm's (1977) prediction that the basement was comprised of basalts (Talwani *et al.*, 1976), supporting the interpretation that the outer plateau was constructed of oceanic crust.

Seaward-dipping reflectors define a zone which consists of an inner part where the dipping wedge commonly rests on a base reflector, and an outer part where there is no apparent base to the wedge (Figure 3-16). Eldholm and Grue (1994) have named it the Zone-III. The continental-oceanic crustal transition (the Zone-III and IV boundaries) is placed at the seaward termination of the base reflector (Skogseid and Eldholm, 1987). The base reflector continues into Zone-II which lies between the apex of the wedge and an escarpment, or a distinct flow front. Zone-I represents

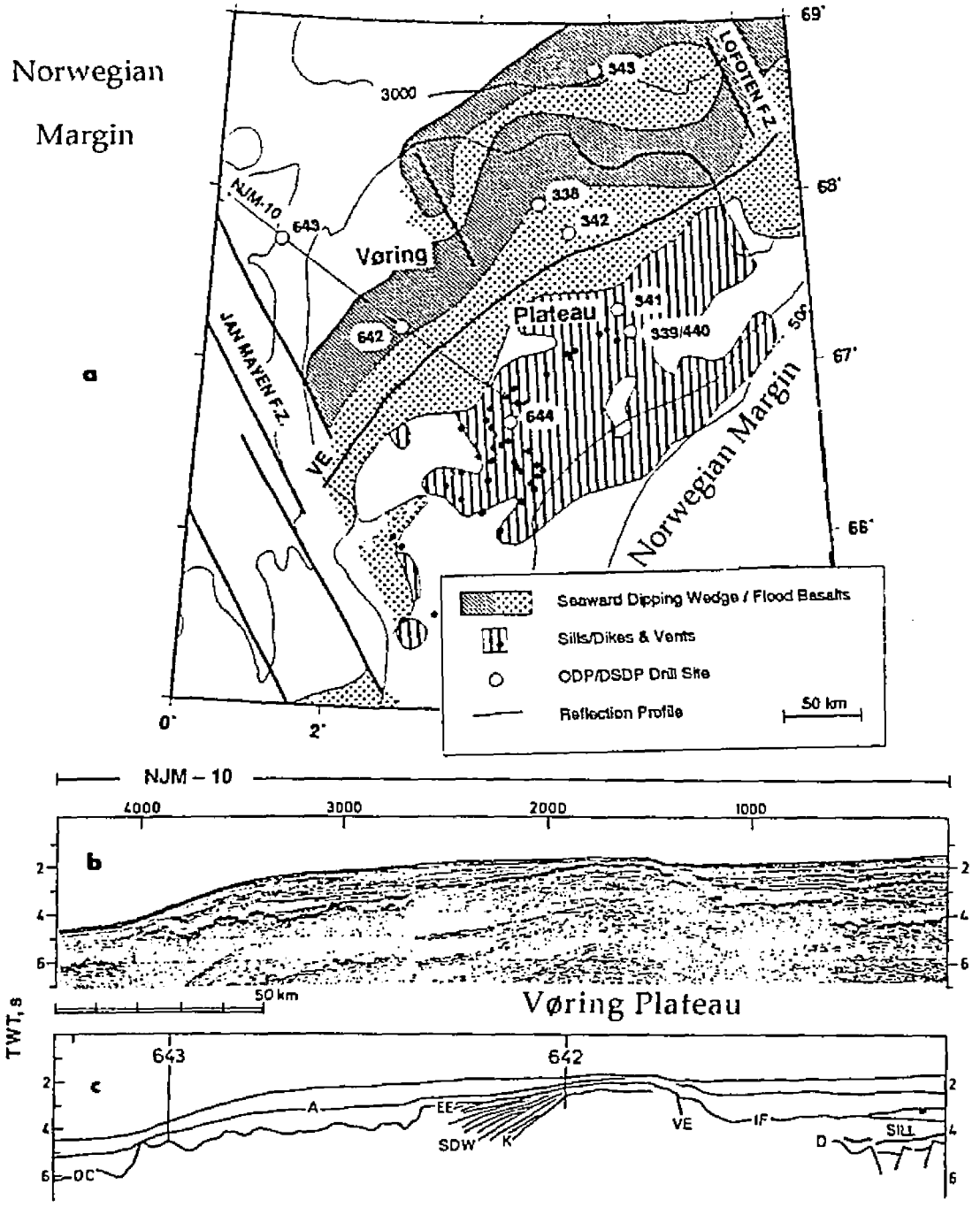

Figure 3-16. A Geoseismic section from the Norwegian Margin. (a) Main structures on the Norwegian Margin (bathymetry in meters, after Planke, 1993).
(b) Seismic record showing the typical character of the acoustic basement and seaward-dipping reflectors (after Eldholm *et al.*, 1984). (c) Line drawings of multichannel seismic reflector profile across the Vøring Plateau. Seaward-dipping reflector sequences (SDW, K), Early Eocene (EE) units, A: post-Eocene, D: top-Jurassic, IF: Landward boundary of lava flow, OC: oceanic crust, VE: Vøring Plateau Escarpment.

lavas landward of the escarpments.

Eldholm *et al.* (1984) have placed the continent-oceanic crustal transition near the seaward termination of reflector-K (Figure 3-16). Mutter *et al.* (1984) believe that this reflector may mark the dike/lava transition. The acoustic basement is overlain by a 1-km thick low-seismic velocity zone of uncertain origin (possibly sedimentary sequences), and broken by several normal faults. The Escarpment is also associated with a zone of smooth opaque basement (5.3-6.3 km/s; Mutter *et al.*, 1984) that separates the Inner Vøring Plateau from the Outer Vøring Plateau (an area with the oldest spreading lineations and thin sediments). North of the Vøring Plateau a similar escarpment in the Lofoten Basin has been noticed with a shallow acoustic basement (Eldholm *et al.*, 1979). Below the sediments of the Lofoten Basin lies a typical oceanic crust increasing in thickness from 5 to 8 km under the escarpment.

The marginal highs contain thick seaward dipping wedges (Mutter *et al.*, 1984; Skogseid and Eldholm, 1989; Eldholm and Grue, 1994). Velocities in the dipping wedges increase with depth, reaching ~6.5 km/s in the deepest part (4-6 km below the top). Local shallow low-velocity layers related to the basalt-dacitic flow transition, have been reported in the Zone-II (Mutter *et al.*, 1984; Mutter and Zehnder, 1988; Mjelde *et al.*, 1992). In the absence of a marginal high on the Lofoten margin, Eldholm and Grue (1994) infer the Zone-I and II boundary from lateral change in the velocity (Mjelde *et al.*, 1992).

The entire Western Svalbard-Barents Margin is characterized by a thick Cenozoic low-velocity sedimentary wedge with velocities of 2.9-4.8 km/s

superimposed upon oceanic crust with an average seismic velocity of 7.1 km/s (Myhre *et al.*, 1982, 1992). The continent-oceanic crustal transition on the Senja and Western Svalbard Margins (Figure 3-17, between 70°N and 77°N) was established based on the structural boundaries seen in the multichannel seismic data (Myhre, 1984; Myhre and Eldholm, 1988; Faleide *et al.*, 1991). The main feature is a north-northwest trending fault system on the continental shelf between 74° and 79°N. The existence of a major fault, representing a significant geological boundary, beneath the shelf was first recognized by Sundvor and Eldholm (1979) who named it the Hornsund Fault Zone. Myhre (1984) mapped the continent-oceanic crustal transition close to the Hornsund Fault Zone. Along the Hornsund Fault Zone the seaward dipping reflectors (4.5 and 5.5 km/s, Myhre and Eldholm, 1988) mark the transition. Myhre and Eldholm (1988) confirmed that this fault zone forms a complex region of continent-ocean transition along the Western Svalbard Margin. Between 75° and 77°N, the fault zone is dominated by a system of downfaulted blocks with small individual throws (Sundvor and Austegård, 1990). To the north this fault zone is characterized by a major fault scarp with a throw of almost 6 km (Sundvor and Austegård, 1990).

The southern part of the Yermak Plateau has been covered by a series of multichannel seismic reflection surveys and sonobuoy reflection experiments (Sundvor *et al.*, 1977, 1978, 1979, 1982a; Austegård, 1982). From near the coast of northern Spitsbergen (81.43°N) an opaque reflector, called 0, has been mapped as acoustic basement (Figure 3-18). It is block-faulted and buried with sediments. The

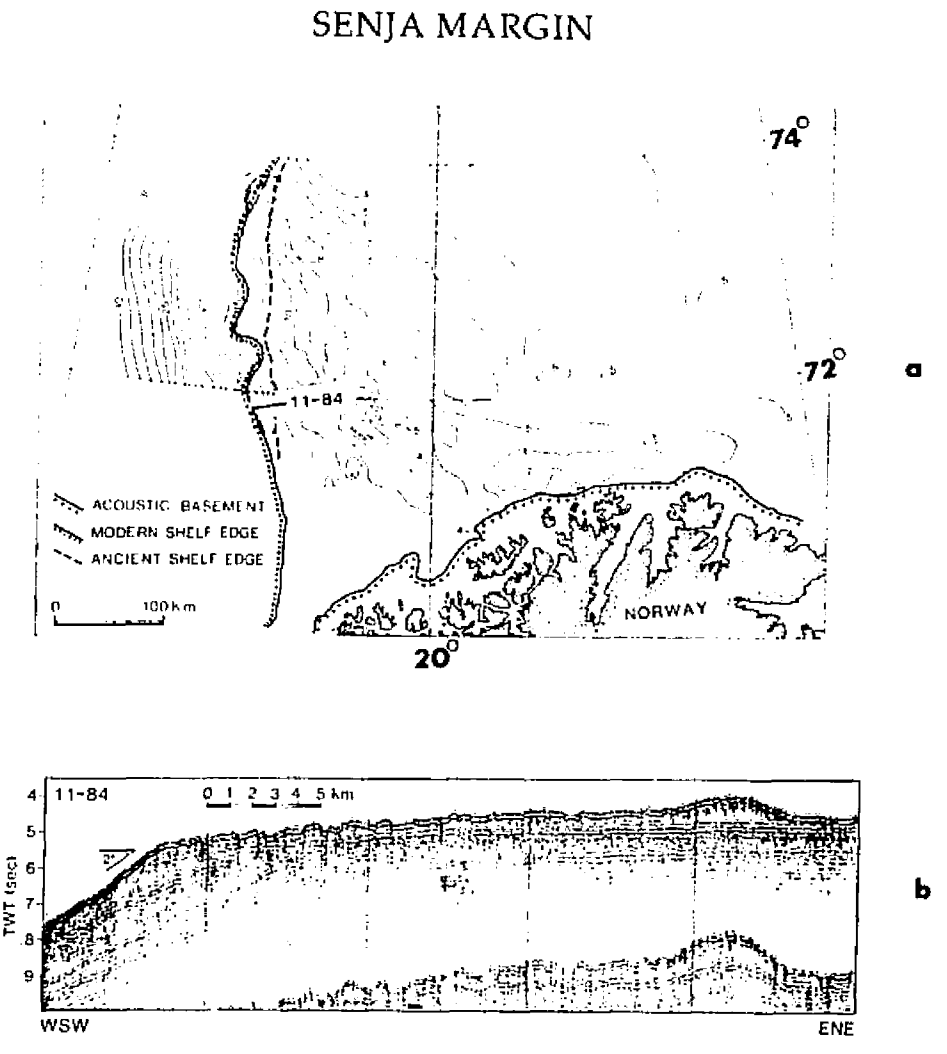

Figure 3-17. A Geoseismic section from the Senja Margin (after Vorren *et al.*, 1989). (a) Location of the geoseismic transect, (b) Multichannel section showing a continuous basement reflector across the shelf break just south of Bjørnøya.

multichannel seismic data (Sundvor and Austegård, 1990) confirm this interpretation with a 4.5 km thick layer of 5-5.7 km/s velocity structure. Based on these seismic data, Sundvor and Austegård (1990) established a tentative continent-ocean boundary on the northern Svalbard Margin.

Sundvor *et al.* (1982a) traced this reflector as far south as 25 km from the northwestern part of Spitsbergen and suggested a connection to the high grade Precambrian gneiss complex (Hecla Hoek) exposed onshore. This continuous basement reflector below a sedimentary basin of a maximum thickness of 4.5 km, correlates with a 5-5.7 km/s refractor velocity (Austegård, 1982). This part of the margin also corresponds to the area of smooth magnetic field reported by Feden *et al.* (1979). The distance between magnetic isochron-24 and the suggested continent-oceanic crustal transition is approximately 100 km, or twice the width of crust of unknown origin indicated by Vogt *et al.* (1979). A 5.5 km/s refractor exists in the entire Hinlopenstretet (Sundvor *et al.*, 1978). In many profiles, another seismic refractor (below this 5.5 km/s layer) appears to have velocities of 5.8-6.6 km/s indicating an acoustic basement along the northern Svalbard-Nordaustlandet Margin (Kristoffersen *et al.*, 1982; Sundvor and Austegård, 1990).

3. Sedimentation Along the Eastern Margins

Sedimentation in the northern Norwegian-Greenland Sea and eastern Arctic basin was influenced by glaciation of the surrounding continents and shelves. The

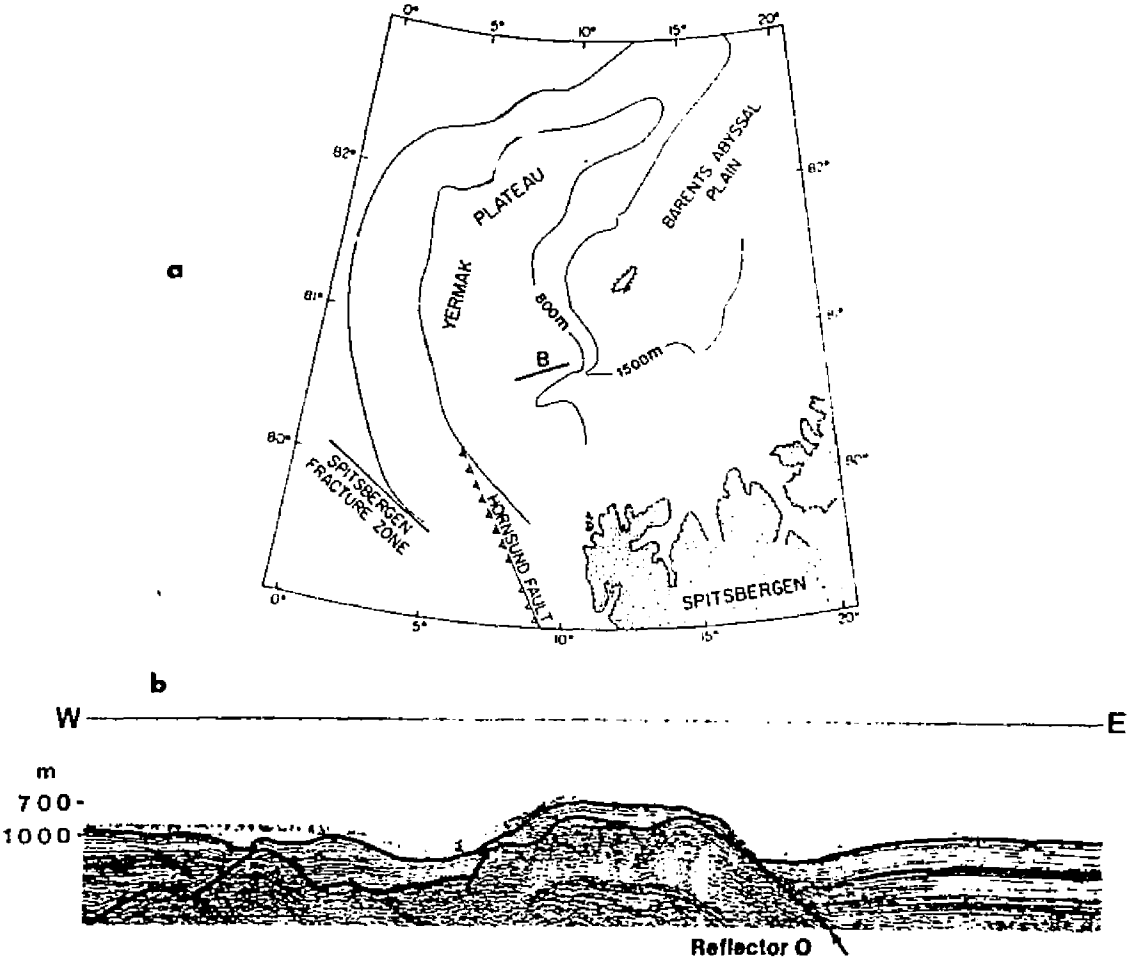

Figure 3-18. A seismic record from the northern Svalbard Margin. (a) Main structures on the Norwegian Margin (bathymetry in meters), B: geoseismic transect, (b) Multichannel section showing a continues basement reflector from nearshore northern Svalbard onto the southern part of the Yermak Plateau (after Sundvor *et al.*, 1982a).

modern depositional environment of the Norwegian-Greenland Sea is highly asymmetric (in an E-W direction) because of the surface water masses and pack ice cover of the Eastern Greenland current regime. Marginal highs which now are buried, acted as barriers to the terrigenous sediments during the early stage of basin formation (Eldholm and Windisch, 1974). Analyses of results from the Ocean Drilling Project-Leg 104 (Eldholm *et al.*, 1987) established that the Northern Hemisphere experienced a multitude of glaciations during at least the past 2.56 Ma (Thiede *et al.*, 1989). In this region, a thick sequence of hemipelagic and pelagic sediments rests on terrigeneous material overlying volcanic basement. Post opening sediment thicknesses range from zero at the axis of the mid-ocean ridge, on some basement highs and on steep escarpments to over 2 km along parts of the continental margin (Grønlie and Talwani, 1978).

On Leg 38 of the Deep Sea Drilling Project the oldest post-opening sediment recovered was late Paleocene-early Eocene, on the crest of the Vøring Plateau (Schrader *et al.*, 1976). A major hiatus was found over the Vøring Plateau which, changed from a high-energy, shallow, terrigenous province to an open-water pelagic, biogenic-dominated depositional region.

The Lofoten-Vesterålen area is characterized by a large accumulation of sediments of which the main part is of pre-Tertiary age, deposited prior to the opening of the Norwegian-Greenland Sea (Eldholm *et al.*, 1984). The total sediment thickness is small (1 to 2 km) and, apart from an irregular thin local upper layer of Quaternary age, sediments are all consolidated (Talwani and Eldholm, 1972).

The age and distribution of the sediments along the Svalbard Margin agrees with the tectonic model for the opening of the Norwegian-Greenland Sea (Myhre *et al.*, 1988). Terrigenous accumulations of 6 to 7 km or more (Senja-Western Svalbard Margin) were laid down on igneous oceanic crust (Eldholm and Windisch, 1974; Myhre *et al.*, 1982, 1992). Sediment sequences of varying thickness overlie an unconformity (upper regional unconformity) along the Senja-Western Svalbard Margin. The thickest sedimentary sequence occurs at the margin and is between 900 and 1000 m's thick (assuming a velocity of 2 km/s in the sediments, Vorren *et al.*, 1989). A massif of salt, found by Faleide *et al.* (1984) was dated as Permian. Nearby in the southwestern Barents Sea a sequence of Lower Cretaceous sediments accumulated with rapid subsidence and subsequent salt mobilization (Myhre *et al.*, 1982).

Further north, along the Western Svalbard Margin, Schlüter and Hinz (1978) mapped an uppermost sedimentary unit which is thought to consist of Pliocene-Pleistocene muds interbedded with turbidites and mass-transported sand related to glacial-interglacial periods. Myhre and Eldholm (1988) proposed that there was a considerable increase in sediment deposition at 5-6 Ma, based on interpretation of seismic profiles. In addition, Myhre and Eldholm (1988) estimate that prior to mid-Miocene the sedimentation rates were approximately 100 mm/y. Since the Miocene (during the last 5 my) the rates have increased to more than 300 mm/y. Faleide *et al.* (1984) suggest an unconformity at the base of the upper Paleocene. It was about this time that block faulting was initiated adjacent to Svalbard. Faleide *et al.* (1984)

interpreted the unconformity as a result of tectonic activity near the present continent-oceanic crustal transition. Myhre *et al.* (1982) proposed that all of the sediment north of 76°N and seaward of the Hornsund Fault Zone was deposited since the mid-Oligocene.

Depocenters occur along the Western Svalbard Margin (Kongsfjørden, Isfjørden, Storfjørdrenna) with approximate velocities of 1.9-2.2 km/s and thicknesses of 1.6-2.4 s (Myhre and Eldholm, 1988). The location of depocenters seaward of east-west fjord systems and submarine depressions indicate high offshore sedimentation rates associated with late Cenozoic glaciations (Myhre and Eldholm, 1988). During the Deep Sea Drilling Program-Leg 38, Site 344 was drilled just east of the Knipovich Ridge (toward the margin). In this site, about 377 m of glacial marine sediments were recovered above the basement. Talwani *et al.* (1976) dated basal sediments as lower Pliocene or upper Miocene. Along the entire continental margin a wedge of Tertiary sediments has prograded into the ocean forming the present passive margin (Myhre *et al.*, 1982).

During glacial periods, the Norwegian-Greenland Sea is thought to have been more or less covered by sea ice including extensive glacier coverage of the Barents and Greenland shelves (Thiede *et al.*, 1990). The last glacial maximum is documented as approximately 18 thousand years ago (CLIMAP, 1976). Fram Strait may have played an important role in the feedback of the glacial-interglacial cycles (Thiede *et al.*, 1990). During the Ocean Drilling Program-Leg 151 (Arctic Gateway-I, Mhyre *et al.*, 1994) physical property measurements on sediments suggest episodic

overcompaction during the Quaternary, which may have resulted from periodic burden by glacial ice. Sediments include minor amounts of biogenic material perhaps because of low productivity due to ice cover, dilution by siliciclastics, and dissolution. Analyses of dropstone abundances indicate an intensification of glacial conditions about 3.5 Ma, marked by the first occurrences of dropstones. These data suggest episodical intensive ice-rafting in the period 3.5 to 1.0 Ma. Sedimentation rates at the Yermak Plateau are extremely high ranging about 10 to 200 m/Ma during the Quaternary.

As the high latitude northern Norwegian-Greenland Sea, and the shallow shelves bordering northern Svalbard might have been covered by a grounded ice sheet during the Quaternary Glaciation, the fault bounded continental margin of Nordaustlandet was substantially modified by glacial scour and later day bottom currents associated with melt waters. Mass sediment transport in response to ice movement is an important process on the northern Svalbard-Nordaustlandet Margin (Okay *et al.*, 1991). Sediments are texturally heterogeneous due to the major role played by ice in their origin, transport and deposition. Sediment surfaces are often strained by the ice impact leaving plow marks and later modified by strong contour currents (Vogt *et al.*, 1994).

4. HEAT FLOW

Heat flow values are high (average 124 mW/m^2) relative to crustal age along/near volcanic marginal plateaus on the eastern margin of the Norwegian-Greenland Sea (Figure 3-8). On the Norwegian Margin there is an increase of heat flow toward the continental margin (reaching from 41 to 87 mW/m^2). Heat flow values on the Vøring Plateau range from 43 to 118 mW/m^2, while heat flow averages 105 mW/m^2 near the East Jan Mayen Fracture Zone. Heat flow reaches 96 mW/m^2 along the Jan Mayen Ridge and 217 mW/m^2 at its southern terminus with northern Iceland (Langseth and Zielinski, 1974).

Heat flow values near the Senja Fracture Zone range from 81-103 mW/m^2. In contrast, although the data are fewer, the heat flow values along the east coast of Greenland at a comparable latitude are considerably lower (67 to 84 mW/m^2). Heat flow reaches 140 mW/m^2 along the Western Svalbard Margin at 75°N (over the Hornsund Fault) and 100 mW/m^2 at 78°N.

Along the northern Svalbard-Hinlopen-Nordaustlandet Margin heat flow data are scarce but range (from 61 to 109 mW/m^2). Over the southern Yermak Plateau on the northern Svalbard Margin (Figure 3-9), heat flow ranges from 104 to 138 mW/m^2 (Crane *et al.*, 1982; Sundvor, 1986; Crane *et al.*, 1991). In contrast, the northern part of the Yermak Plateau is colder ranging from (54-92 mW/m^2, Jackson *et al.*, 1984; Sundvor, 1986; Sundvor and Torp, 1987). Off-axial heat flow highs are also observed along the northeastern Nordaustlandet Margin (109 mW/m^2, Sundvor and

Torp, 1987). No heat flow data have been reported from the region of Kong Karls Land and southern Svalbard within the Barents Sea.

A full analysis of heat flow data will be presented in Chapter 5, corrected for variable rates and durations of sedimentation and then reinterpreted in the context of thermal rejuvenation along the margins.

5. SEISMICITY

Intraplate seismicity is highly concentrated between the Knipovich Ridge area and the eastern margins of the Norwegian-Greenland Sea, as well as on the western Svalbard Platform (Figure 3-19). Earthquakes on Spitsbergen occur along major N-S trending normal faults, such as the Hornsund, Billefjørden, and Lomfjørden Fault Zones. Mitchell *et al.* (1990) suggest that the maximum principal stress axis indicates extension (in the E-W direction), and is perpendicular to the major faults and continental margin orientation.

There are highly active and concentrated seismic zones in Heer Land in southwestern Svalbard (77.8°N, 18°E) and in northern Nordaustlandet where earthquake zones are located close to the landward side of the continental margin (Figure 3-19). The frequency of earthquakes in Heer Land and Nordaustlandet appears to be much higher than that along the oceanic ridge system (Mitchell *et al.*, 1990). In contrast, seismicity is low in the region of the West Spitsbergen Orogeny. Mitchell *et al.* (1990) suggest that the Heer Land Zone correlates intraplate seismicity

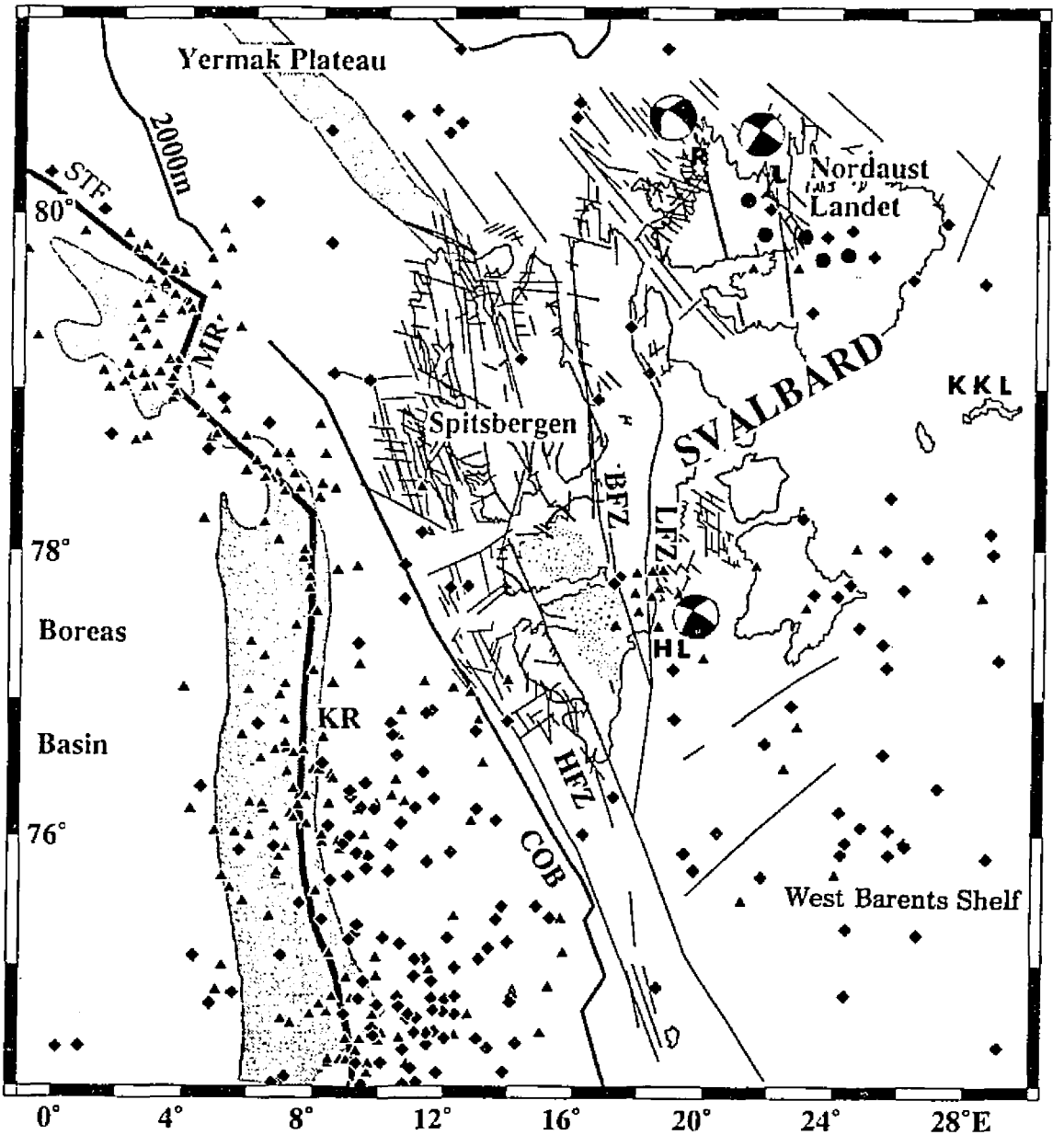

Figure 3-19. Earthquakes in the Svalbard region. Earthquake epicenters are shown as diamonds and triangles determined from different sources (after Müller, 1993). Tectonic lineaments on Svalbard are by Ohta (1972). Shaded areas along the Knipovich Ridge and Yermak Plateau indicate high heat flow (> 150 mW/m^2) as reported by Crane *et al.* (1982, 1988, 1991). The stippled area outlines the Central Tertiary Basin. KR: Knipovich Ridge; COB: Continental-oceanic crustal transition (after Eldholm *et al.*, 1987); MR: Molloy Ridge; HFZ: Hornsund Fracture Zone, STF: Spitsbergen Transform Fault, BFZ: Billefjørden Fracture Zone, LFZ: Lomfjørden Fault Zone, R: Rijpfjørden Fault Zone, HL: Heer Land Seismic Zone, KKL: Kong Karls Land.

having *b*-values of 1.4 to pre-existing faults (mostly compressional and shear movements). On northern Nordaustlandet, two concentrations (extension- and shear-dominated intraplate movements with an apparently NNW-orientation) occur with both *b*-values of 0.5 (Bungum and Kristoffersen, 1980). If the *b*-value is a measure of the relative abundance of large and small earthquakes, (an approximate average for *b* is 1) a small value for *b* indicates that small earthquakes are not so frequent and that large earthquakes are more likely to occur. Small values for *b* are usually characteristic of continental rifts and regions with deep earthquake foci, and large values for *b* are typical of mid-ocean ridges.

6. Magnetic Anomalies

Much of the eastern margin of the Norwegian-Greenland Sea is characterized by "magnetic smooth zones" without hint of clear magnetic anomaly age identifiers (Figure 3-12). The section of the margin most easily dated is the Vøring Plateau. The Vøring Plateau Escarpment is characterized by a distinctive short-wavelength negative magnetic anomaly (Talwani and Eldholm, 1977). Landward of anomaly 24 lies strips of crust about 50 km wide that are magnetically featureless (Vogt *et al.*, 1981; Srivastava, 1985) and thus may mark the continent-oceanic transition (Vogt, 1986). The magnetic character along the Lofoten Margin (northern Vøring Plateau) alters between seafloor spreading anomalies and magnetic smooth zones (Figure 3-11).

In addition to the magnetic smooth zones which characterize parts of the southeastern margin, the magnetic character of the northern Norwegian-Greenland Sea is also confused, not coherent or entirely absent. Åm (1975) from aeromagnetic measurements, suggested Mesozoic doleritic and gabbroic intrusions on the shelf and upper slope along the margin similar to those observed in Svalbard. Although magnetic anomalies align symmetrically about the Mohns Ridge, at its northernmost terminus, where the ridge abuts the paleo-Senja and Greenland Fracture Zones, no clear definition in the background magnetic field is observed (Kovacs *et al.*, 1982).

Even further to the north the high amplitude magnetic anomalies over the Hovgård Fracture Zone may indicate a displacement of this fragment from the Western Svalbard Margin (Myhre *et al.*, 1992). Like parts of the southeastern margins of the Norwegian-Greenland Sea, a magnetic smooth zone was reported by Feden *et al.* (1979) on the southern part of the Yermak Plateau, north of the Spitsbergen Fracture Zone. In contrast, the northern Yermak Plateau is characterized by high amplitude and long-wavelength magnetic anomalies, varying from 300 to 1600 nT (Figure 3-11; Feden *et al.*, 1979; Kovacs *et al.*, 1982; Jackson *et al.*, 1984).

7. GRAVITY

The eastern margins of the Norwegian-Greenland Sea are characterized by locally varying free-air gravity anomalies (from -50 to more than 100 mGal, Figure 3-13, Grønlie and Talwani, 1982; Faleide *et al.*, 1984). On the Vøring Plateau, free-air

gravity anomalies reach 50 mGal (or more). However, a negative gravity anomaly (37 mGal) occurs inside the plateau escarpment. A prominent landward-dipping escarpment has been mapped at 68.9°N coincident with a steep gravity gradient (Talwani and Eldholm, 1972). The Eastern Jan Mayen Fracture Zone is characterized by negative gravity anomalies (37 mGal) and the active portion of the fracture zone is characterized by positive values (>100 mGal). North of the Vøring Plateau in the Lofoten Basin, a large positive anomaly (>100 mGal) may indicate some high density crust under the Lofoten-Vesterålen Islands.

The Senja Gravity High (in excess of 135 mGal) is oriented in a N-NW direction between 70°N and 73.5°N at the Senja Margin (Figure 3-13). In this region, the gravity high is correlated with seaward dipping reflectors and also high heat flow. It is difficult to resolve low-amplitude magnetic features on the shelf and upper slope, where the gravity-field is very quiet except for some local areas of high-amplitude anomalies (Åm, 1975). The anomaly could be explained by a 30 to 60 km-wide subbasement-reflector intrusive. Talwani and Eldholm (1977) suggest that the Senja Gravity High defines the eastern extension of the Greenland Fracture Zone now buried by sediments. Around the Greenland Fracture Zone a large positive anomaly (approximately 117 mGal) may also be indicative of high-density crust located beneath the ridge (Grønlie and Talwani, 1982). A 20- to 50-km wide belt of positive isostatic anomalies is located just seaward of the Greenland Escarpment.

At approximately 74°N, southwest of Bjørnøya, there is a gravity high (10 to 200 km-long) of 80 mGal trending in a NE direction (Faleide *et al.*, 1984; Myhre and

Eldholm, 1988). A series of positive landward anomalies, linearly aligned between Bjørnøya and 76.5°N appear parallel to the shelf edge. The Bjørnøya Gravity Anomaly has a shape and amplitude similar to the anomalies over the neighboring mid-ocean ridge (Myhre, 1984), yet differs from the Senja and the Hornsund anomalies. Myhre (1984) explains this difference and suggests that this gravity anomaly is associated with a structural high trending obliquely to the continental margin. This gravity high has a smaller amplitude than the elongate belts of the Senja and Hornsund Highs and it appears to form a link between them.

In contrast, the Hornsund Fault anomalies trend in a N-NW direction from Bjørnøya to 77.5° N landward of the shelf edge and are thought to mark the continental-oceanic crustal boundary. The anomalies are split into two maxima: Myhre and Eldholm (1988) suggest that the maxima (145 mGal at 75.5°N and 132 mGal at 77°N) are caused by local intrusive bodies surrounded by less dense continental crust along the Hornsund Fault. The shape and location of the main anomaly excludes a topographic edge effect origin (Grønlie and Talwani, 1982; Myhre and Eldholm, 1988). Eldholm *et al.* (1987) suggests that the anomalies may indicate the emplacement of subaerial Icelandic-type basalts during the earliest stage of sea-floor spreading. Along the margin between the Senja and Hornsund Fault Zone, the acoustic basement reflector, forming a marginal high, terminates along northeastern trending faults which are offset along lineaments subparallel with the Senja Fracture Zone and the Hornsund Fault Zone (Myhre and Eldholm, 1988).

C. SUMMARY

The present-day plate boundaries in the Norwegian-Greenland Sea are morpho-tectonically complex features. Both paleo- and presently-active propagating ridges (Aegir, Mohns, and Knipovich) impacted paleo-shear zones (East Jan Mayen, Vøring, Lofoten, Vesterålen, Senja, and Spitsbergen) which defined the nascent transtensional volcanic margins (Norwegian, Senja, and Svalbard). Most recently, the Mohns Ridge intersected and was deflected into the Spitsbergen Shear Zone forming the Knipovich Ridge in the process. If the present is the key to the past then mid-ocean ridge deflection occurred commonly in the early history of the Norwegian-Greenland Sea.

Studies indicate that complex margin formation in the Norwegian-Greenland Sea is associated with episodic magmatic behavior such as early Tertiary and Neo-volcanic activities (Talwani and Eldholm, 1977; Skogseid and Eldholm, 1987; Mutter *et al.*, 1988; Eldholm, 1991; Crane *et al.*, 1991; Okay and Crane, 1993; Eldholm and Grue, 1994). By drilling into the eastern margins' seaward-dipping structure, it was discovered that a series of volcanic flows extruded through continental rock before and during seafloor spreading, thus the continental margins of the Norwegian-Greenland Sea are dominated by deep fracture zones associated with volcanism. The fracture zones were originally defined by a prominent, elongate, gravity anomaly. Seismic, magnetic and gravity data support this relationship (Eldholm *et al.*, 1987; Myhre and Eldholm, 1988). High positive free-air gravity anomalies are associated

with seaward dipping reflector sequences, indicative of high density crust creating the eastern volcanic margins.

The magnetic character also suggests an exceptionally high rate of basalt accumulations at the continent-oceanic transition. Earthquakes occur along the continental-oceanic crustal transition, as well as on the Svalbard Platform with extension-dominated intraplate movements along major N-S trending normal faults associated with diffuse magmatic activity.

The Norwegian-Greenland Sea lies within a broad region of anomalously high heat flow. This high heat flow implies that relatively high temperatures exist at shallow depths in the crust. Thus, in response to the heating, the seafloor in the eastern Norwegian-Greenland Sea is thermally elevated. However, the questions remain about the level of present-day volcanic activity along the margins of the Norwegian-Greenland Sea and its correlation to the unusual patterns of intraplate seismicity and presently high heat flow in the regions where crust was thought to be many ten's of millions of years old. To resolve this problem, we collected SeaMARC-II data to investigate whether or not this area of high seismicity had been volcanically active in the recent past. Our findings from these data are described in the following chapter.

Chapter 4

MORPHO-TECTONIC STUDIES ALONG THE SVALBARD MARGINS: SeaMARC-II RESULTS

A. SeaMARC-II SURVEYS

Two SeaMARC-II expeditions (1989 and 1990) investigated the previously unmapped seafloor in the northern Norwegian-Greenland Sea and the adjacent part of the eastern Arctic Ocean (Crane *et al.*, 1990; Sundvor *et al.*, 1990, 1991; Vogt *et al.*, 1990, 1991, 1993; Okay *et al.*, 1991, 1993; Doss *et al.*, 1991). These expeditions were made possible by the collaboration of several institutions. The Naval Research Laboratory chartered the SeaMARC-II system from the Hawaii Institute of Geophysics. The University of Bergen provided a research vessel, *Håkon Mosby*, including navigation equipment and shipboard-geophysical sensors (3.5 and 38 kHz echo sounders, towed proton precession magnetometer, and gravimeter). Scientific staff, representing the City University of New York, the Lamont-Doherty Earth Observatory of Columbia University, the Hawaii Institute of Geophysics, the Scripps Institution of Oceanography, the Naval Research Laboratory, and the University of Bergen participated. The main objective of my study during these expeditions was to map the regional volcano-tectonic structures and investigate their relationships to the thermal evolution of transtensional volcanic margins adjacent to the northeastern Norwegian-Greenland Sea.

The SeaMARC-II system, as a mapping tool, collects a combination of back-scatter, side-looking sonar imagery and swath-type bathymetry (see Appendix A for a review). This combination facilitates sufficiently accurate descriptions of the seafloor. Volcanics (flows, cones and craters), normal faults, sedimentary and glacial features, and erosional channels are visible on the sonar imagery allowing us to investigate the geological processes operating in the northern Norwegian-Greenland Sea and in adjacent parts of the Eastern Arctic Ocean.

During the SeaMARC-II/1989 Expedition the northern part of the Knipovich Ridge, Molloy Transform Fault along the Western Svalbard Margin and southwestern Yermak Plateau were mapped. In the fall of 1990 more than 200 km of Arctic sea-ice melted north of the Svalbard Archipelago. Favorable ice conditions (more open water than at any time in the previous 43 years) allowed the deep ocean research northeastward to 81.8°N, 29°E. The break from impossible conditions also enabled us to obtain the first side-looking sonar data from the deep-water Arctic Ocean. The SeaMARC-II/1990 investigation covered the NE Lofoten Basin, the Bear Island Fan (Bjørnøya), the Hovgård Fracture Zone, and the northern Svalbard and Nordaustlandet margins. The entire area was surveyed in less than 4 weeks under (sometimes) severe-ice and weather conditions. SeaMARC-II side-looking sonar imagery and swath-bathymetry were generally of good quality throughout the cruise although rough weather resulted in the loss of gravity data along the northern Svalbard-Nordaustlandet Margin.

This chapter combines the results of regional examples of side-looking sonar images, and preliminary geological-geophysical interpretations. Figure 4-1 depicts the track chart of both the 1989 and 1990 SeaMARC-II Expeditions (on a polar stereographic projection). Figure 4-2 illustrates a combination of swath-bathymetry and side-looking sonar imagery mosaics from these expeditions (Plate 1 in Appendix B). These images represent the first side-looking sonar data from the deep-water Eastern Arctic Ocean. As a result of the two-year high-latitude investigations, about 15,000 line kilometers of data were collected, representing approximately 150,000 km^2 of side-scan imagery and 75,000 km^2 swath-bathymetry. The SeaMARC-II side looking sonar images have recently been compiled by Crane and Solheim in the Seafloor Atlas of the Norwegian-Greenland Sea (Crane and Solheim, 1995).

B. GEOLOGY OF THE SVALBARD REGION

1. TECTONICS

Along the northern coast of Svalbard, NW-SE and NNE-SSW trending depressions are dominant on the shelf area. These two directions correspond closely with the conjugate fracture system in the Caledonian rocks (Birkenmajer, 1981; Ohta, 1982; Max and Ohta, 1988). The area from central to southern Spitsbergen is characterized by large NNW-SSE trending fault zones that were first active in

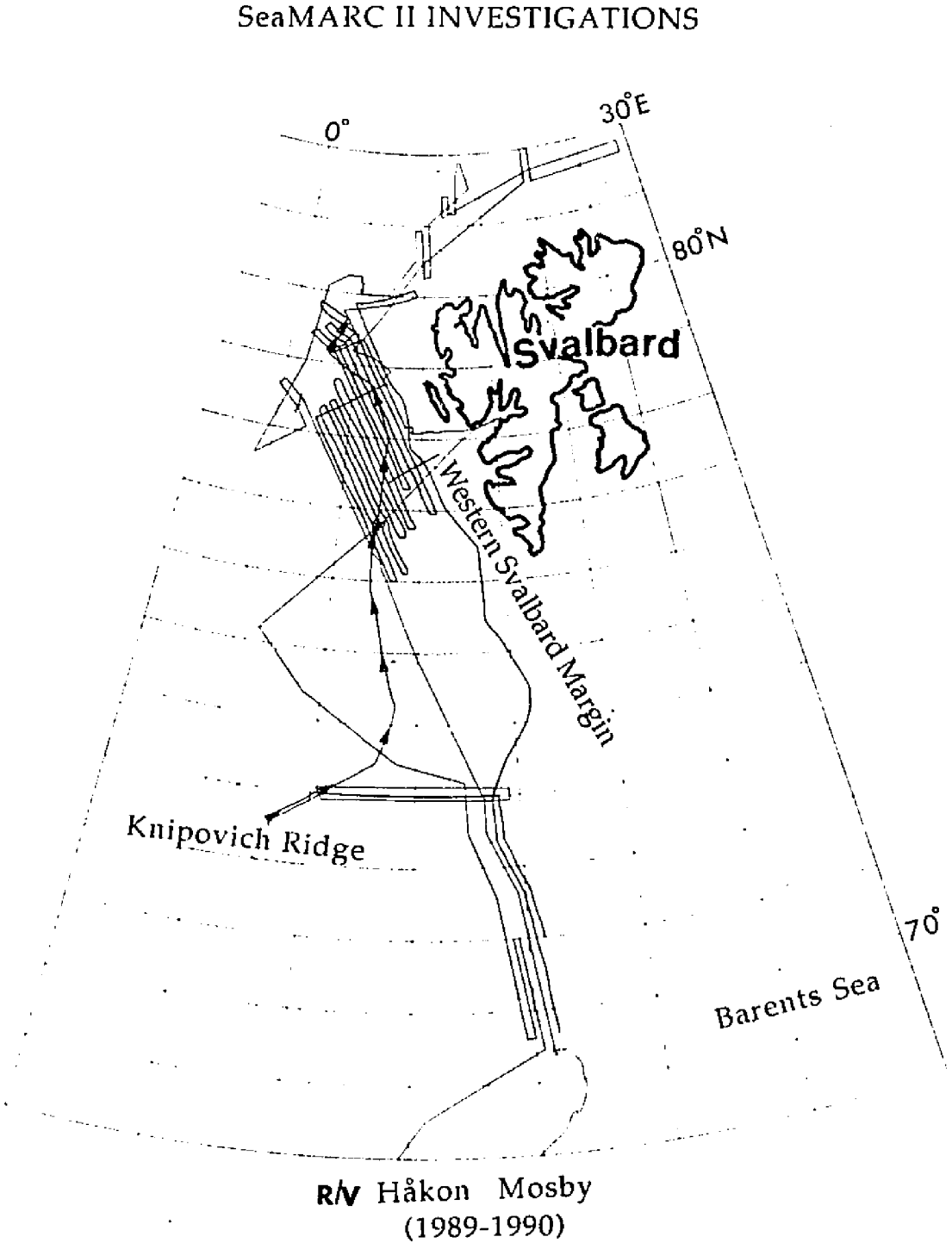

Figure 4-1. Tracks chart of the SeaMARC-II Expeditions (1989 and 1990).

Figure 4-2. SeaMARC-II side-looking sonar imagery and swath-bathymetry (1989 and 1990), from the Seafloor Atlas of the Norwegian-Greenland Sea by Crane and Solheim (1995). Boxes indicate study areas: the northern Svalbard margin (A), the northern Nordaustlandet margin (B).

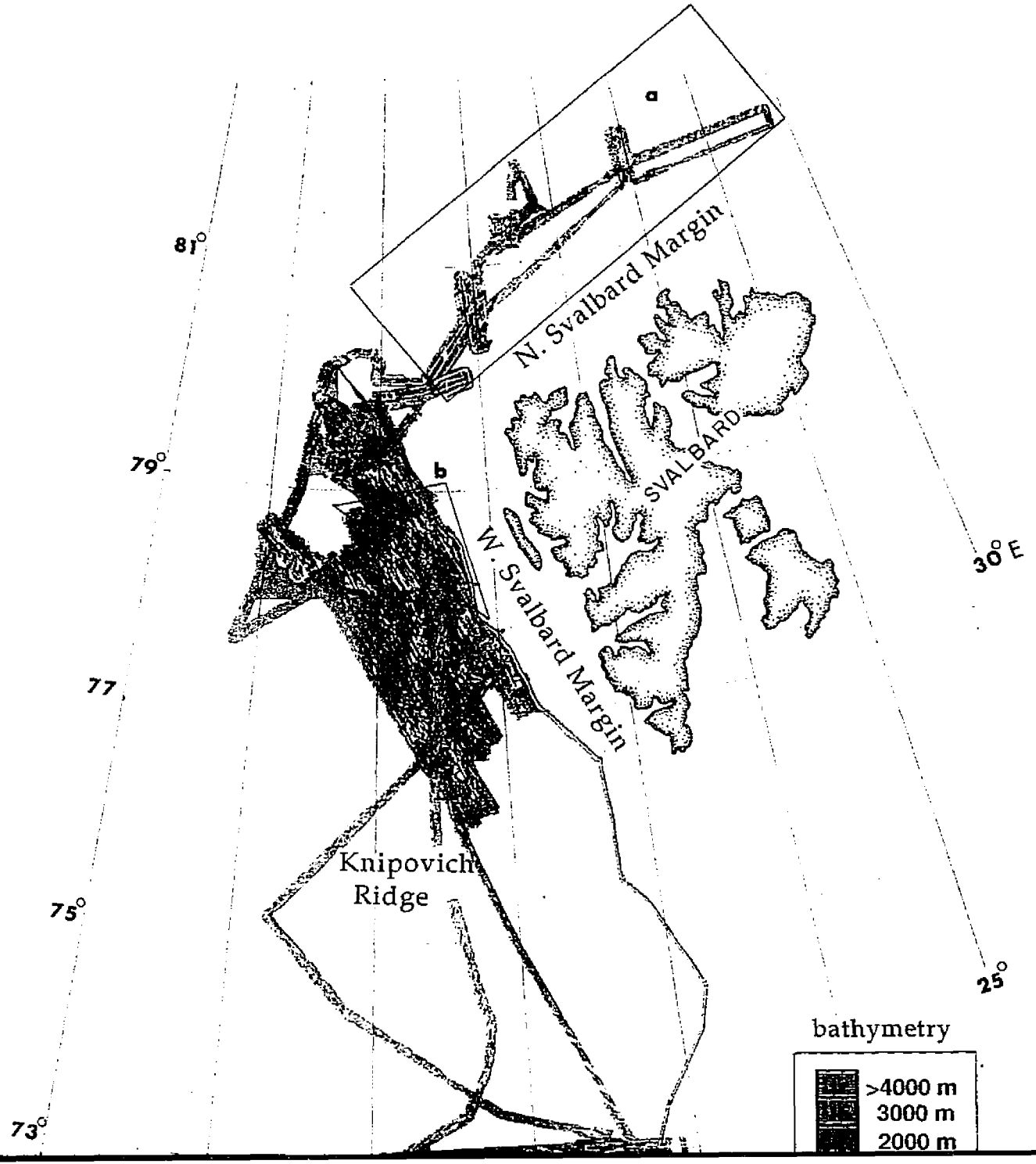
a
b
81°
79°
77°
75°
73°
30° E
25°
N. Svalbard Margin
SVALBARD
W. Svalbard Margin
Knipovich
Ridge
bathymetry
>4000 m
3000 m
2000 m

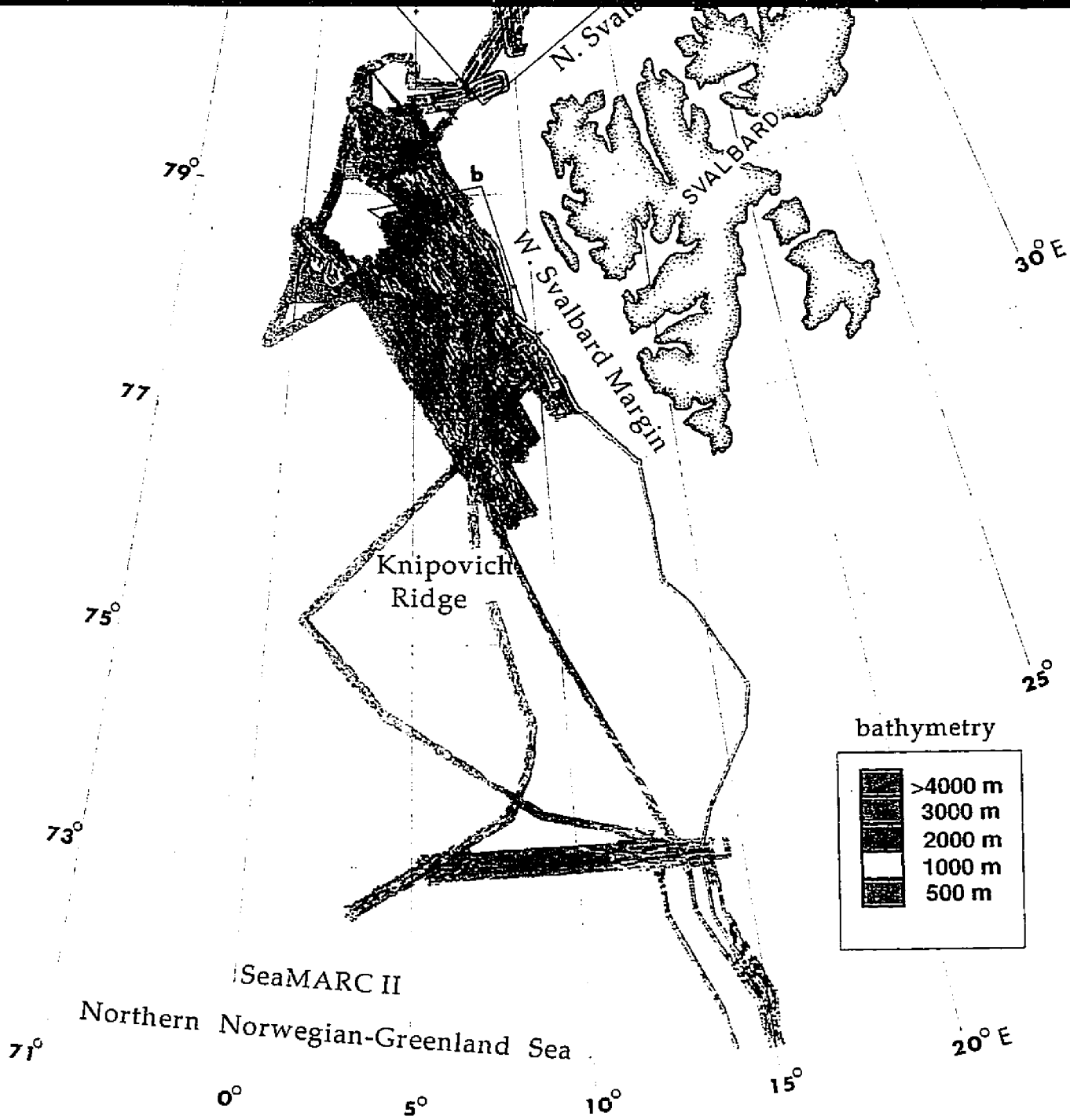
N. Svalbard
SVALBARD
W. Svalbard Margin
Knipovich
Ridge
79°
77
75°
73°
71°
30° E
25°
20° E
15°
10°
5°
0°
bathymetry
>4000 m
3000 m
2000 m
1000 m
500 m
SeaMARC II
Northern Norwegian-Greenland Sea

Devonian times (Ohta, 1982). These are of Tertiary age and older than the NNW-SSE striking graben and horst structures (Ohta, 1982; Steel *et al.*, 1985). They indicate a right lateral transpressive stress, perhaps caused by the northward movement of the Greenland plate in Eocene times prior to the opening of the northernmost Atlantic Ocean (Kristoffersen and Talwani, 1978). The fault zones bounding this area, the Lomfjørden Fault and Billefjørden Fault Zone in the east and the Forland Fault Zone in the west, join to become one fault zone in the Heer Land region; and this junction borders the southern Central Tertiary Basin of Spitsbergen (see Figure 3-19 in Chapter 3). Some minor faults trending NE also occur along the west coast of Spitsbergen.

The Central Tertiary Basin in the southern part of Spitsbergen is generally asymmetric and associated with both strike-slip and thrust faulting. The Basin developed east of a strike slip boundary between the Eurasian and Greenland plates in response to the initiation of rifting, and later seafloor spreading in the northern Norwegian-Greenland Sea (Müller and Spielhagen, 1990). The Tertiary deformation appears to be less pronounced eastward and most of the Tertiary faults are younger than the folding (Harland, 1985; Steel *et al.*, 1985). Kellogg (1975) suggested that the main tectonic face may have been initiated in the late Eocene with culmination in the Oligocene. The compressive phase was followed by a period of tensional stresses resulting in formation of the down-faulted blocks and grabens. Holtendahl (1960) suggested an offshore continuation of this Tertiary fault pattern onto the northern Svalbard margin.

2. SURFACE GEOLOGY

There is a succession of sedimentary rocks from the Cambrian to the Tertiary in Svalbard (Figure 4-3). Within the context of plate tectonics, the late Paleozoic and Mesozoic rocks are similar to those in northern Canada, perhaps indicating a continuous sedimentary basin from the Canadian Arctic across Ellesmere Islands to Svalbard prior to the rifting in the Arctic Ocean (Kellogg, 1975). In the late Cretaceous an epirogenic uplift occurred in Svalbard, therefore no late Cretaceous sediments are observed on land. Most of the Tertiary rocks are located in the southern part of Spitsbergen (the Tertiary Central Basin).

The youngest rocks are believed to be of Oligocene, possibly Miocene age (Flood *et al.*, 1971). The uplifted areas have been a source region for the Tertiary deposits. The older rocks in the northern Spitsbergen and Nordaustlandet were most likely exposed prior to Cenozoic, however, the Hecla Hoek Complex along the Western Svalbard Margin became exposed during the middle Tertiary (Kellogg, 1975). The uplift along the continental margin occurred along a system of northwards trending faults with subsequent erosion of the early Tertiary, Mesozoic and late Paleozoic deposits.

Volcanics are exposed in Spitsbergen and Nordaustlandet, discussed in chapter 3 (Harland, 1971; Prestvik, 1978; Birkenmajer, 1981). Quaternary volcanic centers and active thermal springs are located in western Spitsbergen while Tertiary plateau basalts are found on eastern Spitsbergen. Both Lower Cretaceous and Mesozoic

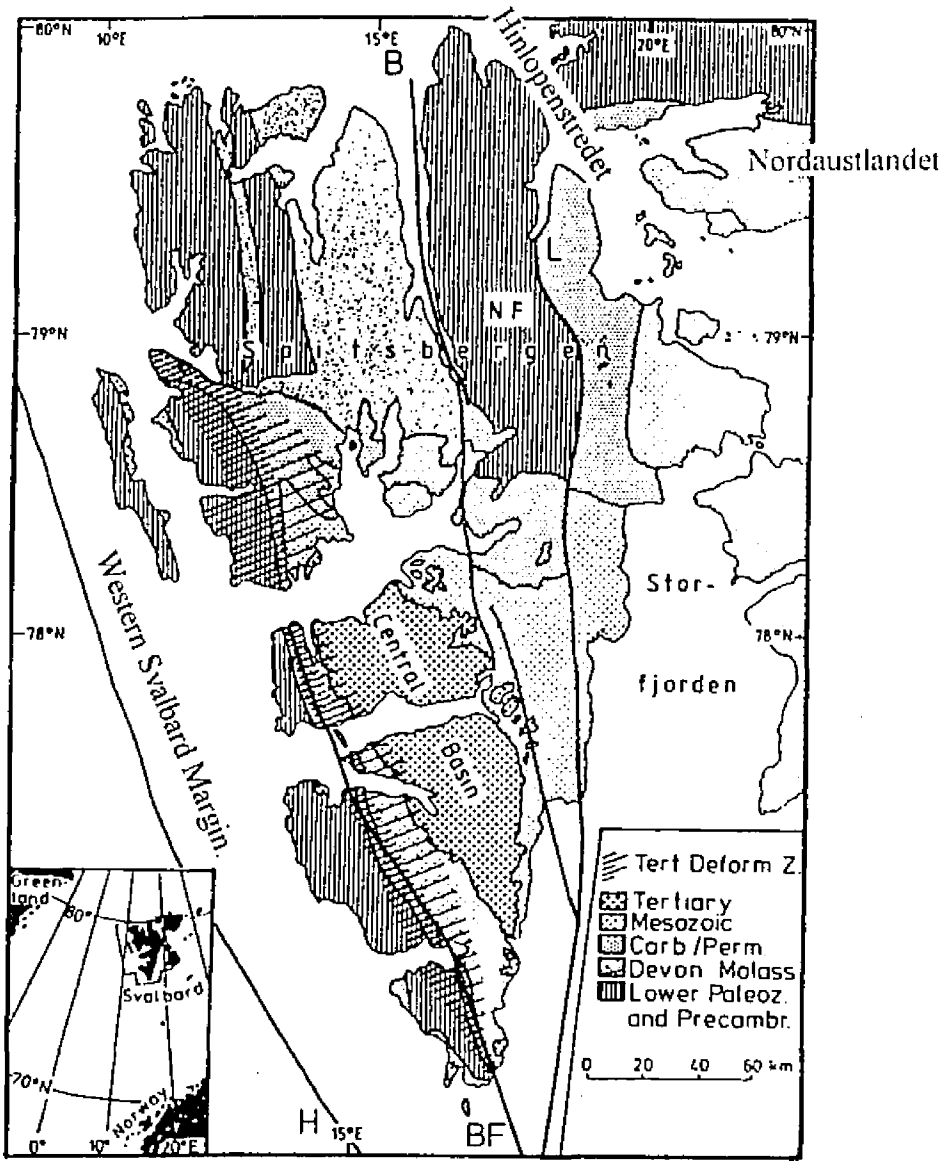

Figure 4-3. General geological basement map of Spitsbergen (Müller and Spielhagen, 1990). Structural features after Birkenmajer (1981) and Ohta (1982). BF: Western Boundary Fault, B: Billefjørden Fault Zone, H: Hornsund Fault, L: Lomfjørden Fault Zone, NF: Ny Friesland.

volcanics (tholeiitic-type) are exposed on both sides of Hinlopenstretet, on Nordaustlandet and Kong Karls Land (Figure 3-6).

C. SeaMARC II-DATA INTERPRETATIONS

1. NORTHERN SVALBARD-NORDAUSTLANDET MARGIN

a. Bathymetry:

Figure 4-4 depicts a bathymetric chart of the northern Svalbard-Nordaustlandet Margin obtained from the SeaMARC-II swath-bathymetry data. Bathymetric contours indicate the arcuate shape of the southern Yermak Plateau, deepening to the northeast (2600 m). The shelf along the northern Svalbard Margin is very shallow (600 m). The bathymetric chart indicates that on the shelf north of Svalbard and Nordaustlandet there are depressions (presumed canyons) perpendicular to the coastline. The shelf is transected by wide transverse channels which appear to be continuations of the main fjord system. The bathymetry of the continental shelf along the northern Nordaustlandet Margin is characterized by several N-S trending canyons reaching depths of 3000 m (Figure 4-4), which may be superimposed upon pre-existing fault grabens which cross through the region.

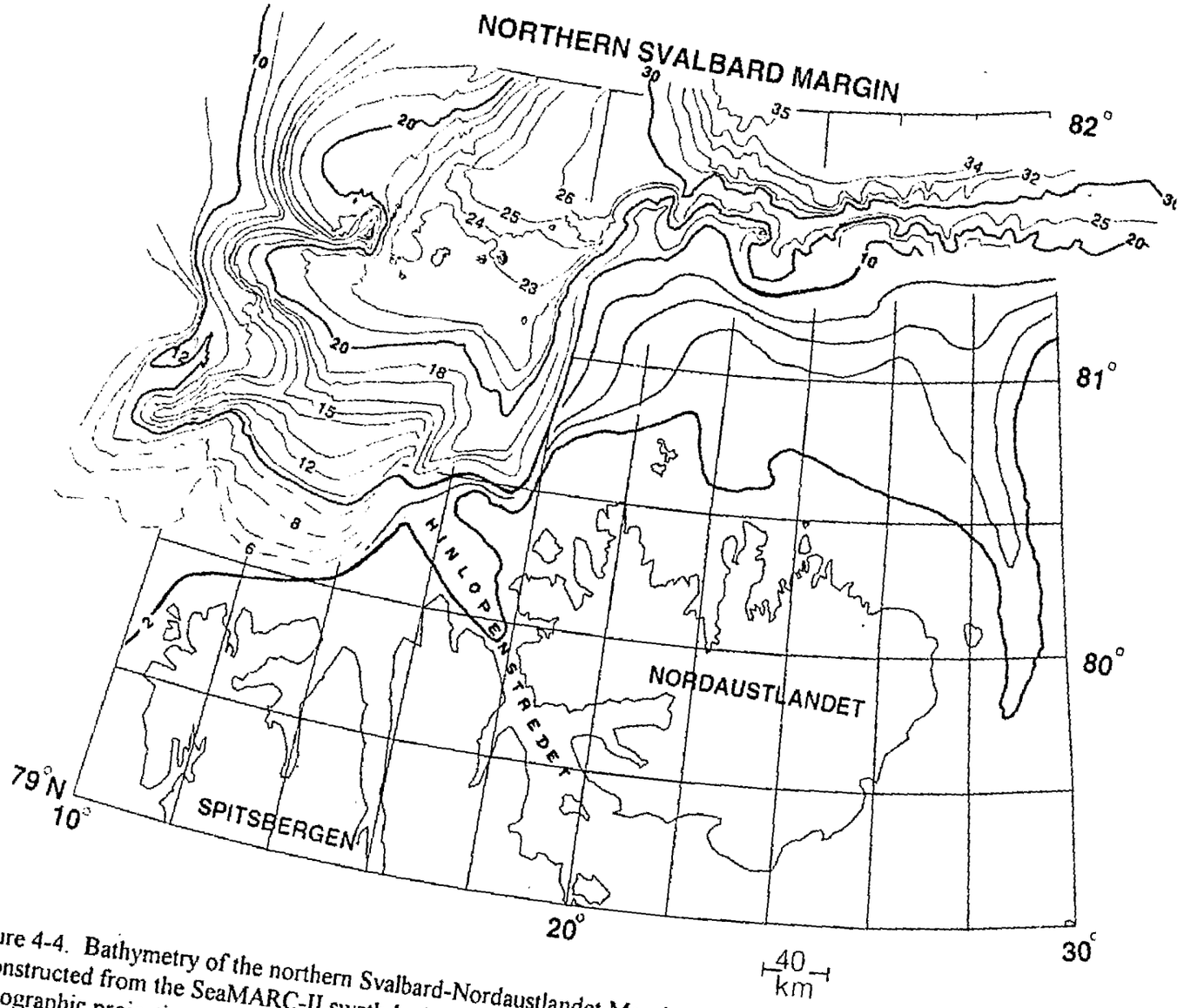

Figure 4-4. Bathymetry of the northern Svalbard-Nordaustlandet Margin. This map is constructed from the SeaMARC-II swath-bathymetry data, placed on a polar stereographic projection. Bathymetry contour intervals 100 m. Northern coastline of Svalbard modified from Cherkis *et al.* (1994).

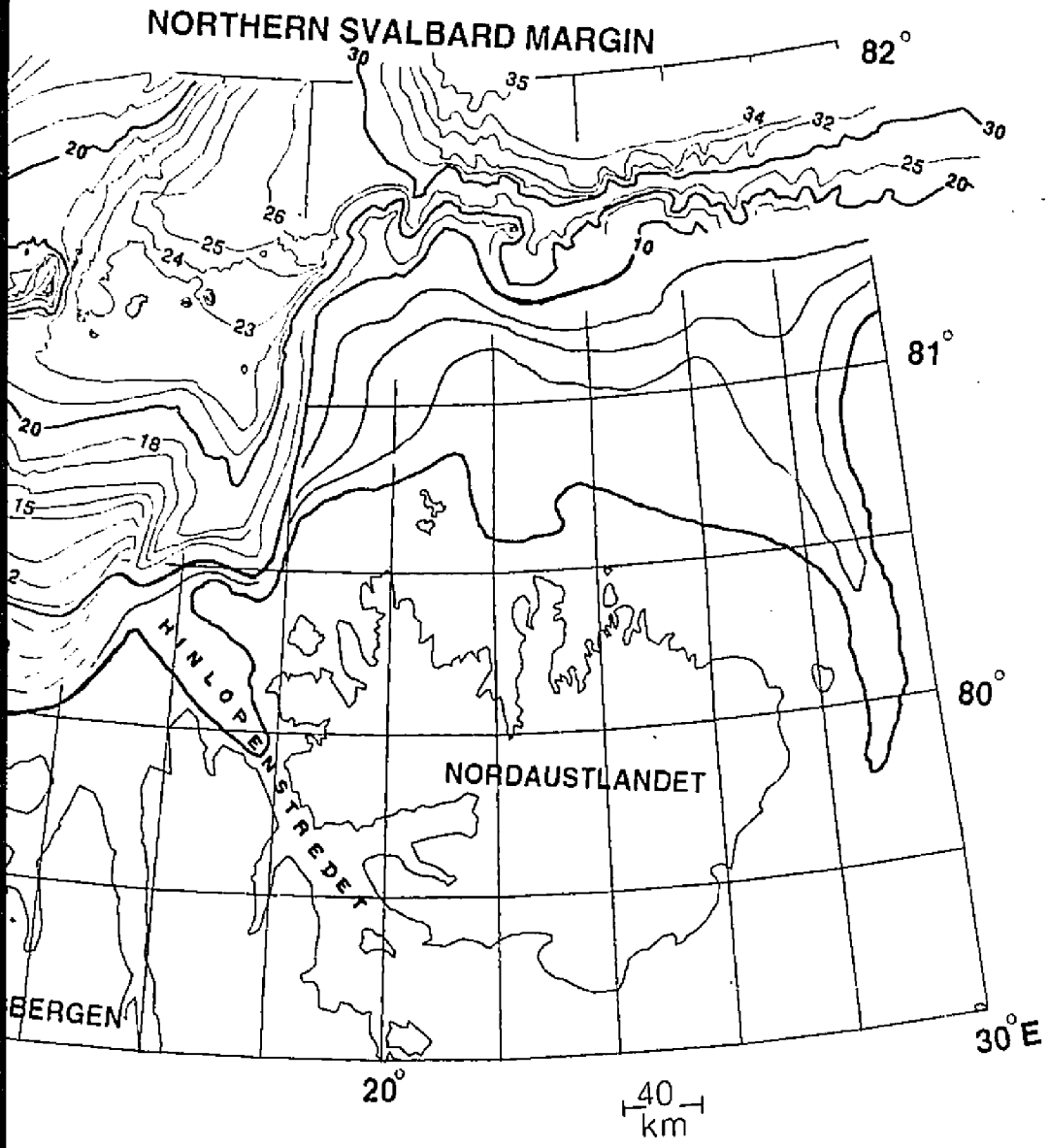

he northern Svalbard-Nordaustlandet Margin. This map
MARC-II swath-bathymetry data, placed on a polar
athymetry contour intervals 100 m. Northern coastline of
rkis *et al.* (1994).

b. Geological Interpretations:

i. Sedimentary and Glacial Features

The main geological features from Plate 1 of SeaMARC-II side-looking sonar images in Appendix B are documented in Figure 4-5. These are sedimentary features, iceberg-plow marks, glacial canyons, erosional channels, faults, volcanic seamounts and volcanic cones surrounded by lava flows and volcanic constructional terrain.

Figure 4-6 is a SeaMARC-II sonar image depicting iceberg-plow marks and sedimentary lineations (on the northwestern tip of Spitsbergen at 8°E). In general, the iceberg-plowmarks are trending in the NE-SW direction, and parallel the western edge of the southern Yermak Plateau. Further north, the orientation of iceberg-plow marks suggests that either large icebergs were carried by the Spitsbergen Current from the Norwegian-Greenland Sea into the Arctic Ocean or that they were formed by a grounded ice sheet moving across the shallow Yermak Plateau. These marks were most likely created during a prior glacial event, because icebergs of such size are no longer observed in this area (Sundvor *et al.*, 1982; Vogt *et al.*, 1994).

A sonar image of the eastern flank of Hinlopenstretet (Figure 4-7), shows erosional channels that indicate large-scale mass wasting and sediment transport along the northern Nordaustlandet Margin (Figure 4-5). If these interpretations of the sonar imagery are correct then glacially derived sediments were/are transported as far as the 3600 m isobath (in Figure 4-4). Active-glacial ice streams are still carving into the heads of fjords, and transporting the glacial sediments. Lineations on the

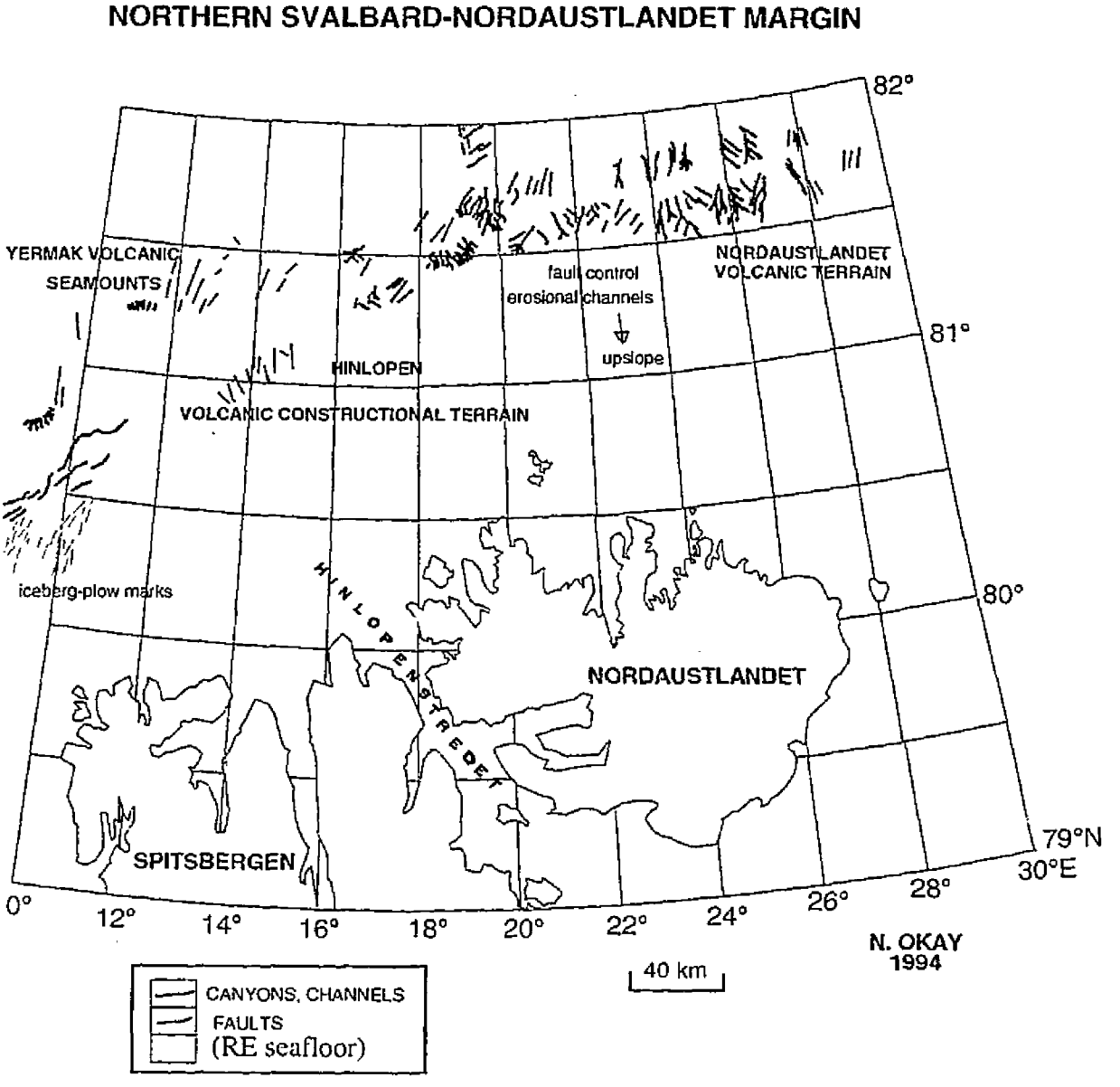

Figure 4-5. A geological interpretation along the northern Svalbard-Nordaustlandet Margin. The main features, obtained from the SeaMARC-II side-looking sonar imagery, are: glacial canyons, erosional channels, iceberg-plow marks, faults, seamounts, and highly reflective seafloor (RE seafloor) either debris terrain or seafloor basalts.

Figure 4-6. Iceberg-plow marks on the southwestern Yermak Plateau. Plow marks trend parallel to the edge of the Yermak Plateau along the northern Svalbard Margin. The orientation of iceberg-plow marks (Upslope) indicates the direction of the Spitsbergen Current during the last glacial event. The SeaMARC-II side-looking sonar imagery (10 km-wide swaths) is projected onto a plan-view, polar stereographic reference frame. The imagery is displayed in shades of gray with acoustic shadows as white and strong reflections as black. The white corridor in the middle of the imagery is the sonar vehicle path.

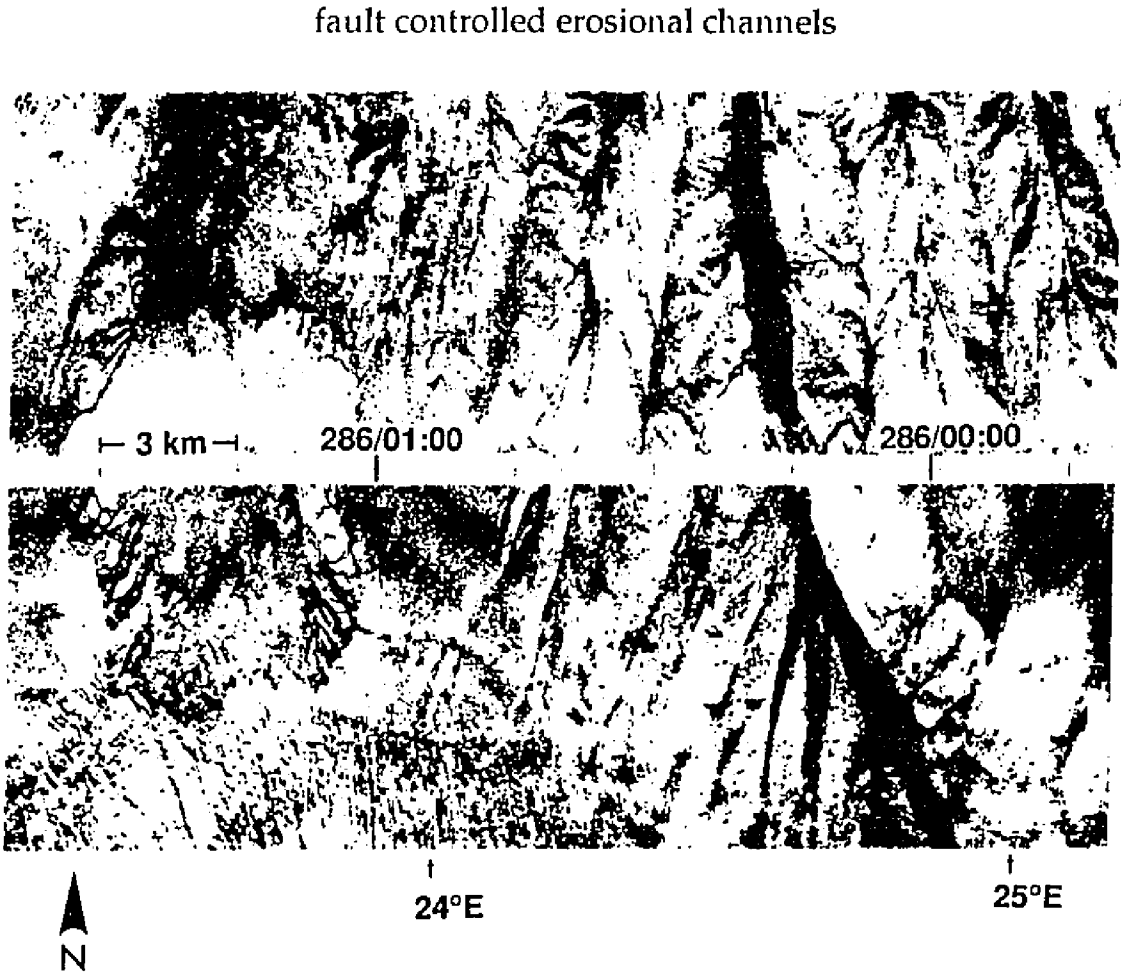

Figure 4-7. Fault controlled glacial canyons and erosional channels on the Nordaustlandet Margin.

surface sediments indicate the presence of strong bottom currents. For example, bottom currents flow northward around Svalbard and may help to modify the glacial valleys and channels along the northern Nordaustlandet Margin (Pfirman, 1989). Canyons appear to be controlled by the many pre-existing N-S trending faults dominating this margin. These faults may still be associated with volcano-tectonic activity in the region. If one traces the faults onto or adjacent to Nordaustlandet, one notices several igneous provinces bounding the steeply dipping scarps.

ii. Volcano-Tectonic Features

Volcanics and faults along the northern Svalbard-Nordaustlandet Margin are indicated in Figure 4-8 (Prestvik, 1978; Hjelle and Lauritzen, 1984; Lauritzen and Ohta, 1984). Basalts are very common in Spitsbergen and Nordaustlandet (Harland, 1971; Prestvik, 1978; Birkenmajer, 1981). Indeed, volcanic and tectonic features often coincide on Svalbard. For example, Quaternary volcanic centers and active thermal springs are located along the Raudfjørden Fault Zone in western Spitsbergen. Tertiary plateau basalts are found along the Billefjørden Fault Zone on eastern Spitsbergen. Lower Cretaceous and Mesozoic volcanics are exposed along the Lomfjørden, Rijpfjørden, and Lady Franklinfjørden Fault Zones on both sides of Hinlopenstretet, on Nordaustlandet and Kong Karls Land.

In the marine environment, three distinctive regions of high reflectivity-high backscatter seafloor associated with highly-reflective fault scarps are observed from sonar images of the northern Svalbard Margin (Figure 4-8). The three regions are:

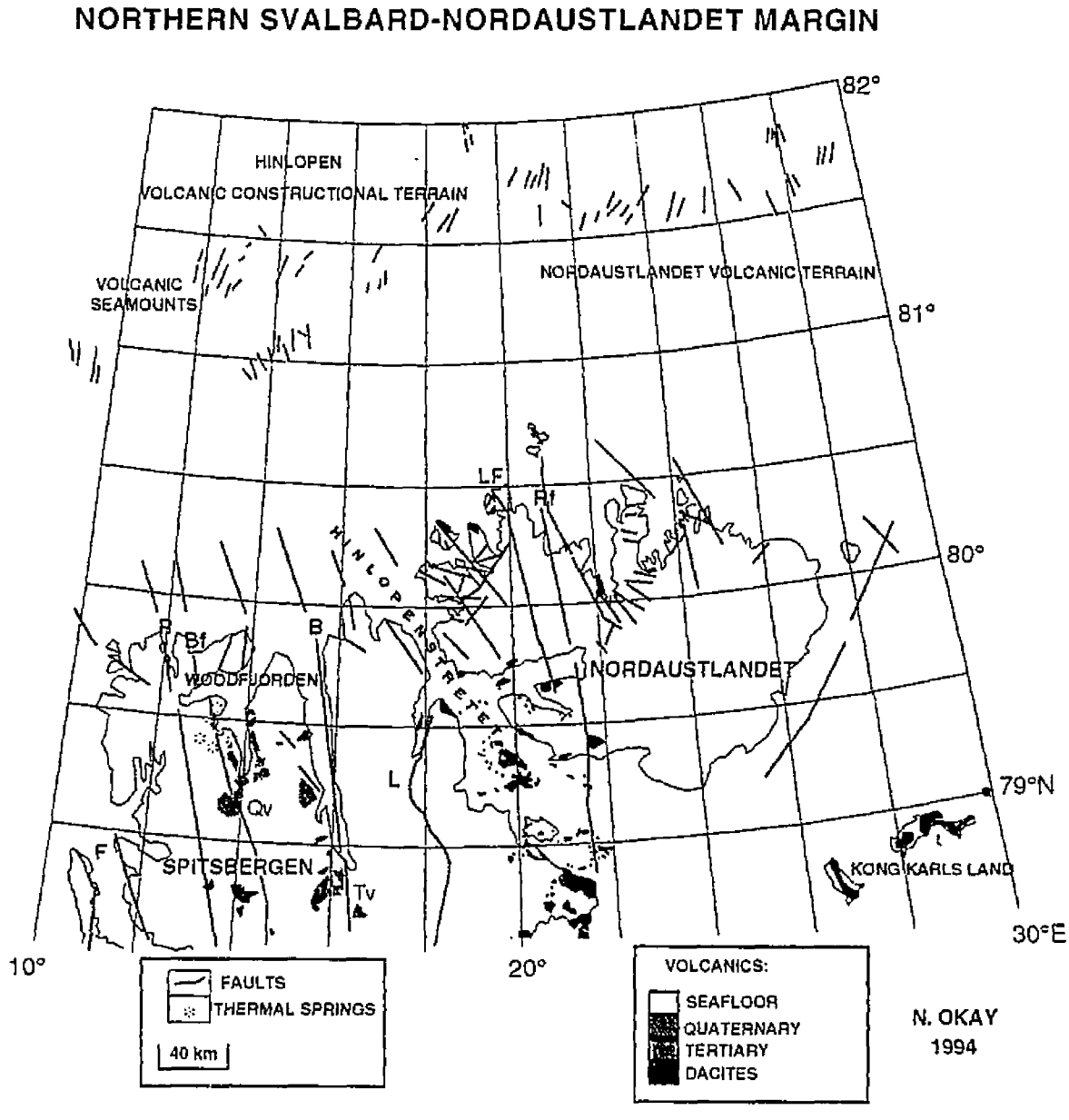

Figure 4-8. Volcanics of Spitsbergen and Nordaustlandet. Various published maps and sources are used (Prestvik, 1978; Hjelle and Lauritzen, 1984; Lauritzen and Ohta, 1984). Regions of highly reflective seafloor (SEAFLOOR) are likely submarine volcanics provinces that occur along the major faults. Qv: Quaternary volcanic centers, Tv: Tertiary volcanics. Fault Zones: Billefjørden (B), Bockfjørden (Bf), Foreland (F), Lomfjørden (L), Lady Franklinfjørden (LF), Raudfjørden (R), Rijpfjørden (Rf).

the Yermak Seamount, the Hinlopenstretet and Nordaustlandet highly-reflective ("presumed volcanic") Terrain. Because they are marine extensions of terrestrial volcanism, it is highly likely that they are volcanic as well.

In the first marine presumed-volcanic region, an elongate seamount (the Yermak Seamount) is found at 12°E. The feature can be seen in both the side-looking sonar imagery and bathymetry (Figure 4-9). The seamount has an overall diameter of about 15-20 km. Highly reflective flank flows are located at its base. Several linear features adjacent to the volcanic feature are characterized by high acoustic back-scatter. These linear features are interpreted to be highly reflective fault scarps that face inwards toward the seamount. The NW-SE trending faults are located directly north of several extensional fault zones, namely: the Raudfjørden Fault Zone (12°E), and the Bockfjørden Fault Zone (13°E) associated with Quaternary volcanic centers in northern Spitsbergen.

The second presumed-volcanic region is observed between 14°E and 17°E (Figure 4-10) and is characterized by several volcanic seamounts, bordered by faults, detected in the sonar imagery. Linear features with high acoustic back-scatter are interpreted to be highly reflective fault scarps trending NW-SE and are located directly north of several extensional fault zones, namely: Billefjørden Fault Zone (16°E), and Lomfjørden Fault Zone (18°E), associated with Tertiary and Quaternary volcanic centers in Spitsbergen. These faults are oriented in the direction parallel to the Billefjørden Fault Zone, which cuts through Spitsbergen south to north along Hinlopenstretet and where Tertiary volcanic centers are exposed. This region is

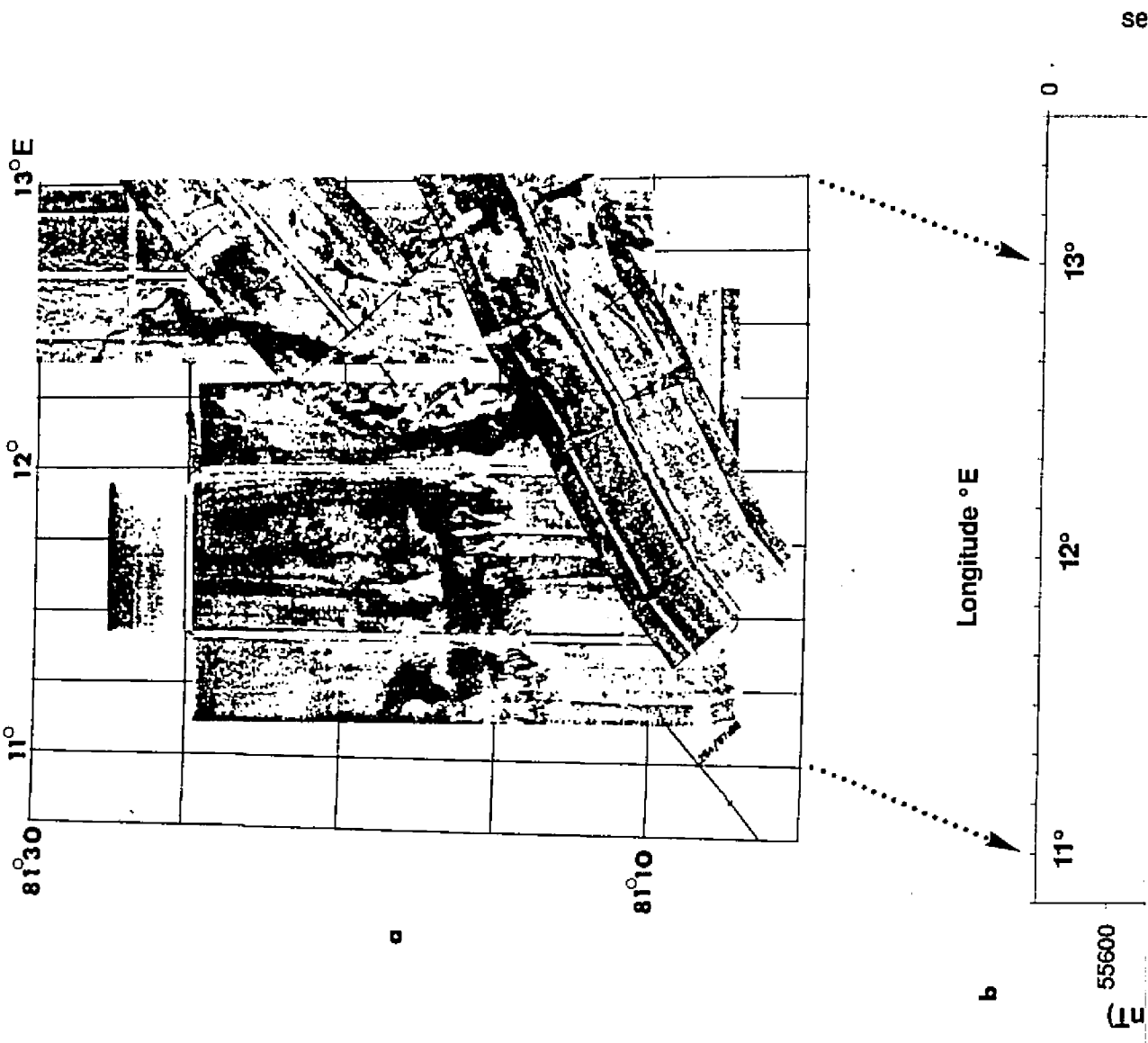

Figure 4-9. (a) Side-looking sonar imagery of the Yermak Seamount on the northern Svalbard Margin ("C" in Plate 1, Appendix B). (b) shaded areas indicate seafloor bathymetry, dark squares total magnetic field over the Yermak Seamount. This region is bordered by faults, and is characterized by a relatively high magnetic field. Major fault zones, and Quaternary volcanic center on Spitsbergen are indicated (11°E on B refer to 11°E on A.)

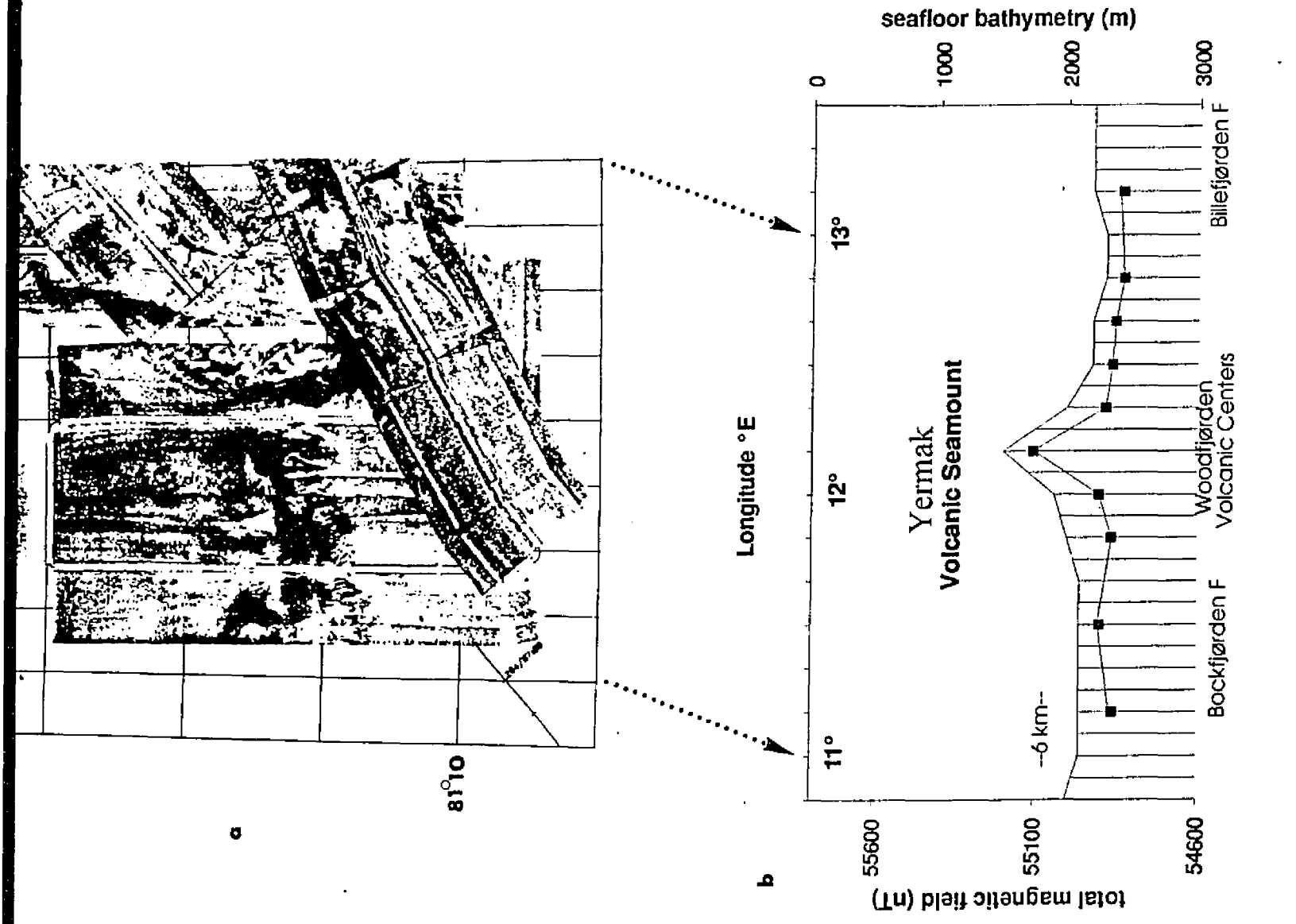

-looking sonar imagery of the Yermak Seamount on the
argin ("C" in Plate 1, Appendix B). (b) shaded areas indicate
dark squares total magnetic field over the Yermak Seamount.
ed by faults, and is characterized by a relatively high magnetic
nes, and Quaternary volcanic center on Spitsbergen are indicated
11°E on A.)

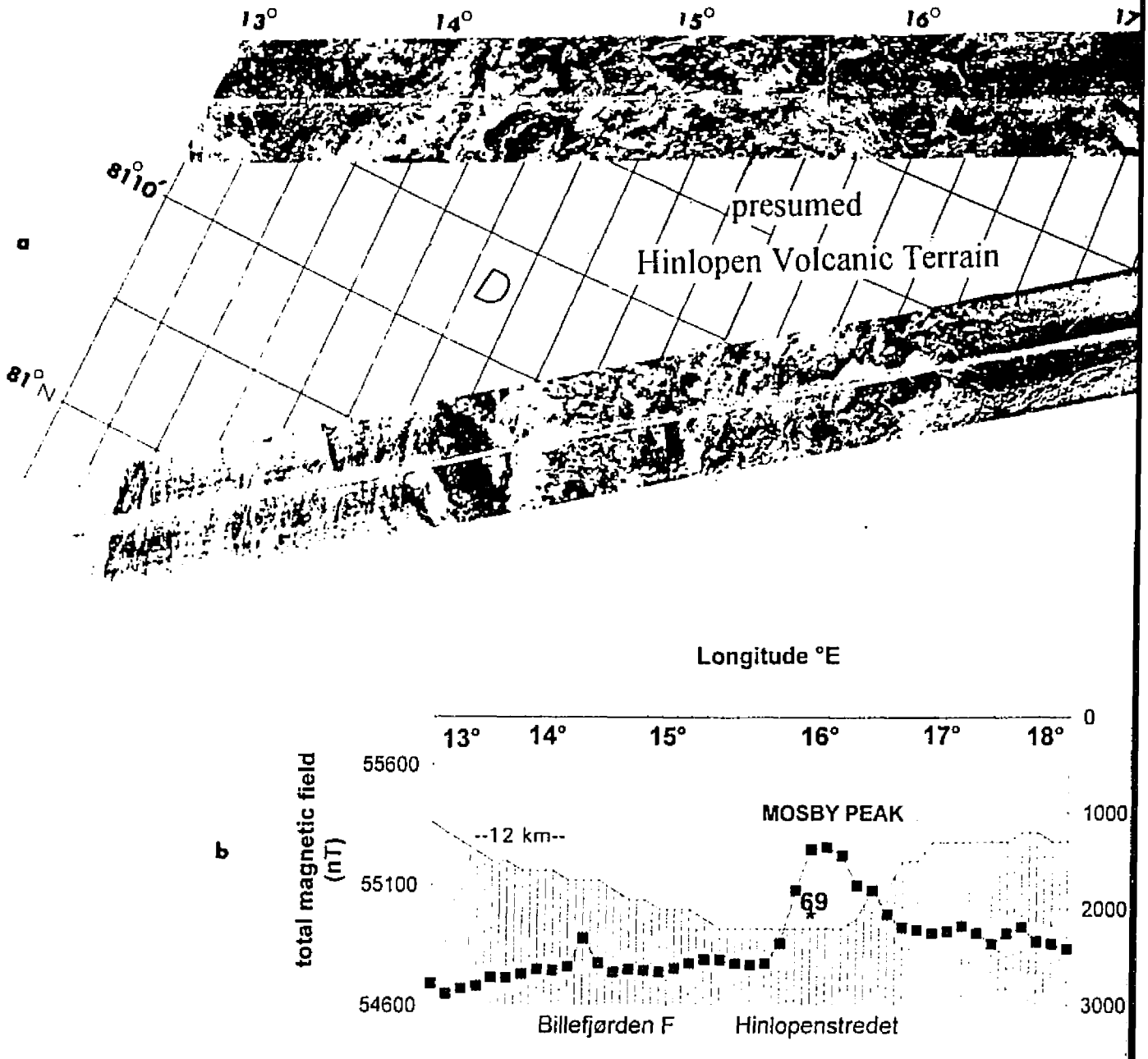

Figure 4-10. (a) Side-looking sonar imagery of the Hinlopen Volcanic Terrain on the northern Svalbard-Nordaustlandet Margin (marked with "D" in Plate 1, Appendix B). (b) Seafloor bathymetry and heat flow are superimposed. This region is bordered by faults and has high total magnetic field (dark squares) over the *Mosby Peak*.

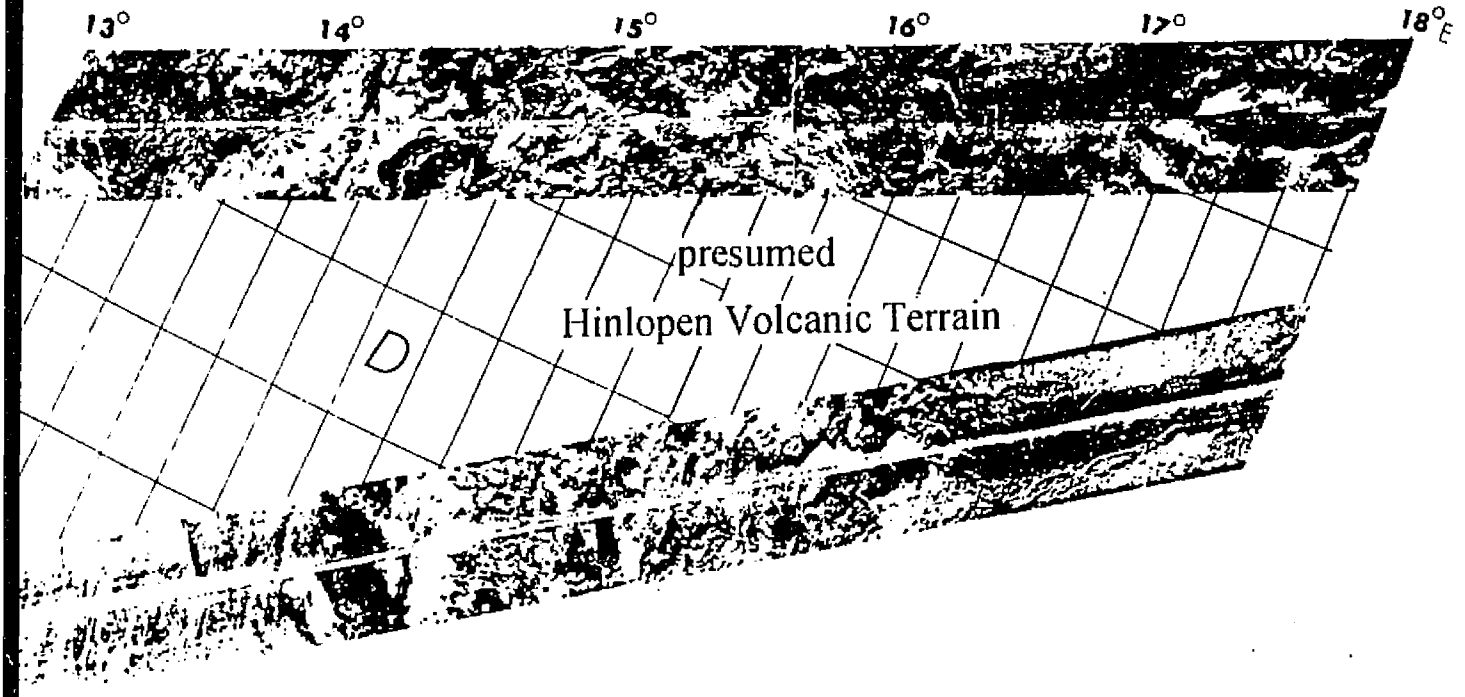

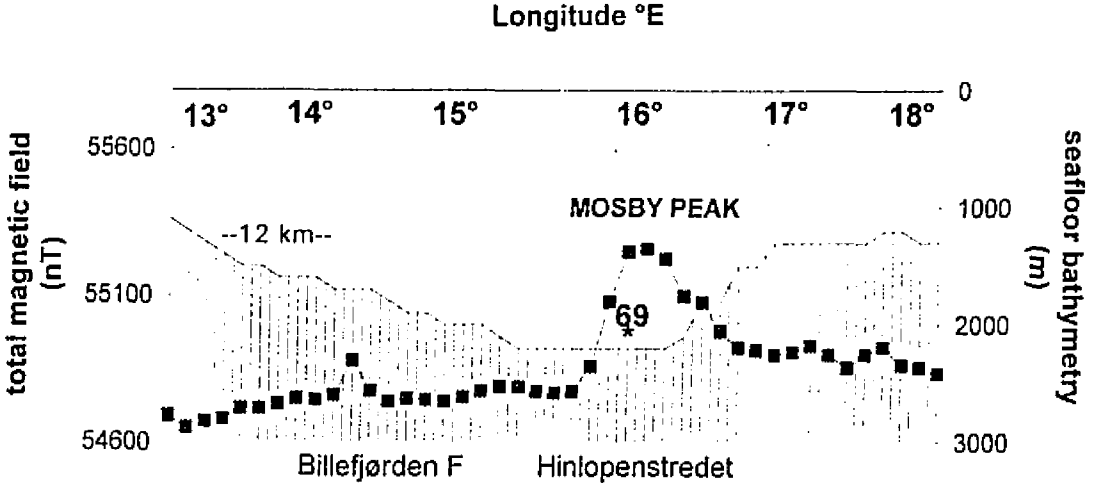

ng sonar imagery of the Hinlopen Volcanic Terrain on
austlandet Margin (marked with "D" in Plate 1, Appendix
and heat flow are superimposed. This region is
gh total magnetic field (dark squares) over the *Mosby*

interpreted to be volcanic constructional terrain (the Hinlopen Volcanic Terrain) covered by volcanic lavas, because the seafloor is also characterized by a large-amplitude magnetic anomaly (Figure 4-10). The Hinlopen presumed-Volcanic Terrain is 60-80 km wide and located between the Widjefjørden and Hinlopenstretet. A volcanic cone (at 16.5°E) is detected in this volcanic constructional terrain. This volcanic cone (*Mosby Peak*) is located directly north of the Quaternary volcanic center in the Woodfjørden region, and is marked by a significantly high amplitude magnetic anomaly (250 nT, Figure 4-10).

The third presumed-volcanic region (Nordaustlandet Terrain) is located north of northeastern Nordaustlandet (Figure 4-11). Here, strong acoustic reflections suggest either volcanic flows or regions covered by glacially derived talus. However, subaerial fissure-fault controlled lavas, associated with Mesozoic plateau basalts on Nordaustlandet and Kong Karls Land probably extend into the submarine Nordaustlandet Terrain. These faults also coincide with the erosional channels that cross the northern Nordaustlandet Margin. In Figure 4-11 a bathymetric profile indicates the rough nature of the seafloor. The faults are located directly north (24°E) of the Rijpfjørden and Lady Franklinfjørden Fault Zones in Nordaustlandet. For this reason it is highly likely that the Nordaustlandet Terrain is at least in part of volcanic origin.

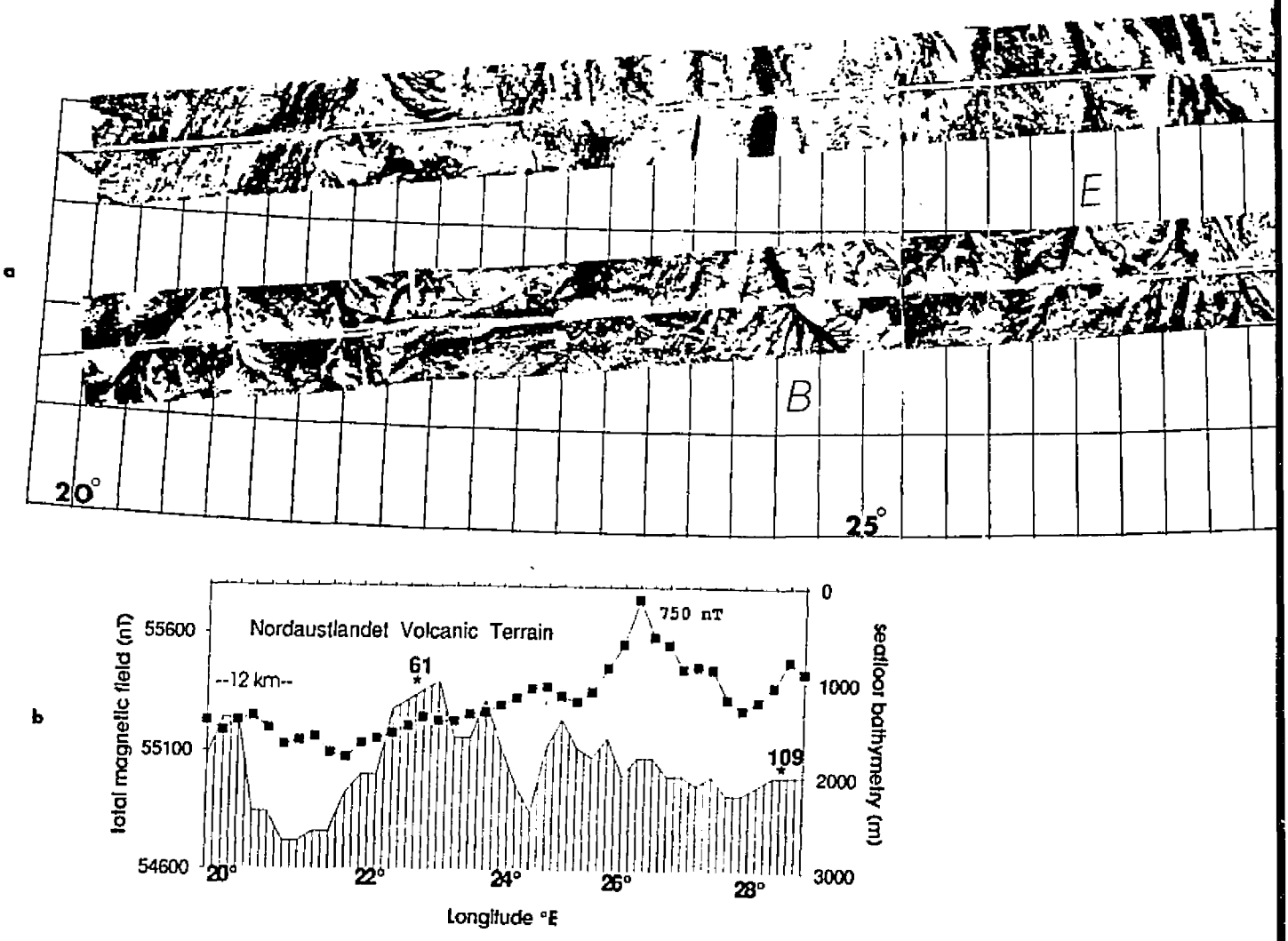

Figure 4-11. (a) Sonar imagery along the northern Nordaustlandet Margin fault controlled patches of highly reflective seafloor, glacial canyons and channels ("B" and "E" regions in Plate 1, Appendix B). (b) Seafloor bathymetry, high heat flow, and high total magnetic field (dark squares) are indicated.

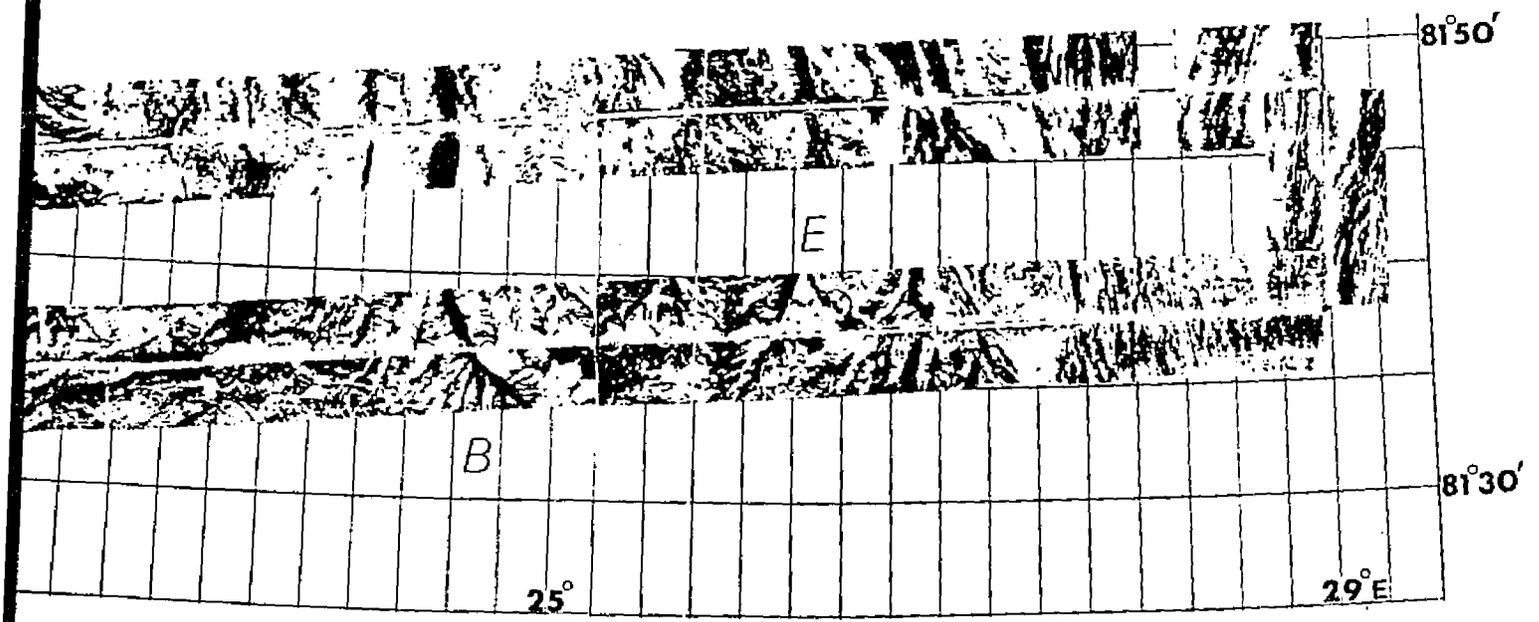

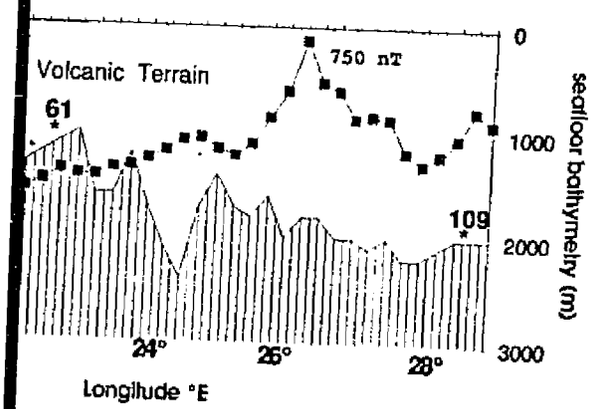

the northern Nordaustlandet Margin fault
eafloor, glacial canyons and channels ("B" and
) Seafloor bathymetry, high heat flow, and
are indicated.

c. Geophysical Characteristics:

The surveyed region lies outside of the clearly defined magnetic anomaly province which is characteristic of the Eastern Arctic Ocean Seafloor. However, high amplitude magnetic fields are indicative of seafloor volcanism in the region (Figure 4-12). The Yermak Seamount in particular is marked by an increase in magnetic amplitude of 102 nT over background (Figure 4-9). The Hinlopen Volcanic Terrain is characterized by a large-amplitude magnetic anomaly and a high heat flow province (Figure 4-10). The region of high heat flow on the southwestern Yermak Plateau (104-138 mW/m^2, Crane *et al.*, 1982) corresponds to a high-amplitude total-magnetic field (250 nT, Okay *et al.*, 1991) which is comparable to the magnetic field of Mosby Peak and nearby Quaternary volcanic centers on Spitsbergen (Prestvik, 1978). Another region where the total magnetic field is noticeably high is at 29°E where faults and volcanic-looking features are detected along the northern Nordaustlandet Margin (Figure 4-11). In addition, along the northeastern Nordaustlandet Margin, the mapped high amplitude total magnetic field (750 nT) correlates with off-axial heat flow highs (77 and 109 mW/m^2 in Figure 4-13; Sundvor and Torp, 1987). High heat flow, and magnetic data suggest that the Nordaustlandet Volcanic Terrain may not be as old as the dacitic lavas in the surrounding area. If this is correct then the crust must be rejuvenated by some sort of magmatic source beneath the Svalbard Archipelago.

The distribution of present-day earthquake activity in the northern Svalbard and Nordaustlandet regions is shown in Figure 4-13. Noticeable earthquake activity has been recorded along the major faults (the Rijpfjorden and Lady Franklinfjorden

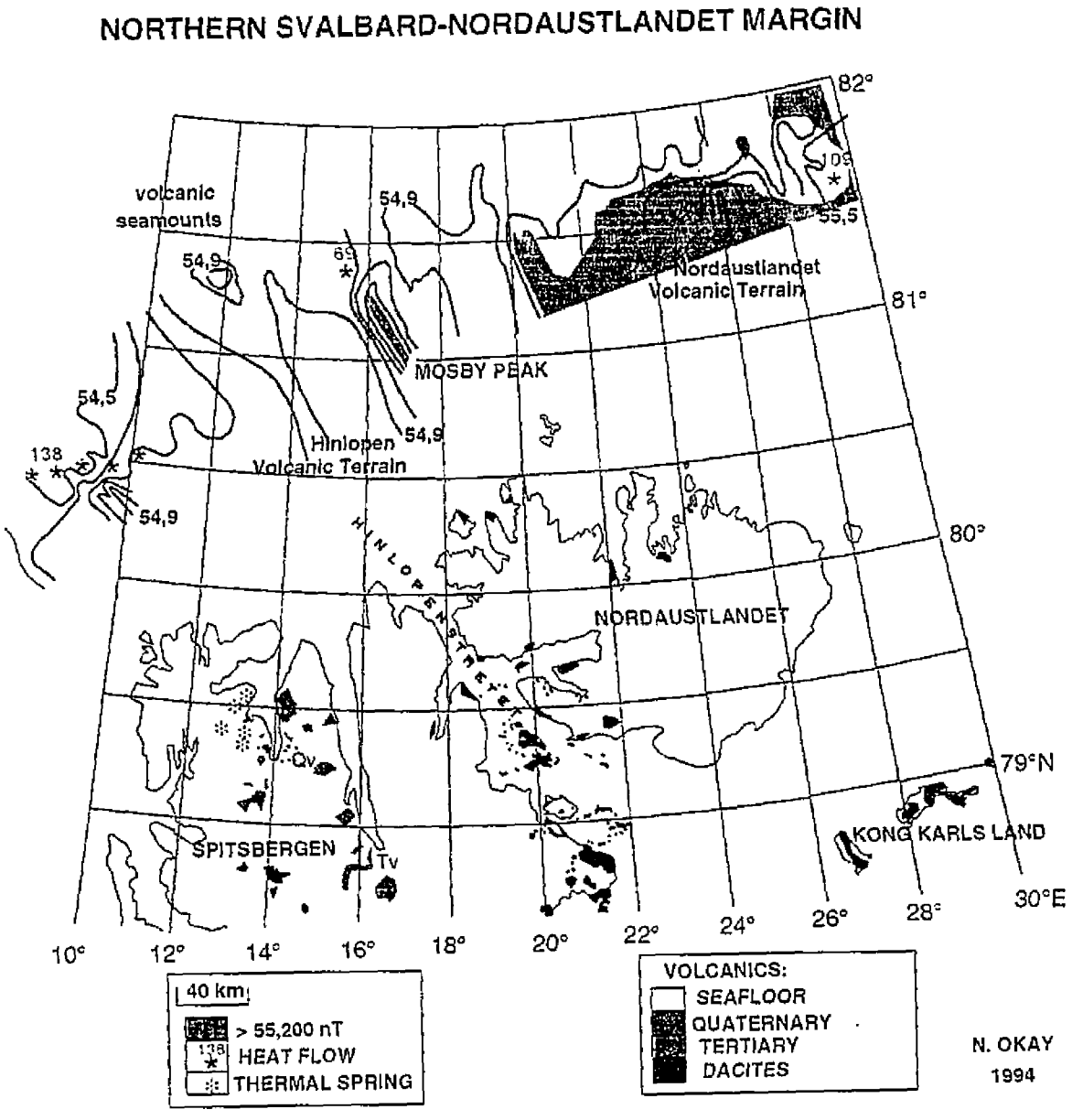

Figure 4-12. Total magnetic field along the northern Svalbard-Nordaustlandet Margin. Contour intervals are in 100 nT. Volcanic, "presumed" seafloor basalts of undetermined age (SEAFLOOR), tectonic features, and heat flow are indicated.

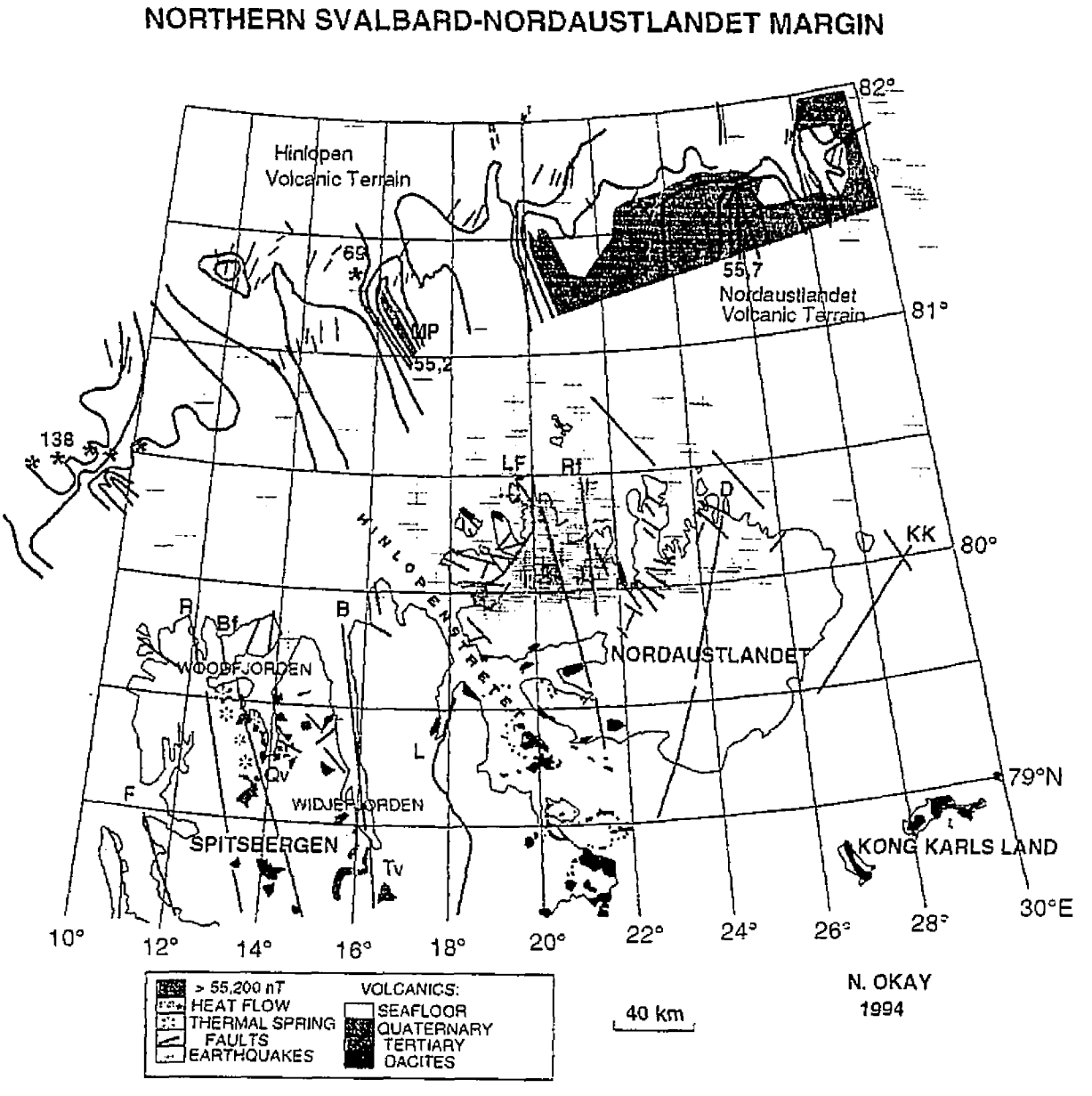

Figure 4-13. Geology and geophysics: Northern Svalbard-Nordaustlandet Margin. Magnetics, "presumed" volcanic provinces, faults and heat flow all correspond to the loci of off-axial volcanic centers along the Nordaustlandet Margin. SEAFLOOR: highly reflective seafloor, Qv: Quaternary volcanic centers, Tv: Tertiary volcanics. MP: Mosby Peak, KK: Kong Karls Land Fault Zone.

Fault Zones) of Nordaustlandet (Mitchell *et al.*, 1979; Bungum *et al.*, 1982; Mitchell *et al.*, 1990). This concentrated earthquake zone extends along the seafloor, where faults can be observed on sonar imagery. Two concentrated seismic zones are observed around 16°-24°E and 30°E (Figure 4-14). Mitchell *et al.* (1990) suggest that fault plane solutions indicate the maximum-principal stress axis to lie E-W (normal to the western continental margin. As this region is more than 200 km away from the plate boundary, earthquake concentrations plus high heat flow and high amplitude magnetic anomalies suggest that the region may be undergoing thermal rejuvenation and diffuse rifting.

2. The Molloy Transform Fault and Western Svalbard Margin

a. Geological Interpretations:

i. Sedimentary and Glacial Features

A geological interpretation of the SeaMARC-II side-looking sonar imagery (Figure 4-15) along the Western Svalbard Margin is illustrated in Figure 4-16. The main features mapped are: faults, volcanic flow, volcanic cones, craters, pock marks, and fault controlled slumping on the Western Svalbard Margin where the propagating Knipovich Ridge intersects the oblique Molloy Transform Fault.

Thick sediments that cover older features on the seafloor (Figure 4-15). Due to its close proximity to the continental margin, the plate boundary (comprised of the northern Knipovich Ridge and the Molloy Transform Fault) are often covered by the thick sediments which cover older features on the seafloor. The continental margin is

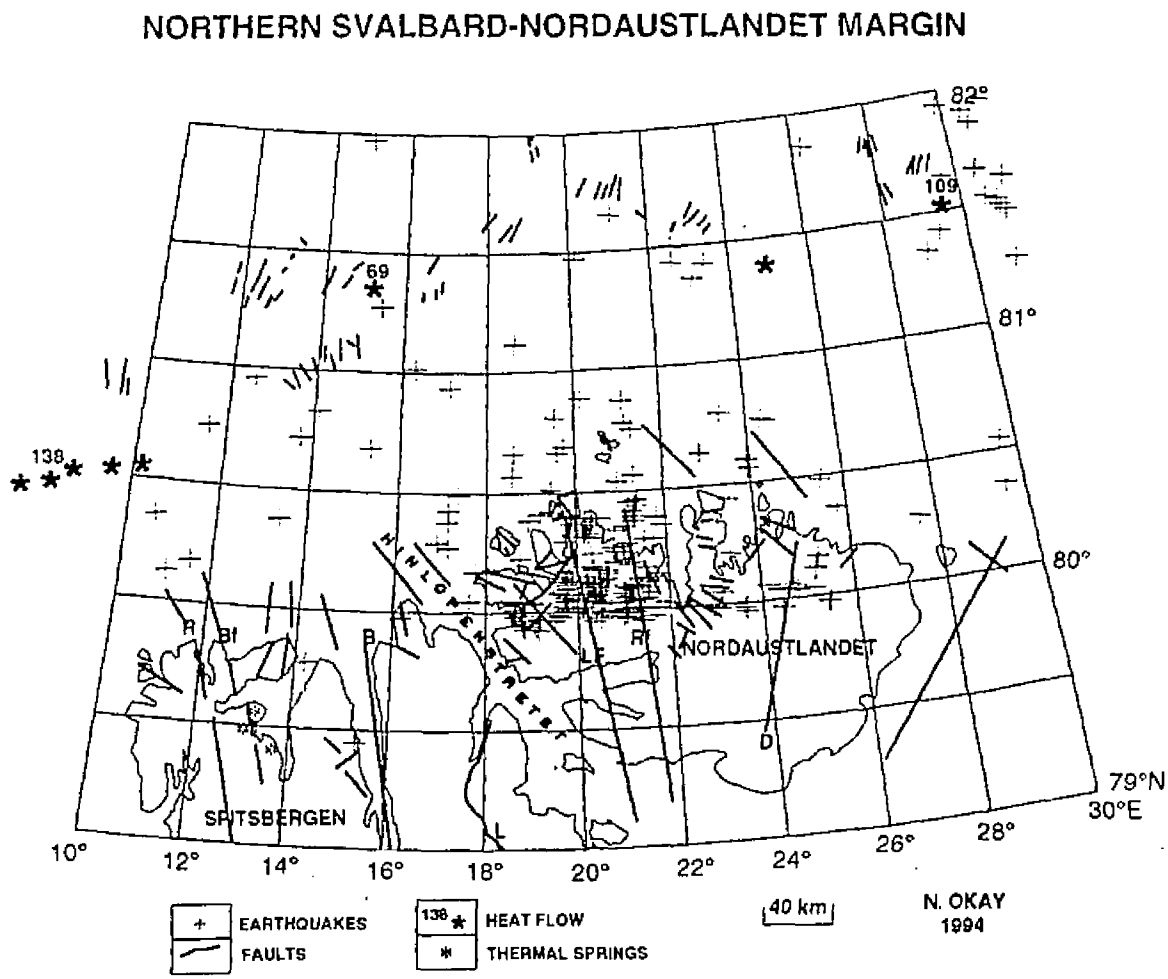

Figure 4-14. Distribution of earthquakes in the Svalbard and Nordaustlandet regions. Earthquakes occur along the major faults in the islands and continue to the seafloor (Mitchell *et al.*, 1979; Bungum *et al.*, 1982; Mitchell *et al.*, 1990). Fault Zones: Foreland (F), Raudfjørden (R), Bockfjørden (B), Billefjørden (Bf), Lomfjørden (L), Lady Franklinfjørden (LF), Rijpfjørden (Rf).

Figure 4-15. SeaMARC-II side-scan sonar imagery along the Western Svalbard Margin. The sonar images reveal the intersection of the Knipovich Ridge with the Molloy Transform Fault.

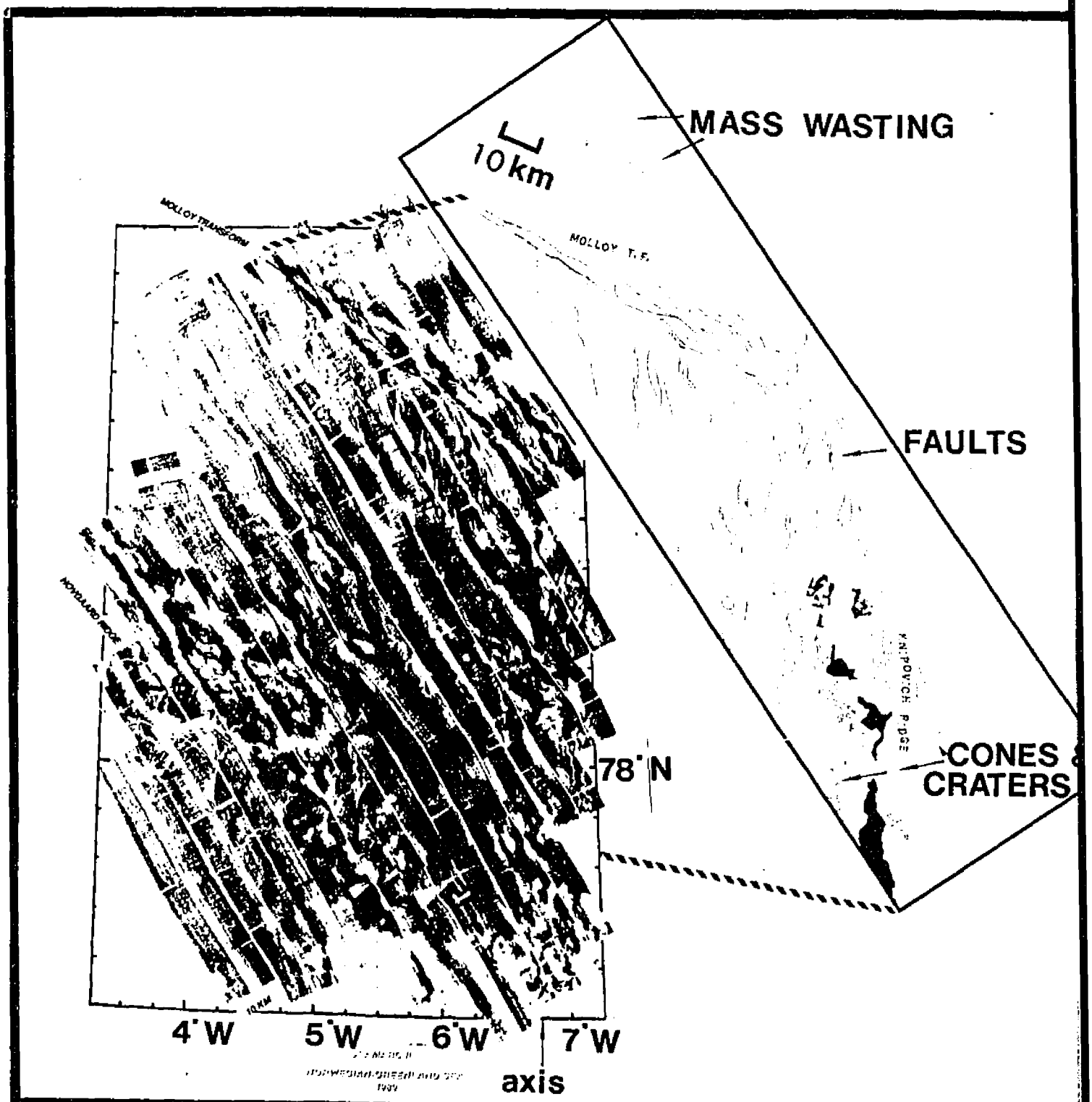
MASS WASTING
10km
FAULTS
CONES &
CRATERS
78°N
4°W
5°W
6°W
7°W
axis
MOLLOY TRANSFORM
MOLLOY T.F.
KNIPOVICH RIDGE

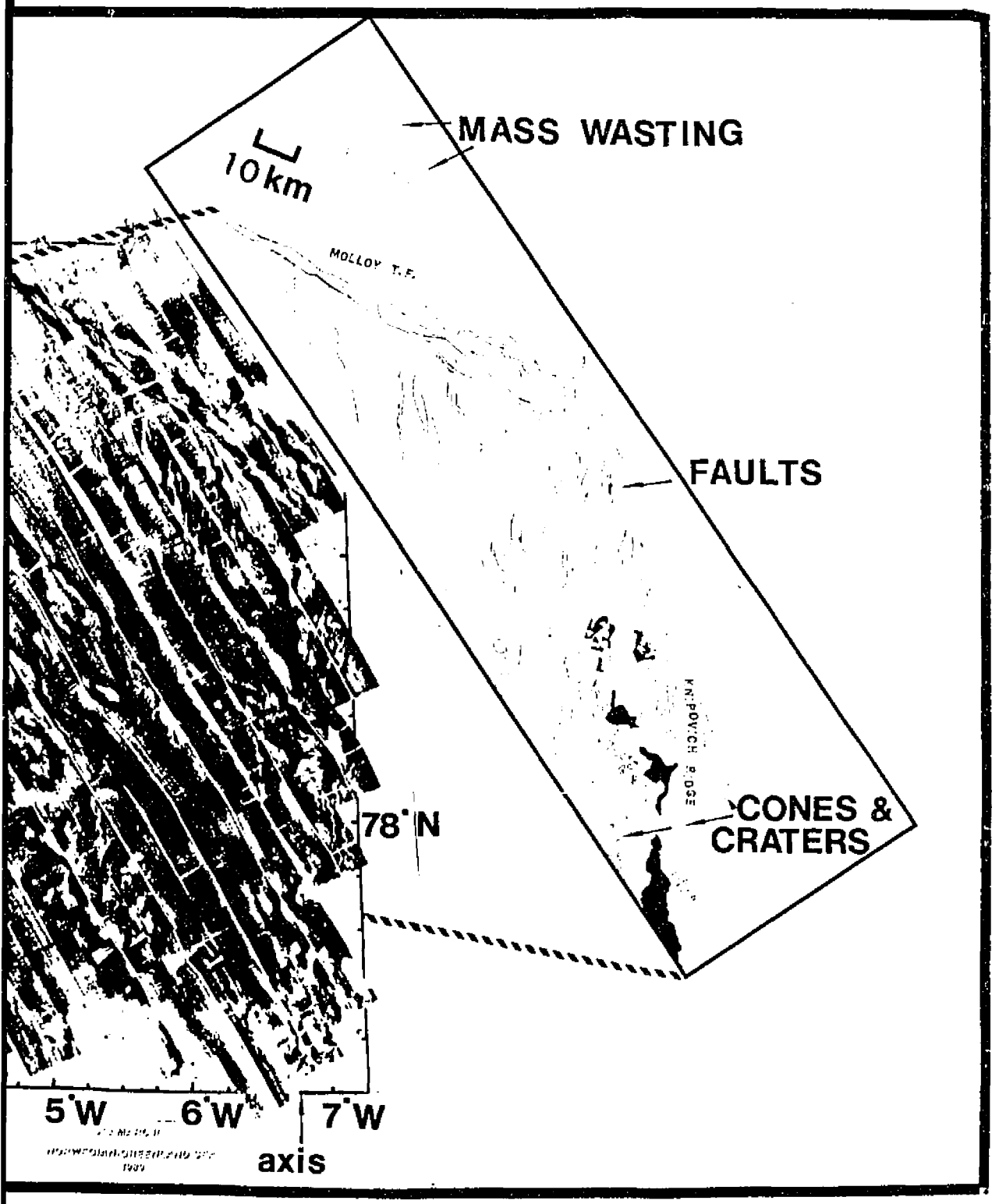
MASS WASTING
10km
MOLLOY T.F.
FAULTS
78°N
CONES &
CRATERS
5°W
6°W
7°W
axis

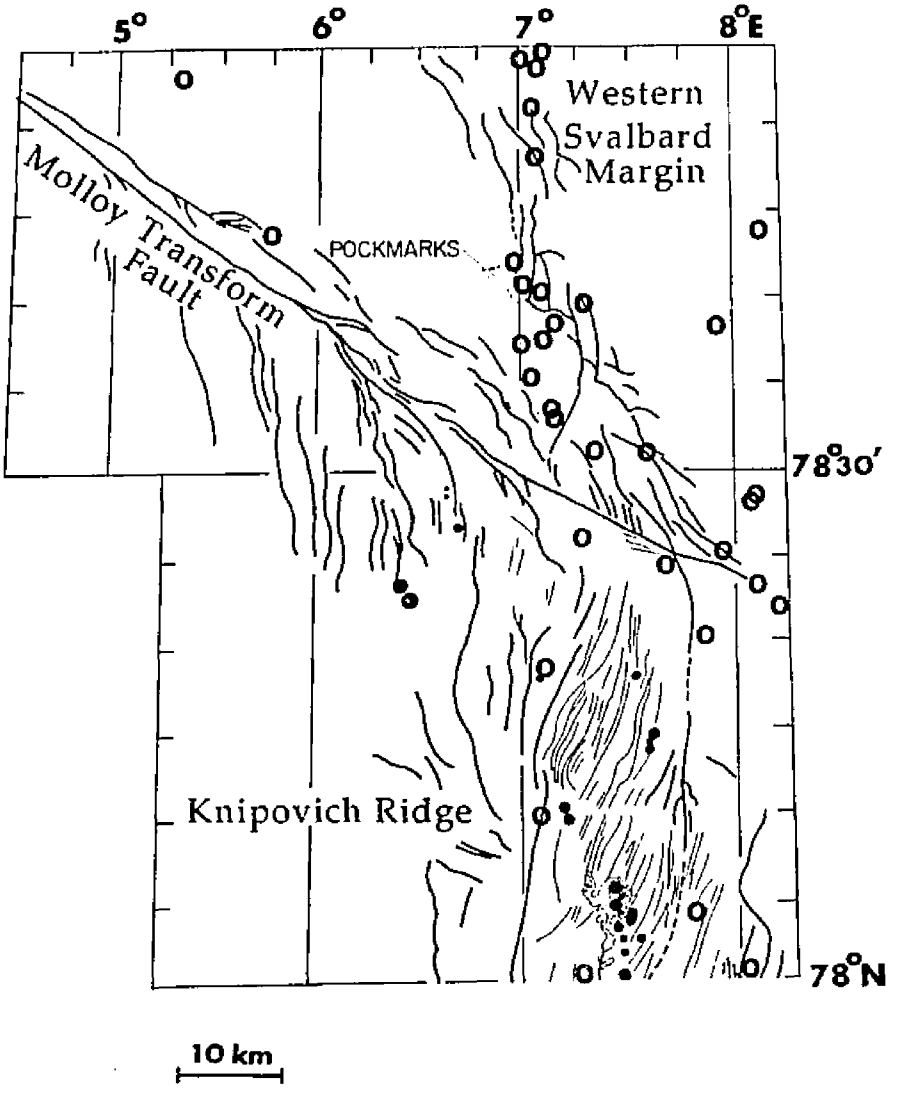

Figure 4-16. Structural and volcanic interpretation of the northern Knipovich Ridge and the Molloy Transform Fault along the Western Svalbard Margin. SeaMARC-II side-scan sonar images reveal the double-fault of the Molloy Transform at its intersection with the northern Knipovich Ridge. Open circles represent earthquakes. Solid lines represent faults, black patches indicate cones, craters and lava flows, stippled areas represent downslope transport of sediment (Crane and Solheim, 1995).

characterized by rapid progradation heavily influenced by repeated Quaternary glaciations and possibly bottom currents. Adjacent to the Svalbard margin the seafloor is subjected to constant mass wasting. Only a few slump scars were imaged near the thickly sedimented slopes at the Molloy Transform area (Figure 4-16). Possible bottom-current generated features appear in side-looking sonar images near the Molloy Transform (Figure 4-15). Their location in proximity to this active fault means that a tectonic origin cannot be ruled out.

Pockmarks were imaged, scattered across the thick sediments atop anticlinal structures. Pockmarks appear as small dark speckles, barely resolvable in the side-looking sonar imagery (Figure 4-16). These features are thought to have been derived by methane venting and their distribution is associated with high heat flow that might cause the thawing of subjacent clathrates below the sedimentary layers (Figure 4-17).

ii. Volcano-Tectonic Features

The most prominent volcano-tectonic features in this region are at the intersection of the northern Knipovich Ridge and the Molloy Transform Fault. This section of the plate boundary is characterized by ultra-slow, oblique and asymmetric spreading along the transform fault. The neo-tectonic Molloy Transform, a double-fault, is covered by thick sediments. Near the intersection of the northern Knipovich Ridge and Molloy Transform Fault (78°30' N, 7°E), the offset between the double faults reaches 8 km. In the intersection region, ridge related faults (and some off-axial

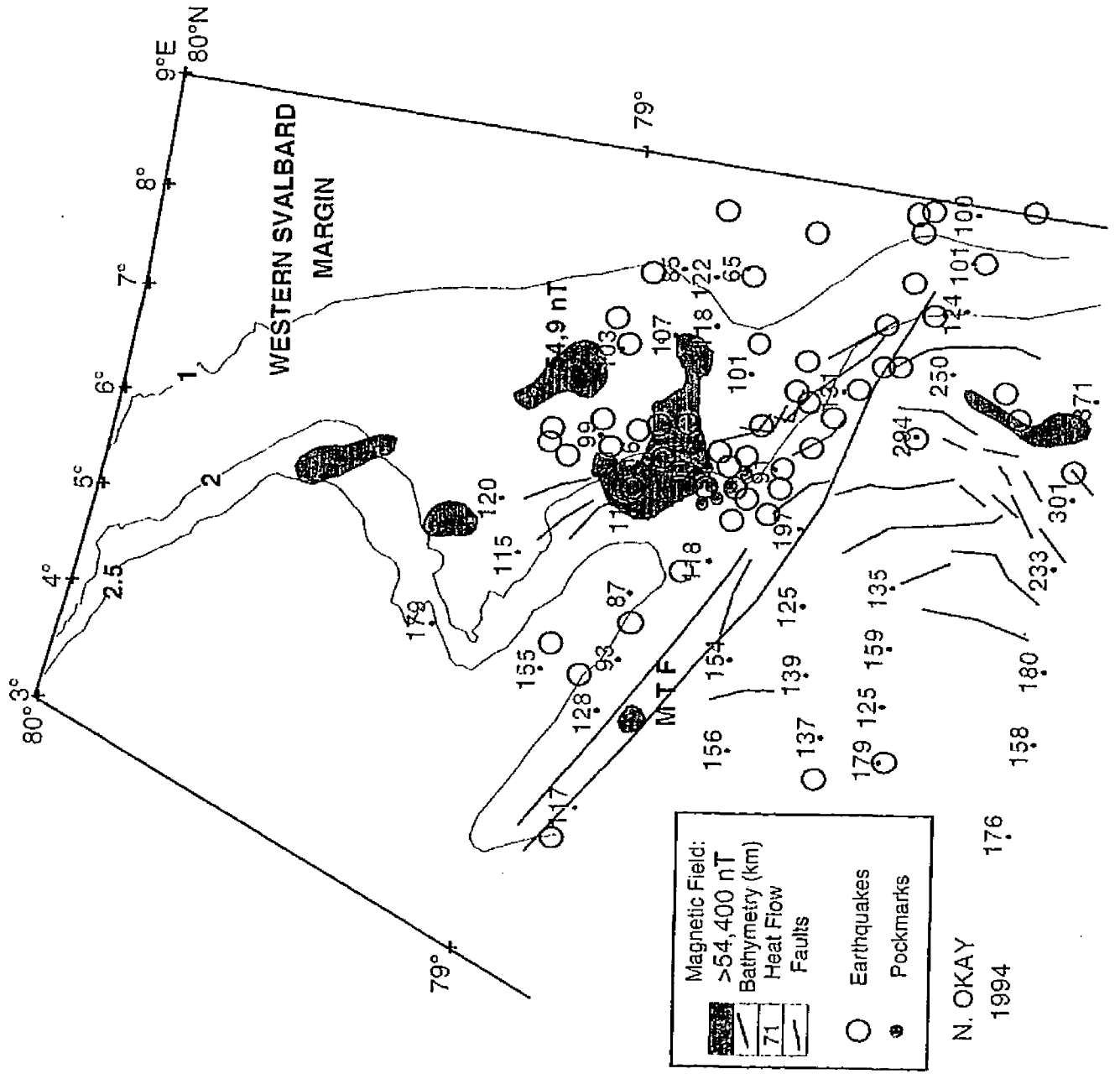

Figure 4-17. Geophysical data at the intersection of the northern Knipovich Ridge/Molloy Transform Fault along the Western Svalbard Margin. Bathymetry is indicated (1 km contour interval). Heat flow data are as reported by Crane *et al.* (1991). High magnetic field regions (>54,400 nT) and earthquakes are indicated. Distribution of earthquakes provided from Bungum *et al.* (1982) and Mitchell *et al.* (1990). Notice concentrated earthquake zone lies south-north (at 7°E, 78°40' N) where pockmarks and high heat flow and high-amplitude total-magnetic field are also found. MTF: Molloy Transform Fault, KR: Knipovich Ridge.

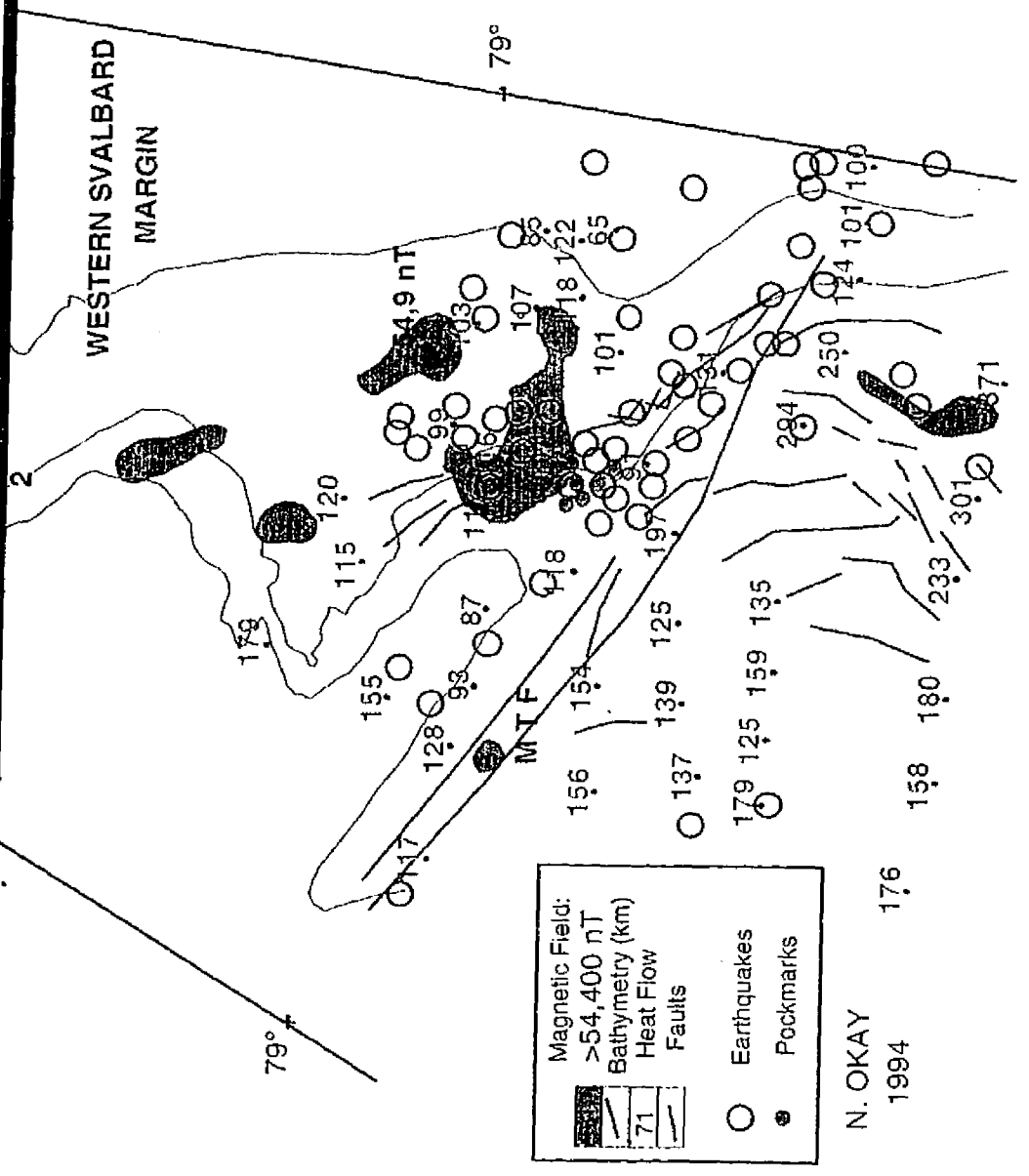

sical data at the intersection of the northern Knipovich
rm Fault along the Western Svalbard Margin. Bathymetry is
ur interval). Heat flow data are as reported by Crane *et al.*
ic field regions (>54,400 nT) and earthquakes are indicated.
uakes provided from Bungum *et al.* (1982) and Mitchell *et al.*
ntrated earthquake zone lies south-north (at 7°E, 78°40' N)
high heat flow and high-amplitude total-magnetic field are also
Transform Fault, KR: Knipovich Ridge.

faults) bend towards the transform trend, north to northwest. A broader belt of deformed lineations striking 30° to 45° with respect to the transform trend, can be found up to 10-30 km SW of the transform axis. Volcanic cones, craters and lava flows are located only in the northern Knipovich Ridge valley (Figure 4-17). South of the intersection region, faults on the flank of the rift valley make a V-shaped pattern which point towards the intersection of the northern Knipovich Ridge and Molloy Transform Fault (Doss *et al.*, 1991; Okay *et al.*, 1993).

b. Geophysical Characteristics:

Seismological data from Sykes (1965), Bungum *et al.* (1979, 1982, 1990) and Mitchell *et al.* (1979, 1990) indicate significant earthquake activity concentrated at the intersection of the northern Knipovich Ridge and the Molloy Transform along the Western Svalbard Margin (Figure 4-16). However, near 7°E, the distribution of earthquakes is highly concentrated in a N-S direction and extends significantly north of the Knipovich Ridge/Molloy Transform Fault intersection. Superposition of the epicenters on the structural map shows the close correlation between sonar imagery, and fault lineations and earthquakes, suggesting that these orthogonal lineations are most likely active faults. That the N-S oriented faults and are a direct extension of the Knipovich Ridge suggests that recent propagation of the ridge may be proceeding north of the Molloy Transform Fault.

High heat flow (>150 mW/m^2) along the Western Svalbard Margin (Figure 4-17) was observed at the tip of the northern Knipovich Ridge and the Molloy

Transform Fault. In addition, certain regions along the northern Knipovich Ridge, Molloy Transform Fault and Western Svalbard Margin were characterized (during the SeaMARC-II Survey) by a total magnetic field higher than 54,400 nT (Figure 4-17). Five of the six zones of high-amplitude magnetic field lie within a corridor of relatively high heat flow (125-150 mW/m^2), which extends northwest of the intersection of the Knipovich Ridge with the Molloy Transform, into and along the seismically active faults mentioned above, lending further credence to the idea that rift propagation is ongoing north of the Molloy Transform Fault. Sandwiched between these two belts of high heat flow lies a 40 km long lenticular-shaped region of low heat flow (<100 mW/m^2) parallel and north of the Molloy Transform Fault (Figure 4-17).

D. SUMMARY OF SeaMARC-II DATA RESULTS

SeaMARC-II data were collected to resolve the plate tectonic evolution of the northern Norwegian-Greenland Sea margins and to map seafloor and geological features. SeaMARC-II data show the interaction between the slow spreading center of the northern Knipovich Ridge and one of the worlds longest fracture zones (the Spitsbergen Fracture Zone). Evidence of further northward rift propagation of the Knipovich Ridge was found on the western Svalbard Margin to the north of the

Molloy Transform. The following represent key geological processes which were detected by the SeaMARC-II imagery:

1. Iceberg-plow marks are observed on the northwestern tip of Spitsbergen (paralleling the edge of the Yermak Plateau). The direction of iceberg-plow marks indicates that large icebergs were either carried by the Spitsbergen Current from the Norwegian-Greenland Sea into the Arctic Ocean during the last glacial event, or were part of an extensive grounded but moving ice sheet in the region. Lineations carved into sediment are evidence that strong bottom currents may at times scour the shallow slopes.

2. SeaMARC-II images along the Western Svalbard Margin reveal the double-faulted Molloy Transform Fault at its intersection with the Knipovich Ridge. Heat flow, magnetics, earthquakes and pockmark terrain on the western Svalbard Margin indicate that the Knipovich Ridge is propagating northwards. Near 7°E, seismic activity is evidence for recent tectonic activity north of the Molloy Transform Fault. Three of the six zones are aligned along the N-S oriented margin boundary faults north of the Molloy Transform and within the corridor of high heat flow described above, suggesting that subjacent magmatic intrusion is now taking place. In addition to this, the identification of multiple ridge/transform trending normal faults (north of the ridge/transform intersection) suggests that the plate boundary is in the process of propagating to the North.

3. SeaMARC-II side-looking sonar imagery along the Northern Svalbard-Nordaustlandet Margin reveals off-axial zones of presumed magmatic intrusions that

have been active along the faults located directly north of the major fault zones of Spitsbergen and Nordaustlandet such as: Raudfjørden, Bockfjørden, Billefjørden, Lomfjørden, and Rijpfjørden Faults. According to interpretations of magnetic, seismic, structural, and heat flow data, I conclude that these NW-SE trending faults associated with the secondary and Tertiary detachment faults bordering the northern Svalbard-Nordaustlandet Margin are the loci of off-plate boundary volcanic intrusions and thermal rejuvenation.

In addition, regions of high total magnetic field, earthquake activity and off-axial high heat flow are coincident with highly-reflective seafloor (presumed-volcanic terrain). The combination of the above suggests that the seafloor in these regions may be volcanic in nature. The SeaMARC-II images also reveal the presence of the Yermak Seamount, a volcanic cone, and the Mosby Peak within the Hinlopen Volcanic Terrain. Higher heat flow, and magnetic data indicate that the crust in the region of the Nordaustlandet Volcanic Terrain is not as old as the dacitic lavas and therefore the continental margin in this region must be rejuvenated by either a subjacent or lateral heat source.

Chapter 5

HEAT FLOW MODELING STUDY OF THE EASTERN NORWEGIAN-GREENLAND SEA MARGINS

A. ANALYSIS OF HEAT FLOW

1. Distribution of Heat Flow Data from the Norwegian-Greenland Sea

Figure 5-1 illustrates collected heat flow in the North Atlantic, Norwegian-Greenland Sea, and eastern Arctic Ocean regions (Lachenbruch and Marshall, 1968; Langseth and Zielinski, 1974; Crane *et al.*, 1982; Jackson *et al.*, 1984; Sundvor, 1986; Sundvor and Torp, 1987; Crane *et al.*, 1988). Heat flow generally decreases with increasing crustal age and distance from the active spreading centers. However, heat flow was found to increase along the eastern margins, and in particular on the volcanic plateaus (Figure 5-1). In general, heat flow averages 124 mW/m^2 on the eastern margins, and is far in excess of heat flow on the western margins of the Norwegian-Greenland Sea (64 mW/m^2). Six regions of high heat flow can be distinguished along the eastern margins: the Vøring Plateau on the Norwegian Margin (87 mW/m^2), the Senja Margin (121 mW/m^2), the Hornsund Fault region (140 mW/m^2) on the western Svalbard Margin (at 75°N), the intersection of the northern Knipovich Ridge and Molloy Transform Fault on the Western Svalbard Margin

Figure 5-1. Heat flow in the North Atlantic Ocean, Norwegian-Greenland Sea and eastern Arctic Ocean regions. The map is compiled from Langseth and Zielinski (1974), Vogt *et al.* (1981), Crane *et al.* (1991). Stations north of 79°N are from Crane *et al.* (1982), Jackson *et al.* (1984), Sundvor (1986), and Sundvor and Torp (1987). The northern Norwegian-Greenland Sea basin adjacent to Svalbard, the Knipovich Ridge (KR), the Mohns Ridge (MR), and the southern Yermak Plateau (YP) are regions of relatively high heat flow (Crane *et al.*, 1982, 1988, 1991): the Vøring Plateau (VP), the Jan Mayen Ridge (JMR), and the Nansen Ridge (NR).

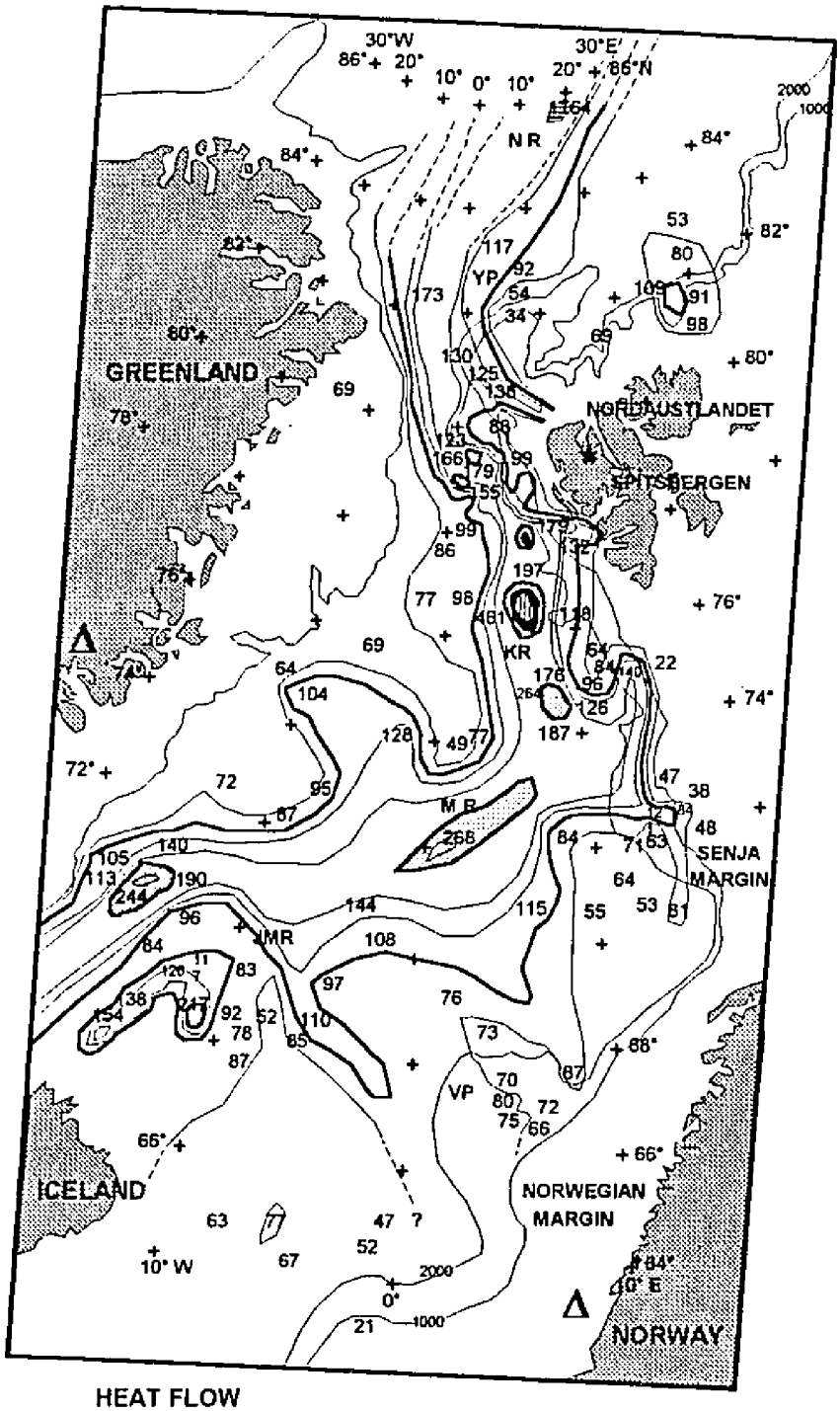

HEAT FLOW
NORWEGIAN-GREENLAND SEA

HEAT FLOW CONTOUR (>200 mW/m²)

ALKALI VOLCANIC CENTERS

THERMAL SPRINGS

N. OKAY
1994

at 78.5°N (197 mW/m^2), the southern Yermak Plateau adjacent to the northwestern Svalbard Margin (138 mW/m^2), and Northern Svalbard-Nordaustlandet Margins (109 mW/m^2).

In this thesis, I analyze heat flow data collected in the eastern Norwegian-Greenland Sea and eastern Arctic Ocean to refine an evolutionary scenario of volcanic plateau formation and thermal rejuvenation of the continental crust along transtensional passive margins. In this region, magnetic anomalies are nearly absent, thus heat flow is a significant tool to reveal the time of geologic events. Magnetic anomalies are absent along much of the Knipovich Ridge and the Senja, Western Svalbard and Northern Svalbard-Nordaustlandet Margins. Therefore, thermal-crustal ages can be compared to magnetic ages at only a few of the analyzed heat flow stations.

In this complex region, I analyze heat flow to estimate thermal crustal ages. In the following sections, I demonstrate how a propagating lateral heat source (controlled by far field kinematics) can create off-axial heat flow highs along transtensional passive margins. Data are applied to heat flow and numerical lithospheric extension models to constrain the evolutionary scenario of the eastern Norwegian-Greenland Sea. I also demonstrate how elevated heat flux can be generated by enchanced lateral thermal gradients created by asymmetric simple-shear lithospheric extension in regions where magma is intruded into paleo-shear zones. Each modeled section compares observed heat flow and seafloor bathymetry along with the best known seismic structure for the area. Seismic records are used to

determine the proximity of heat flow stations to the sediment-basement boundaries. Cross-sections are constructed from data derived from multichannel seismic refraction stations, DSDP and ODP drill sites, and sonobuoy experiment results (Appendix B).

There are still many data gaps in this study area. Due to lack of data the average sedimentation rate (from site to site) was assumed. Another uncertainty was the age of oceanic crust. For instance, poor constraints on the age, extent and direction of spreading of oceanic crust in the region of the southern Yermak Plateau led me to use an alternative method of analyzing the heat flow by applying numerical lithospheric extension modeling. It is worth noting that measured heat flow must be corrected for the blanketing effect due to sedimentary coverage (Hutchison, 1985). Where sediments are thin, such as near the axis, the rough basement topography also causes spatial variability in heat flow. Rapid and irregular sedimentation patterns and fluctuating bottom-water temperatures make measurements of heat flow in the shallow marginal areas, such as the Yermak Plateau, difficult. However, all stations penetrated below the seasonal thermal boundary layer in the sediment making it possible to analyze these data.

2. HEAT FLOW CORRECTIONS

Two methods are applied to analyze heat flow. Firstly, I apply the Hutchison Model (Hutchison, 1985) to correct for the blanketing effect due to sedimentary coverage, and calculate the heat flow at the base of the sediment unit. Secondly, I

apply the cooling oceanic crust model to estimate thermal-crustal ages for corrected heat flow.

a. Blanketing Effect:

Calculating heat flow correction due to sedimentation allows a comparison of observed heat flow values with those predicted by lithospheric extension models. These require a given initial temperature at depth and a constant temperature for a lower boundary condition (Sclater and Francheteau, 1970; Parsons and Sclater, 1977). To correct heat flow accurately, the thermal effects of sedimentation are taken into account. Observed surface heat flow is disturbed in areas of high-relief topography (Von Herzen and Uyeda, 1963). Adjacent to margins, the rapid sediment deposition causes a reduction in the observed surface heat flow (Hutchison, 1985). As continuous plate motion carries the crust away from the axial zone, a gradually thickening sedimentary blanket seals the features, turning the heat transport over to molecular conduction (Vogt *et al.*, 1981; Thiede *et al.*, 1989). A correction for the blanketing effect is used to compensate for this reduction (Appendix A).

This model can be used to help predict the thermal crustal age when magnetic anomalies are not available. Because the sedimentation in this region does not appear to be tied closely to the subsidence rate of a newly evolving oceanic lithosphere (Myhre *et al.*, 1982; Crane *et al.*, 1991), I analyzed the heat flow using the Hutchison (1985) model which accounts for changes in the sedimentation rate, variation in sediment type, compaction of the sedimentary column and surface temperature

changes. Assuming that the heat flow has been constant and the sedimentation rate has been uniform (as the thermal regime can recover slowly) the heat flow at the surface of the sediments can be estimated (Hutchison, 1985). The effects of sedimentation on temperature and heat flow of a slab are determined by using a one dimensional finite difference model (Beaumont *et al.*, 1982; Hutchison, 1985).

I corrected heat flow by using best estimates for sediment type and thickness based on seismic profiles and sound velocity profiles, including DSDP- and ODP-Site results, and core samples taken in these regions. One to two sedimentary layers are assumed based on the in-depth analyses of sedimentation in this region (Myhre *et al.*, 1982). Variable sedimentation rates and durations are input into the Hutchison model (Hutchison, 1985) yielding outputs which are compared to observed values.

b. Extension Rates and Estimation of the Thermal-Crustal Age:

Calculating the blanketing effect of sediment gives a comparison between corrected heat flow values and heat flow values predicted by a model of cooling oceanic lithosphere (Parsons and Sclater, 1977; McKenzie, 1978). The cooling oceanic crust model of McKenzie (McKenzie, 1978) assumes that the oceanic lithosphere cools as it moves from the ridge axis. As a result of this, high heat flow occurs at mid-ocean ridges and decreases with distance from it (Sclater and Francheteau, 1970; Langseth and Zielinski, 1974). The gradual decrease in heat flow with increasing crustal age is explained by the cooling and thermal contraction of the

lithosphere, which is consistent with the gradual deepening of the ocean floor with time (Parsons and Sclater, 1977).

Stein and Stein (1992) also suggest that the systematic variation of ocean depth and heat flow with age became the primary constraint on models of the thermal evolution of the lithosphere. Parsons and Sclater (1977) found that such a model, for a 125 km-thick plate with a basal temperature of 1350°C, provided good fits to the observed heat flow and bathymetry. The model describes the general shape of the depth curve, including the flattening for ages >70 Ma and the heat flow for ages >50 Ma. Both theoretical cooling curves (Parsons and Sclater, 1977 and Stein and Stein, 1992) overlap at crustal ages younger than ~60 Ma.

In this thesis, I attempt to determine local spreading rates by matching the heat flow data, corrected for sedimentation, with a model for the age-dependent cooling of oceanic crust (called the PS-cooling curve by Parsons and Sclater, 1977; Appendix A).

3. Testing Lithospheric-Extension Mechanisms

After sedimentary corrections have been made, corrected heat flow data can be used to constrain which of the lithospheric extension models are most applicable to describe the evolution of the Norwegian-Greenland Sea (pure- and simple-shear, or combination of both). Heat flow and seafloor bathymetry computed by numerical modeling indicate the effects of heat entering the lithosphere. The purpose of using

numerical modeling is to constrain a kinematic development model for the evolution of the Norwegian-Greenland Seafloor. A kinematic model can explain how a continent breaks up, what type of lithospheric extension and heat sources develop, and how a shear zone can trap a mid-ocean ridge forming transtensional volcanic passive margins, plateaus and off-axial multiple-zones of intrusions in this section.

The numerical modeling technique exercises a finite difference method, which simulates two-dimensional time-dependent lithospheric extension. This method employs statistics for the Continuity Equation (Appendix A), which equates horizontal and vertical velocity gradients and conserves volume. The model deals with the advection of heat by prescribing the asthenospheric flow field without regard to material strength or body force (Buck *et al.*, 1988). Heating results from the thinning and extending of the lithosphere. Other additional heat sources such as induced convection and radiogenic heating are not considered in this method. The model properties, assumptions and equations used are discussed in Appendix A.

Model results depend on extension geometries and their development through time even though they all have the same heat input. Pure-shear extension occurs across a zone whose width is changing (depending on time, Figure 2-4). A simple-shear extension occurs on a planar low-angle detachment fault, which cuts the entire lithosphere (Figure 2-1). The most significant parameter of lithospheric extension is the total amount of extension that has occurred which represents the total heat input into the lithosphere.

B. ANALYSIS OF HEAT FLOW FROM THE EASTERN NORWEGIAN-GREENLAND SEAFLOOR: VOLCANIC MARGINAL PLATEAUS AND TRANSTENSIONAL VOLCANIC MARGINS

1. The Vøring Plateau along the Norwegian Margin

Heat flow collected from the Norwegian Margin is shown in Figure 5-2 (most data were collected during the Vema expeditions, Langseth and Zielinski, 1974). Cross sections from the Mohns Ridge to the margin indicate the normal cooling of oceanic crust (from 268 mW/m^2 at the plate boundary to 58 mW/m^2 at the margin ocean/floor interface). However, further landward on the Inner Vøring Plateau, heat flow increases to 87 mW/m^2 along the Inner Vøring Plateau; distinctly warmer than that predicted by local magnetic anomalies. Landward of the plateau is an area associated with a magnetic smooth zone (amplitude relief less than 100 nT reported by Talwani and Eldholm, 1972; in Figure 3-11). The heat flow profile (AA') presented, crosses the magnetic smooth zone and is aligned perpendicular to the Vøring Plateau Escarpment. Heat flow stations, physical properties and seafloor bathymetry are illustrated in Figure 5-3. Detailed information about the stations are given in Figure A-6 (Appendix B). Heat flow corrected for the thermal blanketing effect of sedimentation, is presented in Table 5-1. The decompacted sediment thickness is then estimated for each heat flow station. Sedimentation rate, physical properties and corrected heat flow values are summarized in Tables 5-1a to 5-1d.

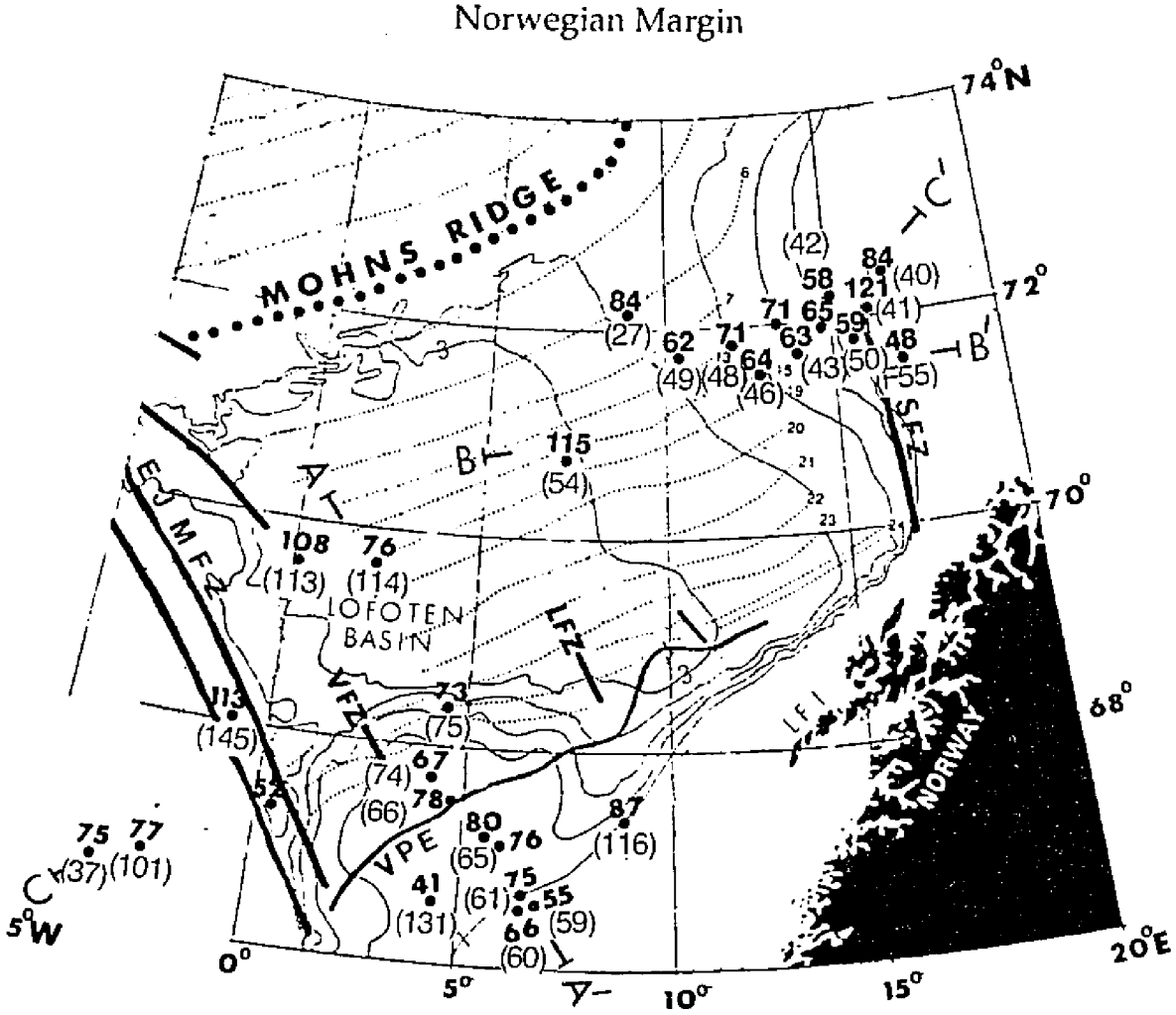

Figure 5-2: Heat flow in the southeastern Norwegian-Greenland Sea. AA': Vøring Plateau transect, BB' transect perpendicular to the Senja Escarpment, CC' transect across the Eastern Jan Mayen, Vøring, and Senja Fracture Zones. Locations of heat flow values (mW/m^2) and station numbers (in parenthesis), bathymetry contour intervals at 0.5 km and magnetic anomalies (dotted lines) are indicated along the Norwegian and Senja Margins. Heat flow data were collected by Sundvor (1986) and Langseth and Zielinski (1974). VPE: Vøring Plateau Escarpment, VFZ: Vøring Fracture Zone, LFZ: Lofoten Fracture Zone, SFZ: Senja Fracture Zone, LFI: Lofoten Islands, EJMFZ: Eastern Jan Mayen Fracture Zone.

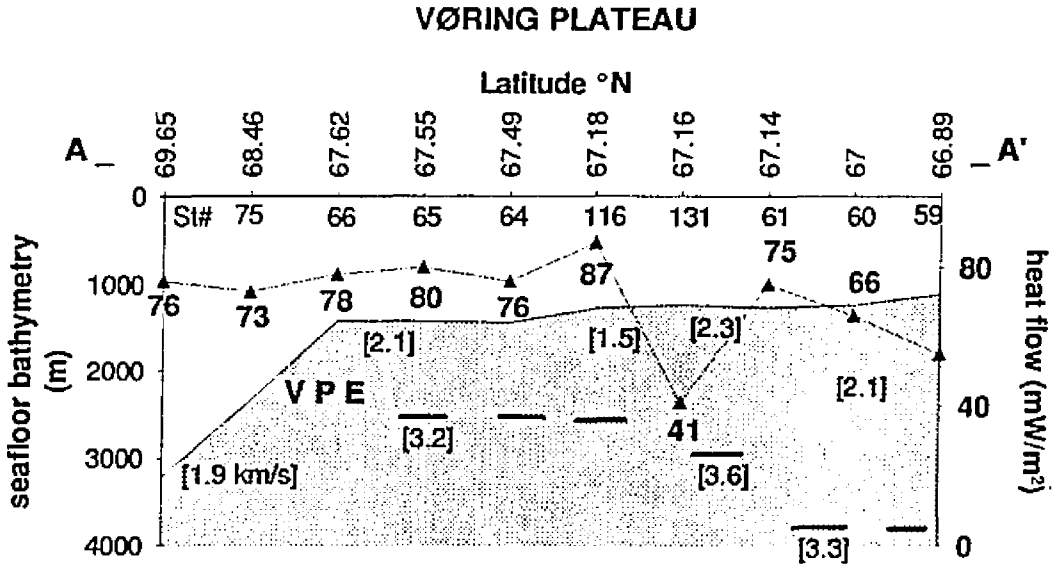

Figure 5-3. Heat flow transect across the Vøring Plateau (A-A' in Figure 5-2). Observed surface heat flow values (triangles) superimposed on seafloor bathymetry normal to the Vøring Plateau Escarpment (VPE). Sediment velocities (km/s) are indicated (Eldholm and Talwani, 1977; Eldholm and Windisch, 1974; Vogt, 1986).

Table 5-1. Heat flow analysis: Vøring Plateau on the Norwegian Margin.

Table 5-1a. Corrected Heat Flow across the Vøring Plateau transect. Layer 1 compacted sediment thickness (H^1, comp, km), seismic velocities (V^1, km/s), decompacted sediment thickness (H^1, decomp, km), magnetically derived crustal age (my), sedimentation rate (m/my), heat flow reduction factor (RF), corrected heat flow (Correct., HF, mW/m^2) for each station on the A-A' Vøring Plateau transect.

Table 5-1b. Layer 2 sedimentation corrections along the Vøring Plateau transect (A-A'). See Table 5-1a for column headers calculation. Porosity $Øz^2$.

Table 5-1c. Layer 1+Layer 2 sedimentation corrections. See caption of Table 5-1a for column header definitions.

Table 5-1d. Corrected heat flow and thermal ages at stations on the Norwegian Margin (Figure 5-2). Difference between thermal ages and magnetic crustal ages (Δage). The mean difference between the magnetic and thermal crustal ages is ~18 mybp.

		Table 5-1a						
		VØRING PLATEAU						
			Layer 1					
H[1]		H[1]	Mag.	Sed.		Obs.	Correct.	St#
comp	V[1]	decomp	Age	Rate	RF[1]	Hf	Hf	
km	km/s	km	my	m/my		mW/m²	mW/m²	
1.06	1.9	1.32	45	29.33	1.08	76±10	82.1	114
0.99	2.1	1.21	44	27.51	1.04	73±3	78.8	75
0.56	2.1	0.64	46	13.91	1.03	78±3	80.3	66
0.56	2.1	0.64	60	27.23	1.04	80±3	83.2	65
1.25	2.1	1.58	60	67.23	1.11	76±6	84.4	64
0.64	1.5	0.73	60	31.06	1.04	87±6	90.5	116
2.01	2.3	2.81	60	119.57	1.19	41±10	48.8	131
2.31	2.1	3.31	60	140.85	1.23	75±2	84	61
2.31	2.1	3.28	60	139.57	1.23	66±2	81.1	60
1.39	2.3	1.75	65	74.47	1.14	55±1	62.7	59

Table 5-1b

VØRING PLATEAU

Layer 2

St #	H^2 comp	V^2	$Øz^2$	H^2 decomp	Mag. Age	Sed. Rate	RF^2	Obs. Hf	Correct. Hf
	km	km/s		km	my	m/my		m/Wm^2	m/Wm^2
DHF 65	0.91	3.17	0.43	1.03	60	17.17	1.04	80±3	83.2
DHF 64	0.85	3.17	0.43	0.97	60	16.17	1.04	76±6	79.04
116	0.81	3.17	0.44	0.9	60	15.13	1.04	87±6	90.48
131	1.82	3.64	0.39	2.22	60	37.11	1.09	41±10	44.69
DHF 61	1.38	3.62	0.41	1.9	60	31.67	1.08	75±2	81
DHF 60	2.71	3.25	0.33	3.62	60	60.33	1.16	66±2	76.56
DHF 59	2.61	3.25	0.34	3.46	65	57.67	1.16	55±1	63.8

Table 5-1c

VØRING PLATEAU

Layer 1+2

St #	H 1+2 comp km	Øz 1+2	H 1+2 decomp km	Mag. Age my	Sed. Rate m/my	RF 1+2	Obs. Hf mW/m²	Corr. Hf mW/m²
DHF 65	1.85	0.35	2.42	60	40.33	1.09	80	87.2
DHF 64	2.11	0.32	2.86	60	47.66	1.14	76	78.7
116	2.29	0.31	3.16	60	52.66	1.14	87	99.2
131	3.88	0.25	5.82	60	97.11	1.26	41	57.7
DHF 61	3.68	0.23	5.67	60	94.51	1.26	75	94.5
DHF 60	5.11	0.19	8.12	60	135.21	1.31	66	85.8
DHF 59	3.99	0.25	5.99	65	99.81	1.26	55	66.8

	Table 5-1d				
	VØRING PLATEAU			thermal rejuvenation	
	Magnetic	Obs.	Corr.	Thermal	Δ
St #	Age	Hf	Hf	Age	Age
	my	mW/m²	mW/m²	my	my
114/V-30	45	76	82.10	35.9	9.1
DHF 75	44	73	78.8	42	18
DHF 66	46	78	80.3	36	10
DHF 65	60	80	87.2	33	27
DHF 64	60	76	78.7	39	21
116/V-30	60	87	99	25	35
131/V-30	60	41	59.7	60	0
DHF 61	60	75	90	30	30
DHF 60	60	66	85.8	32	28
DHF 59	65	55	66.8	55	5
					Δ Age=18 my

Velocity structure and sediment thickness information were obtained from several sources (Eldholm and Windisch, 1974).

Limitations of the seismic data lie in the assumption that velocities greater than 4.9 km/s are assumed to be basement. There is some uncertainty in determining the actual sedimentary thickness in this region, however, I believe that the termination of the main basin westward at the marginal escarpment (Figure 5-3) is well documented. The oldest post-opening sediment (between oldest oceanic crust and continental crust on the crest of the Vøring Plateau) was late Paleocene-early Eocene (Schrader *et al.*, 1976). Two layers and averaged velocities are assumed for each site. Average sedimentation rates are estimated using decompacted sediment thickness and magnetic crustal ages obtained from magnetic anomalies in the region.

Corrected heat flow values are compared to observed heat flow values in Figure 5-4. In Figure 5-5, corrected heat flow is compared to the PS-cooling curve. Determined thermal-crustal ages are compared to magnetic ages in Figure 5-6. In summary, corrected heat flow values indicate that thermal-crustal ages are much younger (by 18 Ma) than the age estimated by magnetic anomaly lineations. Episodes of thermal rejuvenation occurred at both 35 mybp in regions where magnetic ages were determined to be 60-65 Ma, and at 25 mybp in regions where the magnetic ages are thought to be ~45 Ma (Figure 5-5).

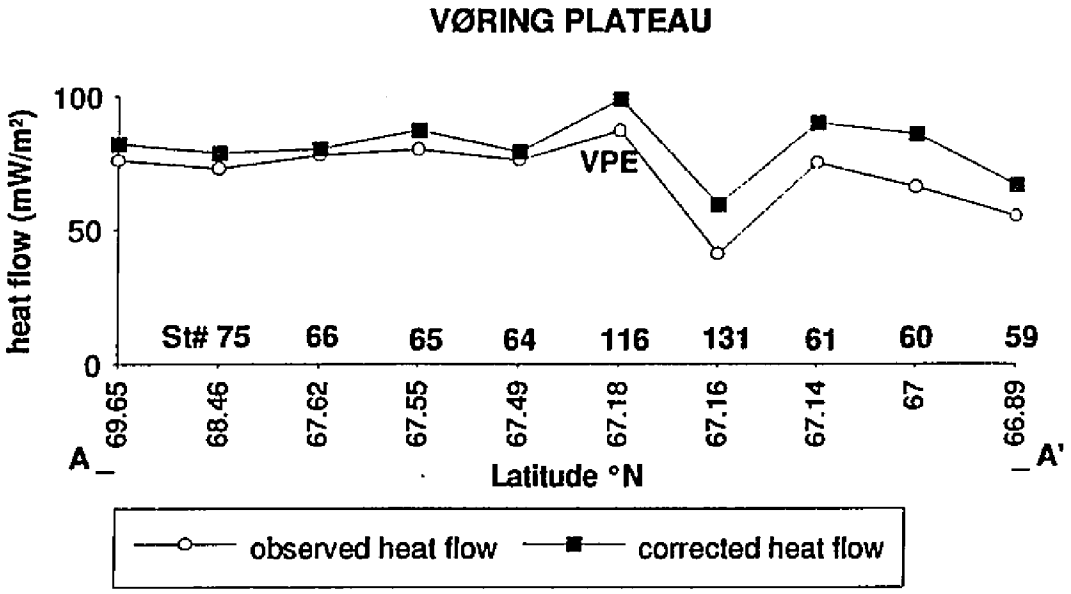

Figure 5-4. Observed vs. corrected heat flow along the Vøring Plateau A-A' transect (Figure 5-2). VPE: Vøring Plateau Escarpment.

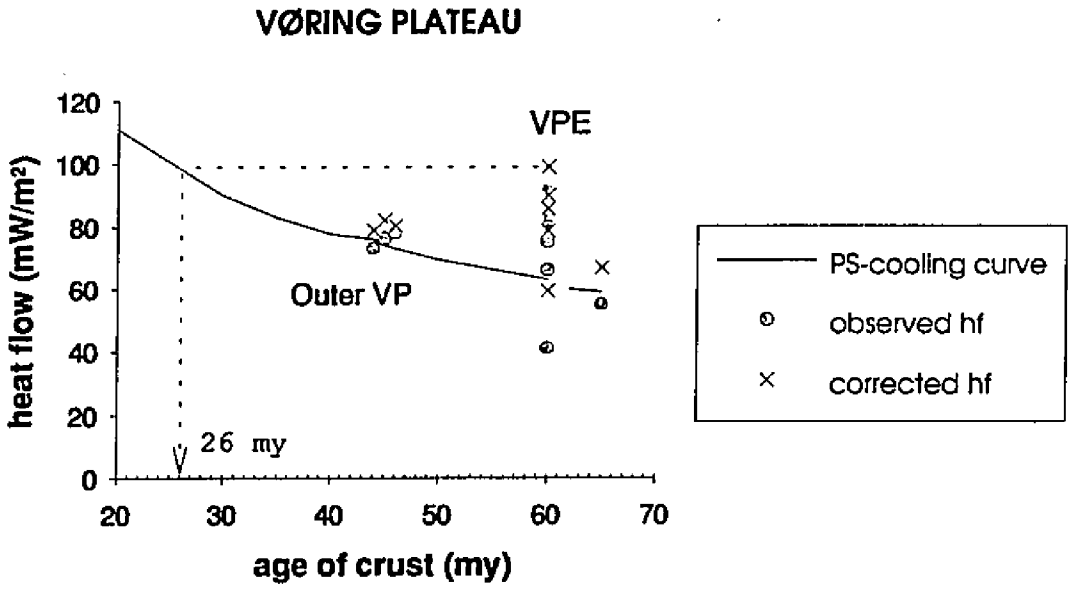

Figure 5-5. Cooling oceanic crust model: Vøring Plateau. Comparison of observed heat flow and corrected heat flow with the PS-cooling curve of Parsons and Sclater (1977). Date of the most recent thermal rejuvenation is estimated to be 26 mybp. VPE: Vøring Plateau Escarpment.

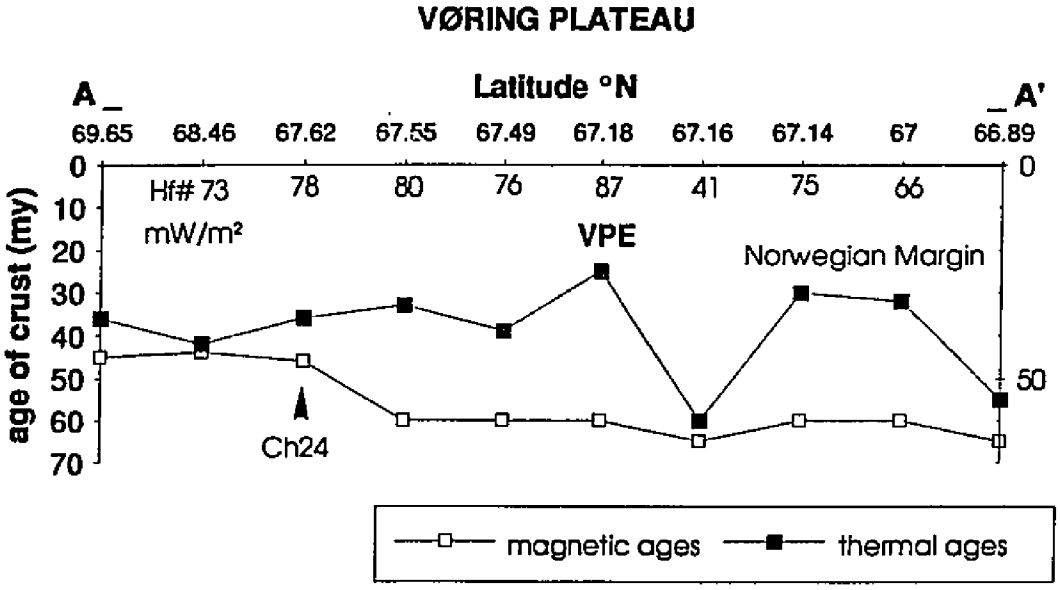

Figure 5-6. Comparison between magnetically and thermally derived crustal ages across the Vøring Plateau (A-A' transect). Mean age difference (Δage) is found to be 18 my at the Vøring Plateau Escarpment (VPE) on the Norwegian Margin. Ch 24 indicates magnetic anomaly-Ch 24.

2. THE SENJA TRANSTENSIONAL VOLCANIC MARGIN

The heat flow profile (BB' profile in Figure 5-2) transects the northern Norwegian Margin to the Senja Margin (Figure 5-7). The heat flow profile indicates that the highest heat flow (121 mW/m^2) is located on the Senja Escarpment. In the same region, a wide magnetic smooth zone (landward of the Senja Margin) is interpreted as shallow magnetic basement (<2 km in depth). However, south of this region between 12°E and 15°E magnetic anomalies are discernible. By projecting the anomalies into our region of interest we can obtain an estimated magnetic crustal age. Detailed information for the stations are given in Figure A-6 (Appendix B).

In this region, sedimentary sequences of varying thickness lie on igneous oceanic crust along the Senja-Western Svalbard Margin (Eldholm and Windisch, 1974; Myhre *et al.*, 1982). The thickest sedimentary sequence occurs at the margin and is between 900 and 1000 m' s thick (assuming a sound velocity of ~2 km/s in the sediments, Vorren *et al.*, 1989). According to Talwani and Eldholm (1972) most of these sediments are pre-Tertiary in age.

To model corrected heat flow, two sedimentary layers of average velocities are assumed at each heat flow site. Decompacted sediment thicknesses are calculated for each heat flow station. Sedimentation rates are determined using estimated decompacted sediment thicknesses and magnetic crustal ages. The results of sedimentation rates, corrected heat flow and thermal-crustal ages are tabulated in

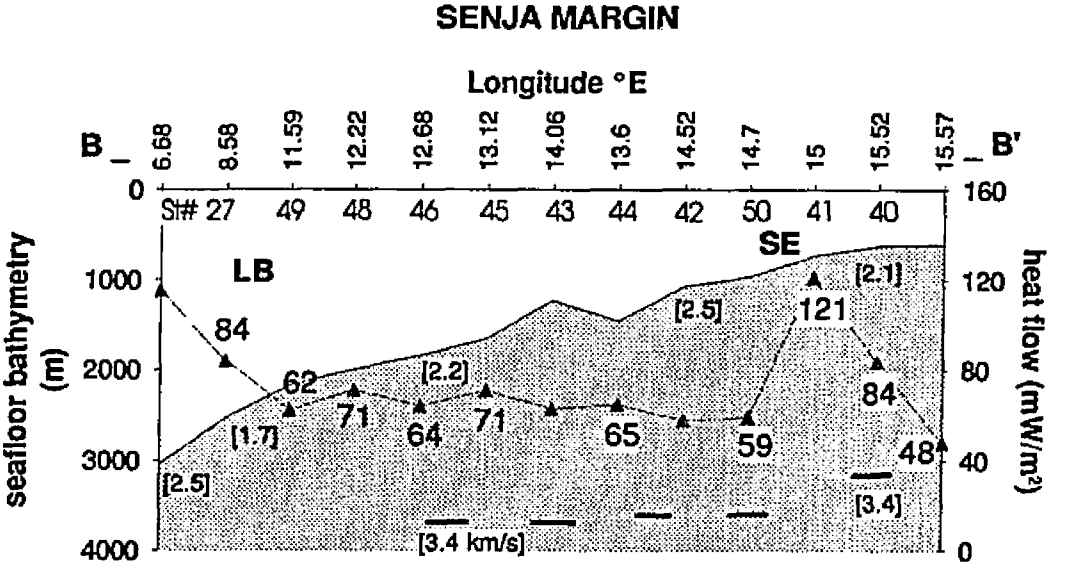

Figure 5-7. Heat flow transect (B-B') across the Senja Margin (see Figure 5-2 for location). Heat flow values (triangles) are superimposed on seafloor bathymetry across the Senja Escarpment (SE) and Lofoten Basin (LB). Sediment seismic velocities (km/s) are derived from Eldholm and Windisch (1974) and Vogt (1986); see Tables 5-2a and 5-2c for details.

Tables 5-2a to 5-2c. Observed surface heat flow is compared to corrected heat flow in Figure 5-8.

In Figure 5-9, corrected heat flow is compared to the PS-cooling curve. Thermal crustal ages are compared to magnetic crustal ages in Figure 5-10. Two high heat flow episodes on crust supposedly 35 and 60 Ma old suggest that the crust in these regions has been thermally rejuvenated to 25 and 10 Ma respectively. Thermal crustal ages are on average 22 my's younger (based on the cooling oceanic plate model) than the estimated magnetic ages.

3. The Eastern Jan Mayen-Vøring-Senja Margin Profile

The heat flow profile CC' crosses the margin between 7°W and 16°E and transects the Eastern Jan Mayen Fracture Zone, Vøring Fracture Zone, Vøring Plateau, Lofoten Fracture Zone, and Senja Fracture Zone (Figure 5-2). Observed surface heat flow, seafloor bathymetry and seismic velocity structure along the profile (modified from Eldholm and Windisch, 1974) are indicated in Figure 5-11a and 5-11b. All of these sites are regions of high heat flow located at considerable distances from the axis of the Mohns Ridge.

To correct each heat flow value for sedimentation, decompacted sediment thicknesses are calculated at each station. Sedimentation rates are estimated using decompacted sediment thicknesses and magnetic ages. Determined sedimentation rates, magnetic crustal ages, corrected heat flow and thermal crustal ages are tabulated

Table 5-2. Heat flow analysis: Senja Margin.

Table 5-2a. Corrected Heat Flow. Layer 1 compacted sediment thickness (H^1, comp, km), seismic velocities (V^1, km/s), decompacted sediment thickness (H^1, decomp, km), magnetically derived crustal age (my), sedimentation rate (m/my), corrected heat flow (Correct., HF, mW/m^2) for each station on the B-B' Senja Margin transect.

Table 5-2b. Layer 1+Layer 2 sedimentation corrections. See captions for Table 5-2a for column header definitions.

Table 5-2c. Heat flow modeling results: Senja Margin. Corrected heat flow values and thermal crustal ages for each station on the Senja Margin. Difference between thermal ages and the ages estimated based on magnetic anomalies is Δage. Mean age (Δage) is found to be 15.6 my.

		SENJA MARGIN					
			Table 5-2a				
			Layer 1				
	H^1		H^1	Mag.	Sed.	Obs.	Correct.
St #	comp	$V1^1$	decom	Age	Rate	Hf	Hf
	km	km/s	km	my	m/my	mW/m²	mW/m²
54/V-23	0.91	2.5	1.06	40	26.5	115±8	123
10/V-27	2.4	1.7	2.21	23	130	84±7	108
F49	2.4	1.8	5.88	26	163.33	62±1	84.9
F48	2.4	1.28	1.59	35	63.6	71±2	90.8
F46	2.4	2.16	4.68	40	187.2	64±2	82.56
F45	2.1	2.16	4.83	40	205.5	71±2	119
F43	2.1	2.18	3.06	40	130.2	63±3	99
F44	2.1	2.18	3.06	50	130.2	65±2	105
F42	2	2.5	3.87	50	164.7	58±6	87
F50	2	2.5	3.87	50	164.7	59±2	94
F41	2	2.1	3.1	50	131.9	121±6	171
F40	2	2.1	3.1	50	131.9	84±6	118
F55	2	2.1	3.1	55	131.9	48±10	68

Table 2b

SENJA MARGIN

Layer 1+2

St #	H^{1+2} comp	V^2	H^{1+2} decom	Mag. Age	Sed. Rate	Obs. Hf	Correct. Hf
	km	km/s	km	my	m/my	mW/m²	mW/m²
F48	2.48	3.4	3.37	35	134.8	71±2	90.8
F46	4.66	3.4	7.36	40	294.4	64±2	83
F45	5.61	3.4	9.37	40	375	71±2	78
F43	4.18	3.4	6.5	40	260	63±3	72
F44	4.18	3.4	6.5	50	226	65±2	78
F42	3.98	3.4	6.7	50	271.6	58±6	87
F50	3.9	3.4	6.1	50	244	59±2	76
F41	3.1	3.4	4.65	50	186	121±6	148
F40	2.5	3.4	3.7	50	66.3	84±6	99
F55	2.5	3.4	3.65	60	60.8	48±10	66

		Table 5-2c			
	thermal rejuvenation				
	Obs.	Corr.	Mag.	Thermal	Δ
	Hf	Hf	Age	Age	Age
	mW/m²	mW/m²	my	my	my
	115	123	40	15	25
	84	108	23	21.8	1.7
	62	84.9	26	23	3
	71	90.8	35	29.6	5.4
	64	83	40	22	18
	71	78	40	16	24
	63	71.8	40	25.4	14.6
	65	78	50	39	11
	58	87	50	26	24
	59	75.5	50	26	24
	121	148	50	15	35
	84	99	50	25	25
	48	66	60	55	5
				Δ Age = 15.6 my	

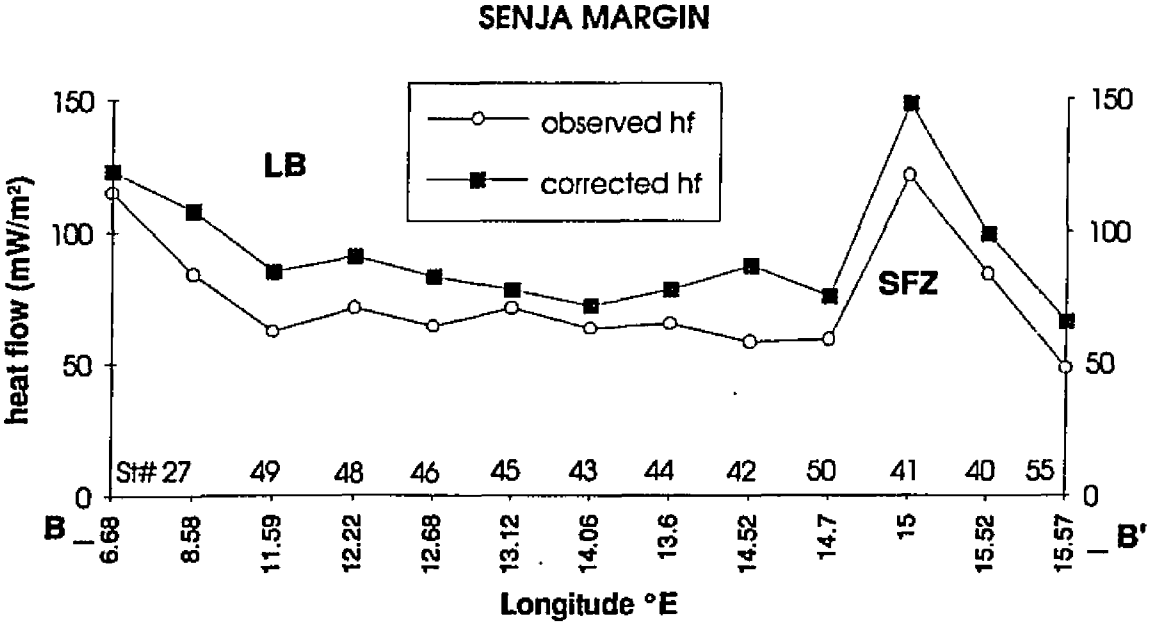

Figure 5-8. Heat flow analysis: Senja Margin. Comparison of the observed heat flow and corrected heat flow across the Senja Escarpment (SFZ), Lofoten Basin (LB).

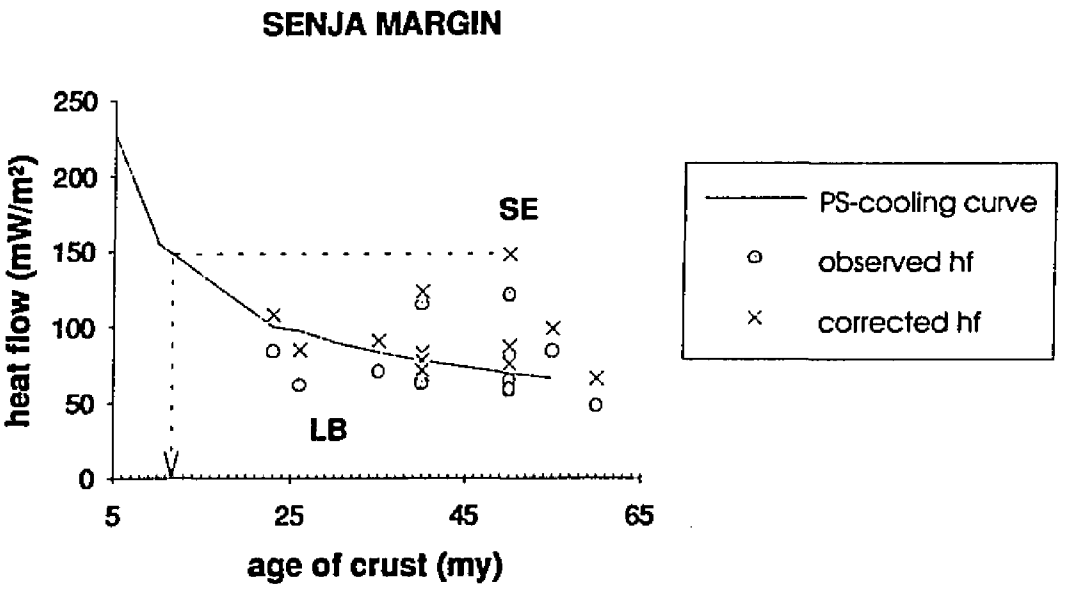

Figure 5-9. Cooling oceanic crust model: Senja Margin. Comparison of observed surface heat flow and corrected heat flow to the PS-cooling curve of Parsons and Sclater (1977). Date of the most recent thermal rejuvenation for the Senja Margin (on crust with magnetic anomaly ages of 50 Ma) can be estimated to be ~12 mybp. SE: Senja Escarpment, LB: Lofoten Basin.

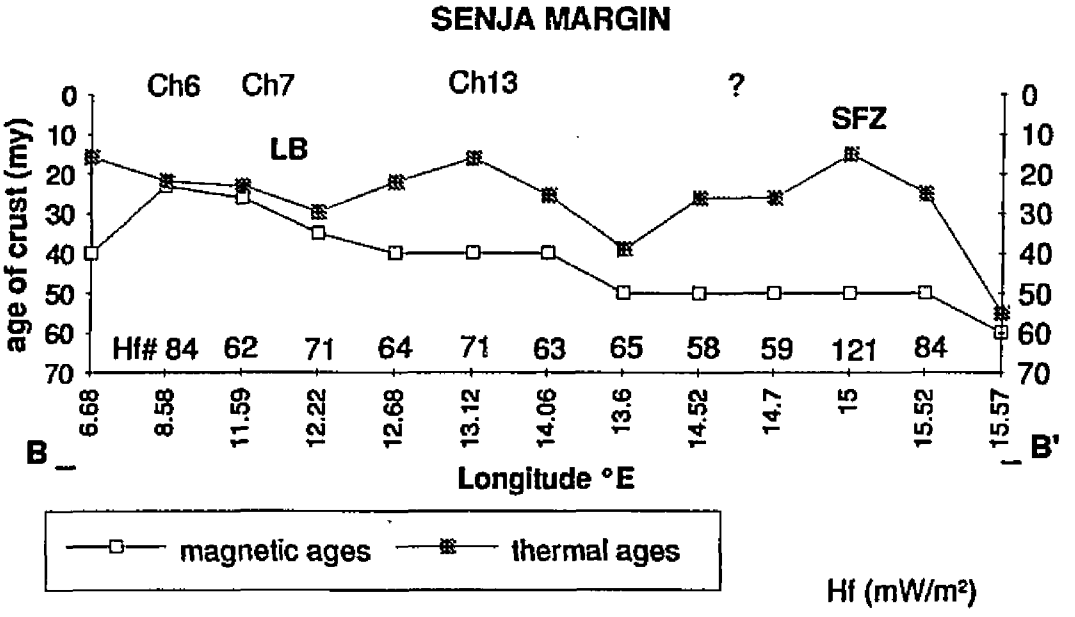

Figure 5-10. Crustal ages: Senja Margin. Comparison of the magnetic ages and thermal ages. Mean age (Δage) is found 15.6 my for the Senja Margin. Hf: heat flow values, Ch (6-22): magnetic anomalies, (?): magnetic smooth zone. SFZ: Senja Fracture Zone, LB: Lofoten Basin.

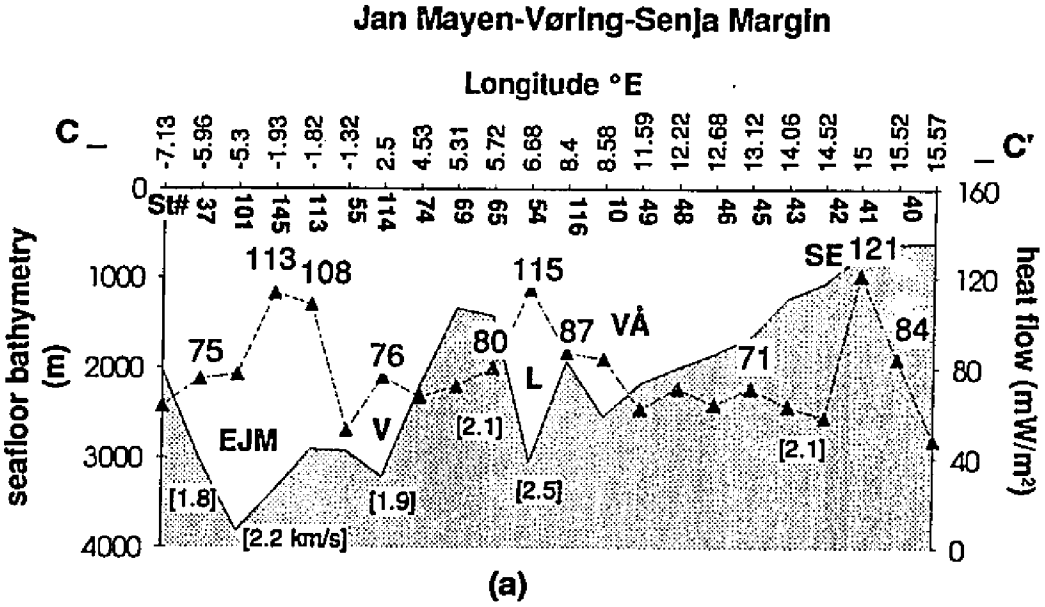

Figure 5-11. (a) Heat flow profile: Eastern Jan Mayen-Vøring-Senja Margin. Heat flow values (triangles) and seafloor bathymetry from the Jan Mayen Fracture Zone and the Outer Vøring Plateau to the Senja Escarpment (CC' transect between 7.13°W and 15.57°E. Heat flow collected by Langseth and Zielinski (1974) and Sundvor and Eldholm (1979). (b) Seismic velocity structure of the Eastern Jan Mayen-Vøring-Senja Margin Profile. Sediment velocity stations on the bottom of the profile are indicated in Table 5-3 (Eldholm and Windisch, 1974; Vogt, 1986) and for further seismic information see Appendix B. EJM: Eastern Jan Mayen Fracture Zone, V: Vøring Fracture Zone, L: Lofoten Fracture Zone, VÅ: Vesterålen Fracture Zone, SE: Senja Escarpment.

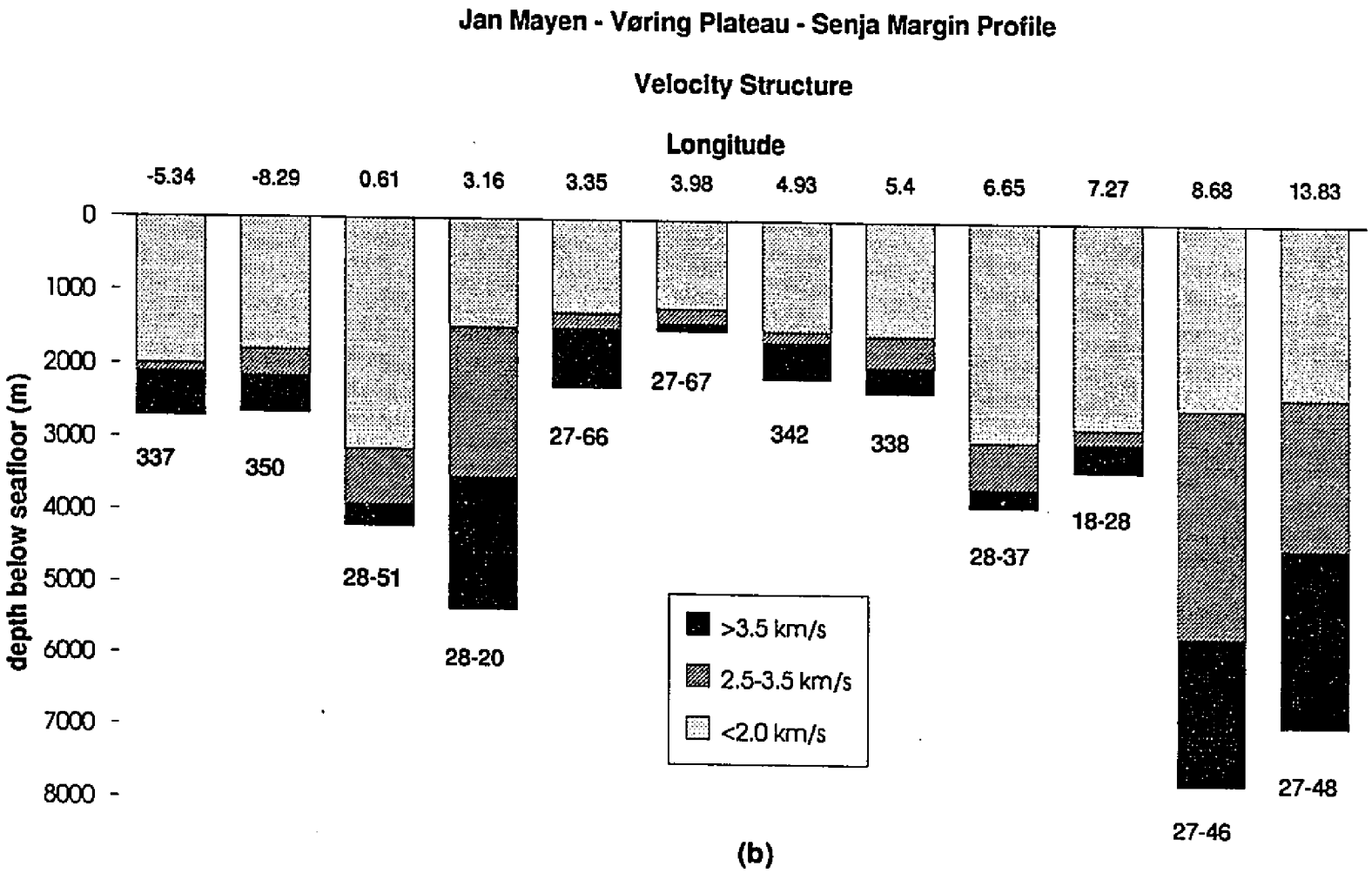
Jan Mayen - Vøring Plateau - Senja Margin Profile
Velocity Structure
Longitude
-5.34
-8.29
0.61
3.16
3.35
3.98
4.93
5.4
6.65
7.27
8.68
13.83
0
1000
2000
3000
4000
5000
6000
7000
8000
depth below seafloor (m)
337
350
28-51
28-20
27-66
27-67
342
338
28-37
18-28
27-46
27-48
>3.5 km/s
2.5-3.5 km/s
<2.0 km/s

(b)

in Table 5-3. Observed surface heat flow is compared with corrected heat flow in Figure 5-12.

Corrected heat flow is compared to the PS-cooling curve in Figure 5-13. Computed thermal crustal ages are compared to magnetic crustal ages in Figure 5-14. Between 24 mybp and 11.5 mybp the crust was repeatedly heated (Figure 5-13). Heat flow analyses imply that there may have been another paleo-fracture zone in the southern Norwegian-Greenland Sea, which I name "the Vesterålen Fracture Zone". The most recent thermal rejuvenation event occurred at 18 mybp along the Senja Fracture Zone, at 24 mybp on the Vøring Fracture Zone, at 25 mybp on the Vøring Plateau, at 17 mybp on the Lofoten Fracture Zone, and at 16 mybp on the Vesterålen Fracture Zone.

In summary, thermally derived crustal ages suggest that the Vøring, Lofoten, Vesterålen Fracture Zone and Senja Fracture Zone (Senja Margin Escarpment) have been repeatedly reheated. Comparing the crustal age differences from both margins (Norwegian and Senja Margins) suggest that heating was more dominant and longer-lived along the Senja Margin. The Lofoten Fracture Zone is closer to the Senja Margin and is presently warmer and hence more recently rejuvenated than the Vøring Fracture Zone.

Table 5-3. Corrected heat flow: Norwegian Margin. Corrected heat flow values and thermal ages for the crust underlying each heat flow station along the Jan Mayen-Vøring-Senja Profile (CC'). Compacted sediment thickness (H^1 comp., km), calculated decompacted sediment thicknesses (H^1 decomp., km), magnetic ages, sedimentation rates (m/my), and observed and corrected heat flow are determined for layers 1 and 2. Sediment seismic velocities are tabulated. Difference between thermal ages and the ages estimated based on magnetic anomalies is Δage. Mean age (Δage) is found 15.3 mybp.

Table 5-3

EASTERN JAN MAYEN - VØRING PLATEAU - SENJA MARGIN PROFILE

St#	V[1]	H[1] comp	H[1] decom	Magnetic Age	Sed. Rate	Obs. Hf	Layer 1 Correct. Hf	Layer 2 Correct. Hf	Thermal Age	Δ Age
	km/s	km	km	my	m/my	mW/m²	mW/m²	mW/m²	my	my
100/V-30	1.8	0.47	0.53	60	10.82	63±8	66		55	5
37/86	1.8	0.4	0.4	45	11.11	75	77		41.3	3.7
101	1.8	0.36	0.44	40	3.06	77±9	79		38.1	2
145/V-29	2.2	0.77	0.88	36	24.4	113±8	118		16.4	19.6
113/V-30	2.2	0.56	0.63	25	25.2	108±8	112		19.8	5.2
55	2.2	0.77	0.88	65	17.6	52	62.4		60	5
114/V-30	1.9	1.06	1.32	45	29.33	76±10	82		35.9	9.1
74	2.1	0.56	0.64	55	11.64	67±1	73		45	10
69	2.1	0.64	0.73	60	31.06	72±2		88	32	28
65	2.1	0.56	0.64	60	27.23	80±3		90	30	30
54/V-23	2.5	0.91	1.06	40	26.5	115±8	123		15.6	24.4
116/V-30	1.5	0.64	0.73	60	31.06	87±6		103	20.3	39.7
10/V-27	2.4	1.7	2.21	23	130	84±7	108		21.8	1.7
F49	2.4	3.88	5.88	26	163.33	62±1	85		23	3
F48	2.4	1.28	1.59	35	63.61	71±2		90.8	30	3
F46	2.4	3.16	4.6	40	187.4	64±2		106	22	18
F45	2.1	3.16	4.83	40	205.5	71±2		119	16	24
F43	2.1	2.18	3.06	50	130.2	63±3		99	25.4	14.6
F42	2	2.18	3.06	50	130	58±6		87	26	24
F41	2	2.18	3.1	50	131	121±6		148	15	35
F40	2	2.18	3.1	50	86.11	84±6		99	25	25
F55	2	2.18	3.1	60	77.5	48±10		66	55	5

Δ Age = 15.3 my

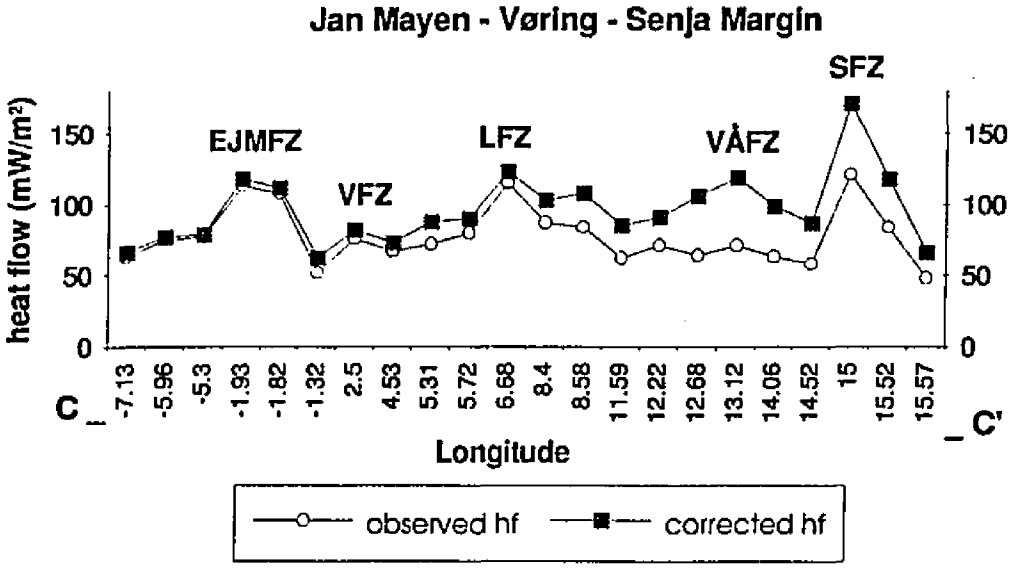

Figure 5-12. Heat flow analysis: Norwegian Margin. Comparison of the observed heat flow and corrected heat flow along the Eastern Jan Mayen-Vøring-Senja Profile (CC'). VÅFZ: Vesterålen Fracture Zone, LFZ: Lofoten Fracture Zone, VFZ: Vøring Fracture Zone, SFZ: Senja Fracture Zone, EJMFZ: Eastern Jan Mayen Fracture Zone.

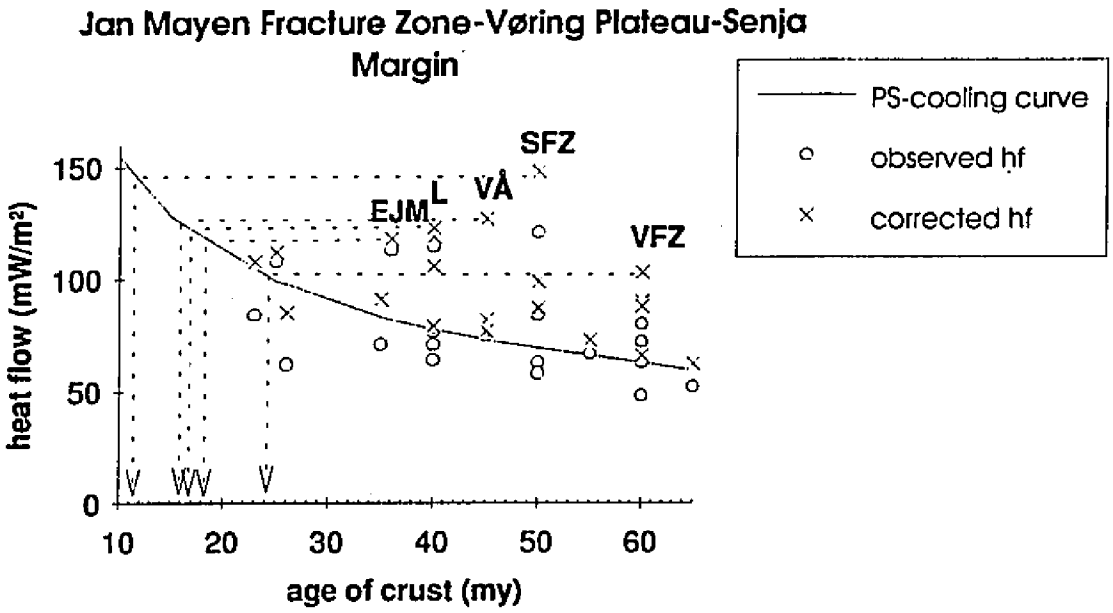

Figure 5-13. Cooling oceanic crust model: Norwegian Margin. Comparison of observed heat flow and corrected heat flow to the PS-cooling curve. EJM: Eastern Jan Mayen Fracture Zone, VFZ: Vøring Fracture Zone, L: Lofoten Fracture Zone, VÅ: Vesterålen Fracture Zone, SFZ: Senja Fracture Zones along the CC' profile. Dates of the most recent thermal rejuvenation episodes along the Eastern Jan Mayen-Vøring-Senja Line: 18 mybp for the Eastern Jan Mayen Fracture Zone, 24 mybp for the Vøring Fracture Zone, 25 mybp for the Vøring Plateau, 17 mybp for the Lofoten Fracture Zone, 16 mybp for the Vesterålen Fracture Zone, up to 11.5 mybp for the Senja Margin.

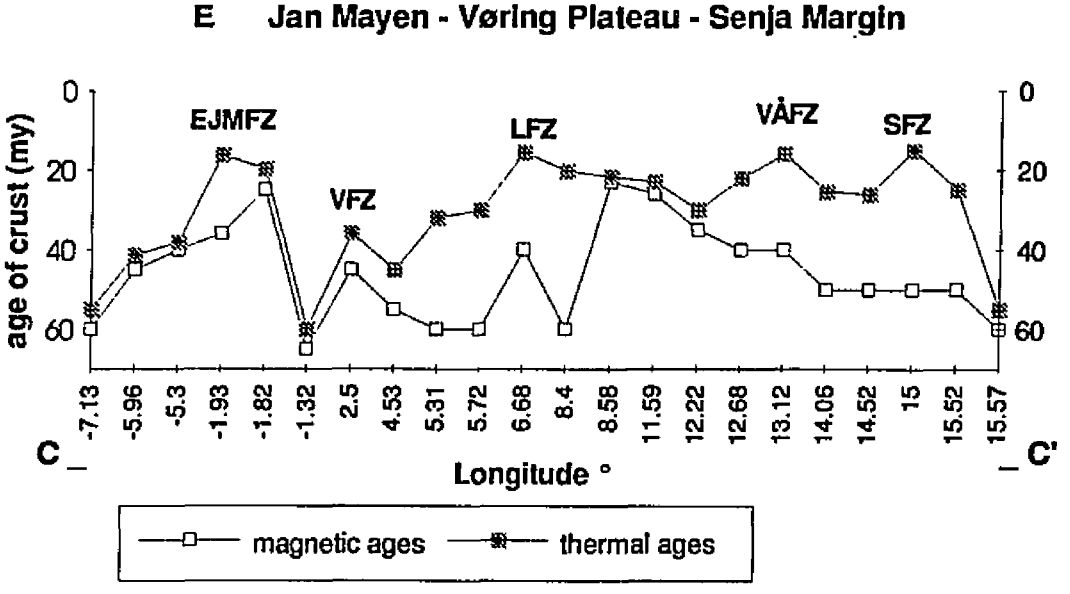

Figure 5-14. Crustal ages: Norwegian Margin. Comparison of the magnetic ages and thermal ages. Mean age difference (Δage) is found to be 15.3 mybp across the Jan Mayen-Vøring-Senja Profile (CC'). EJMFZ: Eastern Jan Mayen Fracture Zone, VFZ: Vøring Fracture Zone, LFZ: Lofoten Fracture Zone, SFZ: Senja Fracture Zone, VÅFZ: Vesterålen Fracture Zone.

4. THE MOLLOY TRANSFORM FAULT-WESTERN SVALBARD MARGIN

Observed heat flow data along the western Svalbard Margin are illustrated in Figure 5-15. Figure 5-16 depicts a heat flow profile transecting from west to east the Western Svalbard Margin (at 78.5°N). High heat flow is observed at the tip of the northern Knipovich Ridge (371 mW/m^2) and the intersection with the Molloy Transform Fault (197 mW/m^2) and along the Western Svalbard Margin (100 mW/m^2). As described in earlier heat flow manuscripts, crustal ages in this region can only be interpreted by using heat flow, because magnetic anomalies are nearly absent.

Sedimentation rates, reduction factors of heat flow, corrected heat flow and thermal crustal ages are tabulated in Table 5-4. Along the Western Svalbard Margin, Myhre and Eldholm (1988) estimate that, prior to mid-Miocene the sedimentation rates were approximately 10 cm/Ma. Since the Miocene (during the last 5 Ma) the rates have increased to more than 30 cm/Ma. They divided the sediments into two layers, referred to as layer 1 and layer 2 (Figure 5-16). The upper layer was deposited during the last 5.5 Ma. Faleide *et al.* (1984) suggest an unconformity at the base of the upper Paleocene. It was about this time that block faulting was initiated adjacent to Svalbard. Faleide *et al.* (1984) interpreted the unconformity to be a result of tectonic activity near the present continent-oceanic crustal transition. Talwani *et al.* (1976) dated basal sediments as lower Pliocene or upper Miocene. Tertiary sediments were prograded toward the ocean basin forming the present passive margin (Myhre, 1984).

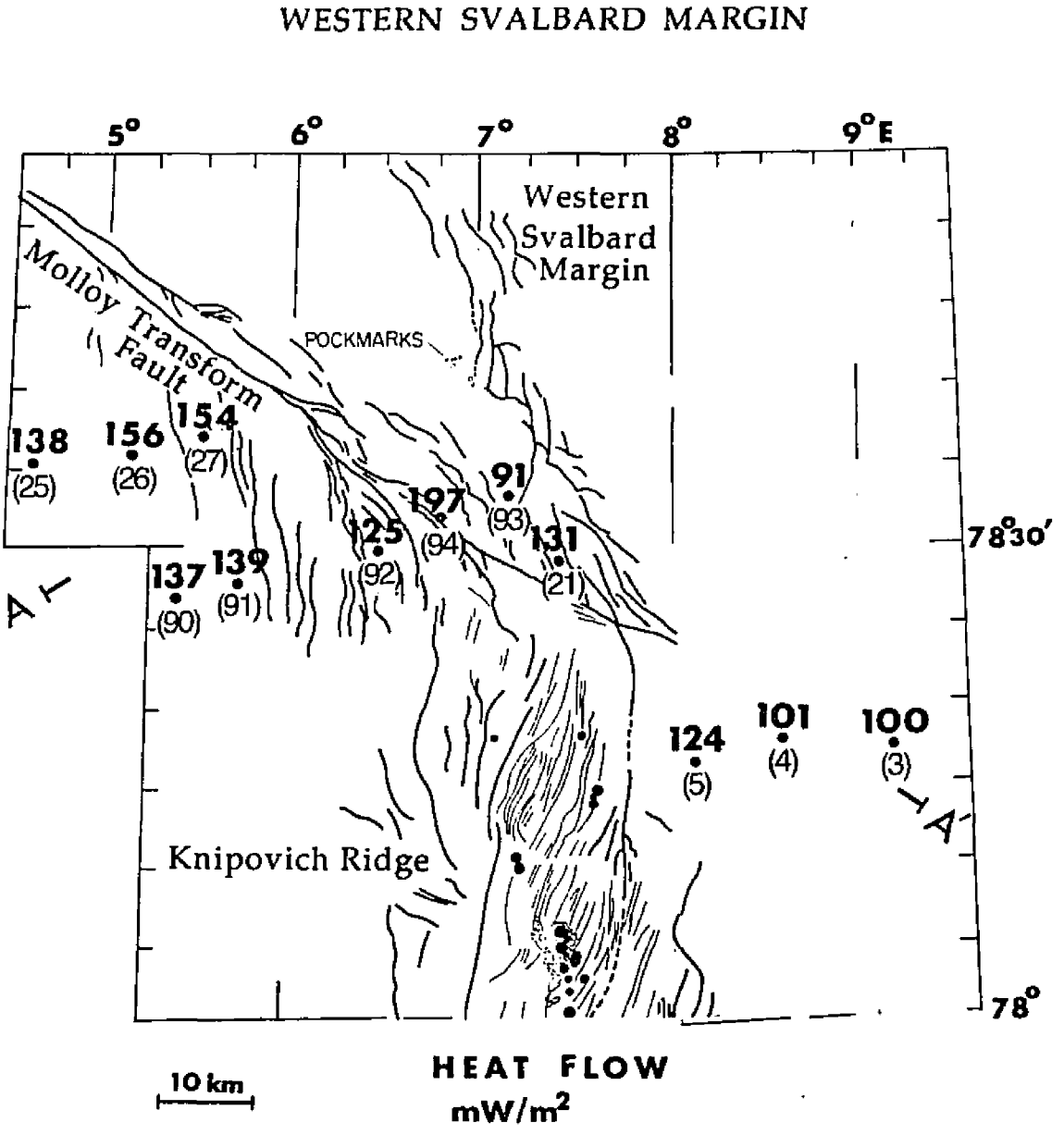

Figure 5-15. Heat flow (with station # ' s) at the intersection of the northern Knipovich Ridge/Molloy Transform Fault along the Western Svalbard Margin. Data (AA' profile) is complied from Langseth and Zielinski (1974) and Crane *et al.* (1982, 1988, 1991). Heat flow values reach 197 mW/m^2 at the intersection and 371 mW/m^2 around the tip of the Knipovich Ridge (within the rift valley). Close to Spitsbergen (only 70 km-distant) heat flow is still high (100 mW/m^2). Structural lineaments and volcanics are obtained from SeaMARC-II data.

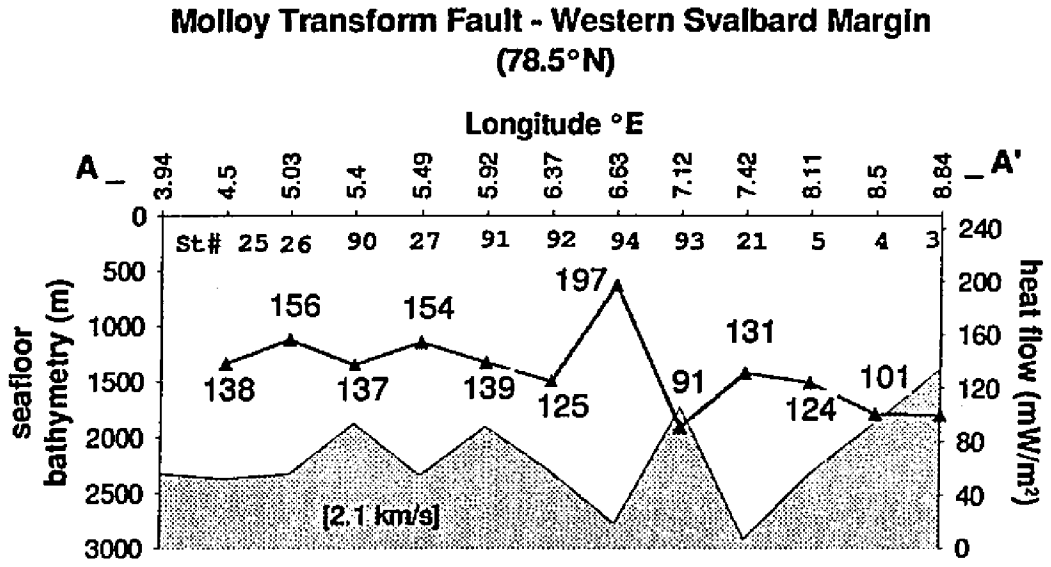

Figure 5-16. Heat flow profile at the intersection of the northern Knipovich Ridge and Molloy Transform Fault. Heat flow stations and values were collected by Crane *et al.* (1982, 1988, 1991), sediment velocity information are interpreted from Torp (1987). Seafloor bathymetry (*shaded*) was collected during the SeaMARC-II Expedition (1989).

Molloy Transform Fault and Western Svalbard Margin (78°30' N)					
	Sed.		Obs.	Correct	Thermal
St#	Rate	RF	Hf	Hf	Age
	m/my		mW/m²	mW/m²	my
25/84	29.25	1.27	138±2	175	9.3
26/84	25.78	1.31	156±14	204	7.8
90/84	2.35	1.16	137±2	160	9
27/84	22.37	1.23	154±6	190	6.7
91/84	3.24	1.25	139±2	175	8.4
92/84	1.53	1.13	125±1	142	9.3
94/84	2.29	1.48	197±9	293	10.5
93/84	5.54	1.26	91±4	115	12
21/V-27	11.25	1.41	131±5	183	13
5/	12.45	1.43	124±4	173.6	3.7
4/	9.39	1.52	101±4	153.5	8.1
3/	9.23	1.52	100±1	152	12

Table 5-4. Heat flow corrections at the intersection of the northern Knipovich Ridge and Molloy Transform Fault. Sedimentation rates, heat flow, reduction factors, observed and corrected heat flow values and thermal ages are tabulated across the Molloy Transform Fault along the Western Svalbard Margin at 78.5°N (between 3.94°E and 8.84°E).

Observed surface heat flow is compared to corrected heat flow in Figure 5-17. Thermal crustal ages and seafloor bathymetry are illustrated in Figure 5-18. The thermal crustal age along the Svalbard Margin is younger (13 Ma old) than expected for a crust 70 km away from the continent. Figure 5-19 compares this corrected heat flow with modeled heat flow predicted by the PS-cooling curve.

Figure 5-20 indicates the thermally derived crustal ages in the area, combined with other thermal modeling results as suggested by Crane *et al.* (1991). On the southern side of the Molloy Transform Fault at the northern Knipovich Ridge, thermal crustal ages approach 0-3.3 mybp. However, heat flow data north of the Molloy Transform Fault and on the West Svalbard/Yermak Plateau Margin show crustal ages of 13 mybp. Crane *et al.* (1988) suggest that the thermal crustal age of the Svalbard margin, further south (at 75°N), is 36 Ma. The young age of the northeastern Svalbard Margin is suggestive of large scale, widespread regional heating.

5. The Southern Yermak Plateau

a. High Heat Flow:

A region of high heat flow (up to 138 mW/m^2) on the southern Yermak Plateau trends NNW-SSE from 81°N along the northern Svalbard Margin (Crane *et al.*, 1982, 1988; Okay and Crane, 1993; Figure 5-21). Magnetic anomalies are absent from this part of the plateau. In the region of the high heat flow transect-AA' a

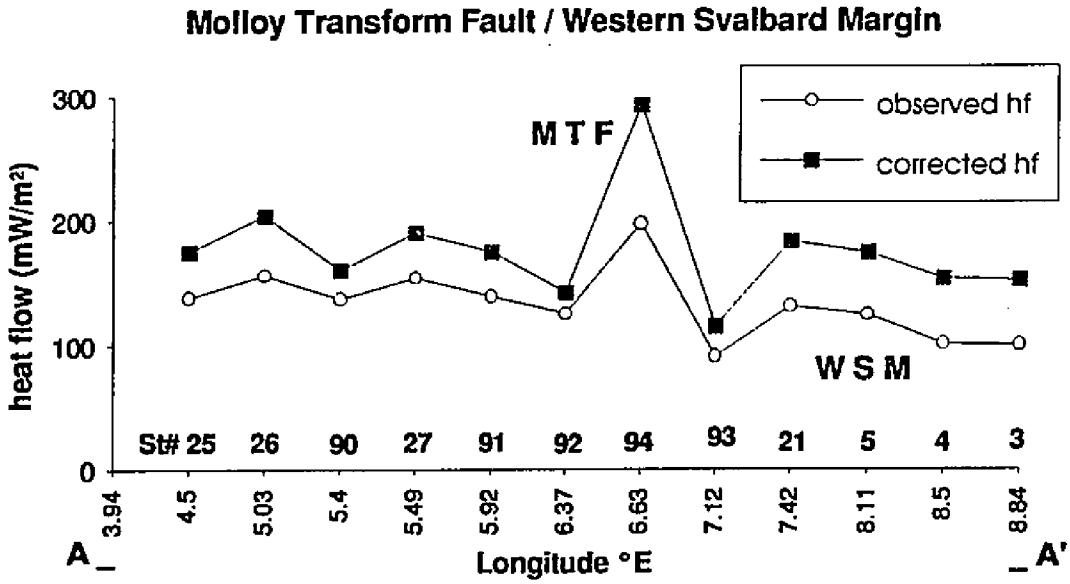

Figure 5-17. Heat flow analysis at the intersection of the northern Knipovich Ridge and Molloy Transform Fault. Comparison of the observed heat flow and corrected heat flow is shown across the Molloy Transform Fault (MTF) along the Western Svalbard Margin (WSM) at 78.5°N.

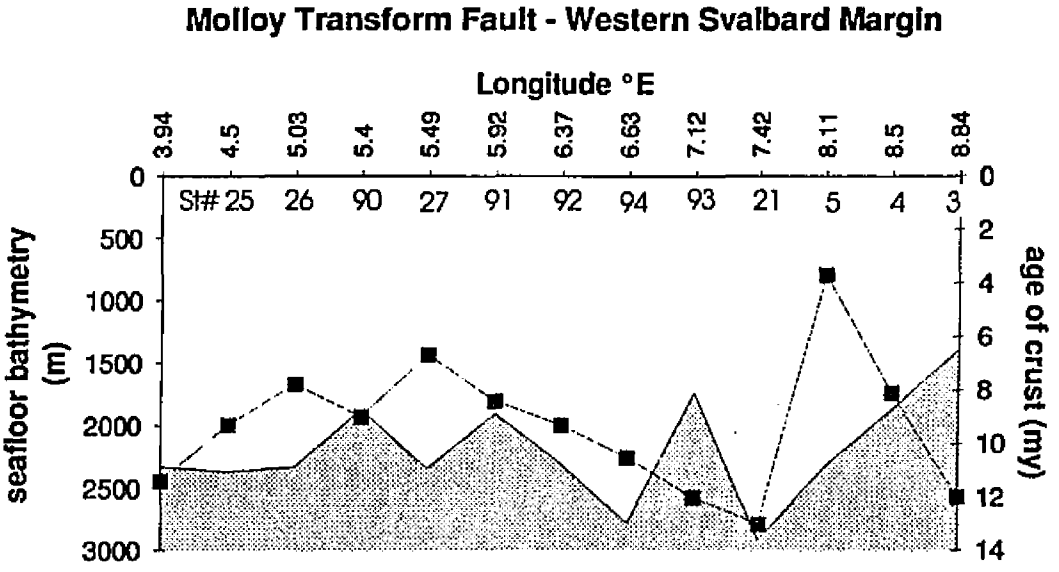

Figure 5-18. Crustal ages at the intersection of the northern Knipovich Ridge and Molloy Transform Fault. Thermally derived crustal ages and seafloor bathymetry are shown across the Molloy Transform Fault.

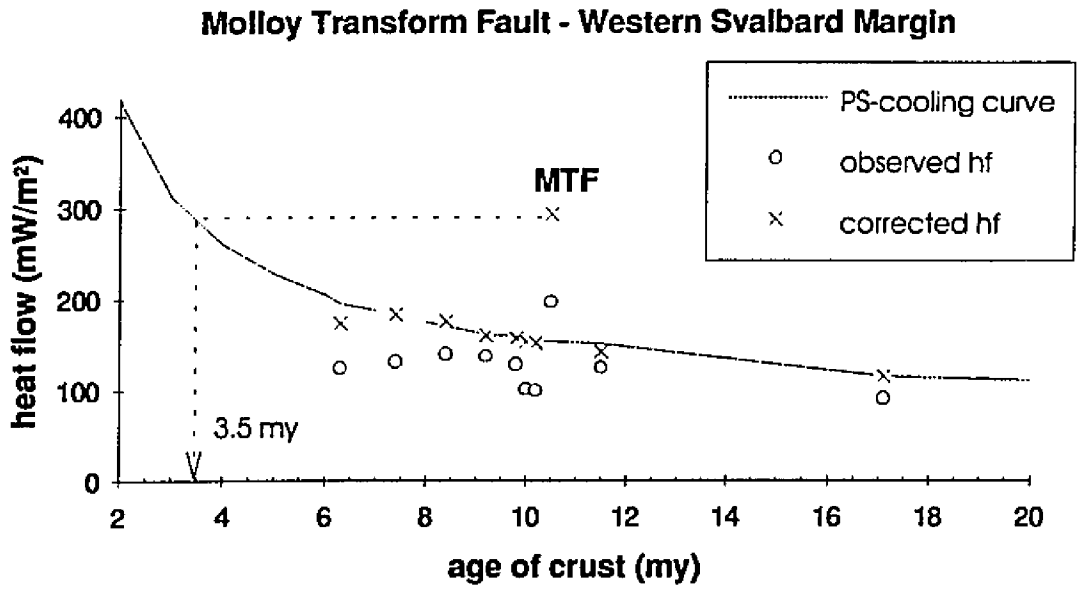

Figure 5-19. Cooling oceanic crust model at the intersection of the northern Knipovich Ridge and Molloy Transform Fault. Comparison of best fitting observed heat flow and corrected heat flow with the PS-cooling curve. Date of the most recent thermal rejuvenation at the intersection is found to be 3.5 mybp. MTF: Molloy Transform Fault.

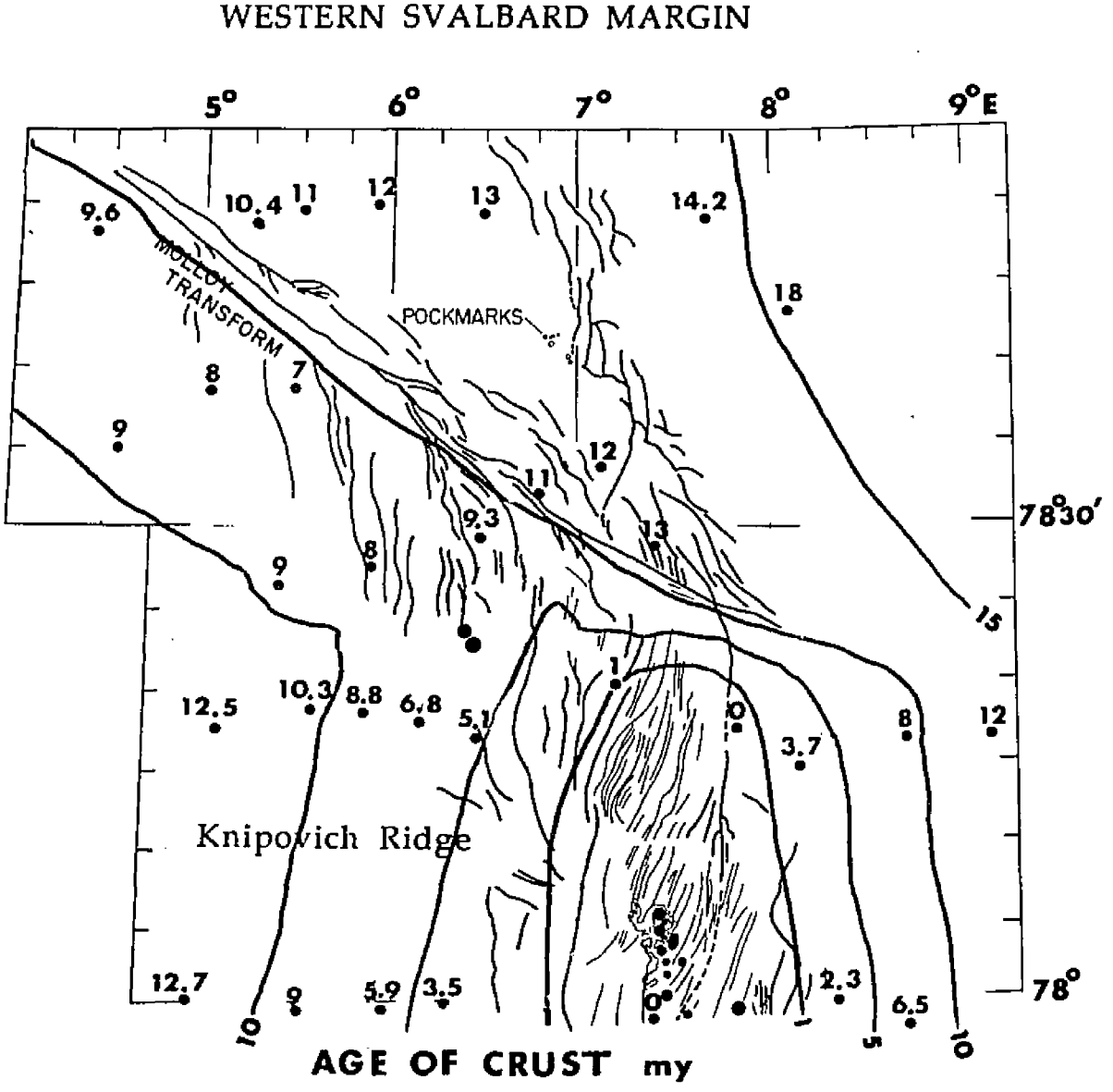

Figure 5-20. Thermal ages at the intersection of the northern Knipovich Ridge and the Molloy Transform Fault along the western Svalbard Margin. Age contours every 5 my Torp (1988) and Crane *et al.* (1991). Structural lineaments and volcanics are obtained from the results of the SeaMARC-II data (Crane and Solheim, 1995).

Figure 5-21. Main structures on the southern Yermak Plateau adjacent to the northern Svalbard Margin. Locations of heat flow values (mW/m^2) along the AA' transect are indicated by dots (collected by Crane *et al.*, 1982; and Sundvor, 1986, and reported by Sundvor and Torp, 1987; Crane *et al.*, 1988). Simplified bathymetry is adapted from Jackson *et al.* (1984) and Cherkis *et al.* (1991). The basement of the plateau is broken by numerous normal faults indicating a large complex graben system (interpreted from seismic cross sections collected by Sundvor *et al.*, 1982b). Faults that define the NW-SE trending Woodfjørden plateau basalts (*stars*) roughly lie in alignment with the western flank of the Yermak Plateau. Hornsund Fault (HF) lies along the western edge of the Yermak Plateau and is bordered by the Spitsbergen Transform Fault (STF), Molloy Ridge (MR) and Molloy Transform Fault (MTF).

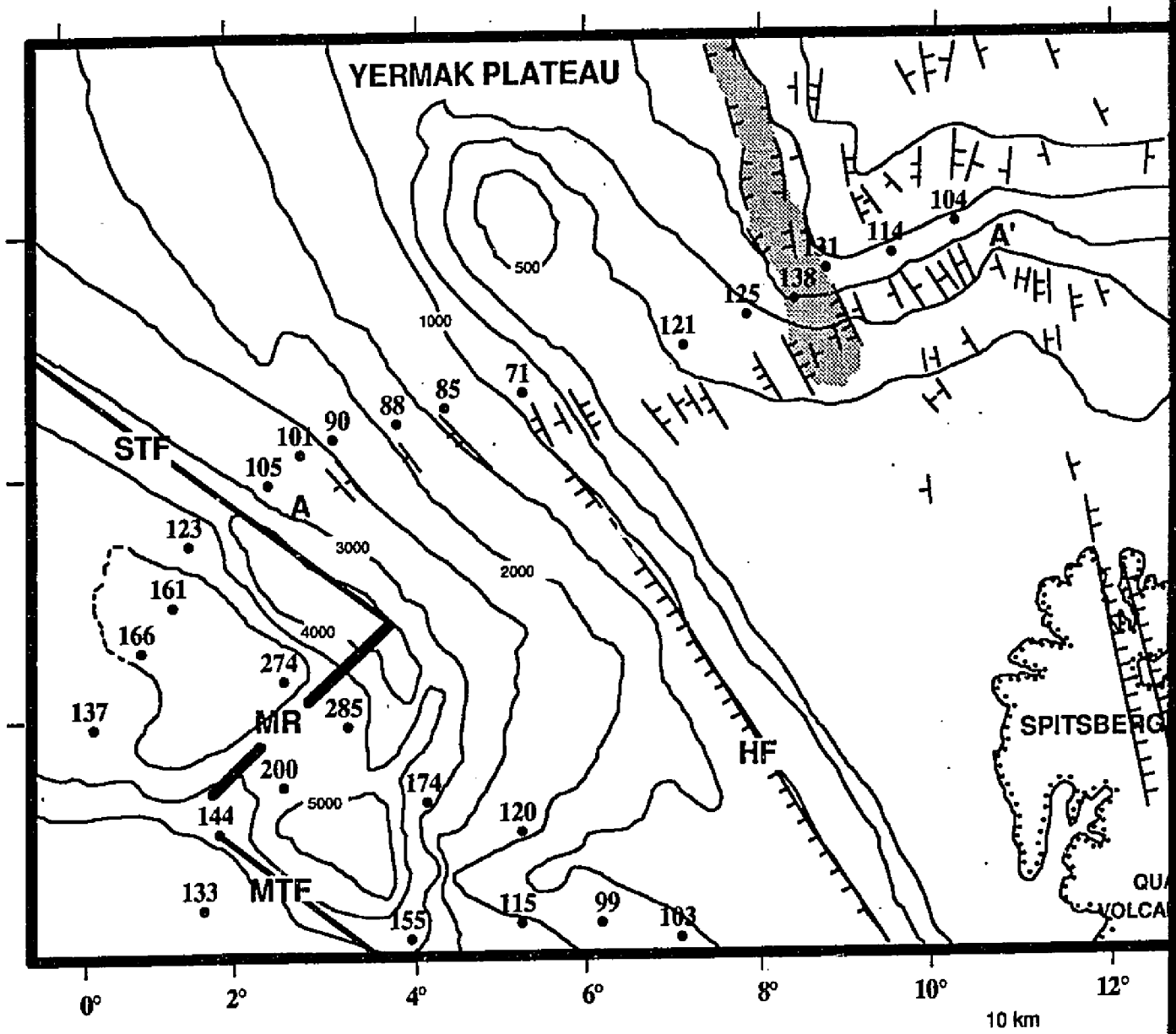
YERMAK PLATEAU
STF
A
A'
MR
MTF
HF
SPITSBERG
500
1000
2000
3000
4000
5000
104
114
131
138
125
121
71
85
88
90
101
105
123
161
166
274
285
137
200
174
144
120
133
155
115
99
103
0°
2°
4°
6°
8°
10°
12°
10 km

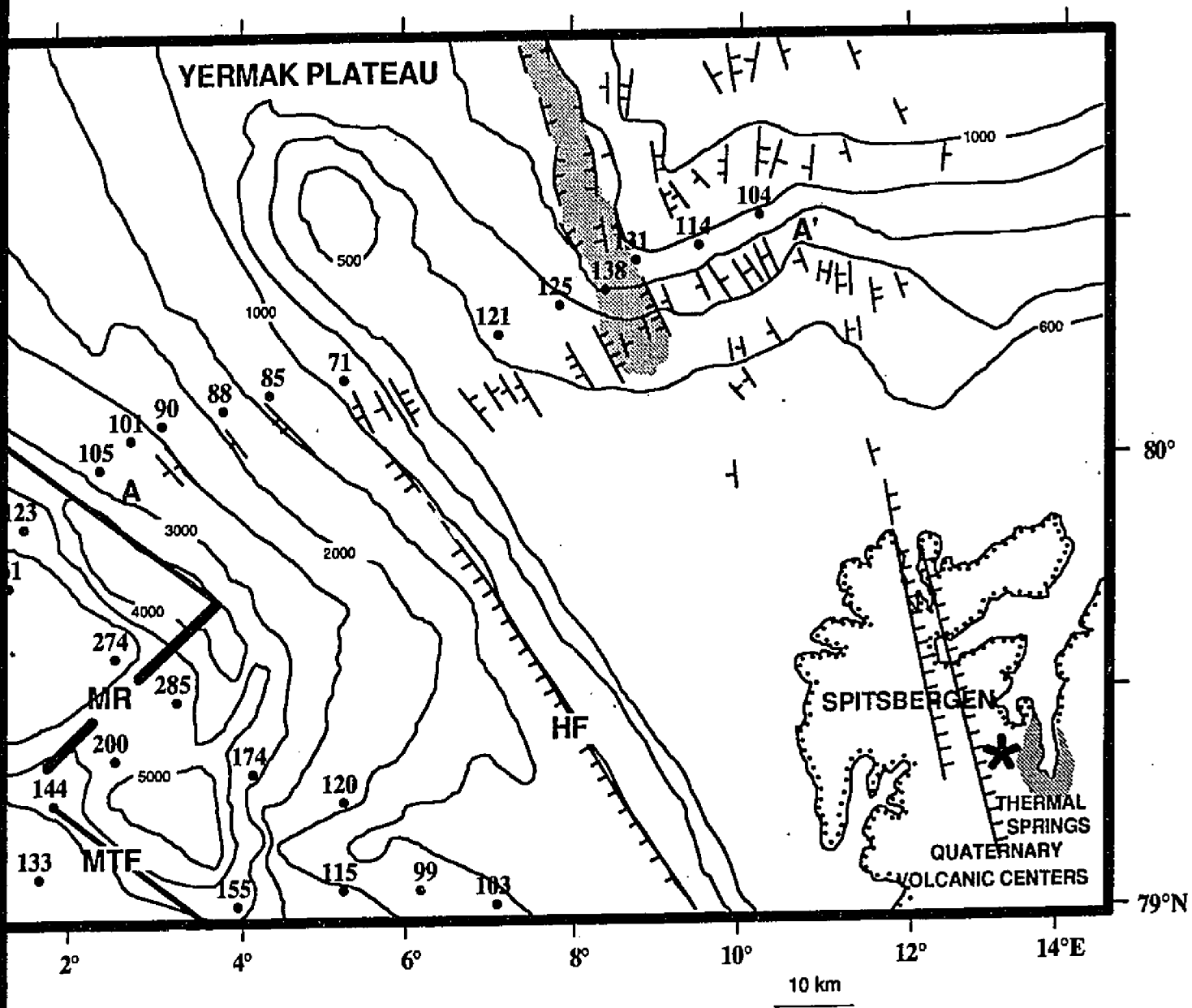
YERMAK PLATEAU
500
1000
1000
600
104
114
131
138
125
121
71
85
88
90
101
105
A
A'
3000
2000
4000
5000
123
1
274
285
MR
200
174
144
120
133
MTF
155
115
99
103
HF
SPITSBERGEN
THERMAL SPRINGS
QUATERNARY VOLCANIC CENTERS
80°
79°N
2°
4°
6°
8°
10°
12°
14°E
10 km

basement reflector is detected, which was interpreted as a volcanic constructional unit by Sundvor *et al.* (1978, 1982a). This basement reflector is highly faulted, and disappears under low velocity sediments (<2.5 km/s, Figure 5-22). Sundvor and Austegård (1990) have established the basement reflector (>5.5 km/s) as a tentative oceanic-continental crustal transition.

b. Correction of Heat Flow:

The compacted sediment thicknesses measured beneath the heat flow stations are corrected for a thermal cold blanketing effect. Decompacted sediment thicknesses are calculated for each time of onset and duration of intrusion. Following this, sedimentation rates are estimated using two-way travel times and sediment seismic velocities (Tables 5-5 and 5-6). Sedimentation rates are calculated using decompacted sediment thickness, based on the age of the crust below the heat flow station.

c. Spreading Rate-Corrections and Thermal-Crustal Age Estimations:

Thus surface heat flow is corrected (for each onset age of intrusion and duration of heating) to determine its value at the base of the sedimentary unit. For each heat flow station (assuming that extension has taken place by an intrusive event during a fixed period of time) corrected heat flow is determined by using the Hutchison Model (Table 5-7).

Figure 5-22. Heat flow profile: Southern Yermak Plateau. Line drawing of a seismic cross section on the southern Yermak Plateau. Observed surface heat flow (q_s) is indicated (AA' transect, see Figure 5-21). Seismic velocities (km/s) from Sonobuoy refraction measurements along the line are indicated (Sundvor *et al.*, 1982). Dark solid lines indicate the interface between layer 1 and layer 2. The basement-reflector correlates with a 5.5 km/s seismic refraction velocity. Depths to subsurface are estimated in seconds of two-way travel time. Numerous normal faults indicate stretching and thinning of the continental crust. The Hornsund Fault is determined to be a continent-oceanic crustal transition.

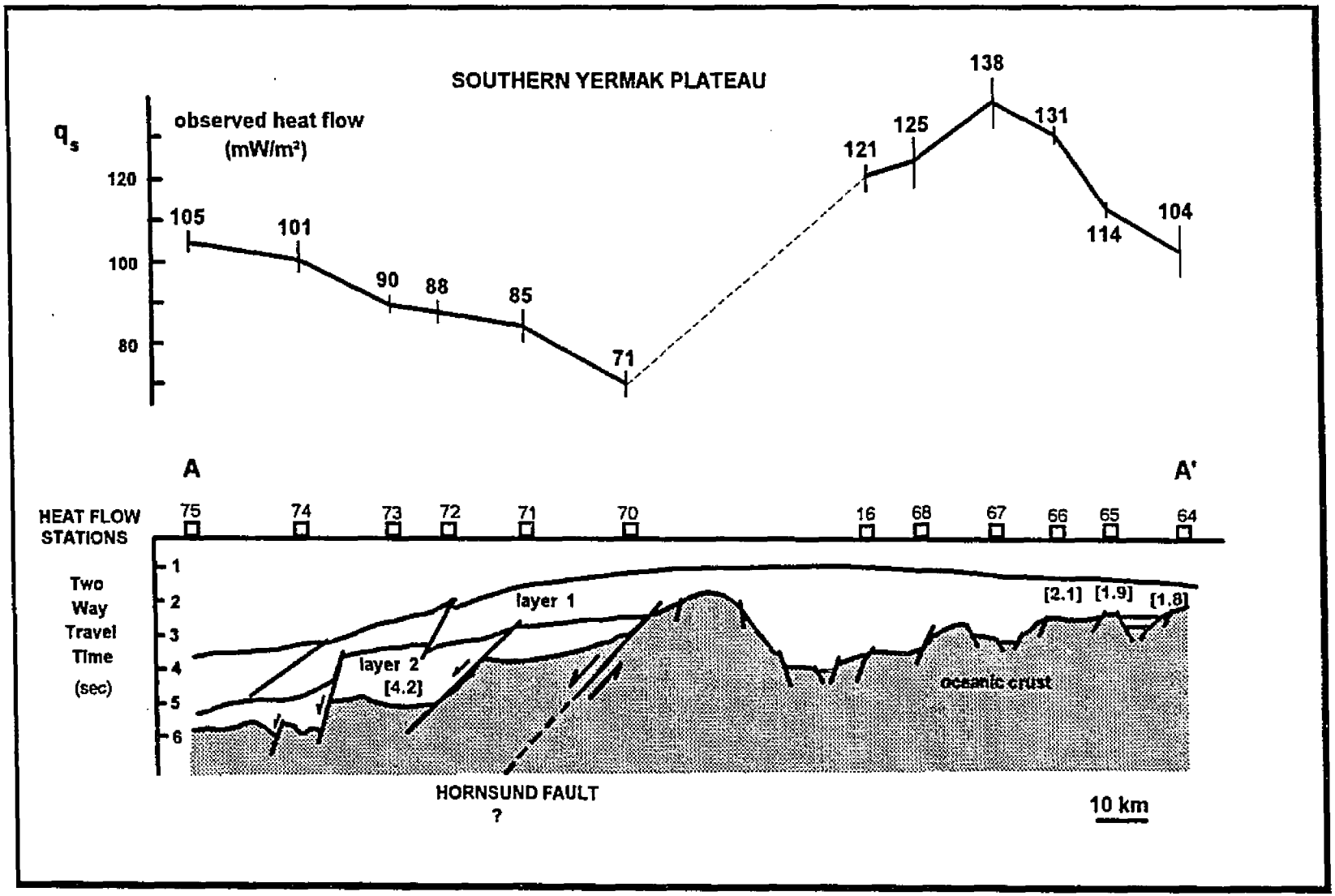
SOUTHERN YERMAK PLATEAU
q_s
observed heat flow
(mW/m²)
120
100
80
105
101
90
88
85
71
121
125
138
131
114
104
A
A'
HEAT FLOW STATIONS
75
74
73
72
71
70
16
68
67
66
65
64
Two Way Travel Time (sec)
1
2
3
4
5
6
layer 1
layer 2
[4.2]
[2.1]
[1.9]
[1.8]
oceanic crust
HORNSUND FAULT
?
10 km

SOUTHERN YERMAK PLATEAU

Layer 1

Heat Flow St.#	Sediment seismic velocity (km/s)	Depth $z = TWT/_2$ (sec)	H_{comp} (km)	H_{decomp} (km)
64	1.80	0.33	0.59	0.68
65	1.97	0.43	0.85	1.01
66	2.10	0.52	1.09	1.34
67	2.10	0.90	1.89	2.57
68	2.10	1.14	2.39	3.43
16	2.10	1.24	2.60	3.80

Table 5-5. Physical properties: southern Yermak Plateau. Depths (*sec*), compacted sediment thicknesses (H_{comp}) and decompacted sedimentary thicknesses (H_{comp}) calculated from two way travel time (*TWT*) and seismic velocities for each heat flow station (*St#*).

SOUTHERN YERMAK PLATEAU

St#	q_s (mWm^{-2})	$\phi(z)$	K	ρ_c ($x10^6$)	κ ($x10^7$km/my)
64	104±6	0.424	1.333	3.336	12.56
65	114±1	0.403	1.373	3.305	13.07
66	131±2	0.386	1.405	3.279	13.48
67	138±6	0.319	1.542	3.179	15.27
68	125±6	0.283	1.621	3.125	16.34
16	121±11	0.269	1.653	3.104	16.78

Table 5-6. Thermal parameters: southern Yermak Plateau. Porosities (ρ), conductivities (K), specific heat of fluid (ρc), and diffusivities (κ) for each heat flow station.

High heat flow (on supposedly thinned continental crust) indicates that some intrusive activity exists on the southern Yermak Plateau. Crane *et al.* (1982) suggest that intrusive activity initiated at 16 Ma and is continuing to the present. This region most likely has undergone the same Cenozoic volcanism that started about 11 mybp, approximately 100 km to the SE on Spitsbergen (Prestvik, 1978; Amundsen *et al.*, 1987, 1988). This interpretation is supported by the Quaternary volcanism and thermal springs (Amundsen *et al.*, 1988; Skjelvåle *et al.*, 1989) in the Woodfjørden area of Svalbard. Rifting, adjacent to Svalbard, began between 35 and 40 mybp as suggested by Crane *et al.* (1988). Therefore, I assumed 40 Ma for the maximum onset age of intrusion in the southern Yermak Plateau. Seven thermal episodes (between 0 and 40 Ma) are used to define the duration of intrusion (Tables 5-7a to 5-7g). Two of these thermal episodes imply that intrusion is still continuing (0 mybp to 35 mybp and 0 mybp to 40 mybp). Five thermal episodes imply that the intrusion ceased 10 to 18 mybp. Lithospheric extension rates (between 0.2 cm/yr and 0.5 cm/yr) are determined for each duration of intrusion responsible for stretching and extension of the plateau (Figures 5-23a to Figure 5-23g).

Thermal episodes are assumed for the different onset ages of intrusion and for the duration of heating, of the continental lithosphere, in the southern Yermak Plateau (Tables 5-8a to 5-8c). Corrected heat flow values are compared to modeled heat flow of the PS-cooling curve (Figures 5-24a and 5-24b). The best fit of surface heat flow and corrected heat flow is assumed to yield the most reasonable onset age of intrusion and duration of heating for the region. The best mean difference between modeled

Table 5-7. Heat flow analysis: southern Yermak Plateau.

Table 5-7a. Thermal Episode 1: assumes a duration of intrusion and thermal rejuvenation between 0 and 40 Ma with a total extension rate of 0.2 cm/yr. The distances between heat flow stations and the point source (where the highest heat flow is observed), decompacted sediment thickness, thermal age of the crust (my), sedimentation rate (m/my) and corrected heat flow values are calculated. The average sedimentation rate is 568 m/my. The difference between observed heat flow (qs) and corrected heat flow (q_b) is Δq, and the average mean heat flow (Δq) is 47.5 mW/m^2.

Table 5-7b. Thermal Episode 2: assumes a duration of intrusion and thermal rejuvenation between 0 and 35 Ma with a total extension rate of 0.23 cm/yr. The average sedimentation rate is calculated to be 675 m/my. The average mean heat flow (Δq) is 53.7 mW/m^2.

Table 5-7c. Thermal Episode 3: assumes a duration of intrusion and thermal rejuvenation between 10 and 40 Ma with a total extension rate of 0.26 cm/yr. The average sedimentation rate is 125 m/my. The average mean heat flow (Δq) is 21.3 mW/m^2.

Table 5-7d. Thermal Episode 4: assumes a duration of intrusion and thermal rejuvenation between 10 and 35 Ma with a total extension rate of 0.32 cm/yr. The average sedimentation rate is 134 m/my. The difference between observed heat flow (q_s) and corrected heat flow (q_b) is Δq and the average mean heat flow (Δq) is 21.3 mW/m^2.

Table 5-7e. Thermal Episode 5: assumes a duration of intrusion and thermal rejuvenation between 11.5 and 40 Ma yielding a total extension rate of 0.28 cm/yr. The average sedimentation rate is 117 m/my. The difference between observed heat flow (q_s) and corrected heat flow (q_b) is Δq and the average mean heat flow (Δq) is 20.3 mW/m^2.

Table 5-7f. Thermal Episode 6: assumes a duration of intrusion and thermal rejuvenation between 11.5 and 35 Ma yielding a total extension rate of 0.34 cm/yr. The average sedimentation rate is 125 m/my. The difference between observed heat flow (q_s) and corrected heat flow (q_b) is Δq and the average mean heat flow (Δq) is 20.3 mW/m^2.

Table 5-7g. Thermal Episode 7: assumes a duration of intrusion and thermal rejuvenation between 18 and 35 Ma yielding a total extension rate of 0.5 cm/yr. The difference between observed heat flow (q_s) and corrected heat flow (q_b) is Δq and the average mean heat flow (Δq) is 18.2 mW/m^2. The average sedimentation rate is 134 m/my.

Table 5-7a

SOUTHERN YERMAK PLATEAU

Thermal Episode 1:0 - 40 my
0.2 cm/yr

Sedimentation Rate

St#	Distance (km)	H_{decomp} (m)	Age of Crust (my)	Sed.Rate (m/my)	q_s	q_b	Δq
64	23.10	680	22.9	29.7	104	109	5
65	13.99	1010	13.8	72.9	114	125	11
66	6.97	1340	6.9	194.2	131	153	22
67	0.96	2570	1.0	2570.0	138	308	170
68	10.82	3430	10.7	320.0	125	169	44
16	17.31	3800	17.1	221.8	121	154	33

Ave.Sed.Rate = 568 m/my

$\Delta\bar{q} = 47.5\ mWm^{-2}$

Table 5-7b

SOUTHERN YERMAK PLATEAU

Thermal Episode 2: 0 - 35 my
0.23 cm/yr

St#	Distance (km)	H_{decomp} (m)	Sedimentation Rate: Age of Crust (my)	Sedimentation Rate: Sed.Rate (m/my)	q_s	q_b	Δq
64	23.10	680	20.01	33.99	104	109	5
65	13.99	1010	12.12	83.35	114	125	11
66	6.97	1340	6.04	221.97	131	155	24
67	0.96	2570	0.83	3090.88	138	335	197
68	10.82	3430	9.37	366.00	125	172	47
16	17.31	3800	14.99	253.46	121	159	38

Ave.Sed.Rate = 675 m/my

$\overline{\Delta q} = 53.7$ mWm^{-2}

Table 5-7c
SOUTHERN YERMAK PLATEAU

Thermal Episode 3:10 - 40my
0.26 cm/yr

Sedimentation Rate

St#	Distance (km)	H_{decomp} (m)	Age of Crust (my)	Duration	Sed.Rate (m/my)	q_s	q_b	Δq
64	23.10	680	17.8	27.8	24.5	104	109	5
65	13.99	1010	10.8	20.8	48.6	114	122	8
66	6.97	1340	5.4	15.4	87.0	131	147	16
67	0.96	2570	0.7	10.7	240.2	138	174	36
68	10.82	3430	8.3	18.3	187.4	125	157	32
16	17.31	3800	13.3	23.3	163.1	121	152	31

Ave.Sed.Rate = 125 m/my

$\Delta\bar{q} = 21.3\ mWm^{-2}$

Table 5-7d

SOUTHERN YERMAK PLATEAU

Thermal Episode 4:10 - 35 my
0.32 cm/yr

Sedimentation Rate

St#	Distance (km)	H_{decomp} (m)	Age of Crust (my)	Duration	Sed.Rate (m/my)	q_s	q_b	Δq
64	23.10	680	14.44	24.44	27.82	104	109	5
65	13.99	1010	8.74	18.74	53.90	114	123	9
66	6.97	1340	4.40	14.40	93.90	131	146	15
67	0.96	2570	0.60	10.60	242.45	138	174	36
68	10.82	3430	6.76	16.76	204.65	125	157	32
16	17.31	3800	10.83	20.83	182.43	121	152	31

Ave.Sed.Rate = 134 m/my

$\Delta\bar{q} = 21.3\ mWm^{-2}$

Table 5-7e

SOUTHERN YERMAK PLATEAU

Thermal Episode 5:11.5 - 40 my
0.28 cm/yr

Sedimentation Rate

St#	Distance (km)	H_{decomp} (m)	Age of Crust (my)	Duration	Sed.Rate (m/my)	q_s	q_b	Δq
64	23.10	680	16.27	27.77	24.49	104	108	4
65	13.99	1010	9.85	21.35	47.30	114	122	8
66	6.97	1340	4.90	16.40	81.70	131	146	15
67	0.96	2570	0.68	12.18	211.07	138	170	32
68	10.82	3430	6.76	19.12	179.40	125	157	32
16	17.31	3800	12.20	23.70	160.40	121	152	31

Ave.Sed.Rate = 117 m/my

$\overline{\Delta q} = 20.3\ mWm^{-2}$

Table 5-7f

SOUTHERN YERMAK PLATEAU

Thermal Episode 6:11.5 - 35 my
0.34 cm/yr

Sedimentation Rate

St#	Distance (km)	H_{decomp} (m)	Age of Crust (my)	Duration	Sed.Rate (m/my)	q_s	q_b	Δq
64	23.10	680	13.43	24.93	27.27	104	109	5
65	13.99	1010	8.14	19.64	51.44	114	122	8
66	6.97	1340	4.05	15.55	86.16	131	147	16
67	0.96	2570	0.56	12.06	213.10	138	169	31
68	10.82	3430	6.29	17.79	192.80	125	157	32
16	17.31	3800	10.07	21.57	176.20	121	152	31

Ave.Sed.Rate = 125 m/my

$\overline{\Delta q} = 20.3\ mWm^{-2}$

Table 5-7g

SOUTHERN YERMAK PLATEAU

Thermal Episode 7: 18 - 35 my

0.5 cm/yr

Sedimentation Rate

St#	Distance (km)	H_{decomp} (m)	Age of Crust (my)	Duration	Sed.Rate (m/my)	q_s	q_b	Δq
64	23.10	680	9.72	26.72	27.82	104	108	4
65	13.99	1010	5.89	22.89	53.90	114	122	8
66	6.97	1340	2.93	19.93	93.06	131	144	13
67	0.96	2570	0.40	17.40	242.45	138	165	27
68	10.82	3430	4.55	17.70	204.65	125	154	29
16	17.31	3800	7.28	21.57	182.43	121	149	28

Ave.Sed.Rate = 134 m/my

$\Delta\bar{q} = 18.2\ mWm^{-2}$

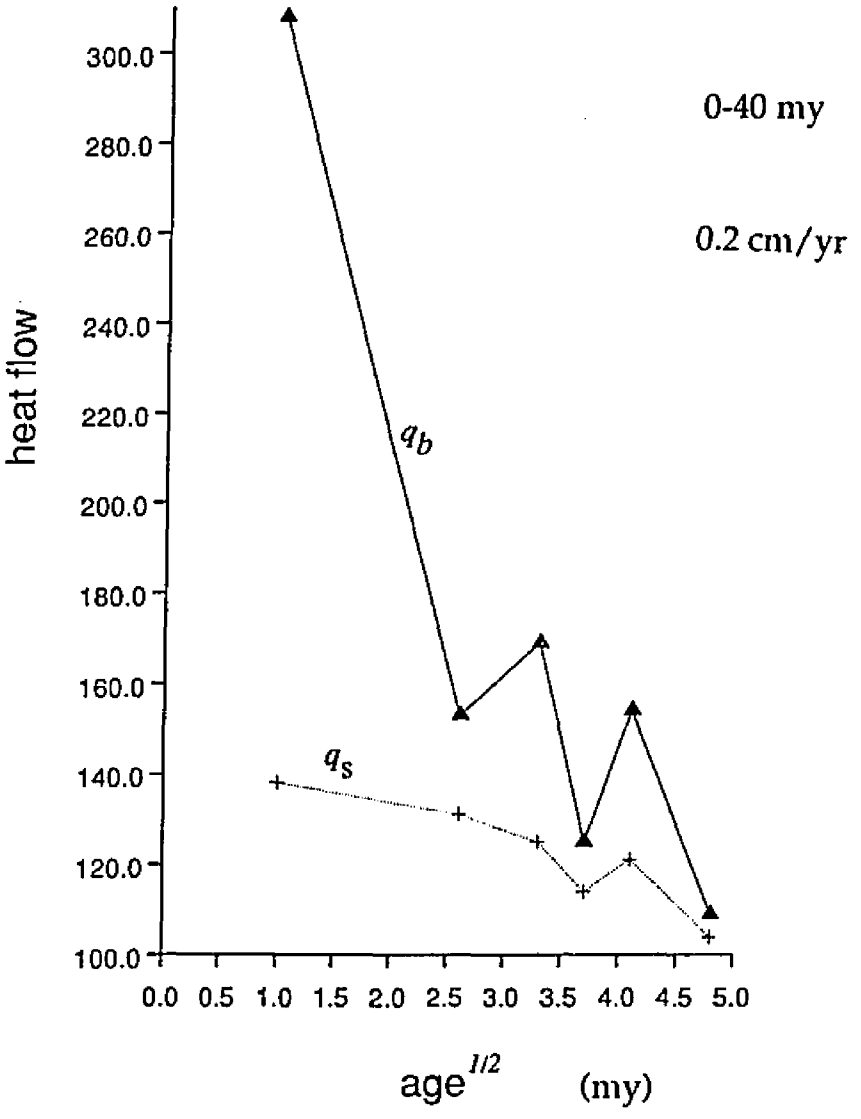

Figure 5-23a. Thermal Episode 1. Observed surface heat flow (q_s) and corrected heat flow at the base of the sediment (q_b) versus thermal age of the crust (age$^{1/2}$) for an assumed duration (0-40 Ma) on the southern Yermak Plateau and the total extension rate of 0.2 cm/yr.

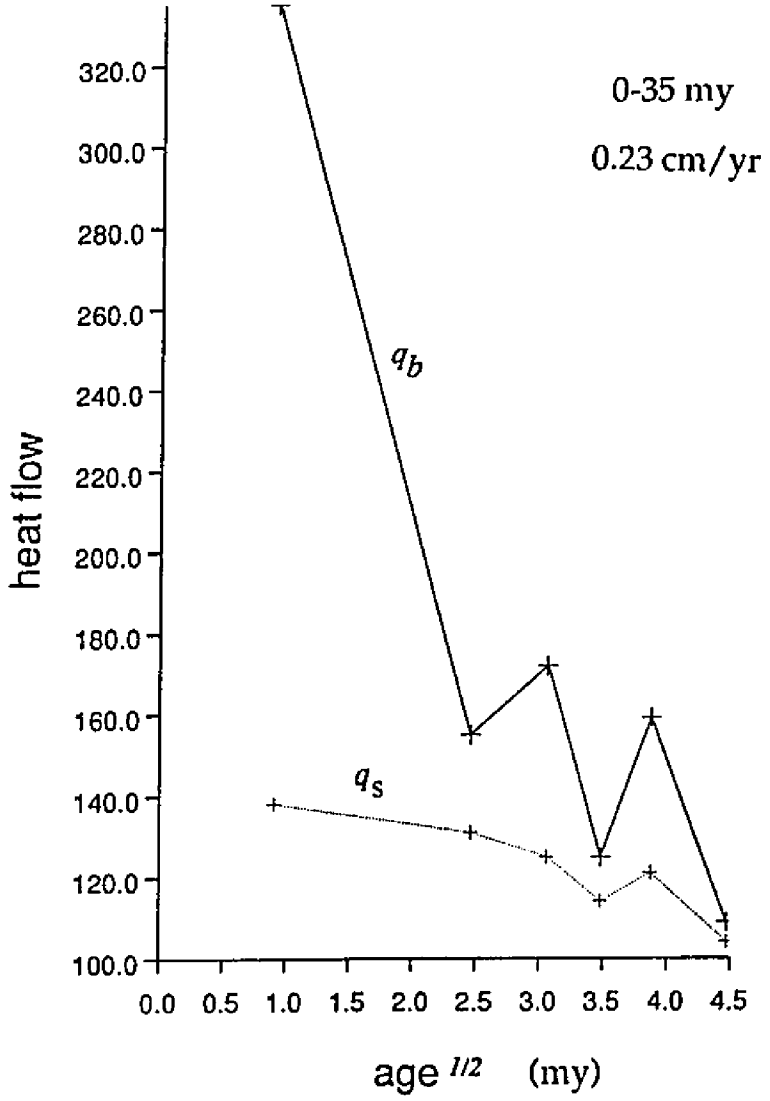

Figure 5-23b. Thermal Episode 2. Observed surface heat flow (q_s) and corrected heat flow at the base of the sediment (q_b) versus thermal age of the crust (age$^{1/2}$) for an assumed thermal rejuvenation duration (10-40 Ma) on the southern Yermak Plateau and the total extension rate of 0.23 cm/yr.

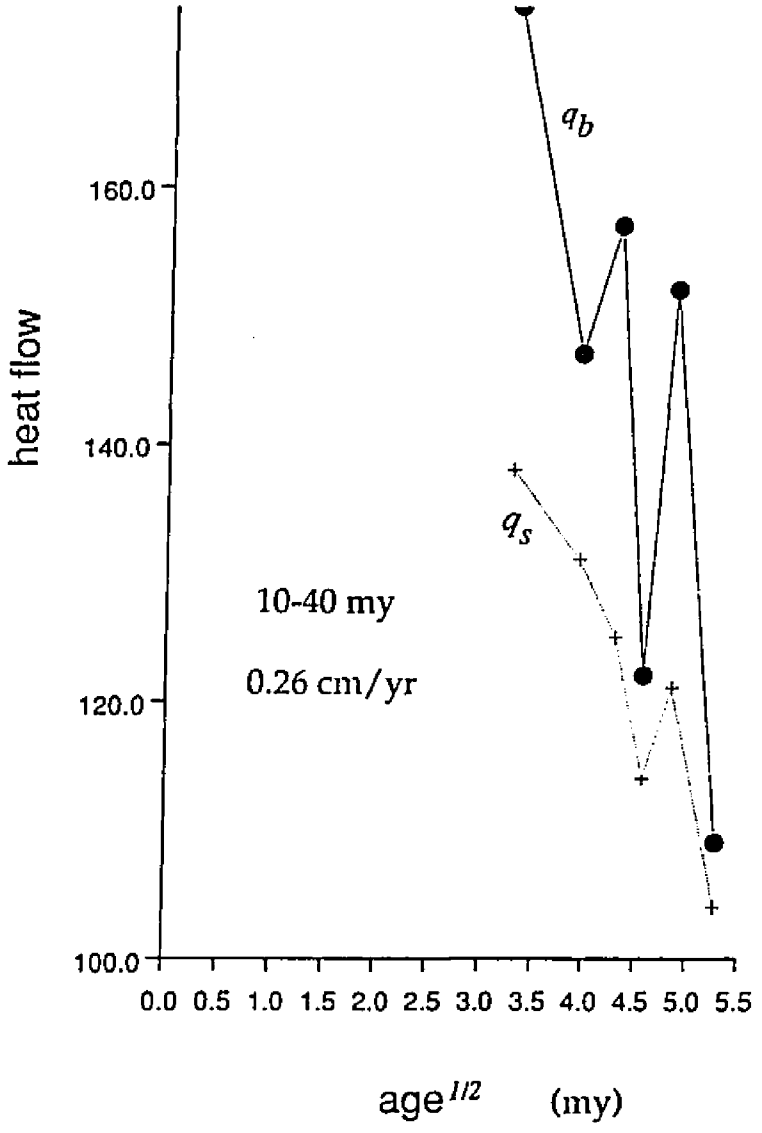

Figure 5-23c. Thermal Episode 3. Observed surface heat flow (q_s) and corrected heat flow at the base of the sediment (q_b) versus thermal age of the crust (age$^{1/2}$) for an assumed thermal rejuvenation duration (10-40 Ma) on the southern Yermak Plateau and total extension rate of 0.26 cm/yr.

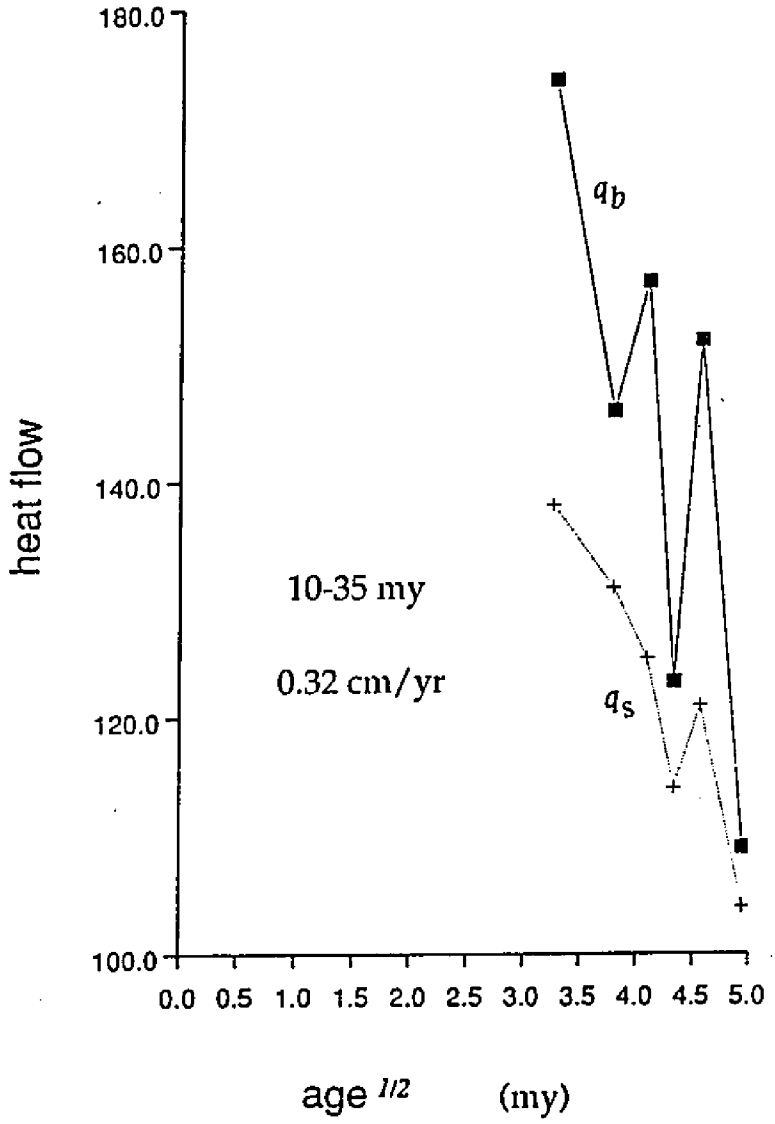

Figure 5-23d. Thermal Episode 4. Observed surface heat flow (q_s) and corrected heat flow (q_b) at the base of the sediment versus thermal age of the crust (age$^{1/2}$) for an assumed thermal rejuvenation duration (10-35 Ma) on the southern Yermak Plateau and the total extension rate of 0.32 cm/yr.

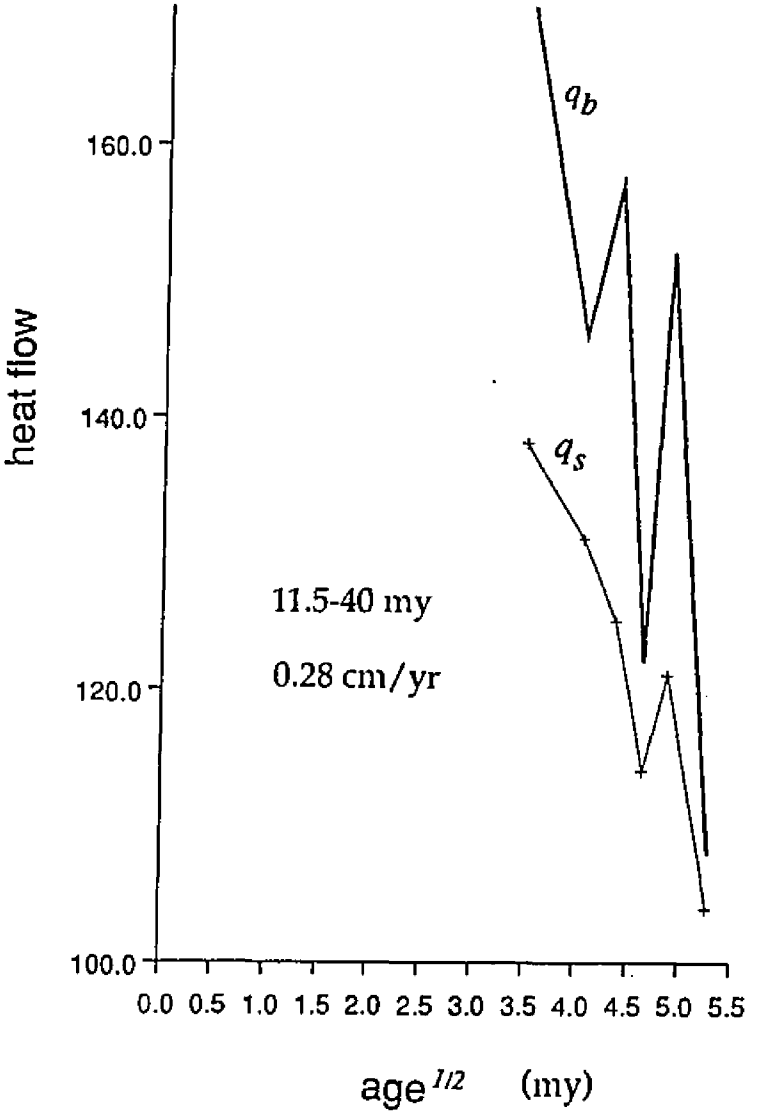

Figure 5-23e. Thermal Episode 5. Observed surface heat flow (q_s) and corrected heat flow (q_b) at the base of the sediment versus thermal age of the crust (age$^{1/2}$) for an assumed thermal rejuvenation duration (11.5-40 Ma) on the southern Yermak Plateau and the total extension rate of 0.28 cm/yr.

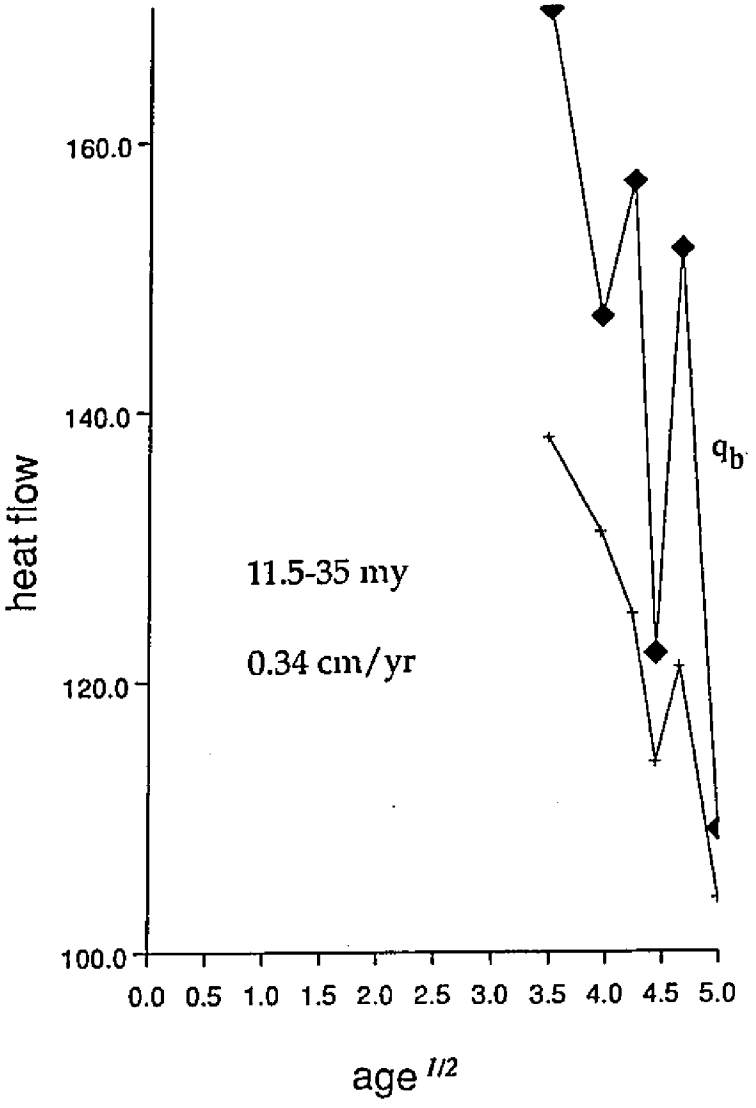

Figure 5-23f. Thermal Episode 6. Observed surface heat flow (q_s) and corrected heat flow (q_b) at the base of the sediment versus thermal age of the crust (age$^{1/2}$) for an assumed thermal rejuvenation duration (11.5-35 Ma) on the southern Yermak Plateau and the total extension rate of 0.34 cm/yr.

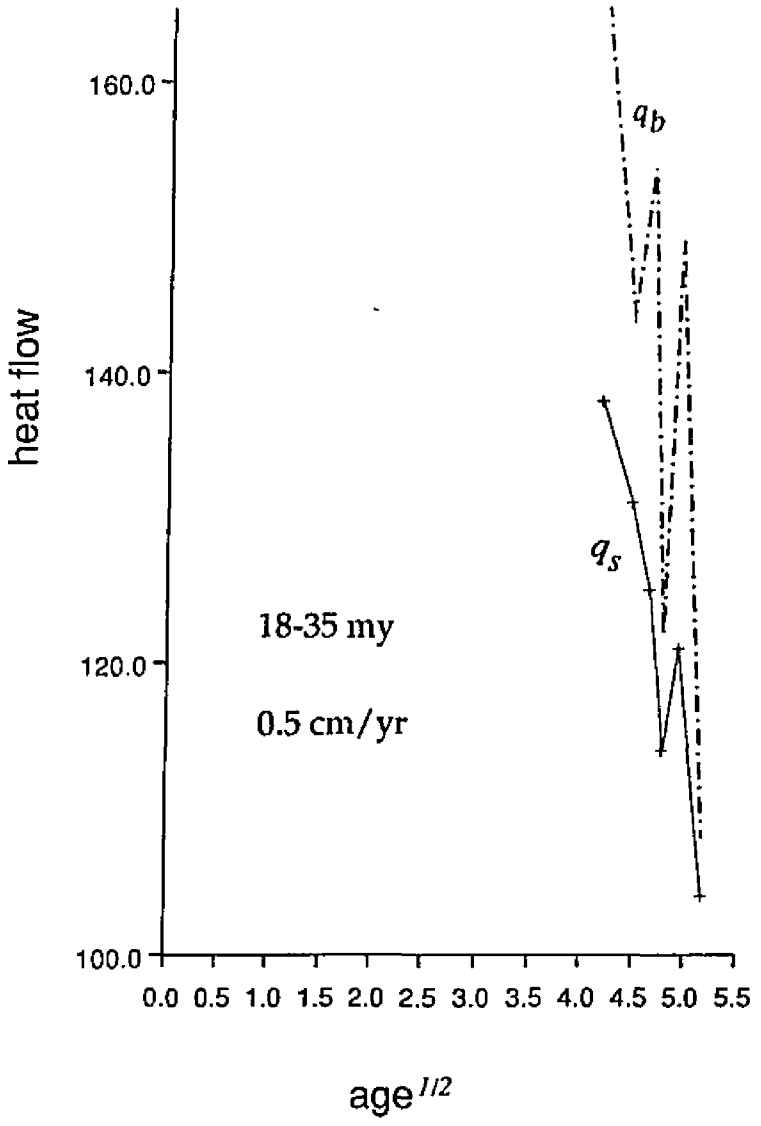

Figure 5-23g. Thermal Episode 7. Observed surface heat flow (q_s) and corrected heat flow (q_b) at the base of the sediment versus thermal age of the crust (age$^{1/2}$) for an assumed thermal rejuvenation duration (18-35 Ma) on the southern Yermak Plateau and the total extension rate of 0.5 cm/yr.

Table 5-8. Cooling oceanic plate model: southern Yermak Plateau.

Table 5-8a. A comparison of corrected heat flow (q_b) to theoretical heat flow values ($q_{s\text{-}p}$) based on the age-dependent cooling of the oceanic crust (Parsons and Sclater, 1977). Thermal age of the crust for each heat flow station are tabulated. Δq: the difference between corrected heat flow (q_b) and the theoretical heat flow ($q_{s\text{-}p}$), Δq: the mean value, it indicates the goodness of fit for Thermal Episodes 1 to 3.

Table 5-8b. A comparison of corrected heat flow (q_b) to theoretical heat flow values ($q_{s\text{-}p}$) for Thermal Episodes 4 to 6. Thermal Episode 4 (for a duration of 10-35 Ma) gives the best fit. Δq: the difference between corrected heat flow (q_b) and the theoretical heat flow ($q_{s\text{-}p}$), Δq is 24.3 mW/m^2 and the total extension rate is 0.32 cm/yr.

Table 5-8c. Thermal Episode 7. The thermal age of the crust for each heat flow station is tabulated. Δq: the difference between corrected heat flow (q_b) and the theoretical heat flow ($q_{s\text{-}p}$). The mean (Δq) value is 36 mW/m^2.

Table 5-8a

SOUTHERN YERMAK PLATEAU

COOLING OCEANIC CRUST

St#	Thermal Episode 1: 0 - 40 my Age my	q_b	q_{sp}	Δq	Thermal Episode 2: 0 - 35 my Age my	q_b	q_{sp}	Δq	Thermal Episode 3: 10 - 40 my Age my	q_b	q_{sp}	Δq
64	22.9	109	100	9	20.1	109	111	2	27.8	109	90	19
65	13.8	125	130	5	12.1	125	140	15	20.8	122	108	14
66	6.9	153	188	35	6.04	155	189	34	15.4	147	125	22
67	1.0	308	840	532	0.8	335	950	615	10.7	174	150	24
68	10.7	169	150	19	9.3	172	160	12	18.3	157	112	45
16	17.1	154	121	33	14.9	159	128	31	23.3	152	100	52
	$\overline{\Delta q}$ = 107 mWm^{-2}				$\overline{\Delta q}$ = 118 mWm^{-2}				$\overline{\Delta q}$ = 29.4 mWm^{-2}			

Table 5-8b

SOUTHERN YERMAK PLATEAU

COOLING OCEANIC CRUST

	Thermal Episode 4: 10 - 35 my				Thermal Episode 5: 11.5 - 40 my				Thermal Episode 6: 11.5 - 35 my			
St#	Age my	q_b	q_{sp}	Δq	Age my	q_b	q_{sp}	Δq	Age my	q_b	q_{sp}	Δq
64	24.4	109	100	9	27.7	108	90	18	24.9	109	99	10
65	18.7	123	115	8	21.3	122	105	17	19.6	122	111	11
66	14.4	146	125	21	16.4	146	120	26	15.5	147	120	27
67	10.6	174	150	24	12.1	170	140	30	12.1	169	140	30
68	16.7	157	120	37	19.1	157	110	47	17.8	157	117	40
16	20.8	152	105	47	23.7	152	100	52	21.6	152	110	42
	$\Delta\bar{q}$ = 24.3 mWm^{-2}				$\Delta\bar{q}$ = 31.7 mWm^{-2}				$\Delta\bar{q}$ = 26.6 mWm^{-2}			

Table 5-8c

SOUTHERN YERMAK PLATEAU

Thermal Episode 7:
18 - 35 Ma

St#	Age Ma	q_b	q_{sp}	Δq
64	26.7	108	93	15
65	22.9	122	100	22
66	19.9	144	110	34
67	17.4	165	120	45
68	21.6	154	105	49
16	24.3	149	97	52

$\Delta q = 36$ mW/m^2

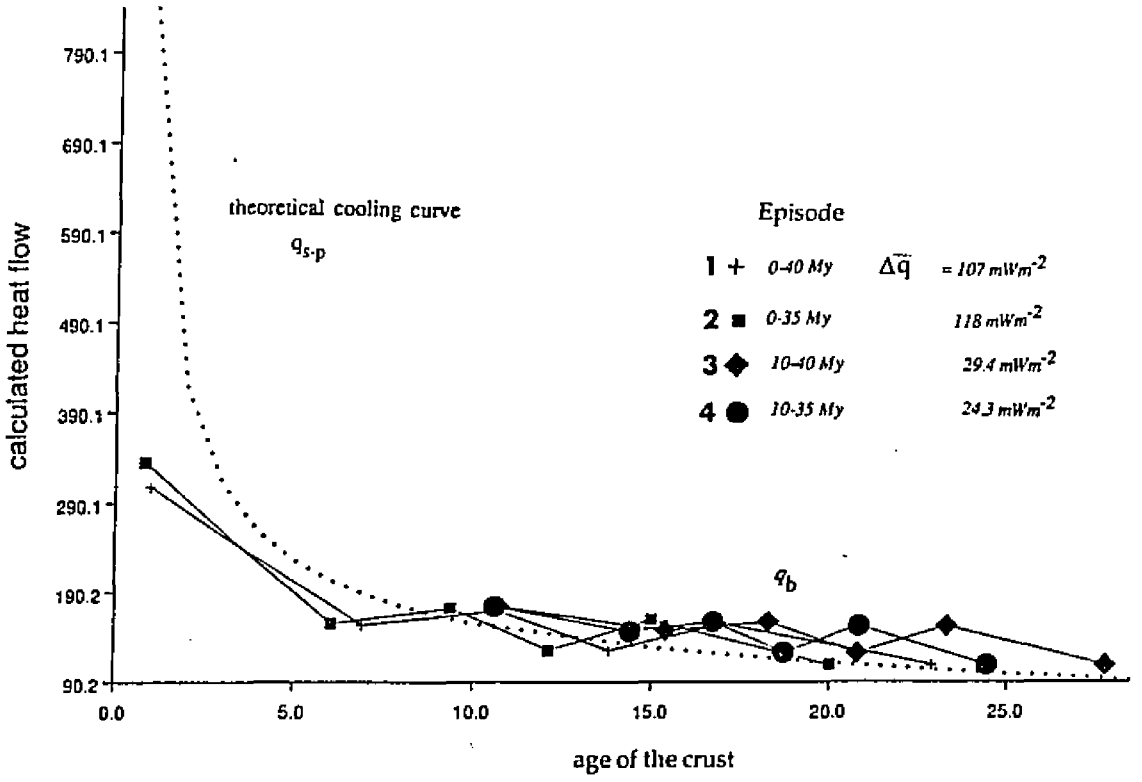

Figure 5-24a. Cooling oceanic crust model: southern Yermak Plateau (Thermal Episodes 1 to 4). Comparison of corrected heat flow (q_b) and theoretical heat flow (q_{sp}) on the southern Yermak Plateau. Theoretical heat flow (dotted line) is based on Sclater and Parsons, 1977). Mean values (Δq) indicate the goodness of fit of four episodes. Note the best fit is Thermal Episode 4 with a mean value of 24.3 mW/m^2 for the duration of intrusion of 25 mybp the thermal rejuvenation occurring between 10-35 Ma with a total extension rate of 0.32 cm/yr.

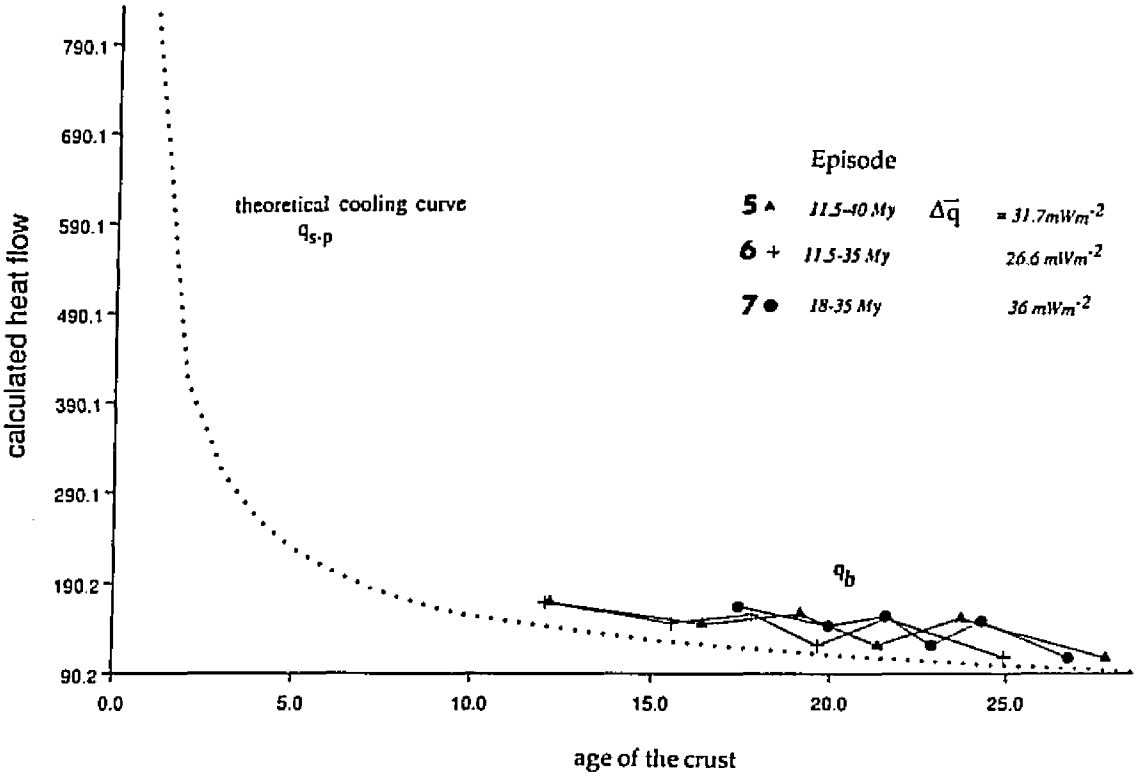

Figure 5-24b. Cooling oceanic crust model: southern Yermak Plateau (Thermal Episodes 5 to 7). Comparison of corrected heat flow (q_b) in the southern Yermak Plateau to theoretical heat flow (q_{sp}) (*dotted line*, based on Sclater and Parsons, 1977). Mean values (Δq) indicate the goodness of fit.

and corrected heat flow (Δq) is 24 mW/m^2 (Thermal Episode 4, for an ongoing intrusion from 35 mybp to present, Table 5-8b). The mean value of worst fit of the thermal episodes is 118 mW/m^2. If the cooling oceanic plate model adequately represents the intrusive activity in this region, the crust was most recently rejuvenated 11 mybp. Figure 5-25 depicts thermal crustal ages demonstrating time of intrusion and thermal rejuvenation on the Yermak Plateau, as determined from Thermal Episode 4. This thermal-crustal age coincides with the commencement of volcanism in the Woodfjørden area of Spitsbergen.

d. Testing the Lithospheric Extension Mechanisms:

If the southern Yermak Plateau is primarily continental crust, the cooling oceanic plate model is not adequate. In this case, it would be more appropriate to apply continental lithospheric extension models to the plateau. I use numerical modeling to determine the thermo-mechanical structure of the plateau and to determine whether or not the plateau is undergoing breakup and rifting by symmetric pure-shear extension (Parsons and Sclater, 1977; McKenzie, 1978) or undergoing asymmetric simple-shear extension along a major detachment fault. The best fit to observed data suggest a spreading rate of 0.32 cm/yr.

In Figures 5-26 and 5-27 the numerical modeling results illustrate different results assuming an initial rift width and total extension rate for crustal thinning, heat flow, thermal uplift and subsidence. Model results depend on the temperature

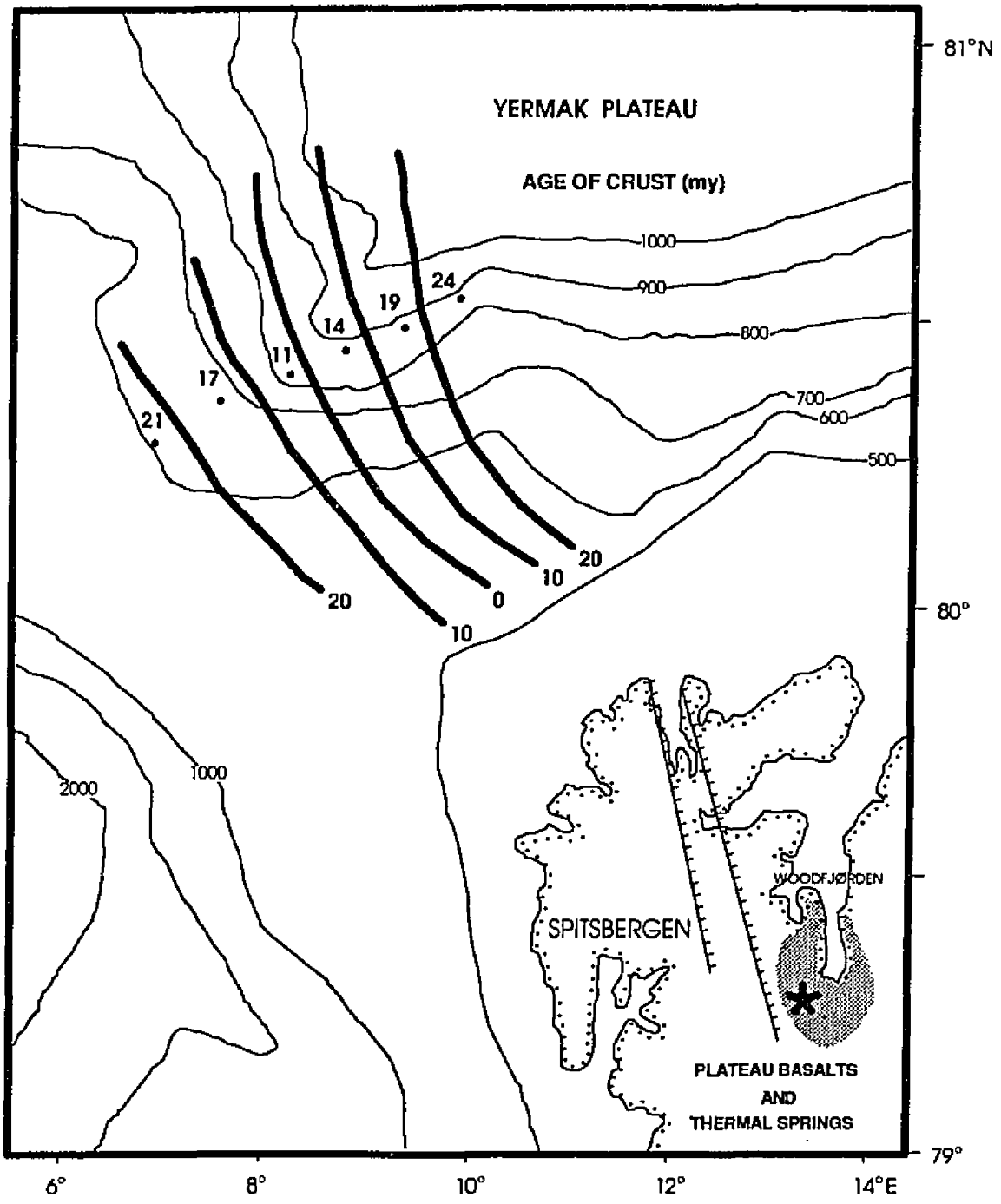

Figure 5-25. Estimated thermal ages (Thermal Episode 4): southern Yermak Plateau. Thermal crustal ages (*dots*) are indicated (see Table 5-8). These thermal crustal age contours (interval of 10 my, *bold lines*) coincide with the ages of plateau basalts (shaded region) and thermal springs (*star*) in the Woodfjørden Volcanic Center in Spitsbergen. Simplified bathymetry (in meters) adapted from Cherkis *et al.* (1991).

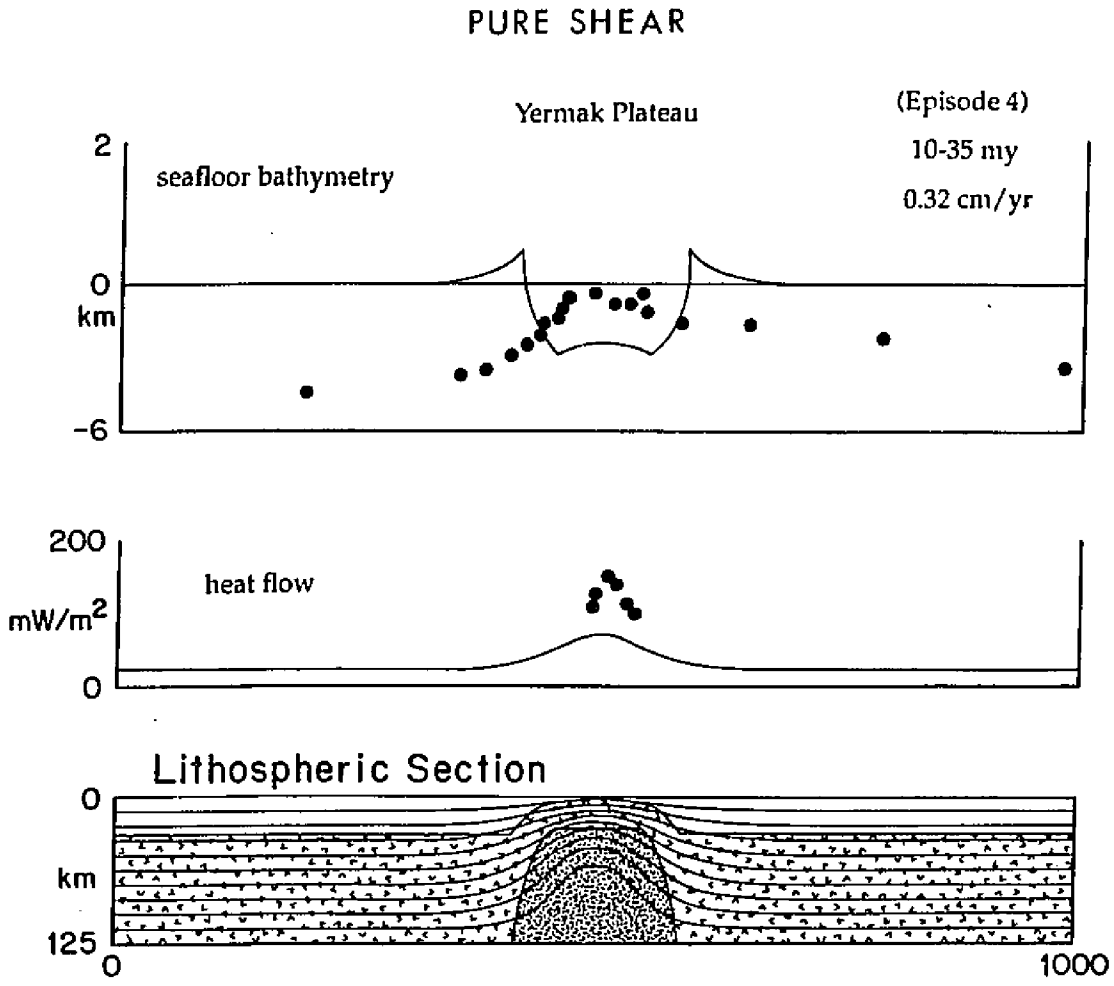

Figure 5-26. Pure-shear lithospheric extension: southern Yermak Plateau. Total extension rate is 0.32 cm/yr (0-35 Ma, Thermal Episode 4) and total present-day offset across is 112 km. The initial crustal thickness was 32 km (un-shaded region of the lithospheric section) and the initial rift width was 48 km. Observed seafloor bathymetry (topography) and heat flow indicated by dots are superimposed on the synthetic topography and heat flow curves. Curvilinear lines in the lithospheric section show isotherms and dark shaded region that indicates an upwelling asthenosphere. Horizontal and vertical scales are in kilometers. Grid dimensions are 13x104.

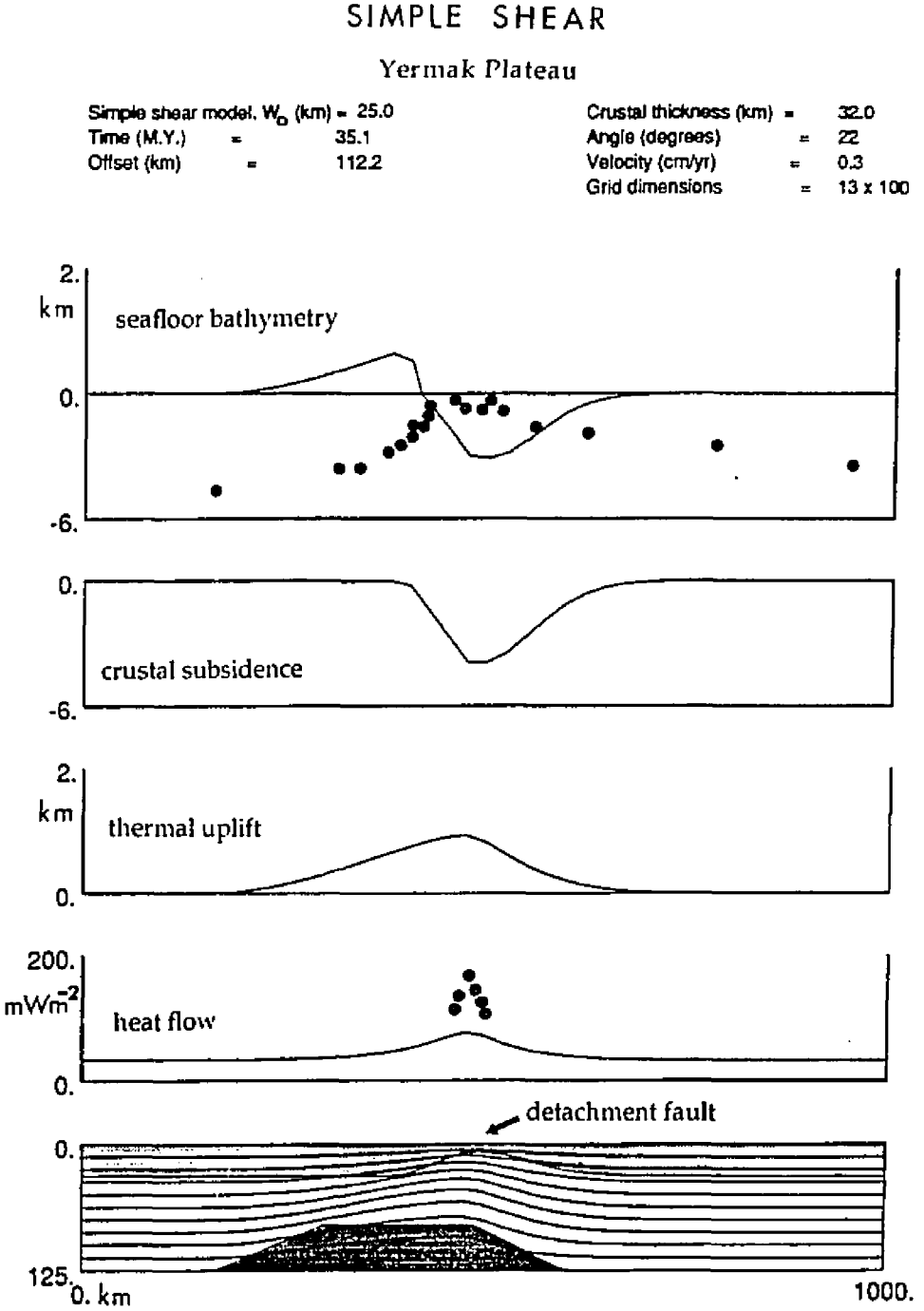

Figure 5-27. Simple shear lithospheric extension model: southern Yermak Plateau. Total extension rate is 0.32 cm/yr for a low-angle (22°) detachment fault (Thermal Episode 4). Observed seafloor bathymetry (topography) corrected for sediment loading (dots) is superimposed on the synthetic topography curve and it is the sum of crustal subsidence and thermal uplift. Initial crustal thickness was 32 km and the initial rift width was 25 km. Present offset observable across the extended region is 112 km.

structure of the model lithosphere and the distribution of crustal thickness. Figure 5-26 is a result of the pure-shear lithospheric extension mechanism. Figure 5-26 shows corrected heat flow superimposed on synthetic heat flow. Heat flow and topography (seafloor bathymetry) numerically produced by pure-shear extension is unlikely to match the heat flow on the southern Yermak Plateau. For a slow extension rate (0.3 cm/yr) the rifting cannot produce enough heat approaching the mantle solidus anywhere in the lithosphere. Numerical modeling of simple-shear is used for various dip angles of the detachment fault, such as, a shallow dipping (22°) detachment fault extending 0.3 cm/yr. Observed heat flow and topography (indicated with circles) are superimposed on synthetic heat flow and topography (Figure 5-27). This model does not match observed topography and corrected heat flow.

The best fit between observed data (the heat flow and the net topography) and the synthetic data is obtained for a detachment fault dipping 45° (Figure 5-28). In this example, an intrusion started at 35 mybp. The extension of the crust (initially 32 km thick) has continued to the present with a total extension rate of 0.32 cm/yr. The modeling result indicates a broad zone of intrusion which, created forty kilometers of mechanically weakened and thermally rejuvenated continental crust. In this model, the detachment fault (dipping to the SW) should intersect another deep-seated major detachment fault dipping beneath the Knipovich Ridge (Crane *et al.*, 1991).

Figure 5-28. Kinematic model of the Yermak Plateau. A numerical modeling result shows two detachment faults dipping at an angle of 45° towards one another. The observed topography and heat flow across the southern Yermak Plateau (*dots*) and the Knipovich Ridge (triangles) are superimposed on the synthetic heat flow and topography curves. The Knipovich Ridge axis (open star) is at 78°N (from Crane *et al.*, 1991). The initial crustal thicknesses for both models was 32 km at the initial point of rifting, and present-day offset across the ridge axis is 321 km.

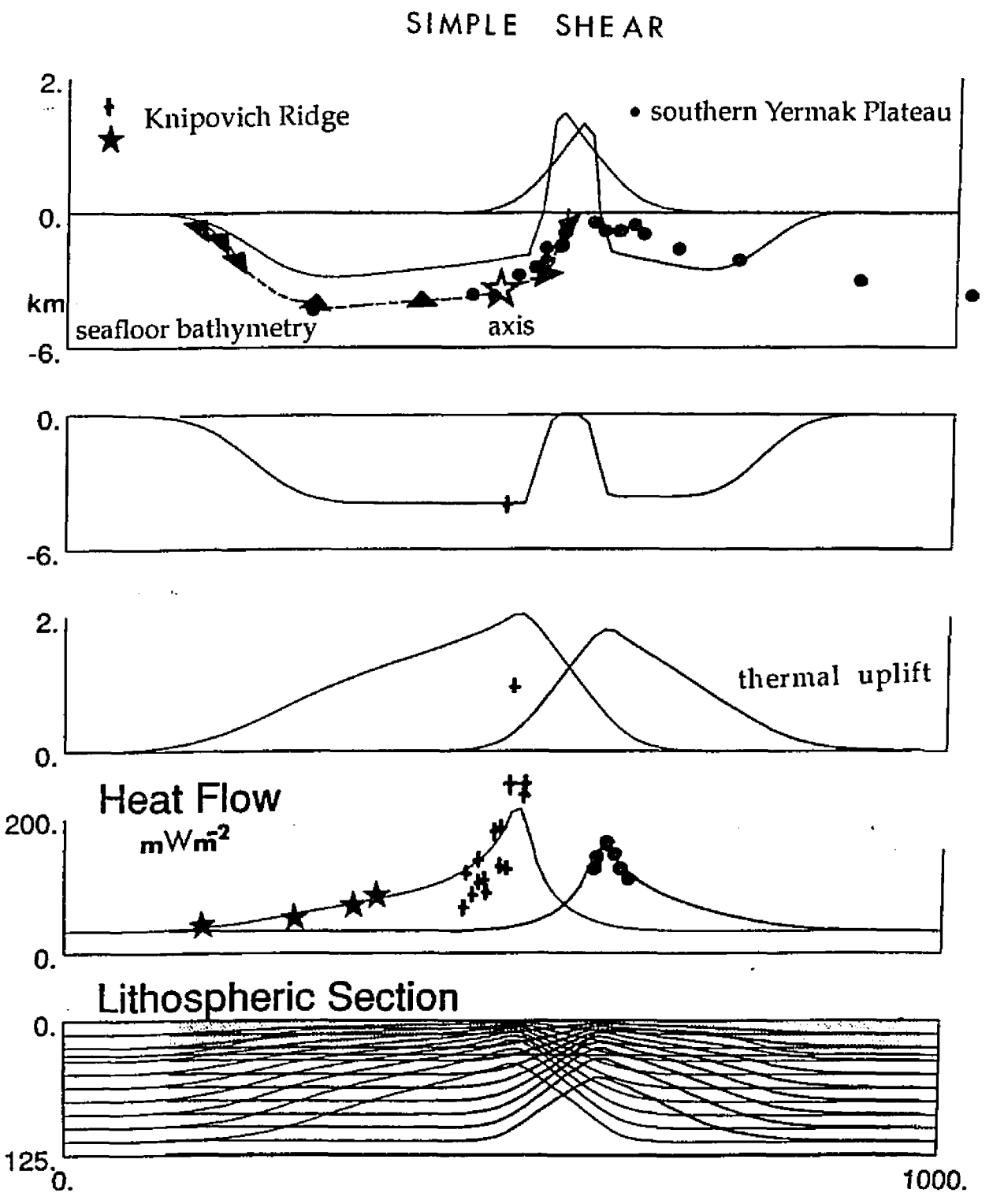
SIMPLE SHEAR
2.
Knipovich Ridge
southern Yermak Plateau
0.
km
seafloor bathymetry
axis
-6.
0.
-6.
2.
thermal uplift
0.
Heat Flow
mWm⁻²
200.
0.
Lithospheric Section
0.
125.
0.
1000.

6. THE NORTHERN SVALBARD MARGIN

A heat flow transect aligned from the Nansen Ridge to the Southern Yermak Plateau along the northern Svalbard Margin (near 8°E, Figure 5-29) reveals gradually decreasing heat flow with increasing distance from the mid-ocean ridge. However, around 82°N heat flow increases towards the northern Svalbard Margin and reaches 138 mW/m^2 on the southern Yermak Plateau. Observed heat flow and seafloor bathymetry are presented in Figure 5-30. Average seismic velocities of the Nansen Basin are indicated in Table A-4 in Appendix B. Magnetic ages are estimated from Jackson *et al.* (1984). Sedimentation rates, magnetic ages, heat flow and thermal crustal ages are tabulated in Table 5-9. During the Ocean Drilling Program-Leg 151 measurements revealed that sedimentation rates at the Yermak Plateau are extremely high ranging from 10 to 200 m/Ma during the Quaternary (Leg 151 Shipboard Party, 1994).

Observed heat flow is compared to corrected heat flow in Figure 5-31. Corrected heat flow is compared to the model heat flow of the PS-cooling curve in Figure 5-32. Magnetic ages are compared to thermal crustal ages in Figure 5-33. Off-axial high heat flow and the younger thermal crustal ages represent thermal rejuvenation in the region. In summary, the age of the crust was found to be as young as 10 Ma old and indicates a period of time (35-10 mybp) when the southern Yermak Plateau was continuously or sporadically reheated (Figure 5-32).

Figure 5-29. Heat flow and respective station locations on the Northern Svalbard-Nordaustlandet Margin. Heat flow data were collected by Crane *et al.* (1982), Jackson *et al.* (1984), and Sundvor (1986). Bathymetry (m) after Cherkis *et al.* (1991). The AA' profile transects the flank of the Nansen Ridge to the northern Svalbard Margin at 8°E. Off-axis high heat flow is located on the southern Yermak Plateau (138 mW/m^2). Magnetic isochrons (*dotted lines*) are superimposed. Heat flow (dots) along the BB' profile was collected by Sundvor and Torp (1987). Off-axis high heat flow is located on the northeastern Nordaustlandet Margin (80-109 mW/m^2). The heat flow profile (CC') transects the Eastern Greenland Margin to the northern Svalbard-Nordaustlandet Margins. Data were collected by Crane *et al.* (1982) and Sundvor (1986). Along this profile several off-axis high heat flow values are found.

Northern Svalbard-Nordaustlandet Margin

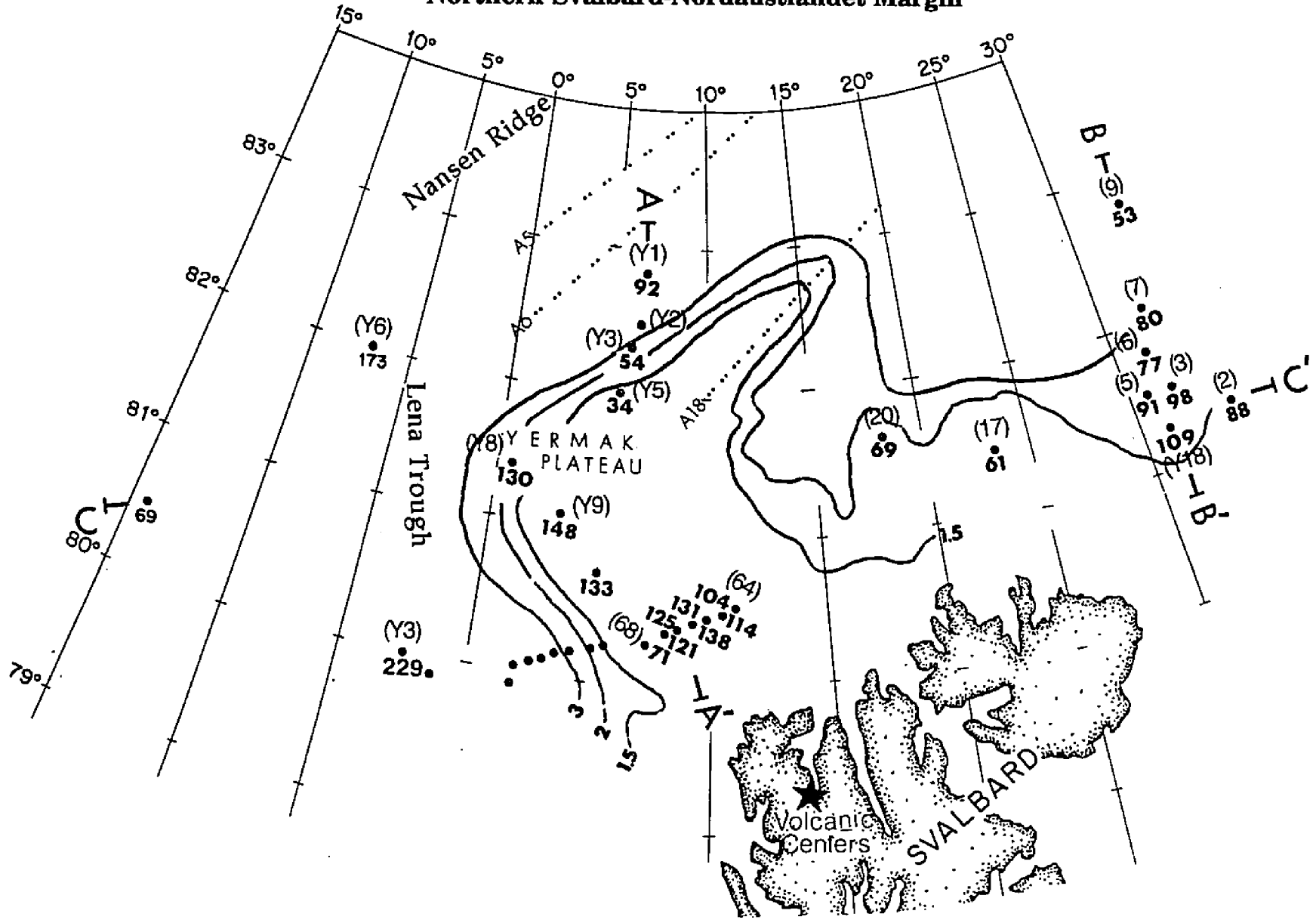

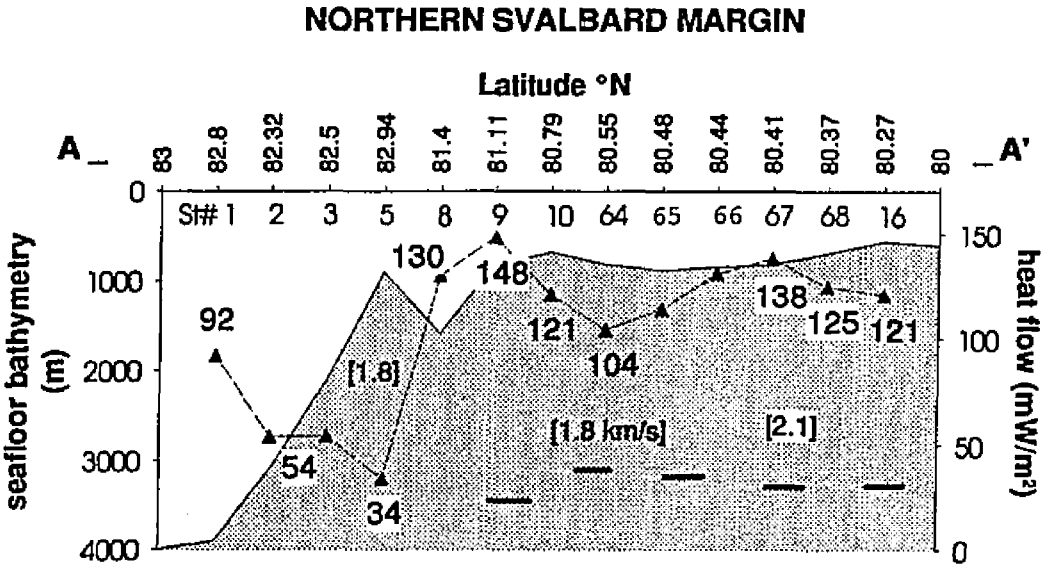

Figure 5-30. Heat flow profile: northern Svalbard. Heat flow values (*triangles*) and seafloor bathymetry along the AA' profile from the flank of the Nansen Ridge to the southern Yermak Plateau (between 83°N and 80°N at 8°E) along the northern Svalbard Margin. Heat flow station numbers are indicated.

NORTHERN SVALBARD MARGIN						
	Obs.	Mag.	Sed.	Correct. Thermal		Δ
St #	Hf	Age	Rate	Hf	Age	Age
	mW/m²	my	m/my	mW/m²	my	my
1	92	23	118.24	107.5	21.8	1.2
2	54	30	67	62	57	-27
3	54	33	61	60	60	-27
5	33.9	37	50.3	47	70	-27
Y8	130	45	103	147	10.5	34.5
Y9	148	45	103	150	13	32
Y10	121	45	103	129	15	30
64	104	55	27.8	109	21	34
65	114	55	54	123	16	39
66	131	55	93.9	146	14	41
67	138	55	242.5	154	11	44
68	125	55	204.7	148	17	38
Y16	121	55	182.4	129	15	40
				Δ Age= 16.3 my		

Table 5-9. Heat flow analysis: northern Svalbard Margin. Listings of sedimentation rates, estimated magnetic ages, corrected heat flow and thermal crustal ages from the flanks of the Nansen Ridge towards the northern Svalbard Margin (at 8°E).

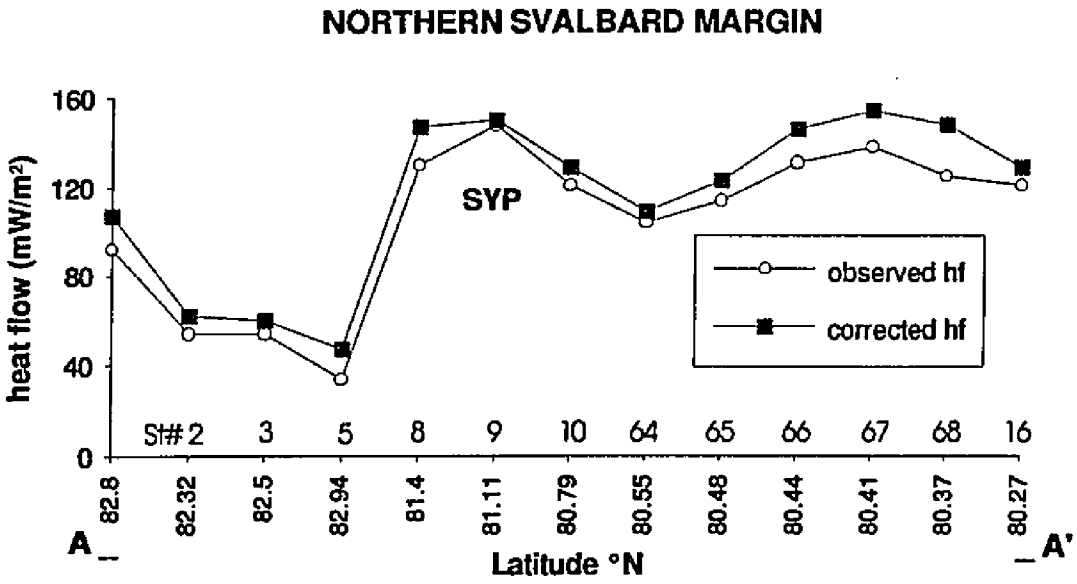

Figure 5-31. Heat flow analysis: northern Svalbard Margin. Comparison of the observed heat flow and corrected heat flow on the northern Svalbard Margin (between 83°N and 80°N at 8°E). From the Nansen Ridge to 82.94°N heat flow gradually decreases away from the active spreading center. Around 82°N heat flow increases towards the northern Svalbard Margin and reaches 148 mW/m^2 on the southern Yermak Plateau (SYP). This off-axial heat flow high represents thermal rejuvenation in the region.

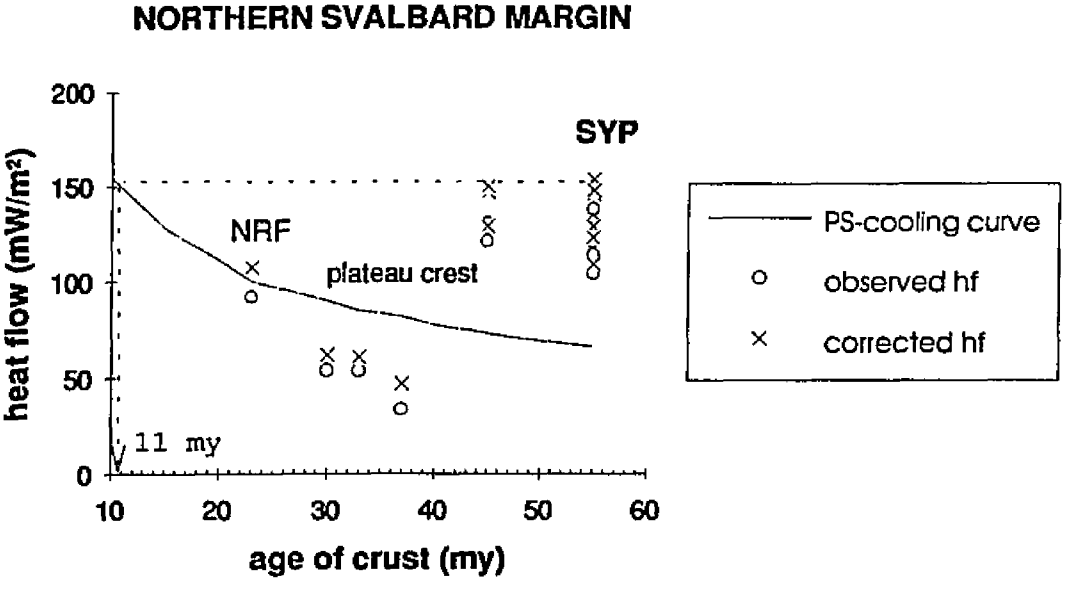

Figure 5-32. Cooling oceanic crust model: northern Svalbard Margin. Comparison of observed heat flow and corrected heat flow to model heat flow of the PS-cooling curve. The most recent thermal rejuvenation for the northern Svalbard Margin is 11 mybp estimated by interpolation. SYP: Southern Yermak Plateau, NRF: Nansen Ridge flank.

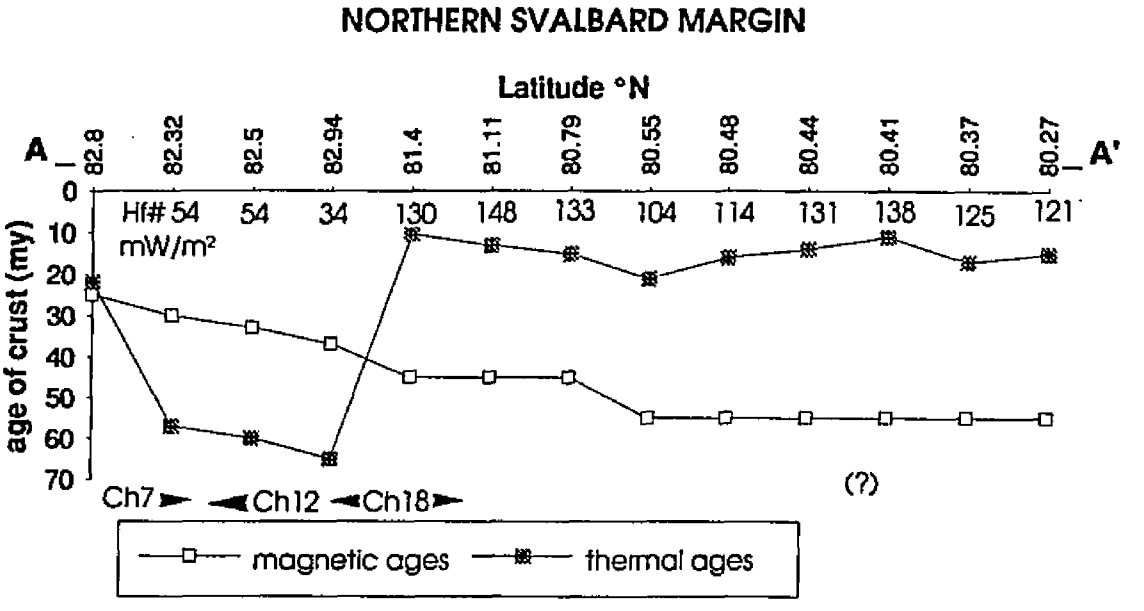

Figure 5-33. Crustal ages: northern Svalbard Margin. Comparison of the magnetic ages and thermal ages on the northern Svalbard Margin (8°E). From the flanks of the Nansen Ridge to 82.94°N thermal ages show gradually increase away from the active spreading center. Around 82°N ages decease to ~10 mybp on the southern Yermak Plateau. Magnetic ages (Ch 7-18) are obtained from Jackson *et al.* (1984) and time scale of LaBrecque *et al.* (1977). Question mark indicates the region with no discernible magnetic anomalies. The younger crustal ages represent thermal rejuvenation in the region. Δage is found to be 16.3 my.

7. THE NORTHERN NORDAUSTLANDET MARGIN

A heat flow profile (BB'), around 30°E, transects the flank of the Nansen Ridge to the northern Nordaustlandet Margin (Figure 5-29). Heat flow data were collected by Crane *et al.* (1982) and Sundvor and Torp (1987). From the Nansen Ridge to 85°N heat flow data show a gradual decrease with increasing crustal age (Figure 5-34). Around 85°N heat flow values increase towards the northern Nordaustlandet Margin and reach 109 mW/m^2. There are no clear magnetic anomalies to define the crustal ages in this region. However, extrapolating from the closest magnetic anomaly, sedimentation rates can be estimated. The distance between magnetic isochron 24 and the suggested boundary is approximately 100 km (Vogt *et al.*, 1979). Using an average half spreading rate of 1 cm/yr the swath of unidentified crust represents an interval of 10 Ma implying an opening time of 66 Ma.

Sundvor *et al.* (1978) discussed the seismic velocity structure for the area north of Nordaustlandet and for the Nansen Basin. They used average seismic parameters and sedimentation rates (Table A-4, Appendix B). Magnetic ages, corrected heat flow and thermal-crustal ages are tabulated in Table 5-10. Observed heat flow values are compared with calculated heat flow in Figure 5-35. Corrected heat flow is compared to the model heat flow of the PS-cooling curve in Figure 5-36. Estimated magnetic ages are compared with calculated thermal crustal ages in Figure 5-37. Figure 5-36 illustrates that sections of the Nordaustlandet Margin are thermally only 20 Ma old compared to its magnetic crustal ages estimated to be >60 Ma.

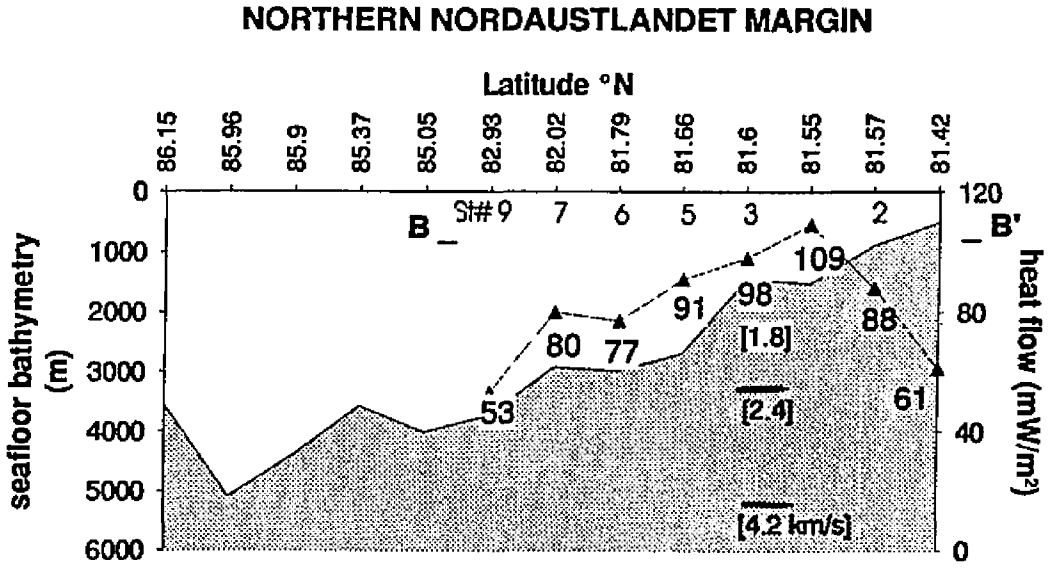

Figure 5-34. Heat flow profile: northern Nordaustlandet Margin. Heat flow values (*triangles*) and seafloor bathymetry from the flanks of the Nansen Ridge to the Nordaustlandet Margin (BB' transect in Figure 5-29).

NORTHERN NORDAUSTLANDET MARGIN						
St#	Obs. Hf	Mag. Age	Correct. Hf	Sed. Rate	Thermal Age	Δ Age
	mW/m²	my	mW/m²	m/my	my	my
9/340	53	46	74	13.9	39	7
7/310	80±1	50	83	12.8	35	15
6/296	77±4	50	80	12.8	37.6	12.4
5/287	91±1	50	94.6	12.8	26.2	23.8
3/282	98±5	55	94.6	11.6	21.9	33.1
Y18	109±6	55	101.9	11.6	17.6	37.4
2/280	88±4	55	92	11.6	27.2	27.8
				Δ age =22.3 my		

Table 5-10. Heat flow analysis: northern Nordaustlandet Margin. Sedimentation rates, observed and corrected heat flow, magnetic and thermal crustal ages along the BB' profile from the flanks of the Nansen Ridge the northern Nordaustlandet Margin are indicated.

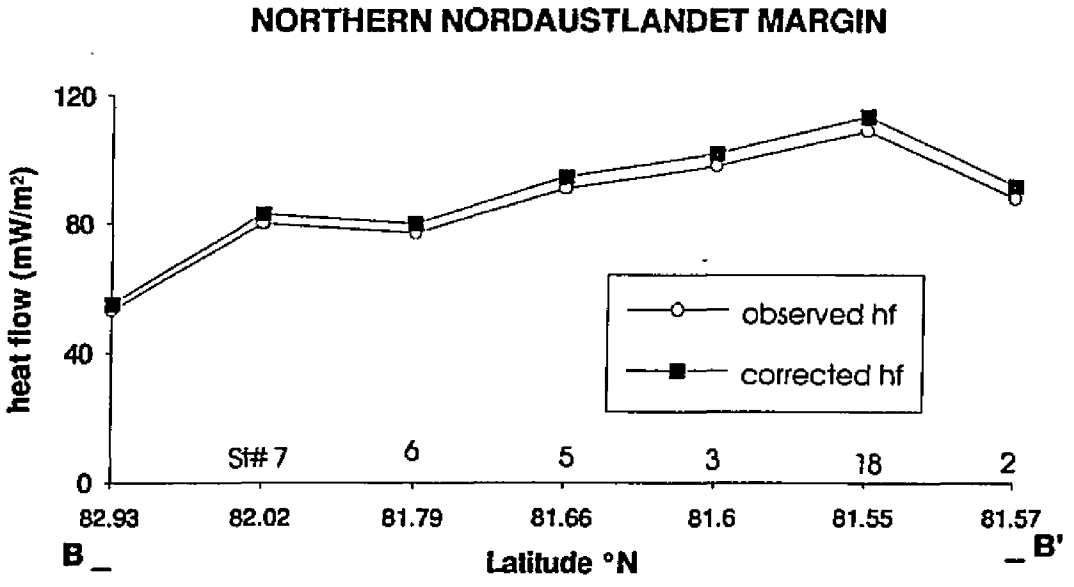

Figure 5-35. Heat flow analysis: northern Nordaustlandet Margin. Comparison of the observed heat flow and corrected heat flow on the northern Nordaustlandet Margin. From the flank of the Nansen Ridge to 85°N heat flow gradually decreases away from the active spreading ridge. Around 85°N heat flow increases towards the northern Nordaustlandet Margin and reaches 109 mW/m^2.

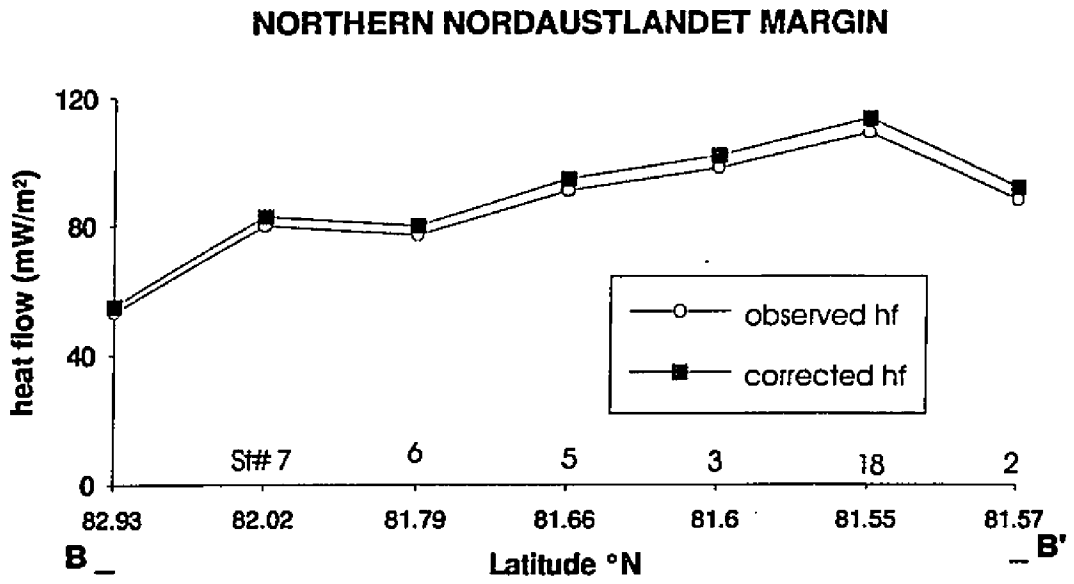

Figure 5-35. Heat flow analysis: northern Nordaustlandet Margin. Comparison of the observed heat flow and corrected heat flow on the northern Nordaustlandet Margin. From the flank of the Nansen Ridge to 85°N heat flow gradually decreases away from the active spreading ridge. Around 85°N heat flow increases towards the northern Nordaustlandet Margin and reaches 109 mW/m^2.

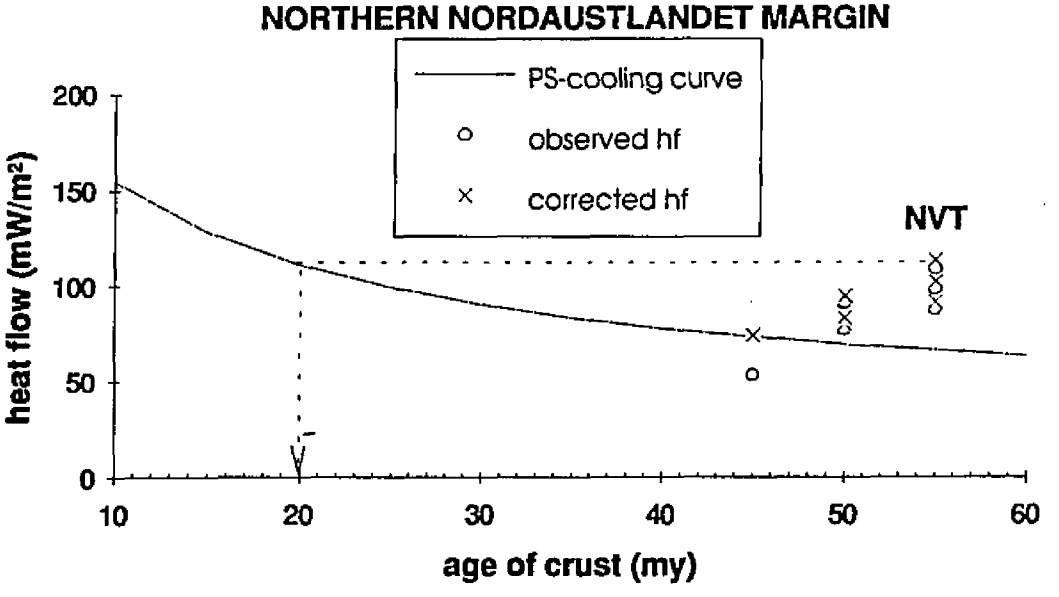

Figure 5-36. Cooling oceanic crust model: northern Nordaustlandet Margin. Comparison of observed heat flow and corrected heat flow to model heat flow of the PS-cooling curve. The interpolated age of the most recent thermal rejuvenation on the northern Nordaustlandet Margin is 20 mybp. NVT: Nordaustlandet Volcanic Terrain.

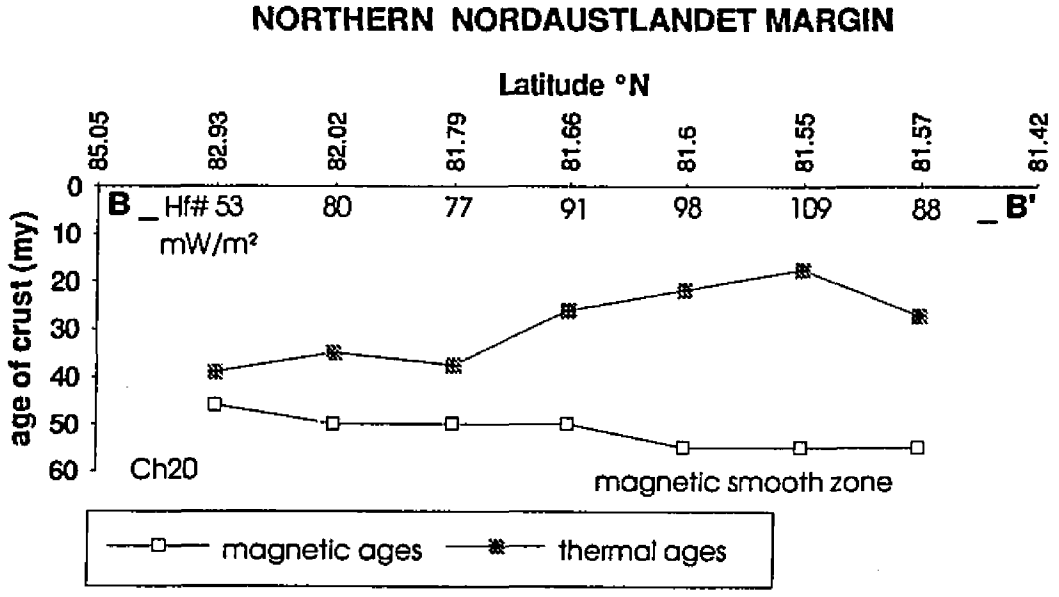

Figure 5-37. Thermal ages: northern Nordaustlandet Margin. Comparison of the magnetic ages and thermal ages on the northern Nordaustlandet Margin. From the Nansen Ridge to 85°N crustal ages increase gradually. Around 85°N crustal ages decrease towards the northern Nordaustlandet Margin and reach 20 my. The younger thermally derived crustal ages (at considerable distance from the Nansen Ridge) and the magnetic smooth zone represent heat injection and thermal rejuvenation. Hf: heat flow values, (Ch 20): magnetic isochrons (from Jackson *et al.*, 1984).

8. The Eastern Greenland and Northern Svalbard-Nordaustlandet Margins Profile

The heat flow profile (CC') transects the Eastern Greenland Margin to the northern Svalbard-Nordaustlandet Margins (between 14.39°W and 32.22°E; Figure 5-29). Heat flow highs are, from west to east, 69 mW/m^2 (on the Eastern Greenland Margin), 229 mW/m^2 (near the Lena Trough), 138 mW/m^2 (on the southern Yermak Plateau), and 109 mW/m^2 (on the northern Nordaustlandet Margin, Figure 5-38). Sedimentation rates, corrected heat flow and thermal crustal ages along CC' are tabulated in Table 5-11. From the Lena Trough to 5°E, heat flow data show a gradual decrease with increasing crustal ages.

Observed heat flow is compared to calculated heat flow in Figure 5-39. Corrected heat flow values are compared to the theoretical heat flow values for the PS-cooling curve in Figure 5-40. Estimated crustal ages (where the magnetic lineaments are available) are compared to thermal crustal ages in Figure 5-41. Around 5°E the heat flow increases toward the southwestern Yermak Plateau and reaches 138 mW/m^2. This off-axial heat flow high (at considerable distance from the Knipovich and Nansen Ridges) and the younger crustal ages represent heat injection and thermal rejuvenation in the region. On the eastern part of the southern Yermak Plateau (on Hinlopenstretet) heat flow decreases, and crustal ages increase, thus Hinlopenstretet may act as a thermal boundary between the southern part of the Yermak Plateau and the northern Nordaustlandet Margin. However, because the data

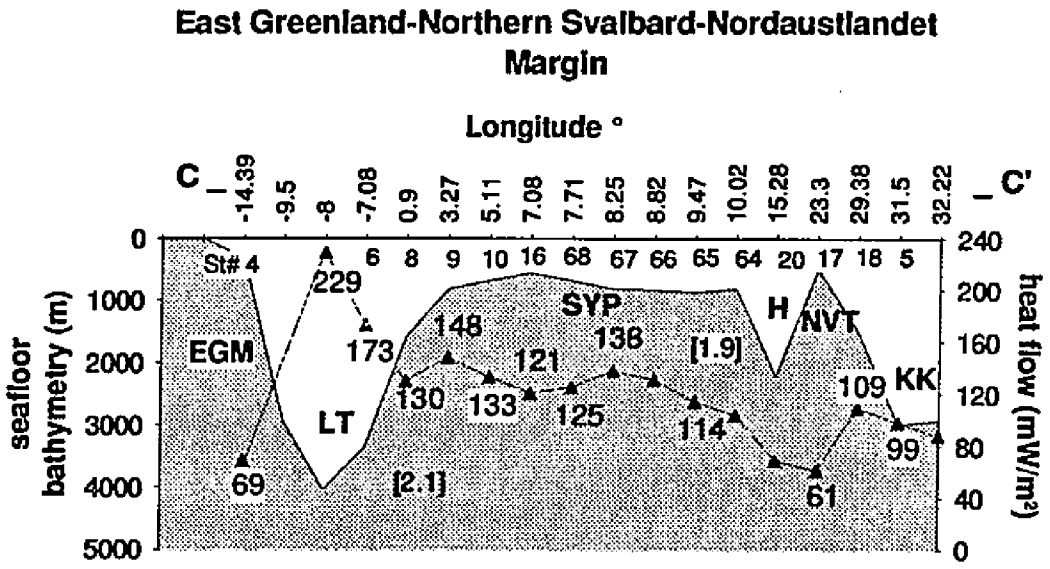

Figure 5-38. Heat flow profile: northern Svalbard-Nordaustlandet Margin. Heat flow values (triangles) and seafloor bathymetry along the CC' profile (Figure 5-29) from the Eastern Greenland Margin and Yermak Plateau to the northern Nordaustlandet Margin (between 14.39°W and 32.22°E). EGM: Eastern Greenland Margin, LT: Lena Trough, SYP: Southern Yermak Plateau, H: Hinlopenstretet, NVT: Nordaustlandet Volcanic Terrain, KK: Kong Karls Land. Sediment seismic velocities are indicated. Most of the area along the profile lacks magnetic anomalies. Deep seafloor bathymetry and low surface heat flow indicate a possible structural and thermal boundary on Hinlopenstretet between the Yermak Plateau and the Nordaustlandet region.

E Greenland - N Svalbard-Nordaustlandet Margin						
	Obs.	Mag.	Sed.	Correct.	Thermal	Δ
St #	Hf	Age	Rate	Hf	Age	Age
	mW/m²	my	m/my	mW/m²	my	my
Y4	69±2	60	27.23	71.76	55	5
12	229±6	5	10.7	286	3.3	2.7
Y6	173±12	15	17.6	207	5.3	9.7
Y8	130±10	45	102.9	147	10.5	34.5
Y9	148±10	45	102.9	150	13	32
Y10	133±8	45	102.9	140	16	29
Y16	121±11	55	182.43	129	15	40
68	125±6	55	204.7	148	17	38
67	138±6	55	242.5	154	11	44
66	131±2	55	93.9	146	14	41
65	114±1	55	53.9	123	15.6	39.4
64	104±6	55	27.8	109	21	34
20	69±5	55	27.2	73	46	9
17	61±9	55	27.2	67	55	0
18	109±6	55	27.2	113	19	36
6	98±4	55	27.2	101.9	22	33
7	88±5	55	27.2	92	27	28
			Δ Age=22 my			

Table 5-11. Heat flow analysis: northern Svalbard-Nordaustlandet Margin. Sedimentation rates, observed and corrected heat flow, magnetic and thermal crustal ages along the CC' transect from the Eastern Greenland Margin to the northern Nordaustlandet Margin.

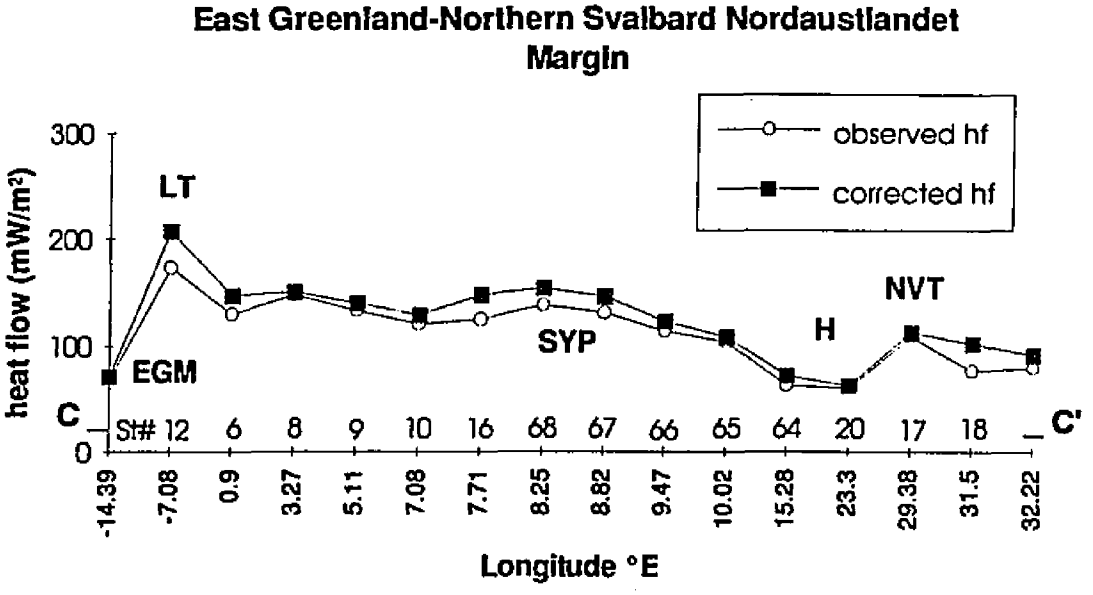

Figure 5-39. Heat flow analysis: northern Svalbard-Nordaustlandet Margin. Comparison of the observed heat flow and corrected heat flow along the East Greenland-Nordaustlandet Profile (CC'). EGM: Eastern Greenland Margin, LT: Lena Trough, SYP: Southern Yermak Plateau, H: Hinlopenstretet, NVT: Nordaustlandet Volcanic Terrain.

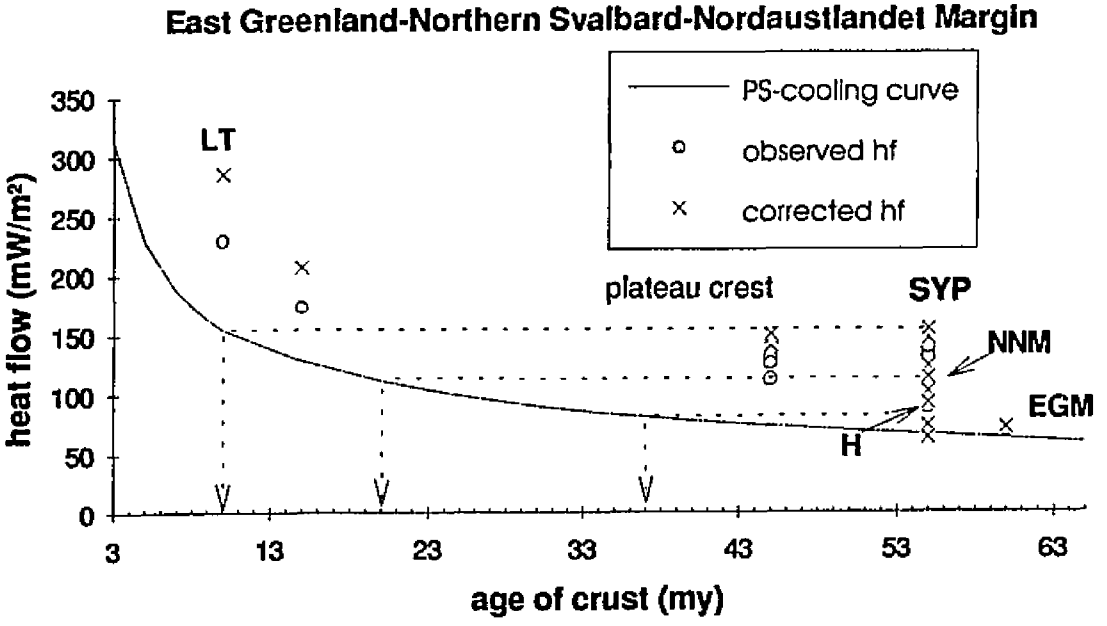

Figure 5-40. Cooling oceanic crust model: northern Svalbard-Nordaustlandet Margin. Comparison of observed heat flow and corrected heat flow with the PS-cooling curve. The ages of the most recent thermal rejuvenation's along the northern Svalbard-Nordaustlandet Margin are estimated by interpolation. On the southern Yermak Plateau (SYP) and northern Svalbard Margin, the thermal rejuvenation occurred at 11 mybp, 37 mybp on Hinlopenstretet (H), and on the northern Nordaustlandet Margin (NNM) the thermal rejuvenation occurred at 20 mybp. EGM: Eastern Greenland Margin, LT: Lena Trough.

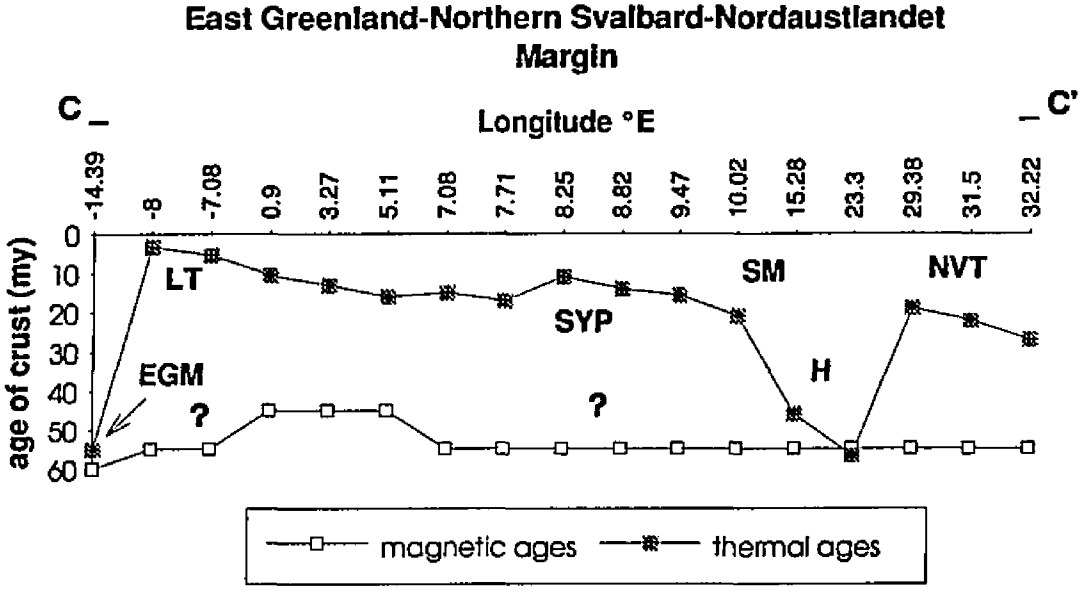

Figure 5-41. Thermal ages: northern Svalbard-Nordaustlandet Margin. Comparison of the magnetic ages and thermal ages along the Eastern Greenland-Nordaustlandet Profile (CC'). EGM: Eastern Greenland Margin, LT: Lena Trough, H: Hinlopenstretet, NM: Nordaustlandet Margin. (?): Magnetic Smooth Zone. SM: Seamounts, NVT: Nordaustlandet Volcanic Terrain, SYP: Southern Yermak Plateau.

are so scarce, further interpretation requires additional heat flow stations in the northern Hinlopenstretet region.

In Figure 5-40 four distinctive groups of heat flow highs and young thermal crustal ages are noticeable along the PS-cooling curve. The first group is located near the Lena Trough region, and suggests that the crust is approximately 6 my old. The second group is located on the southern Yermak Plateau and suggests that the age of the crust is at least 10 my old (in agreement with the Quaternary and recent lavas and thermal spring activity in Svalbard). The third group is located between the islands of Svalbard and Nordaustlandet, and suggests that the age of the crust in this region is 37 Ma (consistent with the ages of Tertiary lavas on Svalbard). The fourth group is situated on the Nordaustlandet Margin, where high heat flow and thermal crustal ages indicate that intrusion took place here from 18-20 mybp.

9. Summary of Heat Flow Results

Figure 5-42 illustrates where thermally rejuvenated crust is associated with present-day earthquake activity within the eastern Norwegian-Greenland Sea and adjacent regions. Thermal-crustal ages on the marginal plateaus and fracture zones are much younger than magnetic crustal ages, indicating thermal rejuvenation (Figure 5-43).

Anomalously high temperatures in the lithosphere result in high heat flow at the surface of the crust. A large amount of heat brought up and injected into

Figure 5-42. Thermally derived crustal ages in the eastern Norwegian-Greenland Sea. Contours indicate that the eastern margins are much younger than expected from magnetic anomalies. This contradicts the pure shear extension model of McKenzie (McKenzie, 1978). Instead, eastern margins of the Norwegian-Greenland Sea have thermal signatures which could be created by asymmetric simple shear. Distribution of earthquakes (BSC: Barents Seismic Corridor and LS: Lofoten-Vesterålen Seismic Zone, HL: Heer Land Seismic Zone, NS: Nordaustlandet Seismic Zone) suggest that highly concentrated seismicity is associated with thermally rejuvenated crust. Earthquake locations are obtained from various sources (Bungum *et al.*, 1982; Mitchell *et al.*, 1990). VP: Vøring Plateau, JMR: Jan Mayen Ridge, S: Senja Margin, SSZ: Spitsbergen Shear Zone, YP: Yermak Plateau, H: Hinlopenstretet, NR: Nansen Ridge, KKC: Kong Karls Corridor, RESEAFLOOR: highly reflective seafloor (*presumably basalts*) and debris fields, SDRS: seaward dipping reflector sequences.

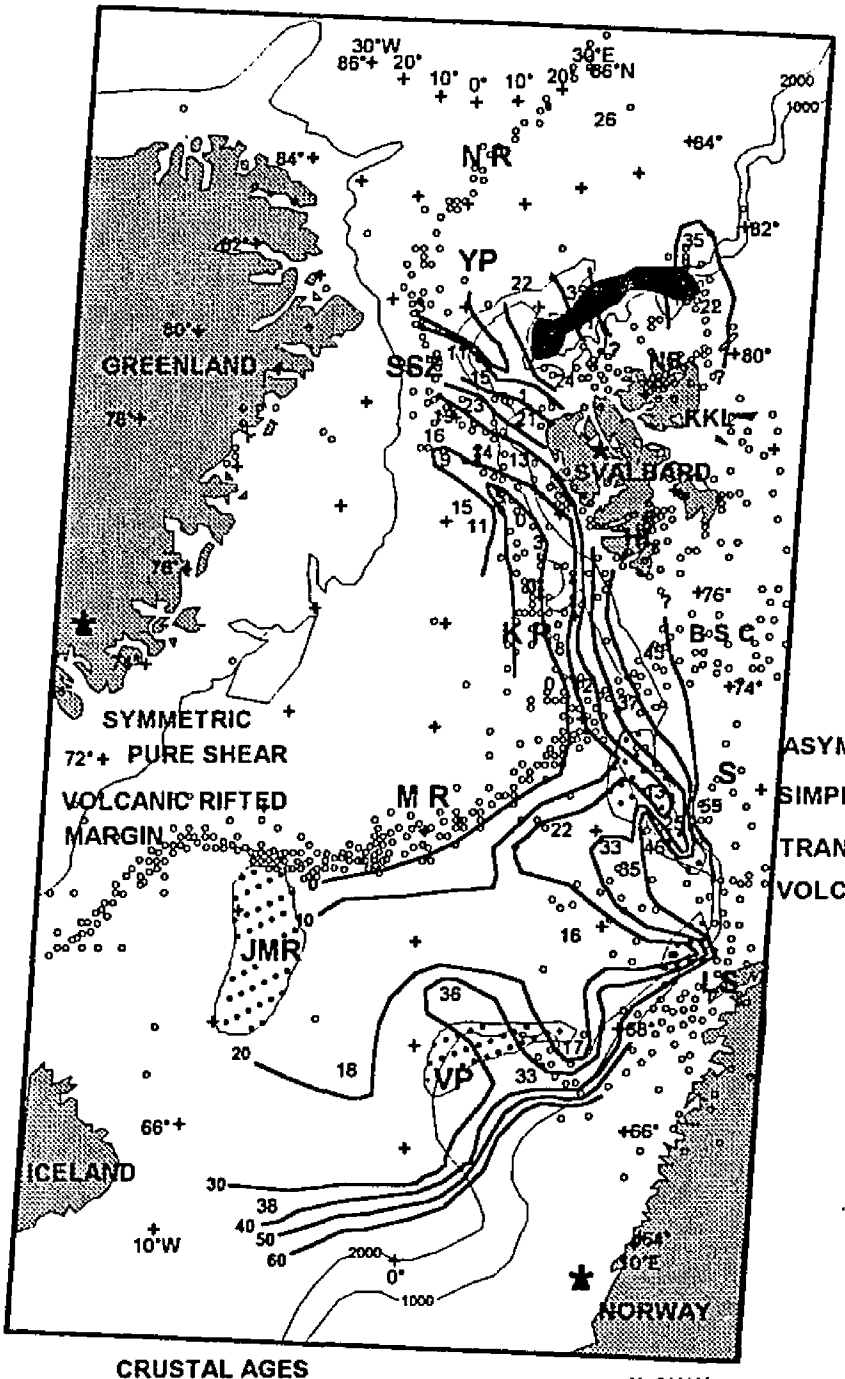
30°W
20°
10°
0°
10°
20°
30°E
86°N
84°
82°
80°
78°
76°
74°
72°
66°
64°
GREENLAND
ICELAND
NORWAY
SVALBARD
YP
NR
SSZ
KKL
KR
BSC
MR
JMR
VP
SYMMETRIC
PURE SHEAR
VOLCANIC RIFTED
MARGIN
ASYMMETRIC
SIMPLE SHEAR
TRANSTENSIONAL
VOLCANIC MARGIN
10°W
10°E
2000
1000
0°
CRUSTAL AGES
NORWEGIAN-GREENLAND SEA
N. OKAY
1994
AGE CONTOUR (my)
EARTHQUAKES
ALKALI VOLCANIC CENTERS
THERMAL SPRINGS
RESEAFLOOR
SDRS

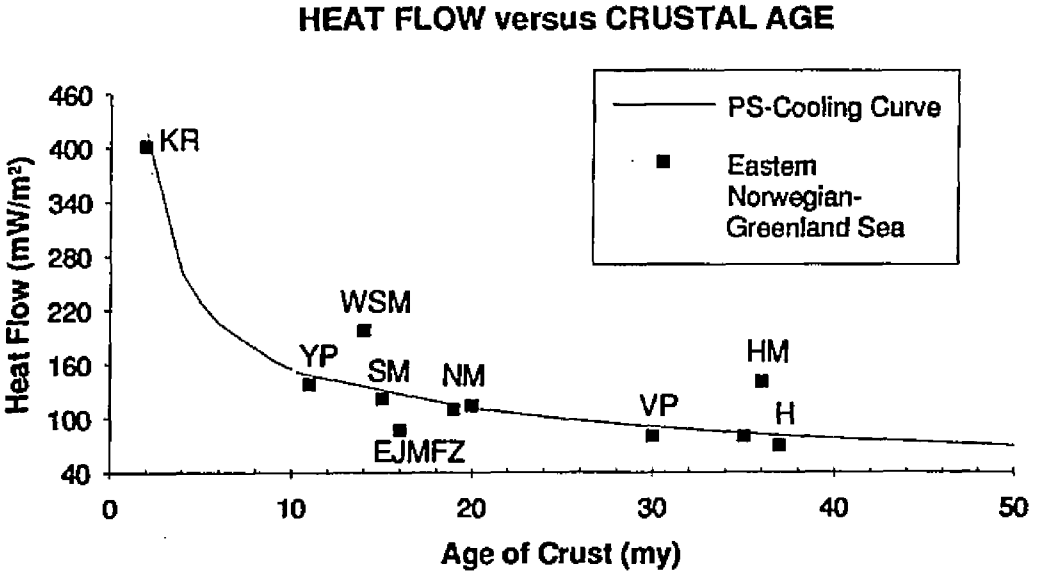

Figure 5-43. Corrected heat flow versus thermal ages (in terms of DNAG Time Scale, Vogt, 1986) in the Eastern Norwegian-Greenland Sea. The Norwegian-Greenland Sea approximately fits the PS-cooling curve. EJMFZ: Eastern Jan Mayen Fracture Zone, VP: Vøring Plateau and Norwegian Margin, SM: Senja Margin, HM: Hornsund Margin, KR: Knipovich Ridge, WSM: Western Svalbard Margin, YP: southern Yermak Plateau, H: Hinlopenstretet, NM: Nordaustlandet Margin.

the lithosphere during the formation of basaltic crust, is a signature of major tectonic events. Langseth and Zielinski (1974), Sclater *et al.* (1980), and Stein and Stein (1992) suggested that there is a balance between spreading rate and heat brought vertically from the asthenosphere to the base of the lithosphere. Their general observation that heat flow and seafloor bathymetry change as a function of age in most oceans, has held. In addition, they proposed that if the vertical heat flux (a mantle plume) governs the thickness of the lithosphere and induces the continental breakup (in the sense of symmetric pure-shear lithospheric extension), then a faster spreading rate will coincide with a higher heat flow. I believe that this concept does not adequately describe the thermal evolution of the ultra-slow spreading ridges (such as the Knipovich Ridge within the northern Norwegian-Greenland Sea) and off-axial high heat flow distant from active spreading centers.

Table 5-12 summarizes the thermal-crustal ages and episodes of thermal rejuvenation along the eastern margins of the Norwegian-Greenland Sea. The continent-oceanic crustal transition on the Norwegian Margin at its intersection with the Lofoten-Vesterålen Fracture Zone was first formed at 60 mybp and heating continued on this margin until 16 mybp. Heat injection along the Vøring Plateau continued until 26 mybp, and thus the region was the site of magmatic intrusions for up to 16 mybp after its oceanic crust was imprinted by magnetic anomalies. Thermal rejuvenation ages along the Senja Margin are 25 to 10 mybp with continued heating for 12 mybp (after the margin was first formed). At present the distribution of

AGES OF THERMAL REJUVENATION
EASTERN MARGINS OF THE NORWEGIAN-GREENLAND SEA

	A G E	
	Magnetic	Thermal
	Ma	
Vøring Plateau	60	26
E Jan Mayen FZ	60 (?)	18
Vøring FZ	45 (?)	24
Lofoten FZ	60-40	17
Vesterålen FZ	(?)	16
Senja FZ/Senja Margin	60 (?)	12
Hornsund Fault (75°N) (181 km)	60 (?)	36
Knipovich Ridge (78°N) along the W. Svalbard Margin (0 km)	(?)	0
Intersection of the northern Knipovich Ridge and the Molloy Transform Fault along the W. S. Margin (<100 km, 78.5°N)	(0)	3.5
the southern part of the Yermak Plateau	50-60 (?)	11
Hinlopenstretet (170 km)	50-60 (?)	37
Nordaustlandet Margin (200 km)	750-60 (?)	20

Table 5-12. Summary of magnetic- and thermal-ages of thermal rejuvenation along the eastern margin of the Norwegian-Greenland Sea. Question marks (?) indicate magnetic smooth zones in the areas, and (km) indicates the distances from the mid-ocean ridge.

earthquakes is highly concentrated around these thermally rejuvenated regions (Figure 5-42).

The thermal-crustal age (13 mybp) along the northwestern Svalbard Margin is younger than expected (35 mybp) according to age estimates of the southwestern Svalbard Margin which corresponds with a plate boundary shift from the Senja Fracture Zone to the Hornsund Fault Zone along the Western Svalbard Margin. Along the northern Svalbard-Nordaustlandet Margin, off-axial thermal rejuvenation events occurred from 35 to 10 mybp. The duration of intrusion (estimated from thermal modeling) indicates that the southern Yermak Plateau was continuously heated between 35 mybp and 10 mybp. These results are in an agreement with the recent volcanics and activity of thermal springs in Svalbard.

Several intersecting detachment faults are proposed for the structural model of the northern Norwegian-Greenland Sea based on numerical modeling results of the northern Knipovich Ridge, the Southern Yermak Plateau, and the Nordaustlandet region. The best fit to the observed data suggest that asymmetric simple-shear lithospheric extension with a 45° major detachment fault dips to the East underneath Svalbard and intersects the seafloor at the northern Knipovich Ridge, as proposed by Crane *et al.* (1991), and Okay and Crane (1993). In addition, secondary and Tertiary (westward dipping) detachment faults probably cut through both the southern Yermak Plateau and the northern Nordaustlandet Margin and intersect the main detachment surface (Okay and Crane, 1993).

All of the detachment faults are thought to have been inherited from the fault system associated with the paleo-Spitsbergen Shear Zone. This indicates that the paleo-Spitsbergen Shear Zone was not a singular structure, but consisted of several deep-seated pre-existing continental faults. These faults, as the secondary-Tertiary detachment faults, make excellent conduits for heat and magma transport. The lateral translocation of magma is probably associated with asthenospheric underplating of Svalbard and parts of the Barents Sea via these faults. The intrusion and extrusion of basalt may still occur within these deep-seated faults and the southern part of the Yermak Plateau (ten's of kilometers from the Knipovich Ridge axis-the major detachment fault) and 100's of kilometers away near the island of Nordaustlandet.

The thermal-crustal age of the Hinlopenstretet region located between the thermally rejuvenated sections of Svalbard and Nordaustlandet is 37 Ma. This result is consistent with the episode of Tertiary lava extrusion on Svalbard. The thermal-crustal age of the margin of eastern Nordaustlandet is found to be younger. In this region thermal rejuvenation has occurred as recently as 20 mybp. A thermal-crustal age contour map of the Norwegian-Greenland Sea indicates that the eastern margins are much younger than expected (Figures 5-42 and 5-43).

In this study, it is primarily those regions where fracture zones intersect the margin, where thermal rejuvenation occurs. Apparently, fracture zones are excellent conduits for the transport of heat, and thus they may continue to transfer heat 10's of million of years after seafloor spreading ceased in the region. In addition, seismic activity is enhanced in these locations. One possible cause of this seismicity is that the

reduction in mechanical plate thickness under regions of localized intrusion and the added heat injection decreases the strength of lithosphere making it far more susceptible to seismic activity (McNutt, 1984).

In addition, thermal data suggest that when the northwards propagating Mohns Ridge intersected the paleo-Spitsbergen Shear Zone, only a portion of the ridge entered the shear zone. The remaining deep-seated "propagating asthenospheric corridor" probably continued moving in its original direction, gradually underplating Svalbard in the process. The timing and the magnitude of thermal rejuvenation can be related to the rate at which the propagating asthenosphere moved underneath Svalbard. Once this asthenospheric corridor intersected Secondary and Tertiary detachment faults (dipping towards the newly formed Knipovich Ridge), then intrusion and extrusion into/along these faults occurred. If the present is the key to the past then it is likely that a similar process occurred along the Vøring Plateau Escarpment when the paleo-Aegir Ridge intersected the paleo-Jan Mayen Fracture Zone.

Further research should be directed to answering to following questions:

1. Will the Knipovich Ridge continue to propagate northwards and deactivate the Molloy Transform Fault completely?
2. Will Nordaustlandet become a site of extensive volcanic activity?
3. Will the underplating of the Svalbard-Barents Sea region evolve into a completely new plate boundary?

Chapter 6

DISCUSSION

A. THERMAL REJUVENATION: EVIDENCE FOR ASTHENOSPHERIC CORRIDORS

The Norwegian-Greenland Sea lies within a broad region of anomalously high heat flow. The heat flow profiles from two marginal plateaus and along transtensional volcanic passive margins, presented in the previous chapter, show a significant surface heating distant from the active spreading centers. The high heat flow implies that a significant amount of heat lies at the base of the lithosphere creating relatively high temperatures at shallow depths. In response, the eastern Norwegian-Greenland Sea seafloor (including the Vøring and Yermak Plateaus and all transtensional margins) as well as the western Svalbard-Barents Platform are anomalously elevated.

Buck and Mutter (1989) suggest, that when a continent breaks up and a passive margin forms along a paleo-shear zone, a transition zone develops between continental and oceanic crust. According to Parsons and Sclater (1977) and McKenzie (1978) the surface expression of the heat flow should be symmetric and dome shaped indicating the cooling of the oceanic crust toward the margins away from the ridge. However, in the case of the Norwegian-Greenland Sea, heat flow

often increases towards the margins. This high heat flow at the margin may mark the point (in time) where partial melting increased because of large lateral thermal gradients either at the onset of rifting or during a later intrusive event. In addition, early extensive partial melting in these regions resulted in lava ponding onto the surface and the creation of seaward dipping basaltic units and marginal volcanic plateaus. These events died down as more new oceanic crust formed and oceanization continued.

However, thermal ages along the eastern Norwegian-Greenland Sea indicate that the eastern margins are much younger than expected. This contradicts the symmetric, pure-shear extension model of McKenzie (1978) but not asymmetric simple-shear extension model. Furthermore, younger thermal ages are also suggestive of recent intrusion of magma both into pre-existing fracture zones and along the margin of the Barents/Svalbard Platform. This may be suggestive of ongoing underplating of the western Svalbard Platform and the Barents Sea. In all likelihood, the propagating ridges (Aegir, Mohns, and Knipovich) were trapped by paleo-shear zones (East Jan Mayen, Vøring, Lofoten, Vesterålen, Senja, and Spitsbergen) within the Norwegian-Greenland Sea and created volcanic plateaus (such as the Vøring and Yermak) along the transtensional eastern margins (Norwegian, Senja and Western Svalbard). Although some magma was intruded into the pre-existing shear zones, in all likelihood, the deep-seated asthenospheric material probably continued to propagate along its original path underplating and thermally

uplifting the margin of the Barents Sea in the process. The details of the propagation events are outlined in the following sections.

B. THE VØRING PLATEAU AND NORWEGIAN VOLCANIC MARGIN

The separation of Greenland and Norway along the Harland Line started about 60 mybp (Birkenmajer, 1981). It was associated with a short-lived but voluminous volcanic activity (Eldholm and Grue, 1994). Eldholm *et al.* (1989b) suggested that early Tertiary magmatism, in some way, was related to the Iceland Hotspot. White (1988) suggested a mushroom-shaped mantle plume (in 2000 km diameter) was centered near the Iceland plume at the time of rifting along the Norwegian Margin. The extinction of the paleo-Aegir Ridge is evidence (subaerial volcanism suggested by Eldholm and Grue, 1994) that the effects of the plume abated rapidly (3.5 Ma) from its center. This observation argues against the concept of the plume model. Eldholm *et al.* (1989a) suggested that instead of a mushroom shape, the upwelling mantle was shaped like a higher temperature carpet.

The main difficulty with the approach of White (1988) is his idea regarding the magnitude of the asthenospheric temperature and the time of volcanic activity due to the mantle plume. The mantle plume should cause symmetric dynamic uplift of the entire area prior to rifting (White, 1988). However, the rocks at the margin off Norway have no record of dynamic uplift (Eldholm *et al.*, 1989b). The Paleocene

uplift at the Vøring Plateau (limited to the area adjacent to the line of break-up) was initiated after the onset of rifting (Eldholm *et al.*, 1989a), reflecting the isostatic response to the changing lithosphere (continent to oceanic). The passive margin and volcanic plateaus along the eastern Norwegian-Greenland Sea can probably be best explained by simple-shear dominated lithospheric extension mechanisms where the impact of a propagating ridge upon an obliquely oriented paleo-shear zone releases a short-lived but voluminous magmatic production.

Although magnetic anomaly lineaments show the Harland Line (the Aegir Ridge and paleo-Mohns Ridge; Birkenmajer, 1981) propagated along the Jan Mayen Transform System (Figure 6-1). Hagevång *et al.* (1983) suggest formation of the crust in the negative polarity interval between magnetic anomalies' (Chron 24-25: 58.7 to 56.6 mybp). A jump in the plate boundary occurred about 57 mybp causing the duplication of the 24A and 24B on the southern Vøring Plateau. At 55 mybp the plate boundary "straightened out" and symmetric spreading started along the Mohns Ridge (Hagevång *et al.*, 1983). Hagevång *et al.* (1983) proposed that maximum magnetic amplitudes occur seaward of the outer Vøring Plateau. Leg 38 of the Deep Sea Drilling Project also showed that Fe-Ti-rich basalts with a high remnant magnetization increases westward, at the plateau, and are classified as hotspot-type by Raschka and Eckhardt (1976). However, Hey *et al.* (1980) suggest that the basaltic rocks responsible for high amplitude magnetic anomalies can occur at the tips of propagating rifts. Although, we cannot demonstrate this, following Hagevång *et al.* (1983), rift propagation may well have occurred prior to Chron 23 time. By

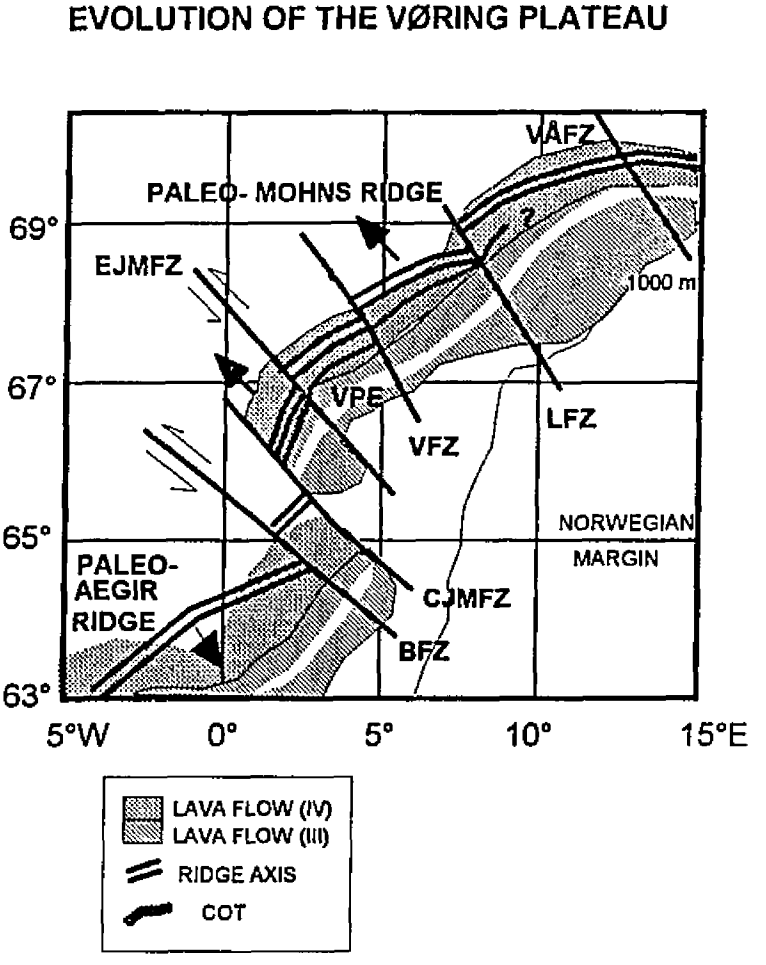

Figure 6-1. Evolutionary model of the Vøring Plateau and the Norwegian Margin. The propagation of the paleo-Aegir and -Mohns Ridges along the Jan Mayen Transform System created the Vøring Plateau and the transtensional volcanic passive margin in the southeastern Norwegian-Greenland Sea. This configuration is revised from magnetic lineaments suggested by Hagevång *et al.* (1983). Bathymetry contour (1000 m) included. The paleo-Mohns Ridge propagated along the BFZ: Basin Fracture Zone, CJMFZ: Central Jan Mayen Fracture Zone, EJMFZ: Eastern Jan Mayen Fracture Zone, VFZ: Vøring Fracture Zone, VPE: Vøring Plateau Escarpment (*white bold-line*), LFZ: Lofoten Fracture Zones, VÅFZ: Vesterålen Fracture Zone, COB: continental-oceanic crustal transition boundary.

analyzing the early spreading rates Hagevång *et al.* (1983) find there are irregular anomalies probably caused by a combination of intrusives and relief in the underlying oceanic crust. The duplication of Chron 24 line (Hagevång *et al.*, 1983) indicates that the paleo-Mohns Ridge axis was offset by segments of the Jan Mayen Transform System (East Jan Mayen Fracture Zone, Vøring Fracture Zone, Lofoten Fracture Zone, and probably Vesterålen Fracture Zone).

During the propagation of the Harland Line, Eldholm *et al.* (1987) and Mutter *et al.* (1988) suggest that early Eocene lavas were extruded, for 2 to 3.5 my, at a high flow rate, and distant from the spreading center. Basalt samples from the Outer Vøring Plateau indicate that high amplitude magnetic anomalies were created at the tip of the northward propagation tip of the Aegir Ridge (Eldholm *et al.*, 1987). During propagation along the Eastern Jan Mayen Fracture Zone (and during the adjustment of the plate boundary along the northern margin), an abrupt crustal transition zone was created (seismic Reflector-K in Figure 3-16; Skogseid and Eldholm, 1987).

Heat flow analyses indicate that the crust on the Norwegian Margin was first heated 60 mybp and continued to be intruded by volcanism up to 16 mybp (Table 5-12). Segments of the Eastern Jan Mayen Fracture Zone, Vøring Fracture Zone, Lofoten Fracture Zone and Vesterålen Fracture Zone, probably trapped or channeled the respective intrusions. The interaction of the Aegir Ridge with the paleo-Jan Mayen Fracture Zone likely resulted in a pulse of voluminous subaerial volcanism forming the Vøring Plateau about 57 mybp. Relatively lower present-day heat flow in

this region is probably the result of rapid heat loss during the period of lava extrusion. However, thermal rejuvenation occurred up to 24 my ago on the Vøring Fracture Zone and 26 my ago on the Vøring Plateau.

The succession of these events probably coincided with the rapid propagation of the paleo-Mohns Ridge northward along the Vøring and Lofoten Fracture Zones. In all likelihood, deep-seated propagating magma from the paleo-Mohns Ridge moved beneath the northern Norwegian Margin and rejuvenated the crust underneath the Lofoten and Vesterålen Islands (16 mybp; Figure 5-42). Free-air gravity anomalies also suggest shallow-paleo magma sources in this region (Figure 3-13) where even today, earthquakes occur (Figure 3-10).

C. THE SENJA AND WESTERN SVALBARD TRANSTENSIONAL VOLCANIC MARGIN

The northeastern propagating Mohns Ridge interacted with the paleo-Senja Shear Zone between approximately Chron 23 and Chron 13. Until the plate reorganization, no-oceanic crust formed along the Senja Margin (Figure 6-2). The Mohns Ridge propagated northward along the paleo-Spitsbergen Shear Zone into the Arctic Basin rather than rifting the continental lithosphere in the Svalbard Platform. However, young thermal-crustal ages underneath and adjacent to Svalbard are evidence that underplating by mantle material is probably occurring in this region.

The paleo-Senja Shear Zone most likely acted as a barrier to the surface expression of the propagating Mohns Ridge blocking the rifting that would have penetrated through the Barents Platform. However, at depth, the asthenosphere associated with the propagating ridge apparently succeeded in underplating the Senja Margin thermally rejuvenating the Svalbard-Barents Platform in the process (Table 5-12). The distribution of earthquakes (*the Barents Seismic Corridor*) indicates recent tectonic activity within the mechanically strong continental lithosphere in the regions where thermal rejuvenation has taken place (Figure 5-42). Thus, underplating and thermal uplift of the Western Barents seafloor may still be occurring. At 35 mybp, transtensional movement occurred from the Senja Fracture Zone to the Hornsund Fault (one of the faults within the paleo-Spitsbergen Shear Zone; Müller and Spielhagen, 1990; Faleide *et al.*, 1991). After Chron 13, when the tensional regime became predominant, a system of down-faulted blocks developed west of the major Hornsund fault. These were later buried by the increasing amount of sediment deposited west of the Hornsund Fault (Myhre, 1984). However, spreading evolved along this transtensional fault system creating the Knipovich Ridge in the process (Figure 6-2a).

Figure 6-2. Evolution of the paleo-Spitsbergen Shear Zone.
(a) Distribution of plate boundaries during the opening of the northern Norwegian-Greenland Sea during Chron 23, adapted by Crane *et al.* (1991). Straight thin lines represent sheared crust. Half-arrows show strike-slip movement. Large arrow head indicates the direction of the Knipovich Ridge propagation.

(b) Present day plate boundaries and main structural features of the northeastern Norwegian-Greenland seafloor. Numbered boxes: 1: the continent-oceanic crustal boundary, 2: bathymetry (m), 3: active spreading ridge, MR: Molloy Ridge, 4: magnetic lineations, 5: Spitsbergen Fold and Thrust Belt, 6: Tertiary Central Basin, 7: Early Eocene Volcanism, LG: Lofoten Gravity High, BG: Bjørnøya Marginal High, 8: marginal free-air gravity anomalies, HG: Marginal Hornsund Gravity High (>100 mGal). H: Hovgård Gravity High, MTF: Molloy Transform Fault, SG: Senja Gravity High.

Evolution of the paleo-Spitsbergen Shear Zone

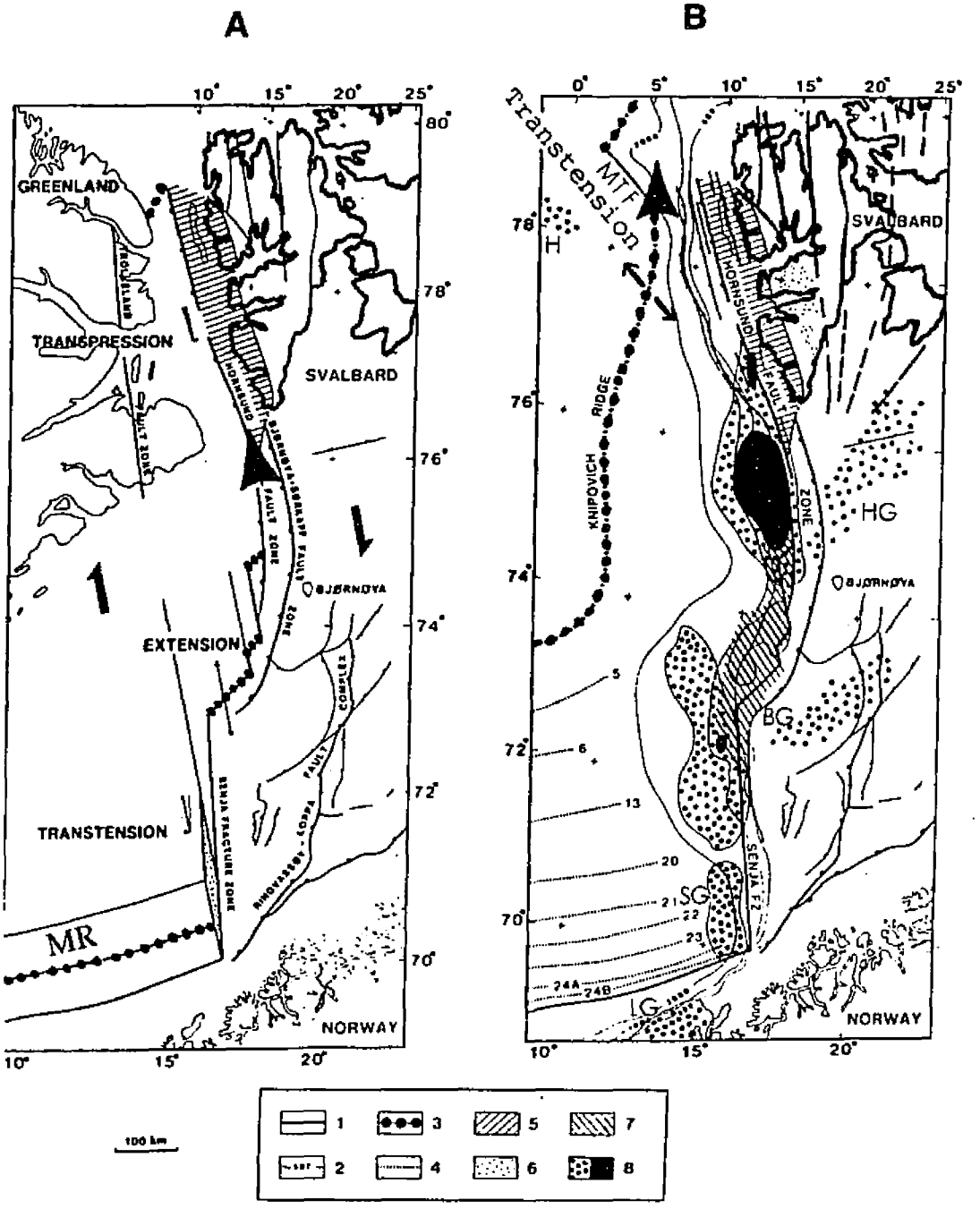

As the ridge propagated northward, it intersected the Spitsbergen Shear Zone producing massive extrusion and compression along the northern Svalbard Margin. Wrench movements along the Hornsund Fault Zone (Sundvor and Eldholm, 1979) were driven by dextral-transpression (Max and Ohta, 1988) related to the northward propagation of the Mohns and Knipovich Ridges. The Bjørnøya Marginal High was also formed by this early Eocene volcanism. Even at present, these intrusions are characterized by high heat flow and the Senja and Hornsund Gravity Highs (Myhre *et al.*, 1982; Crane *et al.*, 1991). Present-day intraplate seismicity is also considerably higher where the Mohns Ridge bends and the propagation continues northwards along the Knipovich Ridge (Figure 6-3).

It is likely that when the stress regime shifted from shear to tension, along the nascent Knipovich Ridge, simple-shear lithospheric extension evolved along the former shear zone creating a detachment fault zone in the process. Based on the analysis of heat flow, the northward propagating Mohns Ridge entered the first of many major detachment faults (part of the Spitsbergen Shear Zone) forming the Knipovich Ridge (Crane *et al.*, 1991). Later deep-seated propagation probably intersected other detachment surfaces and intruded the northwestern Svalbard Margin. A propagation and migration of the Knipovich Ridge from 75°N to 78°N occurred in the middle Miocene. This event deactivated the Hovgård Ridge/Fracture Zone (Myhre *et al.*, 1982; Crane *et al.*, 1991; Okay *et al.*, 1993) resulting in local excess volcanism (15 mybp).

Figure 6-3. Evolutionary model for the development of transtensional volcanic passive margins of the eastern Norwegian-Greenland Sea. Transtensional margins were formed at the intersections of the Mohns Ridge with the Jan Mayen Fracture Zone (JMFZ), the Vøring Fracture Zone (VFZ), the Vesterålen Fracture Zone (VÅFZ), and the Senja Fracture Zone (SFZ), and the intersection of the Knipovich Ridge with the Molloy Transform Fault (MTF) and the Spitsbergen Shear Zone (SSZ). The dotted area marks the present-seismic zones (LS: Lofoten-Vesterålen Seismic Zone, BAC: Barents Asthenospheric and Seismic Corridor, HL: Heer Land Seismic Zone, NS: Nordaustlandet Seismic Zone, KKC: Kong Karls Corridor). Systems of deep-seated faults (RFZ: Raudfjørden Fault Zone, BFZ: Billefjørden Fault Zone, LFZ: Lomfjørden Fault Zone, RfFZ: Rijpfjørden Fault Zone) trending parallel to the paleo-Spitsbergen Shear Zone act like vertical thermal boundaries along the northern Svalbard-Nordaustlandet Margin. SYP: Southern Yermak Plateau, NVT: Nordaustlandet Volcanic Terrain, HVT: Hinlopen Volcanic Terrain.

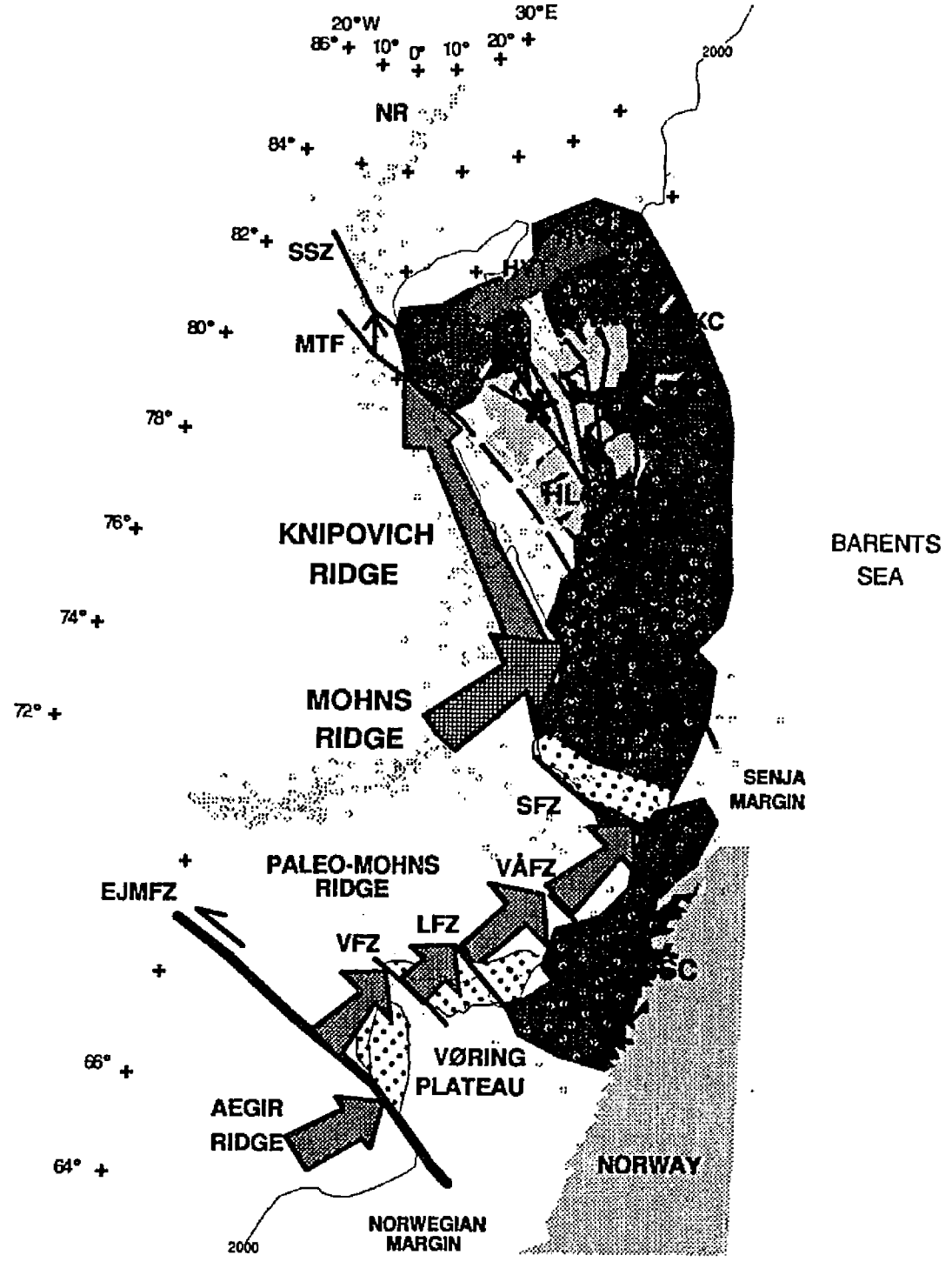
20°W
30°E
86°
10°
0°
10°
20°
2000
NR
84°
82°
SSZ
80°
MTF
78°
76°
KNIPOVICH
RIDGE
74°
72°
MOHNS
RIDGE
BARENTS
SEA
SENJA
MARGIN
SFZ
PALEO-MOHNS
RIDGE
VÅFZ
EJMFZ
LFZ
VFZ
66°
VØRING
PLATEAU
AEGIR
RIDGE
64°
NORWAY
NORWEGIAN
MARGIN
2000
SEISMIC AND PROPAGATING ASTHENOSPHERIC CORRIDOR
EARTHQUAKES
PLATEAU BASALTS
SDRS
HIGHLY REFLECTIVE SEAFLOOR
THERMAL SPRINGS
N. OKAY
1994

Interpretations of SeaMARC-II side-looking sonar imagery indicate that the northern Knipovich Ridge is at present propagating north of the double-troughed Molloy Transform Fault near its intersection with the Knipovich Ridge at 78.5°N (Figure 4-15). In fact, this double-fault transform is probably the result of a recent transform migration (Okay *et al.*, 1993) caused by the northward propagation of the Knipovich Ridge (the age of which we do not know) on the northwestern Svalbard Margin (Crane *et al.*, 1991; Okay *et al.*, 1993). Perhaps more recently, the northwards propagation of the Knipovich Ridge caused the thermal rejuvenation of the northern Svalbard Margin, where the continent-oceanic crustal transition boundary developed 13 my ago (at 79°N; Okay *et al.*, 1993).

The seismic pattern changes abruptly from the Mohns Ridge to the Knipovich Ridge (Figure 3-10). The Svalbard Archipelago is the most active region on the seismicity map of the Norwegian-Greenland Sea (Figure 4-14). Earthquake epicenters on Spitsbergen occur along major pre-existing structures, such as the Hornsund Fault Zone, Billefjørden Fault Zone, and Lomfjørden Fault Zone. Most likely, the oblique-intersection of the Knipovich Ridge with the Spitsbergen Shear Zone continued to generate a compressional front on both the Western Svalbard Margin and on Svalbard (the Heer Land Seismic Zone in southern Spitsbergen) where fault plane solutions show compressional stresses on Heer Land (Mitchell *et al.*, 1990). In additional to compressive stress, it is likely that oceanic mantle has underplated the Svalbard Platform thermally rejuvenating a region extending from the

Mohns Ridge bend, underneath the Barents Seafloor to a region north of Nordaustlandet (*the Barents Asthenospheric Corridor*).

Elverhøi and Solheim (1987) likewise suggest that during the last 5 my or so the Western Barents Shelf has thermally uplifted. Sellevoll *et al.* (1982) show that a 3 km-deep Moho Zone occurs only under the Central Spitsbergen Tertiary Basin and is characteristic of mobilized lower crust or igneous underplating. According to Amundsen *et al.* (1987) evidence from xenoliths and geophysics show that the crust is ca. 27 km thick and has been thinned by rifting for only 10-15 my. Both upper mantle ultrabasic and lower continental crustal high-temperature granulite xenoliths in the volcanics demonstrate subsided continental crust. Thus, shallow Moho depth (average 27 km, Amundsen *et al.*, 1988; Sellevoll *et al.*, 1991; Müller, 1993) suggests that the crust is thinner under the Svalbard Platform and that diffuse rifting and thermal rejuvenation have occurred in the Svalbard Platform as well. Apparently, while lavas erupted out of the Knipovich Ridge (the major detachment fault), the deep-seated Barents Asthenospheric Corridor continued to propagate northeast of the Mohns Ridge under Svalbard up to the northeastern Nordaustlandet region (35 to 20 mybp).

D. THE SOUTHERN YERMAK PLATEAU AND NORTHERN SVALBARD-NORDAUSTLANDET VOLCANIC MARGIN

The southern Yermak and Vøring Plateaus have similar thermo-mechanical histories. They both were created during the development of transtensional volcanic margins, on the compressional sides of ridge/shear-zone impacts. Several studies (Sundvor *et al.*, 1972, 1982b; Jackson *et al.*, 1988) indicate that the southern Yermak Plateau was also deformed by crustal thinning, stretching by later dike intrusion besides undergoing large scale thermal rejuvenation (Okay and Crane, 1993). The high heat flow on the southwestern part of the plateau suggests that intrusive activity occurred from 16 Ma to the present (Crane *et al.*, 1982). Extensional faults oriented in the NW-SE direction range from the region of high heat flow on the southern Yermak Plateau towards the volcanically active Woodfjørden area of Svalbard (Gjelsvik, 1963; Prestvik, 1977; Crane *et al.*, 1982; Amundsen *et al.*, 1988; Skjelkvåle *et al.*, 1989). Heat flow measurements (Sundvor, 1986) also indicate that high heat flow continues onto the southern section of the plateau where crustal thinning was observed by Johnson *et al.* (1982). Sundvor and Austegård (1990) proposed that this process also could have ruptured the continental crust, creating some oceanic crust in the process (Jackson *et al.*, 1984; Sundvor and Austegård, 1990).

In contrast, the northern part of the Yermak Plateau has lower heat flow values in the range of 50-92 mW/m^2 (Jackson *et al.*, 1984; Sundvor and Torp, 1987).

Sundvor and Austegård (1990) suggest that these heat flow values correspond to crustal ages between 41 and 26 Ma which are consistent with ages determined on the basis of extrapolated magnetic lineations (Feden *et al.*, 1979). These observed heat flow values (without corrections of the blanketing effect due to sedimentation) when compared with the theoretical cooling curve (Parsons and Sclater, 1977) represent oceanic crust 56 my old, the assumed age of the shelf edge that marks the continent-oceanic transition in this region (Sundvor and Austegård, 1990).

The southern Yermak Plateau intrusions and extrusions were probably trapped by several deep-seated faults related to the continuation of the Hornsund Fault Zone) trending southeastward from 81°N towards the coast of Western Svalbard just seaward of the continent-ocean transition (Figure 6-4). The northern continuations of the Raudfjørden Fault and Bockfjørden Fault on Spitsbergen dissect the southern Yermak Plateau. These faults likely acted as secondary detachment faults, interacting with the paleo-Spitsbergen Shear Zone, and consequently channeled the heat from the Knipovich Ridge causing intrusions in the southern Yermak Plateau at 11 mybp (Crane *et al.*, 1991; Okay and Crane, 1993). Two detachment surfaces (Knipovich and Yermak) could be inherited from the faults associated with the paleo-Spitsbergen Shear Zone; Figure 6-5).

There is no-indication of pure shear extension on the plateau to explain the off-axial Yermak Plateau's volcanic formation. In addition, field observations do not support a symmetric extension process. Thermal modeling results reveal that heat sources (presumably from *the asthenospheric corridor*) propagated and intruded into

Figure 6-4. Thermal rejuvenation model along the northern Svalbard-Nordaustlandet Margin. The Kong Karls Corridor is the northeastern expression of the propagation of deep-seated magma, creating thermal rejuvenation of the crust around 20 my. As the asthenospheric corridor progressed to the northeast, at 11 mybp, shallower melt injected through multiple-faults creating the Mosby Peak, the Southern Yermak Plateau, and volcanic centers and hot springs in the Woodfjørden region (Svalbard). These regions have undergone and are probably still undergoing thermal rejuvenation. Multiple zones of intrusion are common when continental margins form along paleo-shear zones and when they have been substantially faulted prior to rifting. Highly reflective seafloor interpreted as volcanic flows observed in SeaMARC-II images along this margin are surface expressions of extrusion from multiple-fault zones (secondary detachment faults). The multiple-fault zones are R: Raudfjørden Fault Zone, B: Billefjørden Fault Zone, L: Lomfjørden Fault Zone, Rf: Rijpfjørden Fault Zone. NVT: Nordaustlandet Volcanic Terrain, HVT: Hinlopen Volcanic Terrain, KK: Kong Karls, BAC: Barents Asthenospheric Corridor, SAC: Svalbard Asthenospheric Corridor, SSZ: Spitsbergen Shear Zone.

THERMAL REJUVENATION OF THE CRUST ALONG THE NORTHERN SVALBARD-NORDAUSTLANDET MARGIN

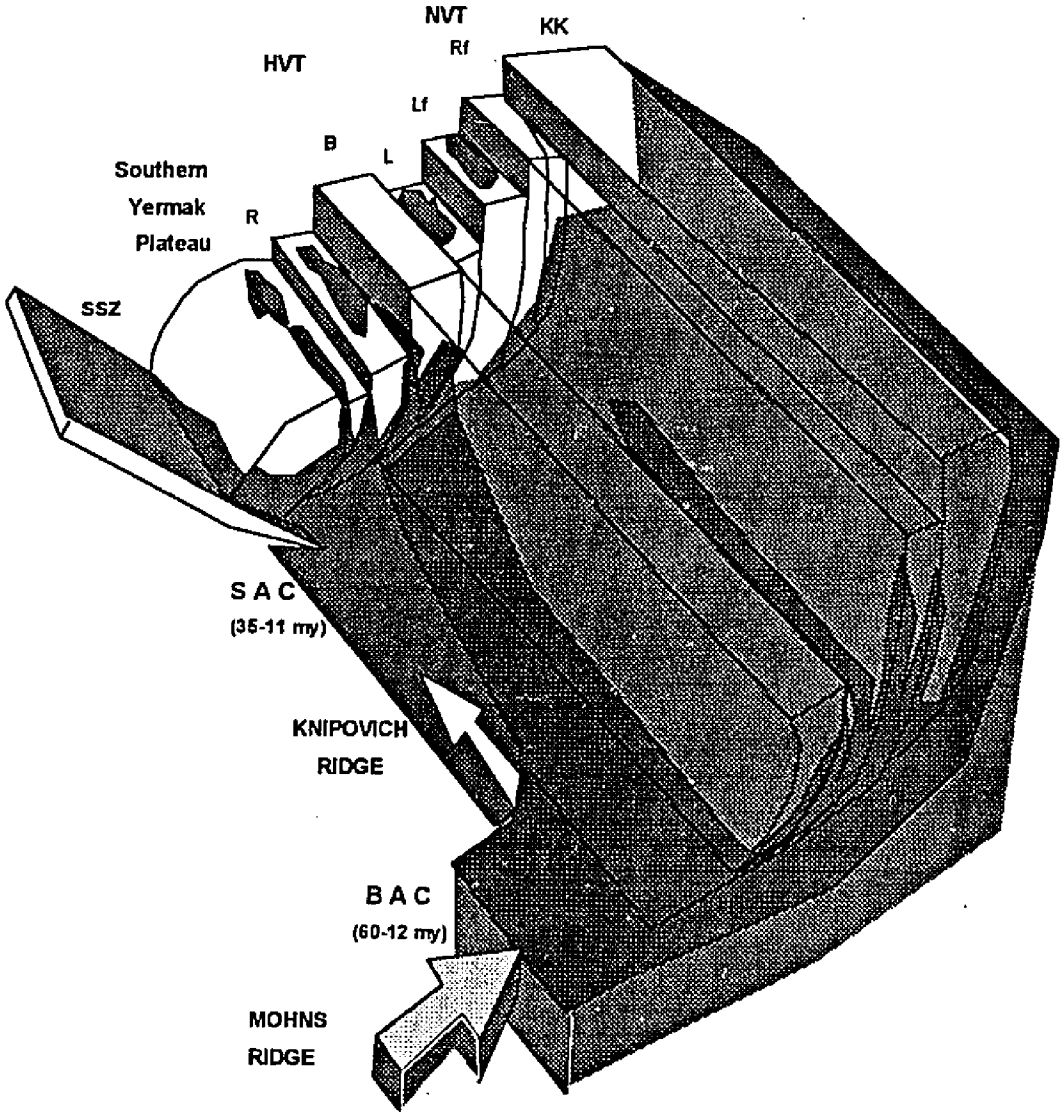

Figure 6-5. Kinematic model of the southern Yermak Plateau formation.
Evolutionary model describes a fault system of the Knipovich Ridge and southern Yermak Plateau.
Faults dip eastward from the Spitsbergen Transform Fault (STF)-Knipovich Ridge, intersecting a secondary fault dipping westward (under Svalbard). AA' profile represents the heat flow for the southern Yermak Plateau. HF: Hornsund Fault Zone.

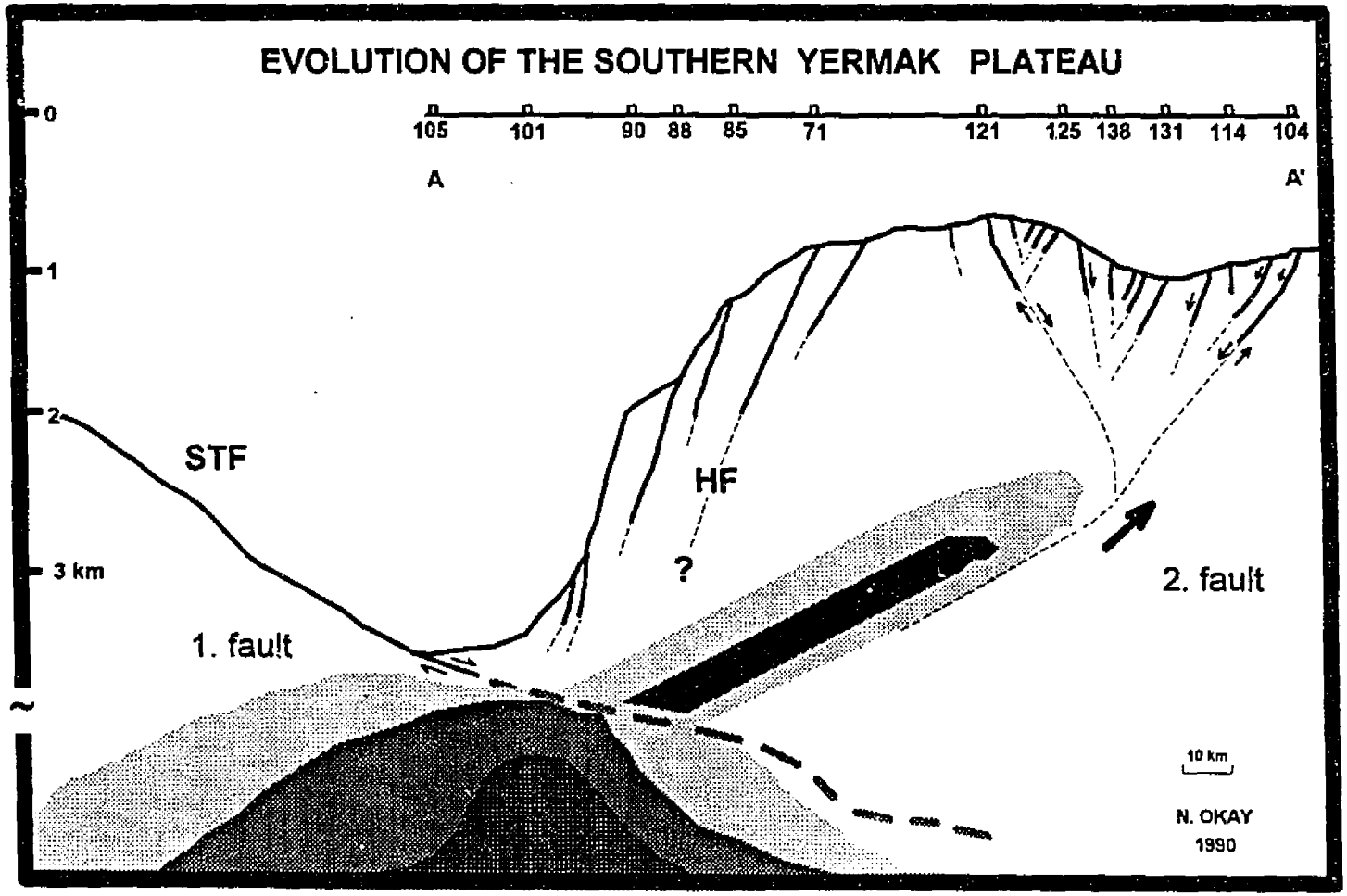
EVOLUTION OF THE SOUTHERN YERMAK PLATEAU
0
1
2
3 km
105
101
90
88
85
71
121
125
138
131
114
104
A
A'
STF
HF
?
1. fault
2. fault
10 km
N. OKAY
1990

the region by an asymmetric simple-shear extension mechanism. Bonatti and Michael (1989) report that fresh peridotites can be found in this area at shallow depth along the northern Svalbard Margin, indicating that the Yermak Plateau had been underplated and heated by oceanic mantle material most likely originating from a source under the Knipovich Ridge (rather than continental mantle). Heat flow analyses also indicate that some of the Barents/Yermak underplating asthenosphere erupted near the Hinlopen Volcanic Terrain creating the Mosby Peak along the northern Svalbard Margin between 35 and 11 mybp. SeaMARC-II side-looking sonar imagery suggests that well defined normal faults cut the seafloor directly north of the active multiple-fault zones on Spitsbergen (the Raudfjørden, Bockfjørden, Billefjørden, and Lomfjørden fault zones). The northern prolongation of these faults is coincident with a positive magnetic anomaly that suggests submarine volcanics (Figure 4-13).

It is likely that the Knipovich Ridge propagated northwards while its subjacent asthenosphere progressed northeastwards, intersecting and intruding the multiple-faults associated with the Paleo-shear zone creating the southern Yermak Plateau, the Mosby Peak, the Yermak Seamount at 12°E and the Woodfjørden volcanics in the process. The regions of high total magnetic field detected during the SeaMARC-II Expedition in 1990, are interpreted as probable dike injections associated with the underplating of the Barents-Svalbard Platform by the Spitsbergen Shear Zone/Knipovich Ridge system. Each distinctive magnetic high is associated with highly reflective seafloor, which also correlates with off-axial heat flow highs and

zones of concentrated earthquakes (Figure 4-16). This suggests that these regions have undergone and are probably still undergoing thermal rejuvenation.

SeaMARC-II data (Sundvor *et al.*, 1991; Okay *et al.*, 1991; Okay and Crane, 1993) indicate that there are also NW-SE trending faults (probably secondary and Tertiary detachment faults associated with the greater Spitsbergen Shear Zone System; Figure 6-5) bordering the northern Nordaustlandet Margin (northern extensions of the Rijpfjørden and Lady Franklinfjørden Fault Zones). These are also probably the loci of off-axial volcanic eruptions (Okay *et al.*, 1991). Based on the analysis of heat flow, a thermal boundary probably exists between the southeastern Yermak Plateau and the northern Nordaustlandet Margin. This boundary between high heat flow and low heat flow coincides with the magnetic and structural boundaries along Hinlopenstretet, but the continental-oceanic crustal transition zone is unclear. According to heat flow analyses, the latest intrusion of magma occurred at ~37 mybp and was associated with Tertiary volcanics.

I suggest, that as the Mohns Ridge propagated northward, creating the Knipovich Ridge in the process, episodic transtensional stress propagated in space and time from Kong Karls Land to the Spitsbergen Shear Zone. Between 60-55 mybp and 35 mybp the Barents Asthenospheric Corridor likely propagated northwards, causing the eruption of dacitic lavas on northeastern Nordaustlandet and Kong Karls Land (Figure 6-4). Dike injections also occurred along the Lady Franklinfjørden Fault. This fault is related to the other multiple-faults (secondary and Tertiary

detachment faults on the northern Svalbard Margin) that trapped the deep-seated asthenosphere.

Fault plane solutions show extensional stresses active today on Nordaustlandet (Mitchell *et al.*, 1990). Mitchell *et al.* (1990) reported small *b*-values for the Nordaustlandet Seismic Zone. This indicates, rather unique, diffuse rifting in the region. Focal mechanisms are not typical of earthquakes that are characterized by compressive stresses occurring at the passive margin or regions of continental rifting (Sykes, 1978). The earthquakes instead are caused by an extensional regime with a strike-slip component (Chan *et al.*, 1985; Mitchell *et al.*, 1990) rather than by intraplate deformation. Savostin and Karasik (1988) suggested a Spitsbergen Microplate which was bordered by the seismic zones (Heer Land and Nordaustlandet), and they suggested that the Billefjørden Fault Zone, a major strike-slip feature in the area, is a major plate boundary. However, the Billefjørden Fault Zone is also a deep-seated secondary extensional fault (Lamar *et al.*, 1986) that most likely served as a magma conduit or a vertical thermal-mechanical boundary. In general, the analyses of these new geophysical data are highly suggestive of large-scale underplating of the Barents-Svalbard Platform and imply that either the axis of spreading now centered along the Knipovich Ridge may either be migrating laterally as well as propagating to the North, or the data may suggest that the plate boundary is very broad in this region (≈450 km).

Chapter 7

CONCLUSIONS

1. Transtensional volcanic plateaus and passive margins form along paleo-shear zones. The orientation of the paleo-shear zones have absolute control on a migrating and propagating ridge during its entrapment by the shear zone. An oblique impact of a ridge and shear zone creates an asymmetric unstable stress configuration generating both extension and compression on either side of the intersection. The impact angle controls the direction of deflection of the propagating ridge, the rate of spreading and style of newly forming oceanic crust. Marginal plateaus, seismic activity, underplating by deep-seated asthenosphere, multiple zones of intrusions, heat injection and thermal rejuvenation of the continental crust are found on the compressional side of the ridge/paleo-shear zone intersection. In these locations, the continent-oceanic crustal transition is characterized by seaward dipping seismic reflectors, high heat flow, high gravity and magnetic smooth zones located on the compressional side of impact along the transtensional margin.

Based on heat flow analyses of the eastern margin of the Norwegian-Greenland Sea the thermal crustal ages indicate that the thermal structure in many sections of the passive margin have been reset to values appropriate for much younger lithosphere. Shear zones and their deep-seated extensional multiple-faults act as vertical magma conduits from the deep-seated asthenosphere associated with a

propagating ridge to the surface. Rejuvenation occurs with lateral heat injection via these paleo-shear zone related deep-seated extensional faults.

2. Pre-existing deep-seated multiple-faults in extensional terrain may also act as detachment faults. Shear zones control the lithospheric extension style (simple shear lithospheric extension by a detachment fault), continental breakup, position, and mode in the upper crust. Major detachment faults are often accompanied by secondary detachment faults. These secondary detachment faults are responsible for the development of a wide continent-oceanic crustal transition (as suggested by seaward-dipping seismic reflectors).

3. An asymmetric simple shear lithospheric extension mechanism (or perhaps a combination of it with symmetric pure shear) is responsible for the emplacement of thick (but narrow) basaltic crust adjacent to the passive margin. Symmetric lithospheric extension models do not explain the wide variations in the passive margin geometry such as marginal plateau formation. There is a notable absence of symmetrical rift structures on the opposing margins of the Norwegian-Greenland Sea. If this region is representative of other transtensional margins, then it is reasonable to suggest that structural asymmetry is a general feature of transtensional volcanic passive margins. By analyzing heat flow it is possible to distinguish the events which occurred during the development of a transtensional volcanic margin and to determine whether or not simple-shear extension has taken place.

4. Suggestions for further studies:

Few heat flow data are available from other transtensional margins in the world. Future analyses of heat flow collected in these areas should be directed towards understanding the thermal characteristics of a changing paleo-shear zone, the off-axial intrusion phenomena, and the magnitude of thermal rejuvenation on a passive margin.

a. For a further study of lithospheric extension modeling, a transect of heat flow stations extending normal to the Eastern Jan Mayen Fracture Zone and additional drilling of the Vøring Plateau is suggested. An important test of the detachment fault model would be to mount a drilling program into basement rocks in the Vøring outer highs, to demonstrate the presence of deeper level sediments and/or metamorphic rocks.

b. Few (or no) heat flow measurements have been collected from the Lofoten Islands, the western and eastern Barents Sea region, the area between Kong Karls Land and Franz Josef Land, and the Hinlopenstretet region, leaving substantial need to complete this picture.

c. A thermal boundary exists somewhere between the Yermak Plateau and Nordaustlandet. This boundary between high heat flow and low heat flow probably coincides with the magnetic and structural boundaries along the margin. The continental-oceanic crustal transition zone along the northeastern coast of Svalbard is unclear and thus both the heat flow and seismic structure in this region need to be resolved to make any further estimation of the intrusion dates and nature of this thermal boundary.

APPENDIX

A. METHODOLOGY

1. SeaMARC-II AND INSTRUMENTATION

SeaMARC-II (Seafloor Mapping and Remote Characterization) is a combination of towed acoustic mapping systems developed by International Submarine technology in collaboration with the Hawaii Institute of Geophysics (Figure A-1). The SeaMARC-II system is a shallow towed-instrumentation package. It simultaneously collects backscatter and bathymetric information for seafloor mapping (Shor, 1990). Acoustic sensors are towed behind a depressor in a streamlined, passively stabilized, naturally buoyant vehicle (Figure A-2).

The system is capable of operating in any water-depth greater than 50 meters. Survey speed depending on weather averages between 3 and 9 knots. The side-looking sonar system is configured to produce a swath of data 10 km wide for sea-floor depths greater than 1 km. A blind zone at nadir is assigned a width of 4% of swath width. The bathymetric data is recorded from nadir to an angle of 60°, or to a swath-width equal to 3.4 times water depth (seafloor multiples cause phase interference at and beyond this range) as suggested by Shor (1990).

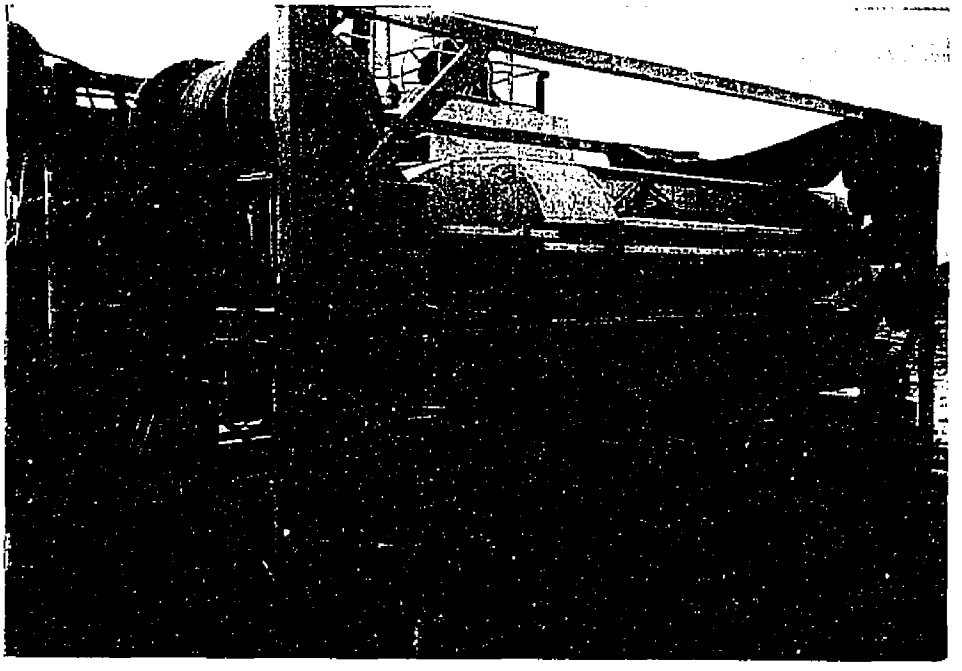

Figure A-1. SeaMARC-II towfish on transportable launch and recovery system.

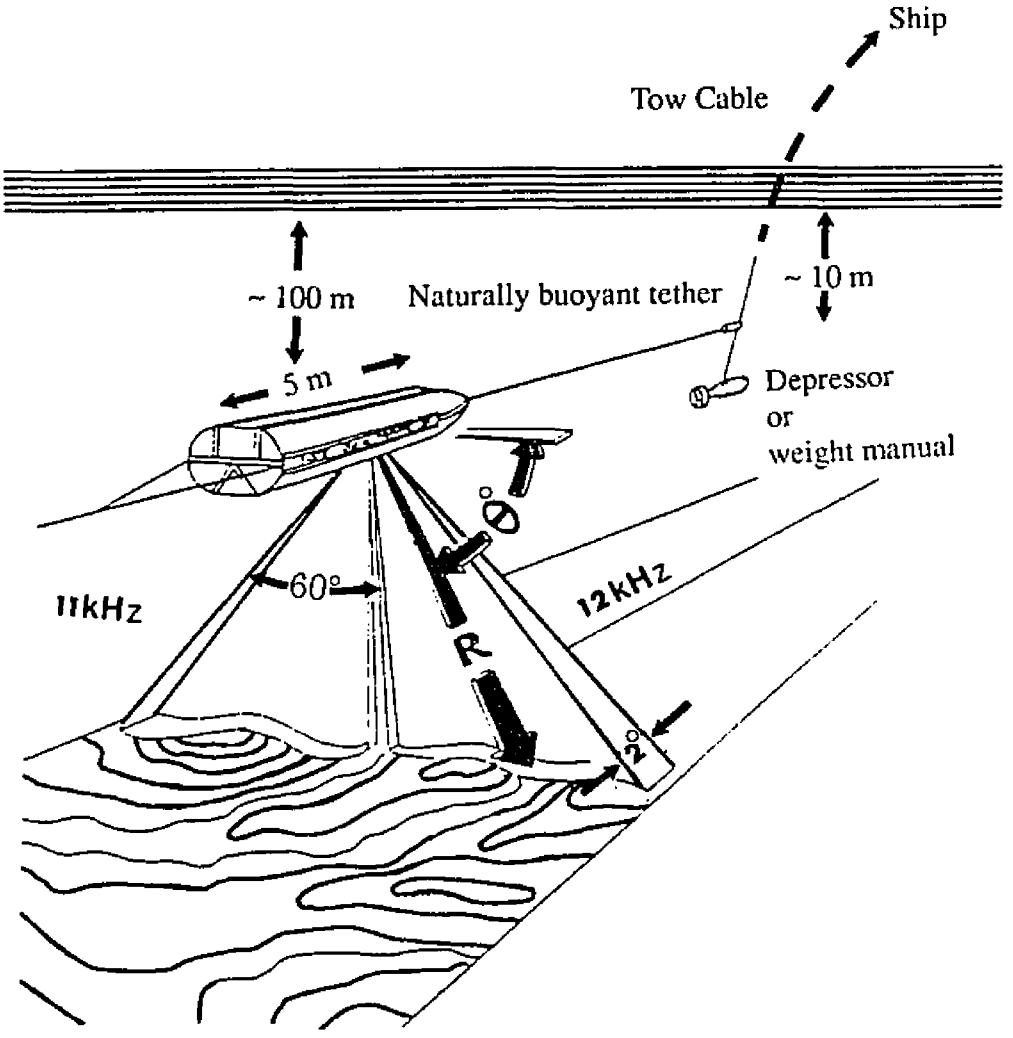

Figure A-2. The schematic SeaMARC-II Mapping System Configuration (after Blanckinton *et al.* (1983). The system operates at 11 *kHz* on the portside and 12 *kHz* to starboard.

Bathymetry is determined by measurements taken 4000 times each second of the magnitude and arrival angle (θ°) of narrow band acoustic energy, phase difference (Ø°), returned from each side of ship's track (Figure A-3). Each array is composed of two banks of transducers. During transmission the two banks are driven in parallel, but while receiving, the two are measured separately. The phase difference can be measured between the two lines. For the system C/FD is ~2° (Shor, 1990; Masnadi-Shirazi and de Moustier, 1990).

SeaMARC-II image resolution is a function of the beam width of the signal 2°, range, ping repetition rate and ship speed (Figure A-2). Side-looking images are a combination of the small scale reflecting properties of the bottom (micro-reflectivity). SeaMARC-II side-looking images contain 1024 pixels of digital data on either side of the swath. This unique combination allows more accurate and rapid understanding of seafloor character (Shor, 1990). SeaMARC-II system is used to investigate the results of tectonic and structural processes. Linear features such as channels and faults are recognizable if they have dimensions of several to a few tens of meters.

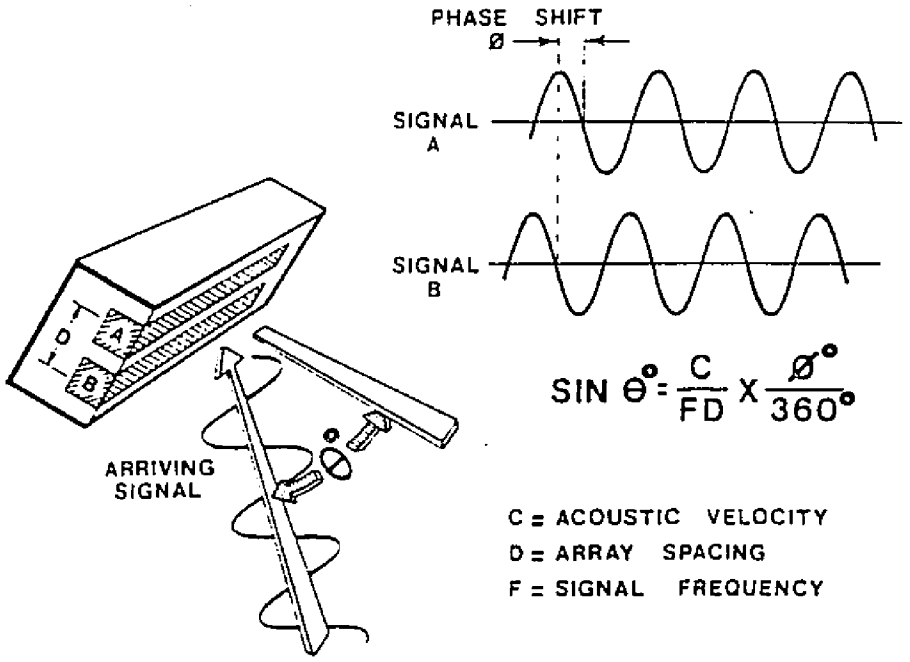

Figure A-3. Schematic illustration of the SeaMARC-II phase difference measurement technique for determining acoustic angle to target on bottom. When combined with precise arrival times, range and depth pairs are calculated across a swath of seafloor out to 60° to either side of the towfish track (Shor, 1990).

2. HEAT FLOW MODELS

a. Sedimentation and Compaction:

The sediment particle rates (V_S) depend only on z, positive downward

$$V_S(z,t) = V_S(z) \qquad [A.1].$$

As the porosity falls with increasing depth of burial, the velocity of the sediment grains is reduced; at depths (>>λ, compaction constant), the porosity, ϕ is effectively zero and the sediment rate is given by

$$V_S(z) = V_0(1 - \phi) / (1-\phi) \qquad [A.2].$$

The conductive and advective heat flux (Crane *et al.*, 1982),

$$- K\, \partial z\, T + [\rho_W C_W V_W \phi + \rho_S C_S V_S (1 - \phi)].\, T \qquad [A.3]$$

where $T(z,t)$ is temperature, function of depth z and time t; $K(z,t)$ is composite thermal conductivity at depth, ρ_W and ρ_S are pore fluid-density and sediment particle-density, C_W and C_S are heat capacity, $V_W(z,t)$ pore fluid-velocity. The heat flow equation,

$$= \partial z\, (K\, \partial z\, T) - \partial_z \{[\rho c_W V_W \phi + \rho c_S V_S (1 - \phi)]\, T\} + IHP \qquad [A.4]$$

$$= [\rho c_W \phi + \rho c_S (1- \phi_0)].\, \partial t\, T \qquad [A.5]$$

where ϕ_0 is the surface porosity for the porosity of sediment at z depth, and IHP is the internal heat production,

$$\phi(z) = \phi_0 .\, exp\, (-z/\lambda) = P(z) \qquad [A.6].$$

A comparison of observed heat flow data with heat flow corrected site by site. Decompacted sediment thickness can be calculated by first estimating where,

$$H_{decomp} = H_{comp}\, [1 - \phi(z) / 1 - \phi(0)] \qquad [A.7].$$

This simplified equation taken from Crane *et al.* (1982) for decompacted sedimentary thickness is determined to yield an average depositional rate at any point.

The thermal conductivity K_S of a rock is the sum of water and water rock matrix conductivities caused by lattice vibrations and by transfer of heat by radiation. Average thermal conductivity of rock,

$$K_S = K_W^{P(z)} \cdot K_R^{1-P(z)}, \qquad [A.8]$$

volume specific heat of fluid,

$$\rho c(z) = \rho c_W [\phi(z) + \rho c_R (1-\phi(z)] \qquad [A.9]$$

average thermal diffusivity is defined by

$$\kappa = K_S / \rho c \qquad [A.10]$$

which is needed to solve problems in heat conduction in which the temperature changes with time. Parameters used for this calculations are given on Table A-1.

b. One-Layer Model:

If it is assumed that the heat flow from depth has been constant and the sedimentation rate has been uniform, then the heat flow at the surface of the sediments can be estimated (Langseth *et al.*, 1980) using an equation derived by Benfield (1949):

$$q_S = q_b [1 - 4i^2 \cdot erfc (V\sqrt{t} / 2\sqrt{\kappa})] \qquad [A.11].$$

Where, q_S is the observed heat flux from the sedimentary surface, q_b the heat flow from great depth, t the duration of sedimentation (*my*), and V the sedimentation rate (*km/my*):

Porosity	$\phi_0 = 0.50$
Compaction constant	$\lambda = 2.0$ km
Conductivities	
	$K_W = 0.6$ W/m°C
	$K_R = 2.4$ W/m°C
Volume Specific Heat	
pore fluid	$\rho c_W = 4.2\times10^6$ J/m^3°C
basement	$\rho c_R = 2.7\times10^6$ J/m^3°C

1 m^2/sec = 3.15×10^7 km^2/my

Table A-1. Initial parameters used in heat flow modeling.

$$Sedimentation\ Rate = H_{decomp} / Age\ of\ Crust$$

The factor by which the heat flow reduced is the following,

$$z = [V(t)^{1/2} / 2(k)^{1/2}]$$

$$\forall\, z \in C^2, \qquad \text{Complex Plane}$$

$$q_S = q_b\,(1 - 4i^2\, erfc\, z)$$

$$\forall\, z = x+iy \qquad [A.12]$$

Thus:

$$erf\, z = \pi^{-1/2}\, \Psi(1/2, z^2) \qquad [A.13]$$

$$erfc\, z = \Pi^{1/2}\, \Gamma(1/2, z^2)$$

where,

$$\Gamma(1/2) = \sqrt{\pi} \qquad [A.14]$$

$$erf\, z = 2/\sqrt{\pi} \int e^{-(t)^2}\, dt \qquad [A.15]$$

$$erfc\, z = 1 - erf\, z \qquad [A.16]$$

$$i^{-1}\, erfc\, z = 2 / \sqrt{\pi}\ e^{-(z)^2} \qquad [A.17]$$

$$i\, erfc\, z = -z\,(1 - erf(z) + 0.5(i^{-1}\ erfc\, z)) \qquad [A.18]$$

and

$$i^2\, erfc\, z = -z/2\ (i\, erfc\, z) + 0.25\ (1 - erfc\, z) \qquad [A.19]$$

c. Cooling Plate Model:

I have attempt to fit the combined heat flow data of the Norwegian-Greenland Sea using the cooling plate model of McKenzie (1978) (Figure A-4). In this model the lithosphere is assumed to be a slab of uniform thermal properties

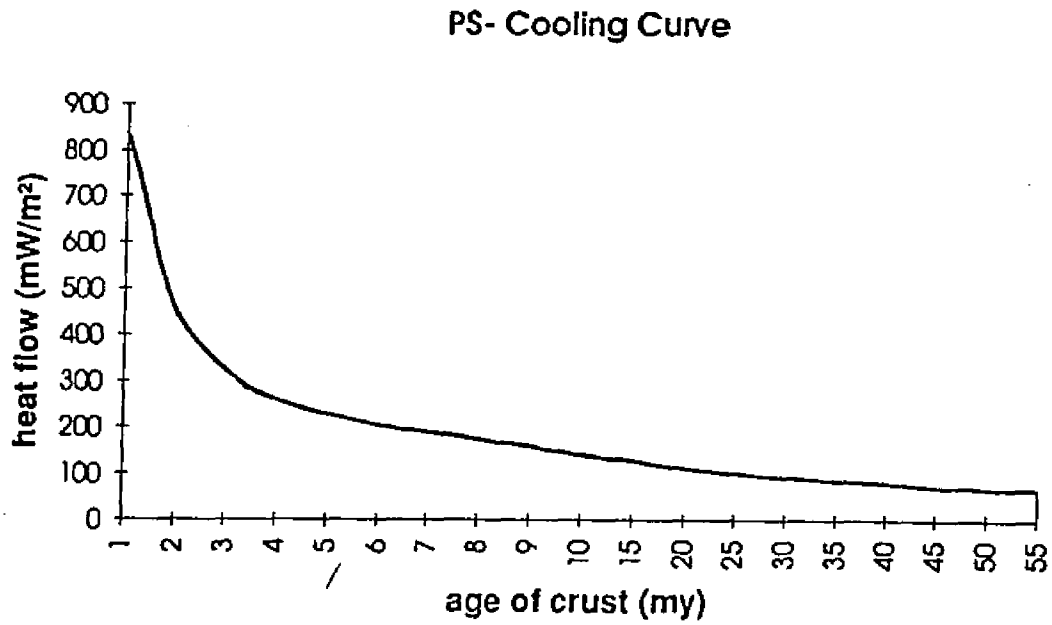

Figure A-4. Theoretical heat flow versus age. Cooling oceanic crust is modeled by PS-cooling curve (Parsons and Sclater, 1977). The solid line represents a fit of the data to the cooling crust model of McKenzie (1978) assuming a spreading velocity of 1 cm/yr, a thickness of 60 km and basal temperature of 1475°C. Both seafloor depth and heat flow vary with age to provide the main constraints on the thermal structure and evolution of the oceanic lithospheric (Stein and Stein, 1992). In the plate tectonic cycle oceanic lithosphere cools as it spreads away from mid-ocean ridges.

moving away from the ridge axis at a constant velocity. The accreting edge of the slab and the base of the slab are assumed to be an isotherm and the surface temperature is assumed to be an uniform colder temperature taken as zero. The lithosphere cools by conduction as it moves away from the mid-ocean ridge axis.

3. NUMERICAL MODELING

a. Pure Shear Lithospheric Extension:

Pure shear is defined by the initial width of the vertical region of the Lithosphere thinning (W_0) and the rate of separation of one side of the rift from the other (U_r), the rate of crustal thinning $W_r(t)$ at any given time (Figure A-5a); after the initiation of rifting is given by:

$$W_r(t) = W_0 + U_r \, . \, t \qquad [A.20]$$

For this model, the horizontal gradient of horizontal velocity, ($\partial U/\partial X$) is constant across the width of the extending region and equal to the vertical gradient of vertical velocity, ($\partial W/\partial Z$). For the general model of the pure shear lithospheric extension, the thickness of the crust within the rift at (t) is given by:

$$D(t) = D_0 \; exp \, [- (U_r / U_b) \, ln \, (U_b \; t / W_0 + 1)] \qquad [A.21]$$

where (D_0) is the initial thickness of the crust and (U_b) is the rate of the extensional boundary extension. If the boundaries of the zone of extension are fixed, $U_b = 0$. Then the crustal thickness within the extending pure shear region will vary as $exp(-U_r \, t / W_0)$ or for extreme pure shear model ($U_b = U_r$) and the thickness of the crust within the shearing region varies as $(U_b \, . \, t / W_0 + 1)^{-1}$.

pure shear

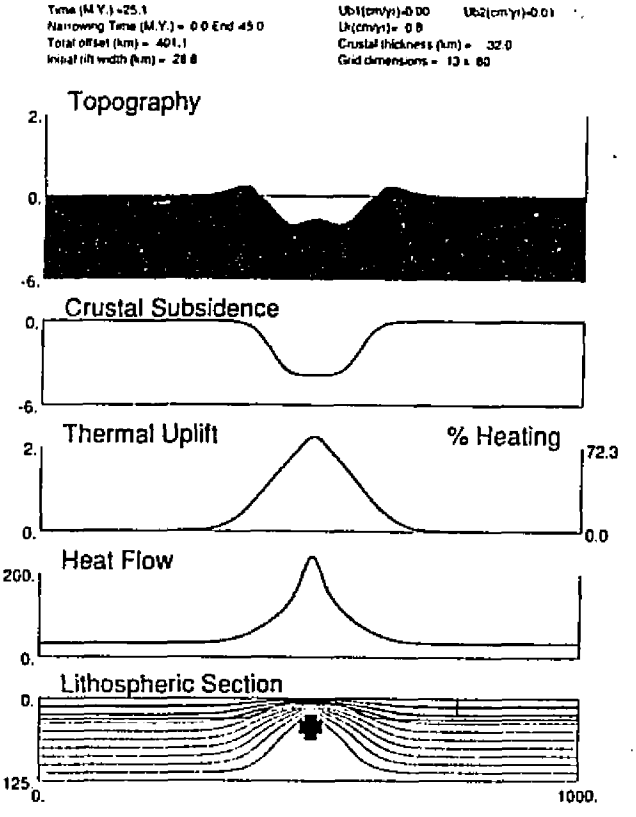

a

Figure A-5a. Numerical modeling of the pure shear lithospheric extension: the initial rift width of the extending area is 28.8 km, and the total extension rate is 0.8 cm/yr during a 25 my time period.

The *2-D* equation of advective and diffusive heat transport:

$$\partial T/\partial t + U \cdot \partial T/\partial x + W \cdot \partial T/\partial z = \kappa \cdot (\partial T^2/\partial X^2 + \partial T^2/\partial Z^2) \qquad [A.22]$$

is solved. In this case, (T) is the temperature in °C, (t) is the time in seconds, (κ) is diffusivity, (x) and (z) are horizontal and vertical directions, (u) and (v) are horizontal and vertical velocities. The boundary conditions for the temperatures are that $T = 0$ °C on the top boundary ($z = 0$ *km*) and $T = 1300$ °C on the bottom boundary ($z = 125$ *km*, see Table A-2). The temperature equation [A.22] is solved using a finite difference method. The values are calculated on a fixed Eulerian Grid representing the Lithosphere. The accurancy of the method was evaluated by repeating calculations at three grid cell spacings and examining the rate of convergence. The smallest grid-spacing is used in the calculations, the distribution of crustal thickness in the models is calculated analytically as a function of position and time.

b. Simple Shear Lithospheric Extension:

For the simple shear model, the strain fields do not change with time but are affected by the separation rate (Buck *et al.*, 1988). Lithospheric simple shear extension models are inefficient at generated melts, they do not produce partial melting unless the plate separation rate is high or the shear zone has a steep dip. Heat flow and uplift increase with increasing rate of extension and dip angle, because the thermal anomaly is distributed over a wide area.

Model Physical Constants

Crustal Thickness	32 km
Crustal Density at 0 °C	2.8 $g.cm^{-3}$
Lithospheric Thickness	125 km
Lithospheric Density at 0 °C	3.33 $g.cm^{-3}$
Thermal Expansion Coefficient	3.4×10^{-5} C^{-1}
Thermal Conductivity	3.2 Wm^{-1} C^{-1}
Thermal Diffusivity	10^{-6} m^{-2} s^{-1}
Surface Temperature	0 °C
Boundary Temperature	1300 °C

Table A-2. Physical constants used in numerical modeling.

$$W_0 = D_0 / (\tan \theta° + W_{SS}) \qquad [A.23]$$

If W_{SS} is the width of the shear zone, and the dip of the shear zone or detachment fault is ($\theta°$), then the initial crustal width W_0 (Figure A-5b) is determined by the initial crustal thickness (D_0) and detachment fault dip.

Illustrations of numerical modeling results for pure and simple-shear lithospheric extension are shown in Figures A-5a and A-5b. In these figures, the top panel shows the compensated topography (seafloor bathymetry) produced by the crustal subsidence component and the isostatic thermal uplift component. Observed surface heat flow and seafloor bathymetry (topography) are two significant constraints imposed on this modeling.

The second panel shows the component of the isostatic Airy subsidence caused by thinning of the crust. The third panel shows the component of the Airy isostatic thermal uplift caused by heating of the lithosphere. The fourth panel shows the synthetic heat flow curve determined by numerical modeling. The lower panel indicates the thermal structure of the lithosphere with isotherms superimposed. The crust is shown in light gray and the material moved from the asthenosphere is shown in dark gray. Temperature is assumed to remain at 0 °C at the surface of the extending crust and 1300°C at the bottom of the extending lithosphere (at approximately 125 km-depth).

Pure- and simple-shear numerical models produce different patterns of topography, heat flow, and thermal structure within an extending region. For

Simple Shear

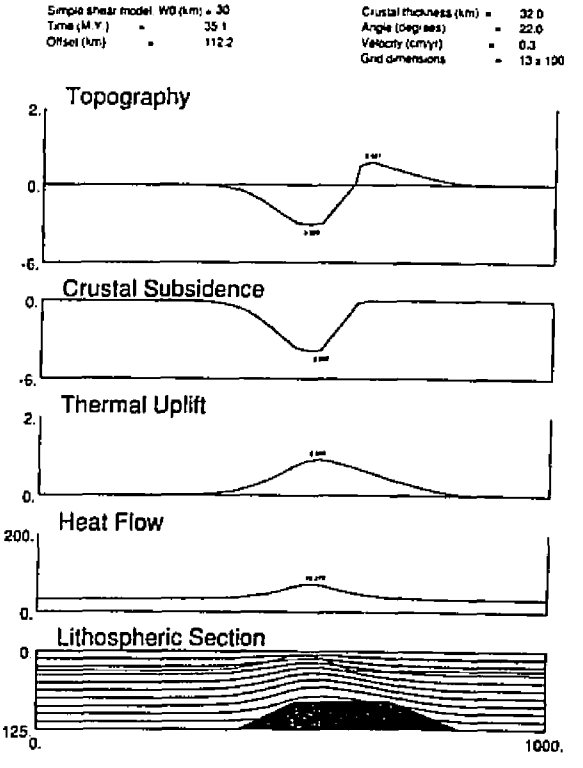

b

Figure A-5b. Numerical modeling of the simple shear lithospheric extension: this extension occurs along a detachment fault with a dipping angle of 22° and a total extension rate of 0.3 cm/yr.

example, the pure-shear extension model is produced by a high extension rate and a narrow rift width. Upwelling asthenosphere (vertical heat flux) and melting are centered symmetrically under the extending region (Figure A-5a). With continued extension, the lithosphere generates a steady-state temperature structure, which is homogeneous everywhere below the mantle solidus. The simple-shear extending model is produced by a detachment fault geometry where there is a finite width of isostatic response. Lower crust is progressively stripped off the center of the extending zone (Figure A-5b). The extension rate and the dip angle of the detachment fault effect the amount and duration of heat input from the asthenosphere into the lithosphere.

1. SeaMARC-II Data

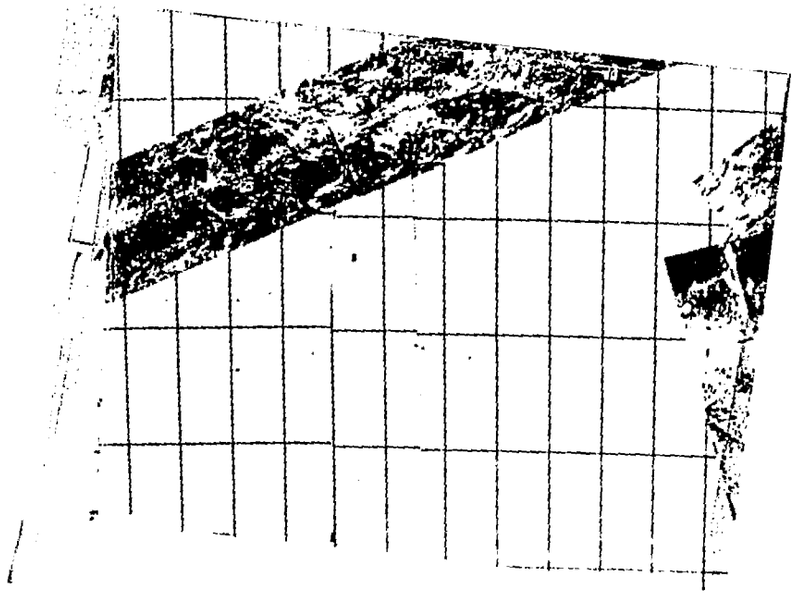

Plate 1. SeaMARC-II side-looking sonar imagery of the Northern Svalbard-Nordaustlandet Margin.

1. SeaMARC-II Data

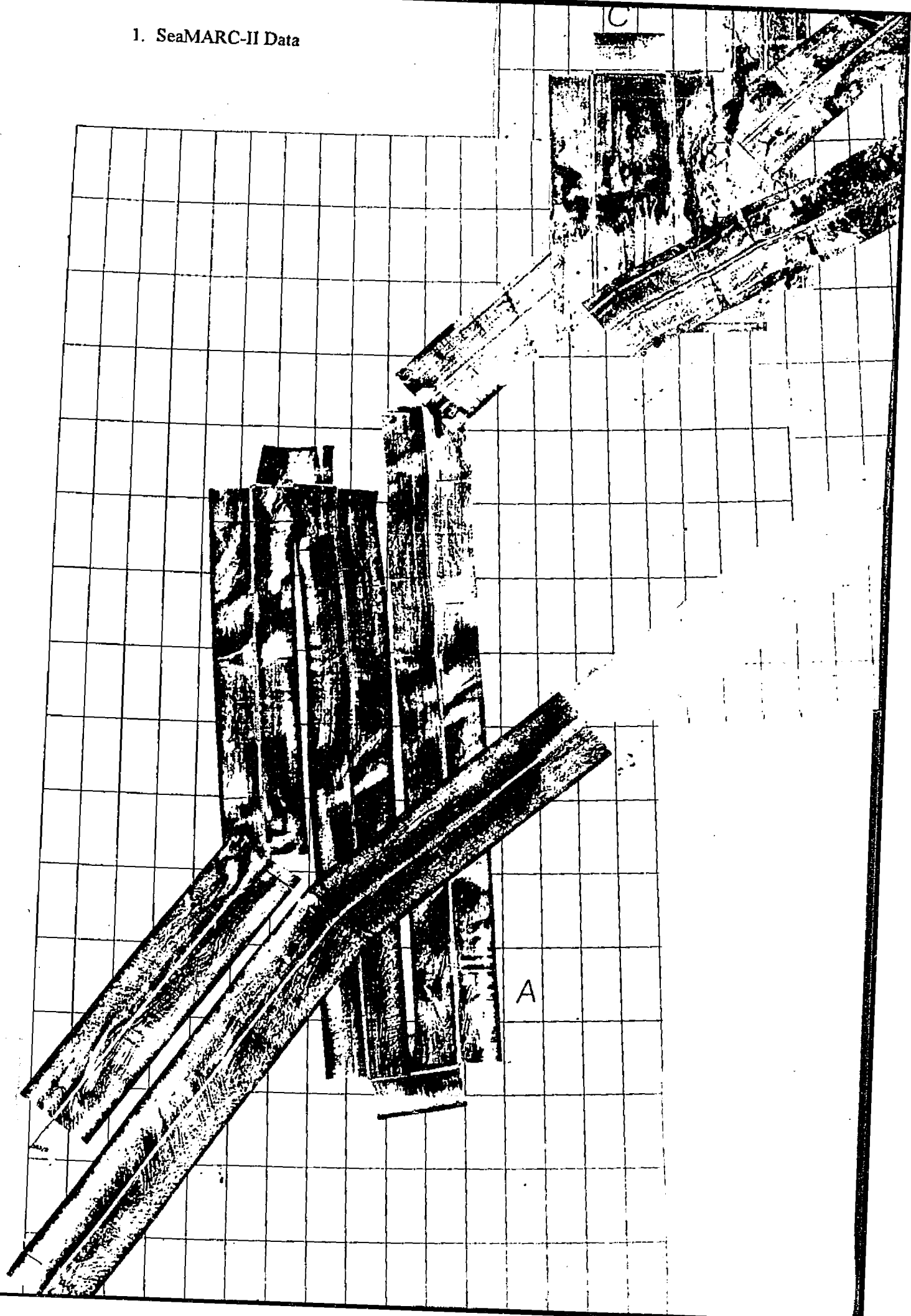

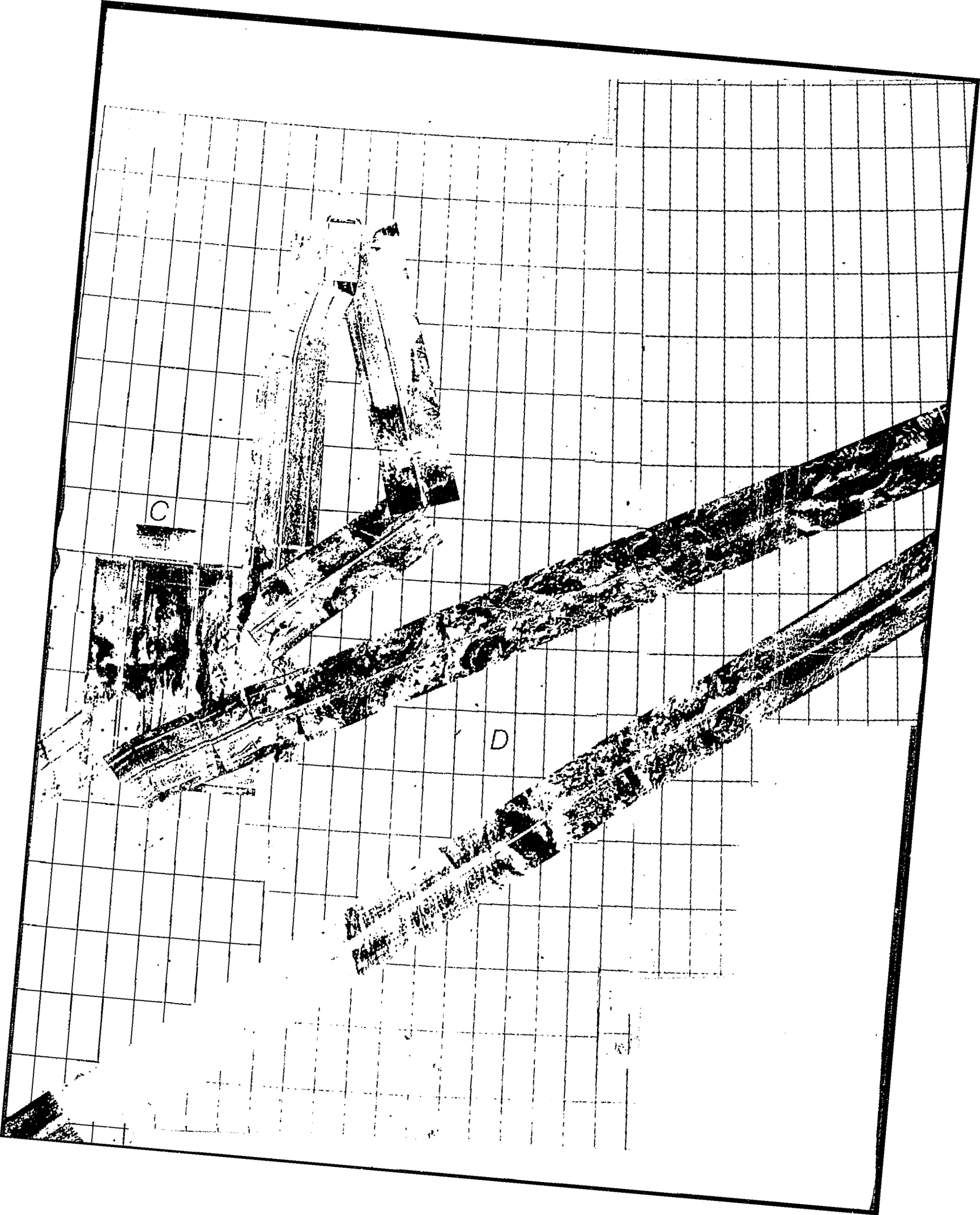
C
D

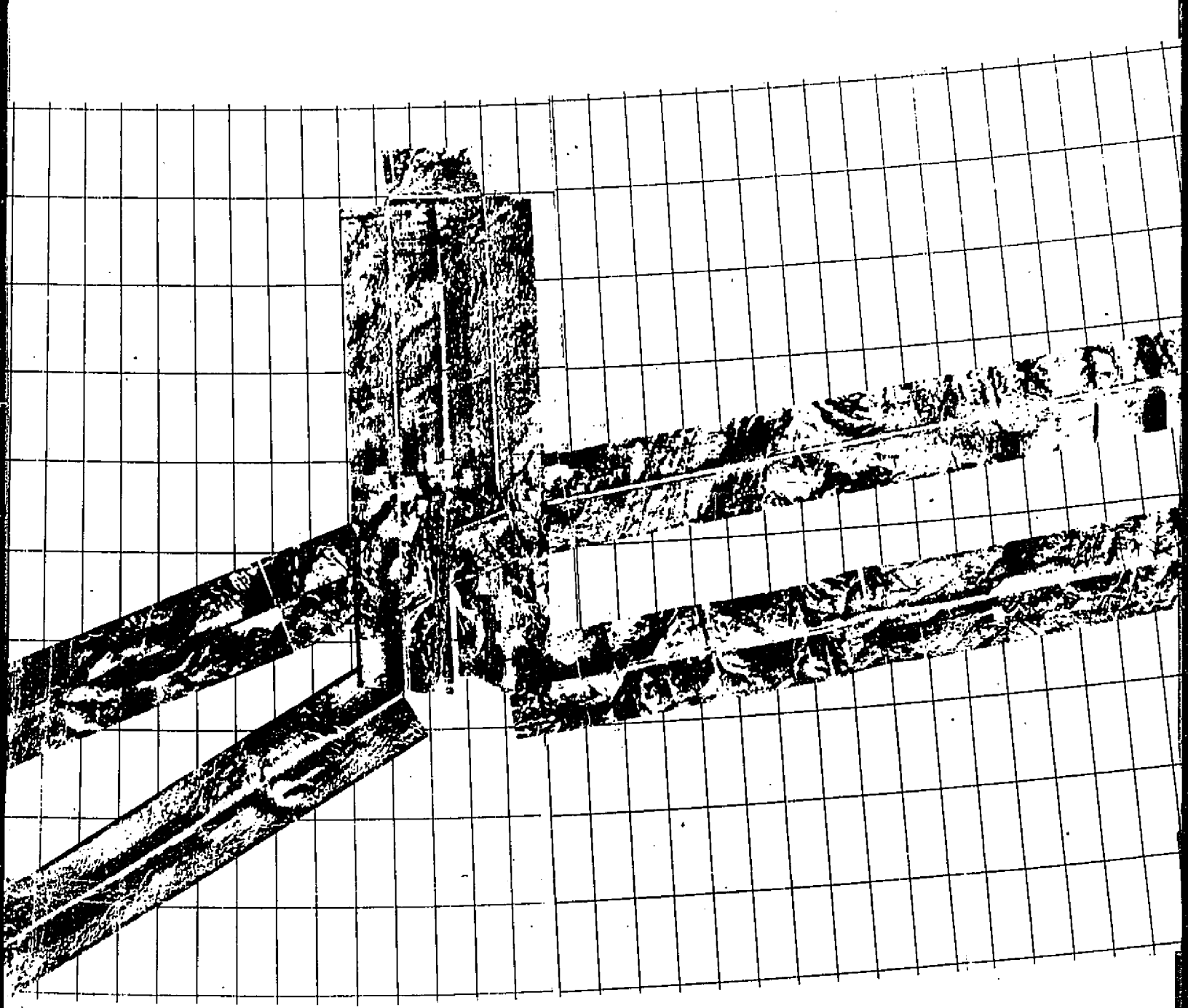

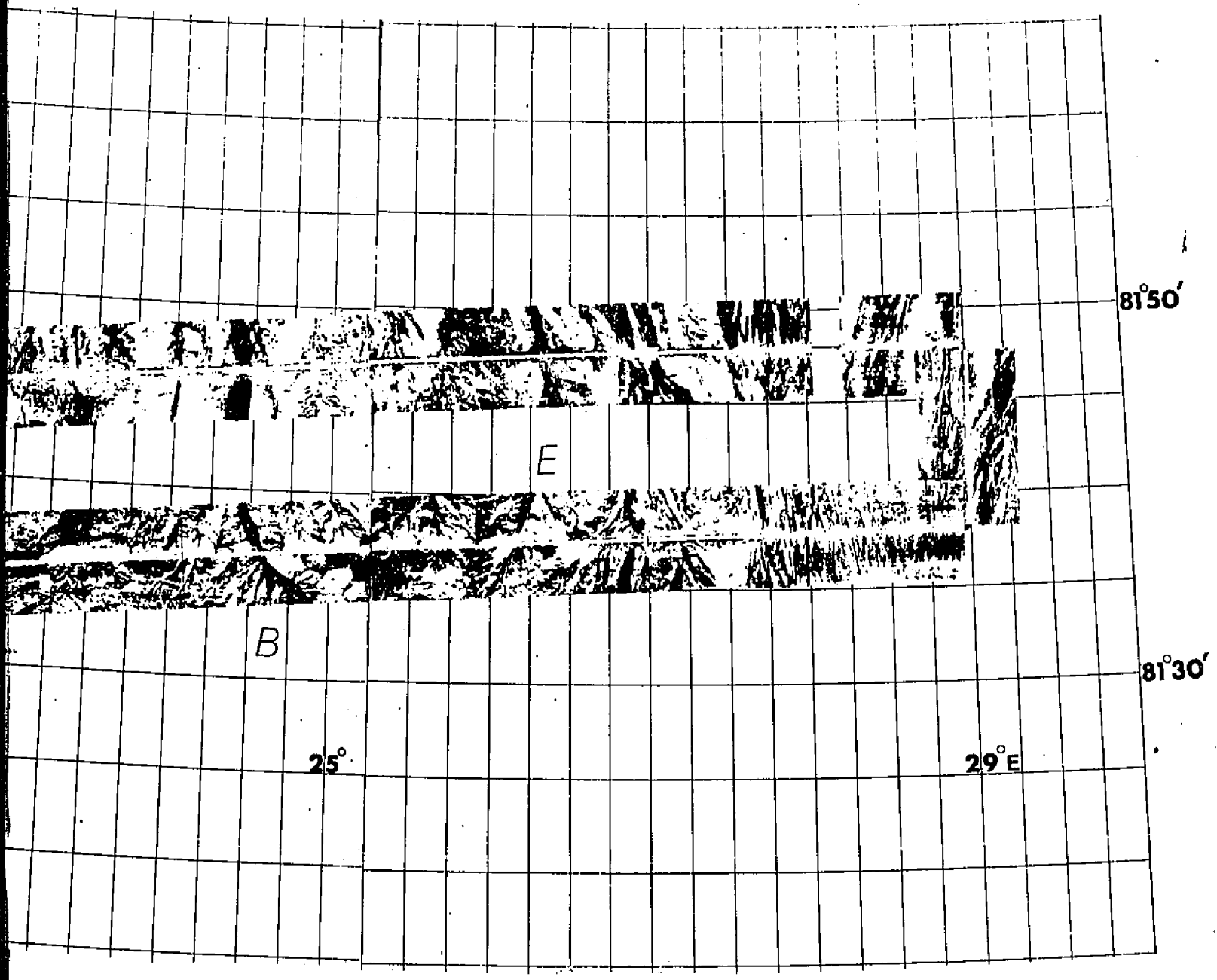
81°50′
E
B
81°30′
25°
29°E

2. HEAT FLOW DATA

	St #	Latitude	Longitude	Water Depth	Obs. Hf	Error
		°N	°E	m	mW/m²	(-/+)
		Northern Nordaustlandet Margin				
#	16-11/371	86°09.09'	22°09.92	3556	192	21
#	15-11/370	85°56.23'	22°41.35'	5100	>1164	
#	14-11/370	85°53.84'	22°50.19'	4390	>885	
#	12-11/364	85°22.30'	26°02.75'	3580	86	4
#	11-11/362	85°03.00'	28°47.14'	4024	26	2
*	1	82°47.70'	06°44.80'		92	
*	2	82°30.10'	06°27.30'		54	
*	3	82°19.10'	06°11.10'		54	
#	7-11/310	82°01.34'	32°13.39'	2925	80	12
*	5	81°56.60'	05°32.30'		33.9	
#	6-11/296	81°47.34'	31°30.14'	2991	77	4
#	5-11/287	81°39.64'	30°48.73'	2698	91	1
#	3-11/282	81°35.82'	31°31.13'	1437	98	5
#	2-11/280	81°34.46'	31°38.47'	886	88	4
	Y18	81°33.00'	29°22.52'	1512	109	65
	Y17	81°25.14'	23°17.89'	509	61	9
#	20-11/423	81°19.51'	15°17.06'	2219	64	5
		Northwestern Svalbard Margin				
	Y4	80°28.99'	14°23.62' W	325	69	2
	Y6	82°00.14'	07°05.00' W	3350	173	12
	Y8	81°24.20'	00°53.81'	1596	130	10
	Y9	81°06.46'	03°16.32'	820	148	10
	Y10	80°47.18'	05°06.42'	682	133	8
	Y16	80°16.44'	07°05.08'	560	121	11

* Jackson et al. (1984)
\# Sundvor and Torp (1987)
Y: YMER (1980)
V: Vema (Langseth and Zielinski, 1974)

Table A-3. Heat flow data from the Norwegian-Greenland Sea.

Table A-3 (cont.)					
St #	Latitude	Longitude	Water Depth	Obs. Hf	Error
	°N	°E	m	mW/m²	(-/+)
Southern Yermak Plateau					
68	80°22.15'	07°42.82'	688	125	6
67	80°24.73'	08°14.86'	813	138	6
66	80°26.62'	08°49.29'	840	131	2
65	80°28.87'	09°28.10'	880	114	1
64	80°32.78'	10°01.25'	813	104	6
Molloy - Western Svalbard Margin					
Y13	79°19.53'	04°03.02'	2910	179	16
Y14	79°15.86'	05°11.33'	1750	120	14
84	79°01.46'	05°01.81'	2184	115	1
85	79°00.18'	05°58.10'	1685	99	4
86	79°00.97'	07°00.02'	1290	103	3
42	78°49.67'	04°29.93'	2405	117	13
41	78°49.92'	05°00.77'	2667	128	4
40	78°49.93'	05°30.08'	2578	93	11
39	78°50.28'	05°58.52'	2454	87	8
38	78°50.14'	06°29.48'	1960	117	1
37	78°49.97'	07°00.53	1426	116	2
36	78°49.96'	07°30.93'	1142	107	4
35	78°50.00'	08°01.43'	1003	85	3
33	78°44.95'	08°10.88'	897	65	4
34	78°45.55'	08°01.02'	978	122	4
32	78°43.81'	07°28.82'	1146	101	5
31	78°42.17'	06°58.54'	1412	114	1
30	78°41.83'	06°44.36'	1560	118	3
29	78°40.96'	06°29.40'	1740	118	2
Y15	78°48.00'	07°29.14'	1154	118	4
88	78°46.74'	05°55.76'	2410	108	1
89	78°41.77'	05°24.85'	2325	113	3

Table A-3 (cont.)

St #	Latitude	Longitude	Water Depth	Obs. Hf	Error
	°N	°E	m	mW/m²	(-/+)
24/84	78°33.05'	03°56.29'	2325	128	5
25/84	78°35.51'	04°29.75'	2369	138	2
26/84	78°37.18'	05°01.68'	2332	156	14
90	78°26.57'	05°24.26'	1874	137	2
27/84	78°38.10'	05°29.31'	2340	154	6
91	78°28.35'	05°55.03'	1905	139	2
92	78°30.95'	06°22.33'	2303	125	1
94	78°32.38'	06°37.86'	2774	197	2
93	78°35.42'	07°07.07'	1735	91	4
21/V-27	78°24'	07°25'	2919	131	5
F17A-B	78°20.28'	01°27.71'	1375	75-80	13
5/	78°16.92'	08°06.52'	2329	124	4
4/	78°18.00'	08°29.82'	1870	101	4
3/	78°17.27'	08°50.42'	1390	100	1
F1	78°01.50'	08°54.05'	1327	114	5
F8	78°01.08'	09°18.49'	727	132	3
F14	78°00.53'	04°55.61'	2863	121	4
F5	78°00.48'	08°16.03'	2089	179	3
F2	78°00.30'	09°09.24'	1000	94-166	
F3	78°00.42'	09°19.70'	733	175	22
F11	78°00.21'	06°22.42'	2037	180	17
F12	78°00.19'	06°00.12'	2350	158	6
F13	78°00.07'	05°30.76'	2570	176	6
F16	78°00.00'	04°00.13'	3046	98	1
F4	77°59.98'	08°29.31'	1780	109	6
F6B	77°59.96'	07°57.54'	2560	297	3
F6A	77°59.79'	07°57.10'	2560	446	4
F15	77°59.76'	04°30.03'	2745	108	2
F10	77°59.70'	06°45.07'	2396	233	1
F18	75°26.50'	14°14.20'	620	22	9
F19	75°25.93'	13°59.30'	860	140	3
F22	75°25.61'	13°48.56'	1014	84	8
F23	75°23.96'	13°38.93'	1165	81	4
F24	75°23.07'	13°23.84'	1344	84	1
F38	75°22.90'	13°14.37'	1448	94	4

		Table A-3 (cont.)			
St #	Latitude	Longitude	Depth	Hf	Error
	°N	°E	m	mW/m²	(-/+)
F39	75°21.73'	13°01.86'	1586	92	2
F26	75°21.01'	12°53.57'	1700	82	4
F27	75°19.88'	12°37.80'	1858	82	3
F36	75°18.90'	12°18.30'	2026	65	2
F28	75°16.36'	11°59.50'	2169	64	2
F29	75°13.43'	11°21.18'	2358	96	4
F30	75°10.06'	10°43.27'	2460	94	5
F31	75°06.76'	10°09.76'	2506	126	7
F32	75°03.40'	09°32.64'	2595	176	6
F34A	74°57.51'	08°43.16'	2642	264	11
F34B	74°57.44'	08°42.97'	2642	258	10
	Senja - Vøring - Jan Mayen Line				
DHF44	72°05.54'	13°36.22	1460	65	2
DHF50	72°18.28'	14°45.89'	965	59	2
DHF55	72°25.60'	15°29.45'	607	48	10
DHF52	72°27.99'	15°42.84'	505	38	4
DHF40	72°24.99'	15°31.12'	620	84	6
DHF41	72°21.19'	15°00.56'	731	121	6
DHF42	72°14.98'	14°31,27'	1065	58	6
DHF43	72°10.52'	14°03.61'	1225	63	3
53/V-23	72°04'	1°24'	2360	268	9
DHF45	72°00.43'	13°07.43'	1650	71	2
10/V-27	72°11'	08°35'	2537	84	7
DHF46	71°55.04'	12°40.54'	1842	64	2
DHF48	71°49.83'	12°13.25'	1995	71	2
DHF49	71°43.84'	11°35.55'	2169	62	1
54/V-23	70°59'	06°41'	3043	115	8
145/V-29	70°54'	04°55' W	1939	144	7
113/V-30	70°11'	01°49' W	2905	108	8
114/V-30	69°39'	02°30'	3210	76	10
37/86	69°12.44'	05°57.41' W	3030	75	2
DHF75	68°27.34'	04°33.27'	2358	73	3
DHF74	68°18.80'	04°31.58'	2198	67	1
32/V-28	67°53'	01°56' W	3376	113	8
DHF69	67°49.84'	05°18.85'	1341	72	2

		Table A-3	(cont.)		
St #	Latitude	Longitude	Depth	Hf	Error
	°N	°E	m	mW/m²	(-/+)
DHF70	67°58.10'	05°06.93'	1346	69	2
DHF68	67°43.68'	05°25.76'	1186	64	2
116/	67°41'	08°24'	1918	87	6
DHF66	67°37.08'	05°37.06'	1421	78	3
DHF65	67°32.95'	05°42.99'	1422	80	3
DHF67	67°37.90'	05°32.21'	1424	70	1
DHF64	67°29.47'	05°47.91'	1438	76	6
131/	67°10'	06°05'	1236	41	10
DHF61	67°08.67'	06°22.16'	1266	75	2
DHF60	67°01.29'	06°31.44'	1240	66	2
DHF59	66°53.56'	06°46.99'	1110	55	1
100/V-30	65°05'	07°08' W	2027	63	8
101/V-30	65°08'	05°18' W	3812	77	9
8	69°47.72'	08°23.76' W	821	79	
11	69°26.88'	07°02.84' W	2442	75	
12	69°28.80'	07°54.23' W	1055	96	
15	69°22.85'	09°23.97' W	2180	83	
16	69°20.21'	10°00.06' W	2225	105	
17	69°19.98'	10°40.88' W	1768	117	
19	69°10.97'	12°04.24' W	1950	121	
20	69°07.39'	12°46.99' W	1830	126	
21	69°00.15'	12°13.42' W	1935	138	
22	68°55.08'	11°39.77' W	1902	109	
23	68°48.01'	11°10.02' W	1950	100	
24	68°48.05'	10°25.12' W	2180	130	
25	68°37.12'	09°53.62' W	2024	92	
30	68°17.09'	07°34.90' W	1750	75	
31	68°12.45'	07°07.69' W	1920	59	
33	68°03.07'	06°06.40' W	2968	71	
37	69°12.44'	05°57.41' W	3030	75	

3. VELOCITY STRUCTURE

Table A-4a								
VELOCITY STRUCTURE IN THE SOUTHERN NGS								
	Water							
Long	Depth	V^1	h^1	V^2	h^2	V^3	h^3	V4
°E	m	km/s	km	km/s	km	km/s	km	km/s
02°28'	3180	1.9	1.06			5.37	3.01	6.94
18°10'	280	1.88	0.87	2.26				
07°16'	2790	2.56	1.78			4.38		
08°41'	2510	2.45	3.16			5.1	2.03	6.05
13°50'	2350	2	2.08	3.43	2.46			
03°21'	1280	1.91	0.56			5.2		
03°59'	1210	2.12	0.14					
03°10'	1480	2.2	2.06	3.64	1.82	4.43		
03°57'	1550	2	0.99			5.35		
06°09'	1030	2.04	2.39	3.62	1.38	4.32		
08°56'	300	2	0.65	2.63				
08°27'	310	2.14	1.39	3.25				
06°15'	1230	1.75	0.34					
06°39'	2980	1.56	0.64					
10°42'	2600	2.13	1.28					
00°37'	3150	2.2	0.77					

Table A-4. Velocity structure in the Norwegian-Greenland Sea.

Table A-4b

VELOCITY STRUCTURE IN NGS

Area	Average velocities (km/s)			Sources
	V^1	V^2	V^3	
Norwegian Shelf (62°-65°N)	2.2	3.6	5.2	(Talwani&Eldholm, 1977)
Barents Shelf	2.2	3.6		(Eldholm&Ewing, 1971)
Vøring Plateau	2.2	3.4	4.4	(Talwani&Eldholm, 1972)
Nansen Ridge Flanks	1.8		8.2	(Kristoffersen et al., 1982)
				(Jackson et al., 1984)

ODP LEG 138 SITES

St #	Lat	Long		Age
	°N	°E		my
338	67°47.11'	05°23.60'	Outer Vøring Plateau	(49-53)
342	67°57.04'	04°56.02'	Outer Vøring Plateau	(44 my)
343	68°42.91'	05°45.73'	Base of the Vøring Plateau	(49-53)
				(Talwani&Eldholm, 1977)

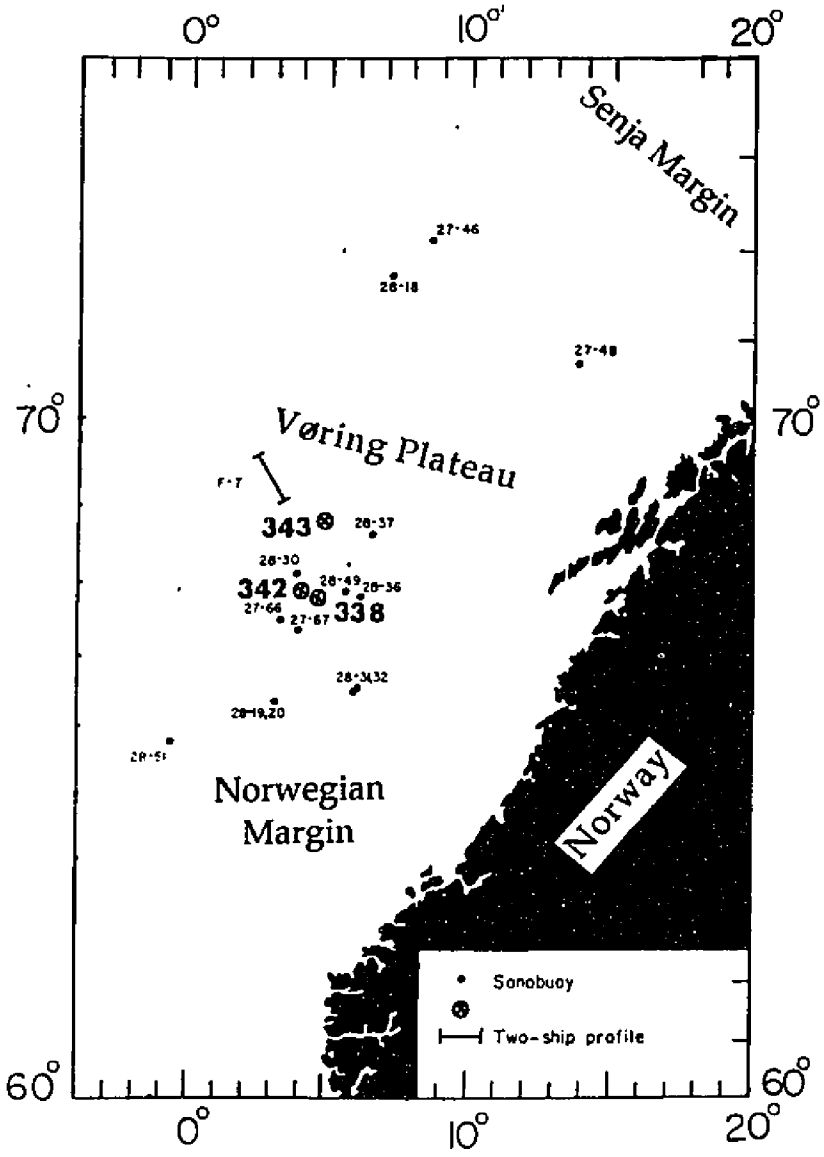

Figure A-6. Location of published seismic stations and Lamont-Doherty sonobuoy profiles in the southern Norwegian-Greenland Sea (see also Table 5-3).

REFERENCES CITED

AHERN, J.L., and TURCOTTE, D.L., 1979. Magma migration beneath an ocean ridge. *Earth Planet. Sci. Lett.*, 45: 115-122.

ÅM, K., 1975. Magnetic profiling over Svalbard and surrounding shelf areas. *Norsk Polarinst. Årb.*, 73: 87-100.

AMUNDSEN, H.E.F., GRIFFIN, W.L., and O'REILLY, S.Y., 1987. The lower crust an upper mantle beneath northwestern Spitsbergen: evidence from xenoliths and geophysics. *Tectonophysics*, 139:169-185.

AMUNDSEN, H.E.F., GRIFFIN, W.L., and O'REILLY, S.Y., 1988. The nature of the lithosphere beneath northwestern Spitsbergen: xenolith evidence. *Nor. Geol. under. Special Publ.*, 3: 58-65.

ARTYUSHKOV, E.V., 1973. Stresses in the lithosphere caused by crustal thickness inhomogeneities. *J. Geophys. Res.*, 78: 7675-7708.

ATWATER, T.M., and MACDONALD, K.C., 1977. Are spreading centers perpendicular to their transform faults? *Nature*, 270: 715-719.

AUSTEGÅRD, A., 1982. Velocity analysis of Sunobuoy data from the northern Svalbard margin. Univ. Bergen, Seism. Obs., *Sci. Rep.*, 9: 25 pp.

AUSTIN, J.A., and UCHUPI, E., 1982. Continental-oceanic crustal transition off Southwest Africa. *Am. Ass. Pet. Geol.*, 66 (9): 1328-1347.

BEAUMONT, C., KEEN, C.E., and BOUTLIER, R., 1982. Evolution of rifted continental margins; comparison of models and observations for the Nova Scotia margin, J. *R. Geophys. Astr. Soc.*, 70: 667-715.

BENFIELD, A.E., 1949. The effect of uplift and denudation on underground temperatures. *J. Applied Phys.*, 20: 66-70.

BHATTACHARJI, S., and KOIDE, 1978. The origin and evolution of rifts and rift valley structures: A mechanistic interpretation, Tectonics and Geophysics at Continental Rifts, Ramberg, I. B., and Neumann, E. R. (eds.), pp: 29-37.

BIRKENMAJER, K., 1981. The geology of Svalbard, the western part of the Barents Sea, and the continental margin of Scandinavia, In: *The Ocean Basins and Margins, The Arctic Ocean*, A. E. Nairn, M. Churkin, and F. G. Stehli (eds.), Plenum Press, New York, 5: 265-330.

BLOCK, L., and ROYDEN, L., 1990. Core complex geometries and regional scale flow in the lower crust. *Tectonics*. 9: 557-567.

BLOCKINTON, J.G., HUSSONG, D.M., and KOSALOS, J., 1983. First results from a combination side-scan sonar and seafloor mapping system (SeaMARC-II), *Offshore Tech. Conf.* (OTC), 4478: 307-311.

BOILLOT, G., GRIMAUD, S., MAUFFRET, A., MOUGENOT, D., MERGOIL-DANIEL, J., KORNPROBST, J., and TORRENT, G., 1980. Ocean-continent boundary off the Iberian margin: A serpantinite diapir west of the Galicia Bank, *Earth Planet. Sci. Lett.*, 48: 23-34.

BONATTI, E., 1985. Punctiform initiation of seafloor spreading in the Red Sea during the transition from a continental to an oceanic rift. *Nature*, 316: 33-37.

BONATTI, E., 1994. The Earth's mantle below the oceans. *Sci. American*, 270: 3: 44-51.

BONATTI, E., and CRANE, K., 1982. Oscillatory spreading explanation of anomalously old uplifted crust near oceanic transforms. *Nature*, 300: 343-345.

BONATTI, E., and CRANE, K., 1984. The geology of oceanic transform faults. *Sci. American*, 250 (5): 40-51.

BONATTI, E. and MICHAEL, P.J., 1989. Mantle peridotites from continental rifts, to ocean basins to subduction zones. *Earth Planet. Sci. Lett.*, 91: 297-311.

BONATTI, E., COLANTONI, P., DELLA VEDOVA, B., and TAVIANI, M., 1984. Geology of the Red Sea Transitional region (22°N-25°N). *Oceanologica Acta*, 7: 385-398.

BONATTI, E., OTTONELLO, G., and HAMLYN, P.R., 1986. Peridotites from the island of Zabargad (St. John) Red Sea: petrology and geochemistry. *J. Geophys. Res.*, 91: 599-631.

BOTT, M.H.P., 1982. *The Interior of the Earth:* Its Structure, Constitution and Evolution, Elsevier Publ., N.Y., 2nd ed., 403 pp.

BROWN, C., and GIRDLER, R.W., 1982. Structure of the Red Sea at 20° N from gravity data and its implication for continental margins. *Nature*, 298: 51-53.

BOYD, L.A., 1948. The coast of northeast Greenland, Spec. Pap. Am. Geog. Soc., 30: 339 pp.

BUCK, W.R., 1986. Small-scale convection induced by passive rifting: the cause for the uplift of rift shoulders. *Earth Planet. Sci. Lett.*, 77: 362-372.

BUCK, W.R., 1988. Flexural rotation of normal faults. *Tectonics*, 5: 959-973.

BUCK, W.R., 1991. Modes of continental lithospheric extension, *J. Geophys. Res.* 96 (B12): 20161-20178.

BUCK, W.R., and MUTTER, J.C., 1989. Convective partial melting II: factors controlling melting.

BUCK, W.R., MARTINEZ, F., STECKLER, M.S., and COCHRAN, J.R., 1988. Thermal consequences of lithospheric extension: pure and simple. *Tectonics*, 7: 213-234.

BUKOVICS, C., and ZIEGLER, P.A., 1985. Tectonic development of the mid-Norway continental margin. *Mar. Pet. Geol.*, 2: 2-22.

BUNGUM, H., GJØYSTDAL, H., HOKLAND, B., and KRISTOFFERSEN, Y., 1978. Seismicity of the Svalbard region: a preliminary report on the microearthquake activity. *NORSAR Tech. Rep.*, 2/78, NTNF/NORSAR, Kjeller, Norway.

BUNGUM, H., and KRISTOFFERSEN, Y., 1980. A micro-earthquake survey of the Svalbard region, Final report, Phase I, *NORSAR Tech. Rep.*, 1/80, NTNF/NORSAR, Kjeller, Norway.

BUNGUM, H., MITCHELL, B.J., and KRISTOFFERSEN, Y., 1982. Concentrated earthquake zone in Svalbard. *Tectonophysics*, 82: 175-188.

BURR, N.C., and SOLOMON, S.C., 1978. The relationship of source parameters of oceanic transform-earthquakes to plate velocity and transform length. *J. Geophys. Res.*, 1193-1205.

CAMPBELL, I.H., and GRIFFITHS, R.W., 1990. Implications of mantle plume structure for the evolution of flood basalts. *Earth Planet. Sci. Lett.*, 99:79-93.

CAMPSIE, J., RASMUSSEN, M.H., HANSEN, N., LIEBE, C.J., LAURSEN, W., BROCHWICZ-LEVINSKI, W., and JOHNSON, L., 1988. K-Ar ages of Basaltic rocks collected during a traverse of the Frans Josef Land Archipelago (1895-1896). *Polar Res.*, 6: 173-177.

CANDE, S.C., HERRON, E.M., and HALL, B.R., 1982. The early Cenozoic tectonic evolution of the southeast Pacific. *Earth Planet. Sci. Lett.*, 57: 63-74.

CHAN, W. W. and MITCHELL, B. J. and KRISTOFFERSEN, Y., 1985. Surface wave dispersion, crustal structure, and sediment thickness variations across the Barents shelf. Geophys. *J. R. Astr. Soc.*, 80: 329-344.

CHERKIS, N.Z., FLEMING, H.S., MAX, M.D., VOGT, P.R., and CZARNECKI, M.F., 1991. Bathymetry of the Barents and Kara Seas. Naval Res. Lab., Washington, D.C., *Map and Chart Series* MCH047.

CHERKIS, N.Z., and VOGT, P.R., 1994. Regional bathymetry of the northern Norwegian-Greenland Sea. Map Ser., Naval Res. Lab., Washington, D.C.

CLIMAP Project Members, 1976. The surface of the ice-age earth, *Science*, 191: 1131-1137.

COCHRAN, J.R., 1982. The magnetic quiet zone in the eastern Gulf of Aden: implications for the early development of the continental margin. *Geophys. J. Roy. Astr. Soc.*, 68: 171-201.

COCHRAN, J.R., MARTINEZ, M.S., STECKLER, M.S., and HOBART, M.A., 1986. Conrad Deep: A new northern Red Sea deep. Origin and implications for continental rifting. *Earth Planet. Sci. Lett.*, 78: 18-32.

COCHRAN, J.R., GAULIER, J-M., and LePICHON, X., 1991. Crustal Structure and the mechanism of extension in the northern Red Sea: constraints from gravity anomalies. *Tectonics*, 10 (5): 1018-1037.

COFFIN, M.F., MUNSCHY, M., COLWELL, J.B., SCHLICH, R., DAVIES, H.L., and LI, Z.G., 1990. Seismic stratigraphy of the Raggat Basin, southern Kerguelen Plateau: Tectonic and paleo-oceanographic implications. *Geol. Soc. Am. Bull.*, 102: 563-579.

COFFIN, M.F., and ELDHOLM, O., 1991. Large Igneous Provinces: *JOI/USSAC Workshop Rep.*, Inst. Geophys., Univ. Texas, Austin. 114: 79 pp.

COFFIN, M.F., and ELDHOLM, O., 1993. Stretching the surface: estimating dimension of large igneous provinces. *Geology*, 21: 515-518.

COFFIN, M.F., and ELDHOLM, O., 1994. Large Igneous Provinces: Crustal Structure, dimensions, and External Consequences. *Rew. Geophys.*, 32 (1): 1-36.

COURTILLOT, V.E., 1982. Propagating rifts and continental breakup. *Tectonics*, 1: 239-250.

CRANE, K., 1976. The intersection of the Siqueiros Transform Fault and the East Pacific Rise. *Mar. Geol.*, 21: 25-46.

CRANE, K., 1985. The spacing of rift axis highs: dependence upon diapiric processes in the underlying Asthenosphere? *Earth Planet. Sci. Lett.*, 72: 405-414.

CRANE, K. and BONATTI, E., 1987. Fracture zone control on the opening of the Red Sea: SIR-A data. *J. Geol. Soc. London*, 144: 407-420.

CRANE, K., ELDHOLM, O., MYHRE, A.M., and SUNDVOR, E., 1982. Thermal implications for the evolution of the Spitsbergen transform fault. *Tectonophysics*, 89: 1-32.

CRANE, K., SUNDVOR, E., FOUCHER, J.P., HOBART, M., MYHRE, A.M., and LeDOUARAN, S., 1988. Thermal evolution of the western Svalbard margin. *Mar. Geophys. Res.*, 9: 165-194.

CRANE, K., VOGT, P.R., SUNDVOR, E., DeMOUSTIER, C., DOSS, H., and NISHIMURA, C., 1990. SeaMARC-II and associated geophysical investigation of the Knipovich Ridge, Molloy Ridge/Fracture Zone and Barents/Spitsbergen continental margin: Part II Volcanic/Tectonic structure. *EOS*, Trans. (Abs.), 71 (17): 622.

CRANE, K., SUNDVOR, E., BUCK, R., and MARTINEZ, F., 1991. Rifting in the Northern Norwegian-Greenland Sea: thermal tests of asymmetric spreading. *J. Geophys. Res.*, 96 (B9): 14529-14550.

CRANE, K., and SOLHEIM, A., 1995. Norwegian-Greenland Sea Atlas. *JOI/USSAC.*

DAVIS, G.A., 1988. Rapid upward transport of midcrustal mylonitic gneisses in the footwall of a Tertiary detachment fault, Whipple Mountains, southern California. *Geo. Rundschau*, 77: 191-209.

DAVIS, E.E., and LISTER, C.R.B., 1974. Fundamentals of ridge crest topography. *Earth Planet. Sci. Lett.*, 21: 405-413.

DAVIS, G.A., LISTER, G.S., and REYNOLDS, S.J., 1986. Structural evolution of the Whipple and South Mountains shear zones. Southwestern U.S. *Geology*, 14: 7-10.

DEWEY, J.F., and ŞENGÖR, A.M.C., 1979. Relative timing of rifting and volcanism on earth and its tectonic implications. *Geophys. Res. Lett.*, 5: 419-421.

DIXON, T.H., IVINS, E.R., and FRANKLIN, B.J., 1989. Topographic and volcanic asymmetry around the Red Sea: constraints on rift models. *Tectonics*, 8: 1193-1216.

DİLEK, Y., and ROWLAND, J.C., 1993. Evolution of a conjugate passive margin pair in Mesozoic southern Turkey. *Tectonics*, 12 (4): 954-970.

DİLEK, Y., MOORES, E.M., DELALOYE, M., and KARSON, J.A., 1991. A magmatic extension and tectonic denudation in the Kızıldağı ophiolite, southern Turkey: implications for the evolution of Neotethyan oceanic crust. In: *Ophiolite Genesis and Evolution of Oceanic Lithosphere*, T. Peters, A. Nicolas, and R.G. Coleman, Kluwer Publ., Boston, Mass., pp: 485-500.

DGP Report, 1991. North Atlantic rifted Margins Detailed Planning Group (Executive Summary) Joint Oceanographic Inst. Deep Earth Sampling J., 17: 24-26.

DOSS, H., CRANE, K., VOGT, P.R., and SUNDVOR, E., 1991. Evolution of the Western Svalbard Margin: Results from analysis of SeaMARC-II data. Part II: Tectonics. *EOS*, Trans. (Abs.), 72 (17): 274.

DUNBAR, J.A., and SAWYER, D.S., 1989. How pre-existing weaknesses control the style of continental breakup? *J. Geophys. Res.*, 94: 7278-7292.

EATON, J.P., 1963. Crustal structure from San Francisco, California to Eureka, Nevada from seismic refraction measurements. *J. Geophys. Res.*, 68: 5789-5806.

ENGLAND, P.C., 1983. Constraints on extension of continental lithosphere. *J. Geophys. Res.*, 88: 1145-1152.

ELDHOLM, O., 1991. Magmatic-tectonic evolution of a volcanic rifted margin. *Mar. Geol.*, 102: 43-61.

ELDHOLM, O., and EWING, J., 1971. Marine geophysical survey in the southwestern Barents Sea. *J. Geophys. Res.*, 76: 3832-3841.

ELDHOLM, O., and WINDISCH, C.C., 1974. Sediment distribution in the Norwegian-Greenland Sea. *Geol. Soc. Am. Bull.*, 85: 1661-1676.

ELDHOLM, O., and GRUE, K., 1994. North Atlantic Volcanic Margins: Dimensions and production rates. *J. Geophys. Res.*, 99 (2): 2955-2965.

ELDHOLM, O., SUNDVOR, E., MYHRE, A.M., 1979. Continental margin off Lofoten-Vesterålen Northern Norway. *Mar. Geophys. Res.*, 4: 3-25.

ELDHOLM, O., SUNDVOR, E., MYHRE, A.M., and FALEIDE, J.I., 1984. Cenozoic Evolution of the Continental Margin off Norway and Western Svalbard, Petroleum Geology of the North European Margin. *Norwegian Petr. Soc.*, pp: 3-18.

ELDHOLM, O., FALEIDE, J.I., and MYHRE, A.M., 1987. Continental-ocean transition at the western Barents Sea /Svalbard continental margin. *Geology*, 15: 1118-1122.

ELDHOLM, O., THIEDE, J., and TAYLOR, E., 1989a. The Norwegian continental margin: tectonic, volcanic and paleoenvironmental framework. In: *Proceedings of the ODP*, O. Eldholm, J. Thiede and E. Taylor (eds.), Sci. Results, 104: 5-104.

ELDHOLM, O., THIEDE, J., and TAYLOR, E., 1989b. Evolution of the Vøring volcanic margin. In: *Proceedings of the ODP*, O. Eldholm, J. Thiede and E. Taylor (eds.), Sci. Results, 104: 5-104.

ELVERHØI, A., and SOLHEIM, A., 1987. Shallow geology and geophysics of the Barents sea- a discussion. *Polar Res., New Ser.*, 5: 285-287.

ETHERIDGE, M.A., SYMONDS, P.A., and LISTER, G.S., 1990. Application of the detachment model to reconstruction of conjugate passive margins, In: Extensional Tectonics and Stratigraphy of the North Atlantic Margins, A.J. Tankard and H.R. Balkwill (eds.), *AAPG Mem.*, 46: 23-40.

FALEIDE, J.I., GUDLAUGSSON, S.T., JOHANSEN, B., and MYHRE, A.M., 1984. Free-air Gravity Anomaly Maps of the Greenland Sea and the Barents Sea. *Norsk Polarinst. Skr.*, 180: 63-67.

FALEIDE, J.I., GUGLAUGSSON, S.T., ELDHOLM, O., MYHRE, A.M., and JACKSON, H.S., 1991. Deep seismic transects across the sheared western Barents Sea-Svalbard continental margin. *Tectonophysics*, 189: 73-89.

FAVRE, P., and STAMPFLI, G., 1992. From rifting to passive margins: The examples of the Red Sea, Central Atlantic, and Alpine Tethys, *Tectonophysics*, 215: 69-97.

FEDEN, R.H., VOGT, P.R., and FLEMING, H.S., 1979. Magnetic and bathymetric evidence for the "Yermak" hot spot northwest of Svalbard in the Arctic Ocean. *Earth Planet Sci. Lett.*, 4: 18-38.

FLOOD, B., NAGY, J., and WINSNES, T.S., 1971. Geological Map of Svalbard (1:500,000), *Norsk Polar. Skr.*, 154A.

FOUCHER, J-P., LePICHON, X., and SIBUET, J-P., 1982. The ocean-continent transition in the uniform lithospheric stretching model: role of partial melting in the mantle. *Philos. Trans. R. Soc. London*, 305: 27-43.

FURLONG, K.P., and FOUNTAIN, D.M., 1986. Continental crust underplating: Thermal considerations and seismic petrological consequences. *J. Geophys. Res.*, 91: 8285-8294.

GAHAGAN, L.M., ROYER, J.-Y., SCOTESE, C.R., SANDWELL, D.T., WINN, K., TOMLINS, R., ROSS, M.I., NEWMAN, J.S., MÜLLER, R.D., MAYES, C.L.,

LAWYER, L.A., and HUEBECK, C.E., 1988. Tectonic fabric map of the ocean basins from satellite altimetry data. *Tectonophysics*, 155: 1-26.

GÉLI, L., RENARD, V., and ROMMEVAUX, C., 1994. Ocean crust formation processes at very slow spreading centers: A model for the Mohns Ridge, near 72°N, based on magnetic gravity, and seismic data. *J. Geophys. Res.*, 99 (B2): 2995-3013.

GJELSVIK, T., 1963. Remarks on the structure and composition of the Sverrefjellet volcano, Bockfjørden West Spitsbergen. *Norsk Polarinst. Årb.*, 50-54.

GREEN, A.R., KAPLAN, A.A., and VIERBUCHEN, P.C., 1984. Circum-Arctic Petroleum potential. *Am. Assoc. Petrol. Geol.*, Sp. Is. of Wallace E. Pratt Mem. Conf. Future Petrol. Prov. of the World, p: 29.

GRØNLIE, D., and TALWANI, M., 1978. Geophysical Atlas of Norwegian-Greenland Seas. LDEO, Columbia University, *Vema Res. Ser.* 4.

GRØNLIE, G., and TALWANI, M., 1982. The free-air gravity field of the Norwegian-Greenland Sea and adjacent areas. *Earth Evol. Sci.*, 2: 79-104.

HAGEVÅNG, T., ELDHOLM, O., and ÅLSTAD, I., 1983. Pre-23 magnetic anomalies between Jan Mayen and Greenland-Senja Fracture Zones in the Norwegian Sea. *Mar. Geophys. Res.*, 5: 345-363.

HÅKANSSON, E., and SCHACK-PEDERSEN, S.T., 1982. Late Paleozoic to Tertiary Tectonic Evolution of the Continental margin in North Greenland. In: Arctic Geology and Geophysics by A.F. Embry and H.R. Balkwill (eds). *Can. Soc. Geol. Mem.*, 8: 331-348.

HAMILTON, C.D., 1987. Crustal extension in the Basin and Range Province, In: *Continental Extensional Tectonics*, M.P. Coward, J.F. Dewey, and P.L. Hancock (eds.). Geol. Soc. Special Publ., 28: 155-176.

HARLAND, W.B., 1971. Tectonic transpression in Caledonian Spitsbergen. *Geol. Mag.*, 108: 27-42.

HARLAND, W.B., 1985. Caledonite Svalbard. In: *The Caledonian Orogen-Scandinavia and related Areas*, D. Gee and B. Sturt (eds.), John Wiley, NY., pp: 999-1016.

HENRY, S.G., and POLLACK, H.N., 1988. Terrestrial heat flow above the Andean Subduction Zone in Bolivia and Peru. *J. Geophys. Res.*, 93: 15153-15162.

HEY, R., DUENNEBIER, F.K., and MORGAN, W.J., 1980. Propagating rifts on mid-ocean ridges. *J. Geophys. Res.*, 85: 3647-3658.

HILL, R.I., 1991. Starting plumes and continental break-up. *Earth Planet. Sci. Lett.*, 104:398-416.

HINZ, R.I., 1981. A hypothesis on terrestrial catastrophes: wedges of very thick oceanward dipping layers beneath passive margins-their origin and paleoenvironment significance. *Geol. Jahrb.*, E22: 345-363.

HINZ, R.I., 1990. The Argentine Eastern Continental Margin: Structure and Geological Development. *Amer. Assoc. Petrol. Geol. Bull.*, 74 (5): 675-676.

HINZ, K., and WEBER, J., 1976. Zum Geologischen Aufbau des Norwegischen Kontinentalrandes und der Barentssee nach Reflexionsseismischen Messungen. *Erdöl, Kohle, Erdgas, Petrochem.*, Comp., 75/76: 3-29.

HINZ, K., MUTTER, J.C., ZEHNDER, C.M., and Norwegian-Greenland Transect Study Group, 1987. Symmetric conjuction of continent-ocean boundary structures off the Norwegian and East Greenland margins. *Mar. Petrol. Geol.*, 4: 167-187.

HJELLE, A., and LAURITZEN, Ø., 1984. Geological map of Svalbard, 1:500000, Sheet 3G, Spitsbergen, northern part. *Norsk Polarinst. Skr.*, 154C: 15 pp.

HOEL, A., and HOLTEDAHL, L., 1911. Les nappes de lava les volcans et les sources thermales dans les environs de la Baie Wood au Spitsbergen. *Vid. Selsk. Skr.*, 1, Kristiania, no. 8.

HOPPER, J., MUTTER, J.C., LARSON, R.L., MUTTER, C., Z., and Northwest Australia Study Group, 1992. Magmatism and rift margin evolution: Evidence from northwest Australia, *Geology*, 20: 853-857.

HOTENDAHL, O., 1960. On supposed marginal faults and the oblique uplift of the landmass in Cenozoic times, in Geology of Norway, *Norges Geol. Undersökelse*, 208: 351-357.

HOUSEMAN, G.A., and ENGLAND, P.C., 1986. A dynamic model of lithospheric extension and sedimentary basin formation. *J. Geophys. Res.*, 91: 719-729.

HUSEYBE, E.S., GJØYSTDAL, H., BUNGUM, H., and ELDHOLM, O., 1975. The seismicity of the Norwegian and Greenland Seas, and adjacent continental shelf areas. *Tectonophysics*, 26: 55-70.

HUTCHISON, I., 1985. The effects of sedimentation and compaction on oceanic heat flow. *Geophys. J. R. Astr. Soc.*, 82: 439-459.

ILLIES, J. H., 1974. Intra-Plattentektonik in Mitteleuropa und der Rheingraben Oberrhein. *Geol. Abh.*, 23: 1-24.

JACKSON, H.R., JOHNSON, G.L., SUNDVOR, E., and MYHRE, A.M., 1984. The Yermak Plateau: formed at a triple junction. *J. Geophys. Res.*, 89 (B5): 3223-3232.

JOHNSON, G. L., and Eckhoff, O.B., 1966. Bathymetry of the north Greenland Sea. Deep Sea Res., 13: 1161-1173.

JOHNSON, G. L., and Heezen, B. C., 1967. Morphology and evolution of the Norwegian-Greenland Sea, Deep Sea Res., 14: 755-771.

JOHNSON, G.L., and RICH, J.E., 1986. A 30 million year cycle in Arctic Volcanism? *J. Geodynam.*, 6: 111-116.

JONGSMA, D., 1974. Heat flow in the Aegean Sea. Geophys. *J. R. Ast. Soc.*, 37: 337-346.

KASTENS, K.A., MACDONALD, K.C., BECKER, K., and CRANE, K., 1979. The Tamayo Transform Fault in the mounth of the Gulf of California. *Mar. Geophys. Res.*, 4: 129-152.

KEEN, C.E., 1987. The dynamics of rifting: deformation of the lithosphere by active and passive driving mechanisms, Geophys. *J. R. Astron. Soc.*, 80: 95-120.

KEEN, C.E., and KEEN, M.J., 1974. The continental margins of eastern Canada and Baffin Bay. In: *The geology of continental margins*, C.A. Burk and C.L. Drake (eds.), Springer-Verlag, NY., p: 381-389.

KEEN, C.E., and DeVOOGD, B., 1988. The continent-ocean boundary at the rifted margin off eastern Canada: new results from deep seismic reflection studies. *Tectonics*, 7: 107-124.

KEEN, C.E., and BEUMONT, C., 1990. Geodynamics of rifted continental margins, In: *Geology of the Continental Margin of Eastern Canada*, Geology of Canada, M.J. Keen and G.L. Williams (eds.), Geol. Survey of Canada, Ottawa, vol. 2: 391-472.

KEEN, C.E., KAY, W.A., and ROEST, W.R., 1990. Crustal anatomy of a transform margin. *Tectonophysics*, 173: 527-544.

KEEN, C.E., COURTNEY, R.C., DEHLER, S.A., and WILLIAMSON, M.-C., 1994. Decompression melting at rifted margins: comparison of model predictions with the distribution of igneous rocks on the eastern Canadian Margin, *Earth Planet. Sci. Lett.*, 121: 403-416.

KELLOGG, T.B., 1975. Late Quaternary Climatic changes in the Norwegian-Greenland Seas. In: Climate of the Arctic, G. Weller and S. Bowling (eds.). *J. Geophys. Res.*, 81: 4061-4070.

KENT, R.W., STOREY, M., and SAUNDERS, A.D., 1992. Large Igneous Provinces: sites of plume impact or plume incubation? *Geology*, 20: 891-894.

KLEIN, E.M., and LANGMUIR, C.H., 1989. Global corrections of ocean ridge basalt chemistry with axial depth and crustal thickness, J. Geophys. Res., 92: 8089-8115.

KRISTOFFERSEN, Y., and TALWANI, M., 1978. The extinct triple junction south of Greenland and the Tertiary motion of Greenland relative to North America. *Geol. Soc. Am. Bull.*, 88: 1037-1049.

KRISTOFFERSEN, Y., HUSEYBE, E.S., BUNGUM, H., and GREGERSEN, S., 1982. Seismic investigations of the Nansen Ridge during the Fram-I Experiment. *Tectonophysics*, 82: 57-68.

KOVACS, L.C., and VOGT, P.R., 1982. Depth-to-magnetic source analysis of the Arctic and Norwegian-Greenland Sea. Tectonophysics, 89: 255-294.

KOVACS, L.C., BERNERO, C., JOHNSON, G.L., PILGER, R.H.Jr., TAYLOR, P.T., and VOGT, P.R., 1982. *Residual Magnetic Chart of the Arctic Ocean Region*, Nav. Res. Lab. and Nav. Oc. Res. and Development Activity, Washington, D.C.

LaBRECQUE, J.L., and HAYES, D.H., 1979. Seafloor spreading history of the Agulhas Basin. *Earth Planet. Sci. Lett.*, 45: 411-428.

LaBRECQUE, J. L., KENT, D. V., and CANDE, S. C., 1979. Revised magnetic polarity time scale for late Cretaceous and Cenozoic time. *Geology*, 5: 330-335.

LACHENBRUCH, A.H., and SASS, J.H., 1978. Models of an extending lithosphere and heat flow in the Basin and Range Province, In: Cenozoic Tectonics and Regional Geophysics of the Western Cordillera, R.B. SMITH and G.P. EATON (eds.). *Geol. Soc. Am. Mem.*, 152: 209-250.

LACHENBRUCH, A.H., and MARSHALL, B.V., 1968. Heat flow and water temperature fluctuations in the Denmark Strait. *J. Geophys. Res.*, 73: 5829-5842.

LAMAR, D.L., REED, W.E., and DOUGLASS, D.N., 1986. Billefjorden Fracture Zone, Spitsbergen: Is it part of a major Late Devonian transform? *Geol. Soc. Am. Bull.*, 97: 1083-1088.

LANGSETH, M. G., and ZIELINSKI, G. W., 1974. Marine heat flow measurements in the Norwegian-Greenland Sea and in the vicinity of Iceland. In: *Geodynamics of Iceland and the North Atlantic Area*, L. Kristjansson (ed.), Reidel, Dordrecht, p: 277-295.

LARSEN, C-H., and JACOBSDÓTTIR, S., 1988. Distribution, crustal properties and significance of seawards-dipping sub-basement reflectors off East Greenland. *Geol. Soc. London Spec. Publ.*, 39: 95-114.

LARSEN, L.M., WATT, W.S., and WATT, M., 1989. Geology and petrology of the Lower tertiary plateau basalts of the Scoresby Sund region, East Greenland. *Bull. Geol. Surv. Greenland*, 157: 1-164.

LASE Study Group, 1986. *Mar. Petrol. Geol.*, 3: 234-242.

LATIN, D., and WHITE, N., 1990. Generating melt during lithospheric extension: pure shear vs. simple shear. *Geology*, 18: 327-331.

LAURITZEN, Ø., and OHTA, Y., 1984. Geological map of Svalbard, 1:500000, sheet 4G, Nordaustlandet. *Nor. Polarinstitutt Skr.*, 154 (B): 14 pp.

LEG 151 Shipboard Party, 1994. ODP Leg 151 accomplishes the successful drilling in the gateway to the Arctic Ocean. *The Nansen Ice breaker*, 5: 1-11.

LEG 152 Shipboard Party, 1994. Drilling Unearths "Fire and Ice" at Southeast Greenland Margin, *EOS*, Trans., AGU, 75 (35): 401-404.

LEMOINE, M., TRICART, P., BOILLOT, G., 1987. Ultramafic and gabbroic ocean floor of the Ligurian Tethys, in search of a genetic model. *Geology*, 15: 622-625.

LePICHON, X., and SIBUET, J-C., 1981. Passive margins: A model of formation. *J. Geophys. Res.*, 81: 239-256.

LIN, J., and PARMENTIER, E.M., 1989. Mechanism of lithospheric extension at mid-ocean ridges. Geophys. *J. Roy. Astron.*, 96: 1-22.

LISTER, G.S., ETHERIDGE, M.A., and SYMONDS, P.A., 1986. Detachment faulting and the evolution of passive continental margins. *Geology*, 14: 246-250.

LISTER, G.S., ETHERIDGE, M.A., and SYMONDS, P.A., 1991. Detachment models for the formation of passive continental margins. *Tectonics*, 10 (5): 1038-1064.

LITHP WHITE PAPER, 1993. Joides Lithosphere Panel (draft document-for comment), JOI for Deep Earth Sampling.

LITVIN, V.M., 1964. Bottom relief of the Norwegian Sea (in Russian). Trudy polyar. nauchno-issled. Inst. morsk. ryb. Khoz. Okernogr. (PINRO), 16: 89-109.

LORENZO, J.M., MUTTER, J.C., LARSON, R.L., and Northwest Australia Study Group, 1991. Development of the continent-ocean transform boundary of the southern Exmouth Plateau. *Geology*, 19: 843-846.

MAKRIS, J., 1982. The crust and upper mantle of the Aegean region from deep seismic soundings. *Tectonophysics*, 46: 269-284.

MACDONALD, K.C., SCHEIRER, D.S., and CARBOTTE, S.M., 1991. Mid-Ocean Ridges: Discontinuities, segments and Giant Cracks. *Science*, 253: 986-994.

MARSHALL, J.F., and LEE, C.S., 1987. Tectonic framework of the northern Perth basin western Australia (abs.) in Applied extension tectonics: Bureau of Mineral Res. Australia, Record 1987/51: 173-177.

MART, Y., 1991. The Dead Sea rift: from continental rift to incipient ocean. Tectonophysics, 197: 155-179.

MARTINEZ, F., and COCHRAN, J.R., 1988. Structure and tectonics of the northern Red Sea: catching a continental margin between rifting and drifting. *Tectonophysics*, 150: 1-32.

MARTINEZ, F., and COCHRAN, J.R., 1989. Geothermal measurements in the northern Red Sea: implications for lithospheric thermal structure and mode of extension during continental rifting. *J. Geophys. Res.*, 94: 12239-12266.

MASNADI-SHIRAZI, M., and DeMOUSTIER, C., 1990. On differential phase measurements with the SeaMARC-II, Bathymetric Side Scan Sonar Systems. *J. Acous. Soc. Am.*, 88 (S1): 132.

MAX, M. D., and OHTA, Y., 1988. Did major fractures in continental crust control orientation of the Knipovich Ridge-Lena Trough segment of the plate margin? *Polar Res.*, 6: 85-93.

McKENZIE, D. P., 1978. Some remarks on the development of sedimentary basins. *Earth Planet. Sci. Lett.*, 40: 25-32.

McKENZIE, D., 1985. The extraction of magma from the crust and mantle, *Earth Planet. Sci. Lett.*, 74: 81-91.

McKENZIE, D., and BICKLE, M.J., 1988. The volume and composition of melt generated by extension of the lithosphere, *J. Petrol.*, 29: 625-679.

McNUTT, M., 1984. Lithospheric flexure and thermal anomalies. *J. Geophys. Res.*, 89 (B13): 11180-11194.

McNUTT, M., 1988. Thermal and mechanical Properties of the Cape Verde Rise. *J. Geophys. Res.*, 93 (B4): 2784-2794.

MEISSNER, R., 1986. The continental crust. A geophysical approach. Academic Publ., San Diego, Calif.

MENARD, H.W., and ATWATER, T., 1968. Changes in directions of seafloor spreading. *Nature*, 219: 463-467.

MENARD, H.W., and McNUTT, M., 1982. Evidence for and consequences of thermal rejuvenation. *J. Geophys. Res.*, 87: 8570-8580.

MICHAEL, P. J., and BONATTI, E., 1985. Peridotite composition from the North Atlantic: regional variations and implications from partial melting, *Earth Planet. Sci. Lett.*, 73: 91-104.

MITCHELL, B.J., ZOLLWEG, J.E., KOHSMANN, J.J., CHENG, C.C., HAUG, E.J., 1979. Intraplate earthquakes in the Svalbard Archipelago. *Geophys. Res.*, 84: 5620-5626.

MITCHELL, B.J., BUNGUM, H., CHAN, W.W., MITCHELL, P.B., 1990. Seismicity and present-day tectonics of the Svalbard region. *Geophys. J. Int.*, 102: 139-149.

MJELDE, R., SELLEVOLL, M.A., SHIMAMURA, H., IWAZAKI, T., and KAWASAWA, T., 1992. A crustal study off Lofoten, N. Norway, by use of 3-component ocean bottom seismographs. *Tectonophysics*, 212: 269-288.

MUTTER, J.C., 1993. Margins declassified. *Nature*, 364: 393-394.

MUTTER, J.C., and ZEHNDER, C.M., 1988. Deep crustal structure and magmatic processes: the inception of seafloor spreading in the Norwegian-Greenland Sea, In: Early Tertiary Volcanism by A.C. MORTON and L.M. PARSON, *Spec. Publ. Geol. Soc. London*, 39: 35-48.

MUTTER, J.C., TALWANI, M., and STOFFA, P.L., 1982. Origin of seaward dipping reflectors in oceanic crust off the Norwegian margin by subaerial sea-floor spreading, *Geology*, 10: 353-357.

MUTTER, J.C., TALWANI, M., and STOFFA, P.L., 1984. Evidence for a thick oceanic crust adjacent to the Norwegian Margin, *J. Geophys. Res.*, 89: 483-502.

MUTTER, J.C., BUCK, R.W., and ZEHNDER, C.M., 1988. Convective partial melting: 1. A model for the formation of thick basaltic sequences during the initiation of spreading. *J. Geophys. Res.*, 93 (B2): 1031-1048.

MUTTER, J.C., LARSEN, R.L., and 10 others, 1989. Extension of the Exmouth Plateau, offshore northwestern Australia: Deep seismic reflection and refraction evidence for simple/pure shear mechanisms. *Geology*, 17: 15-18.

MÜLLER, R. D., 1993. Extremely lithified sandstones from the Central Tertiary Basin of Spitsbergen: evidence for Post-rift thermal rejuvenation? *Geology*.

MÜLLER, R. D. and SPIELHAGEN, R. J., 1990. Evolution of the Central Tertiary Basin of Spitsbergen: towards a synthesis of sediment and plate tectonic history. *Paleogeography, Paleoclimatology, Paleoecology*, 80: 153-172.

MYHRE, A.M., 1984. Complication of seismic velocity measurements along the margins of the Norwegian-Greenland Sea, *Norsk Polarinst. Skr.*, 180: 41-61.

MYHRE, A. M. and ELDHOLM, O., 1988. The Western Svalbard Margin (74° - 80°N). *Mar. Petrol. Geol.*, 5, 134-156.

MYHRE, A. M., ELDHOLM, O., and SUNDVOR, E., 1982. The margin between Senja and Spitsbergen Fracture zones: implications from plate tectonics. *Tectonophysics*, 89: 33-50.

MYHRE, A. M., ELDHOLM, O., SKOGSEID, J., FALEIDE, J.I., GUDLAUGSSON, S.T., PLANKE, S., STUEVOLD, L.M., and VÅGNES, E., 1992. The Norwegian continental margin. In: *Geologic Evolution of Atlantic Continental Rises*, C.W. Poag and Graciansky (eds.), Van Nostrand Reinhold, NY, pp: 157-185.

MYHRE, A. M., THIEDE, J., and ODP Leg 151 Shipboard Scientific Party, 1994. Exploring Arctic history through scientific drilling. *EOS*, 75 (25), 281: 285-286.

NANSEN, F., 1904. A Geological sketch of Cape Flora and its neighbourhood, In: The Norwegian Polar Expedition, 1893-1896 by F. NANSEN, Sci. Res. 1, 1-32.

NIELSEN, T. H., 1983. Influence of the Greenland-Scotland Ridge on the geological history of the North Atlantic and Greenland-Norway Sea Areas, In: *Structure and Development of the Greenland-Scotland Ridge*, M. H. P. Bott *et al.* (eds.), NATO Conference Series, IV: 457-482.

NUNNS, A., 1982. The structure and evolution of the Jan Mayen Ridge and surrounding regions. *Am. Assoc. Petrol. Geol. Bull., Mem.* 24: 193-208.

NUNNS, A., 1983. Plate tectonic evolution of the Greenland-Scotland Ridge and surrounding regions. In: *Structure and Development of the Greenland-Scotland Ridge*, M. H. P. Bott *et al.* (eds.), NATO Conference Series, IV: 11-30.

OHTA, Y., 1982. Morpho-tectonic studies around the Svalbard and the northernmost Atlantic. In: *Arctic Geology and Geophysics*, A.F. Embry and H.R. Balkwill (eds.). Can. Soc. Geol. Mem., 8: 415-429.

OKAY, N., 1990. Thermal Modeling of the Yermak Plateau within the Norwegian-Greenland Sea. *MS Thesis*, New York City Univ., New York, 117 pp.

OKAY, N., 1994. Evidence for propagating asthenospheric corridors: along the transtensional volcanic margins of the Norwegian-Greenland Sea. *EOS*, Trans. (Abs.), 75 (16): 321.

OKAY, N., 1995. Magmatism and rift margin evolution: evidence from the northern Norwegian-Greenland Sea, *TERRA nova* (Abs.), 7: 151.

OKAY, N. and CRANE, K., 1990. Thermal Modeling of the Yermak Plateau within the Norwegian-Greenland Sea, *EOS*, Trans. (Abs.), 71 (17): 622.

OKAY, N., CRANE, K., VOGT, P.R., and SUNDVOR, E., 1991. Diffuse rifting and associated volcanism on the Yermak Plateau in the Arctic Ocean: SeaMARC-II results, Part IV. *EOS*, Trans. (Abs.), 72 (17): 274.

OKAY, N., DOSS, H., and CRANE, K., 1993. Evidence for migratory fracture zones along the propagating Knipovich Ridge. *EOS*, Trans. (Abs.), 74 (43): 562.

OKAY, N., and CRANE, K., 1993. The thermal rejuvenation of the Yermak Plateau. *Mar. Geophys. Res.*, 15 (4): 243-263.

PALMASÓN, G., 1980. A continuum model of crustal generation in Iceland: kinematic aspects. *J. Geophys. Res.*, 47: 7-18.

PARSONS, B. G., and SCALTER, J., 1977. An analysis of the variation of ocean floor heat flow bathymetry with age. *J. Geophys. Res.*, 82: 803-827.

PAUTOT, G., GUENNOC, P., COUTELLE, A., and LYBERIS, N., 1986. La depression axiale du segment nord Mer Rouge (de 25°N à 28°N): Nouvelles données géologiques et géophysiques obtenues au cours de la campagne TRANSMEROU 83. *Bull. Soc. Geol. Fr.*, 8: 381-399.

PEDERSEN, T., and SKOGSEID, J., 1989. Vøring Plateau volcanic margin: extrusion, melting, and uplift. *Proc. ODP, Sci. Results*, 104: 985-991.

PERRY, R. K., FLEMING, H. S., CHERKIS, N. Z., FEDEN, R.H., and VOGT, P.R., 1980. *Bathymetry of the Norwegian-Greenland and Western Barents Seas*, (1: 2333230 map) US Naval Res. Lab., Acoustic Div., Washington D.C.

PERRY, R. K., FLEMING, H. S., WEBER, J. R., KRISTOFFERSON, Y., HALL., J. K., GRANTZ, A., JOHNSON G. L., CHERKIS, N. Z., and LARSEN, B., 1985. Bathymetry Map of the Arctic Ocean (1:600000 map), *Geol. Soc. Am. Map Series* MC-56.

PHILLIPS, J. D., FEDEN, R., FLEMING, H. S., and TAPSCOTT, C., 1982. Aeromagnetic studies of the Greenland/Norwegian Sea and Arctic Ocean, unpublished manuscript, Naval Research Laboratory, Washington, D.C.

PHIRMAN, S., 1989. Sediment distribution of the Greenland sea and the Fram Strait. *Polar Res.*, 5: 319-320.

PITMAN, W.C., III, and HEIRTZLER, J.R., 1966. Magnetic anomalies over the Pacific-Antarctic ridge. Science, 154: 1164-1171.

PLANKE, S., 1993. Rifting and continental breakup: seismic response and crustal evolution with emphasis on the Voring volcanic margin, *Cand. Sci. Thesis*, Univ. Oslo.

PRESTVIK, T., 1978. Cenozoic plateau lavas of Spitsbergen-a geochemical study. *Nor. Polarinst. Årb.*, 127-143.

RABINOWITZ, P.D., and LaBRECQUE, J.L., 1977. Isostatic gravity anomaly: a key to the evolution of the ocean-continent boundary. *Earth Planet. Sci. Lett.*, 35: 145-150.

RASCHKA, H., and ECKHARDT, F-J., 1976. Geochemistry of basalts from the Norwegian-Greenland Sea, Leg 38. *Proc. DSDP*, Talwani, Udinsev *et al.* (eds.), pp: 719-730.

REKSNES, P. A. and VÅGNES, E., 1985. Evolution of the Greenland Sea and Eurasian Basin. *Cand. Sci. Thesis*, Univ. Oslo, 136 pp.

ROBERTS, D.G., and GINZBURG, A., 1984. Deep crustal structure of southwest Rockall Plateau. *Nature*, 308: 435-439.

ROBERTS, D.G., BACKMAN, J., MORTON, A.C., MURRAY, J.W., and KEENE, J.B., 1984. Evolution of volcanic rifted margins: Synthesis of Leg 81 results on the west margin of Rockall Plateau, In: *Init. Repts. DSDP 81*, D.G. ROBERTS *et al.* (eds.), Washington D.C. (US Govt. Print.), pp: 883-911.

ROSENDAHL, B.R., 1987. Architecture of continental rifts with special reference to east Africa. *An. Rev. Earth Planet. Sci. Lett.*, 15: 445-503.

ROWLAND, J.C., and DİLEK, Y., 1992. Rifting and passive margin evolution via asymmetric extension in Mesozoic southern Turkey and analogies with Atlantic margins. *Geol. Soc. Am. Abstr. Prog.* 24:71.

SAVOSTIN, L.A., and KARASIK, A.M., 1981. Recent plate tectonics of the Arctic Basin and of northeastern Asia. *Tectonics*, 74: 111-145.

SAWYER, D.S., 1985. Brittle failure in the upper mantle during extension of continental lithosphere. *J. Geophys. Res.*, 90: 3021-3025.

SAWYER, D., and HARRY, D.L., 1991. Dynamic modeling of divergent margin formation: Application to the US Atlantic margin. *Mar. Geol.*, 102: 29-41.

SAWYER, D., and WHITEMARSH, R., 1993. ODP begins rifted margin transect, Drill Bits, *News from the JOI/US Science Support program* (Assoc. Ocean Drilling Program), 6: 1-3.

SCHRADER, H-J., BJØRKLUND, K., MANUM, S., MARTINI, E., and HINTE, J., 1976. Cenozoic Biostratigraphy, Physical stratigraphy, Paleooceanography in the Norwegian-Greenland Sea, DSDP-Leg 38, Paleontological Synthesis, In: *Init. Rep. DSDP*, M. TALWANI and G. UDINSEV *et al.* (eds.), 38: 1197-1211.

SCHÜLER, H.U., and HINZ, K., 1978. The continental margin of West-Spitsbergen. *Polarforschung*, 48: 151-169.

SCLATER, J. G., and FRANCHETEAU, J., 1970. The implication of terrestrial heat flow observations in current tectonic and geochemical models of the crust and upper mantle of the earth. *Geophys. J. Roy. Astron. Soc.*, 20: 509-542 .

SCLATER, J. G., JAUPART, C., and GALSON, D., 1980. The heat flow through Oceanic and continental crust and the heat flow loss of the Earth. *Rev. Geophys. Space Phys.*, 18 (1): 269-311.

SCOTT, D.L., and ROSENDAHL, B.R., 1989. North Viking Graben: An East African Perspective. *Am. Ass. Petrol. Geol. Bull.*, 73 (2): 155-165.

SELLEVOLL, M. A., DUDA, S. J., GUTERCH, A., PAJCHEL, J., PERCHUC, E., and THYSSEN, F., 1991. Crustal structure in the Svalbard region from seismic measurements. *Tectonophysics*, 189: 55-71.

ŞENGÖR, A.M.C., and BURKE, K., 1978. Relative timing of rifting and volcanism on earth and its tectonic implications. *Geophys. Res. Lett.*, 5: 419-421.

ŞENGÖR, A.M.C., BURKE, K., and DEWEY, J.F., 1978, Rifts at high angles to orogenic belts: tests for thin origin and the upper Rhinegraben as an example. *Am. J. Sci.*, 278: 24-40.

ŞENGÖR, A.M.C., YILMAZ, Y., and SUNGURLU, O., 1984. Tectonics of the Mediterranean Cimmerides: Nature and evolution of the western termination of Paleo-Tethys, In: The geological evolution of the Eastern Mediterranean, J.E. Dixon and A.H.F. Robertson (eds.). *Geol. Soc. London Spec. Publ.*, 17: 77-112.

ŞENGÖR, A.M.C., GÖRÜR, N., and ŞAROĞLU, F., 1985. Strike-slip faulting and related basin formation in zones of tectonic escape: Turkey as a case study, In: Strike-slip deformation basin formation and sedimentation, Biddle, K.T., and Christie-Blick, N. (eds.). *Soc. Eco. Paleo. and Min. Spec. Publ.*, 37: 227-264.

SHERIDAN, R.E., MUSSER, D.L., GLOVER III, L., TALWANI, M., EWING, J.I., HOLBROOK, W.S., PURDY, G.M., HAWMAN, R., and SMITHSON, J.I., 1993. Deep seismic reflection data of EDGE US mid-Atlantic continental-margin experiment: Implications for Appalachian sutures and Mesozoic rifting and magmatic underplating. *Geology*, 21: 563-567.

SHOR, A., 1990. SeaMARC-II seafloor mapping system: seven years of Pacific Research. Proceedings of the Pacific Rim Congress (PACRIM 90), *Australian Ins. Min. Metall.*, 3: 49-61.

SKJELKVÅLE, B., AMUNDSEN, H. E. F., O'REILLY, S.Y., GRIFFIN, W.L., and GJELSVIK, T., 1989. A primitive alkali basalts stratovolcano and associated eruptive centers, northwestern Spitsbergen: volcanology and tectonic significance. *J. Volconol. Geotherm. Res.*, 37: 1-19.

SKOGSEID, J., and ELDHOLM, O., 1987. Early Cenozoic crust at the Norwegian volcanic passive margin and the a conjugate Jan Mayen Ridge. *J. Geophys. Res.*, 92: 11471-11491.

SKOGSEID, J., and ELDHOLM, O., 1987. Early Cenozoic crust at the conjugate Jan Mayen Ridge. *J. Geophys. Res.*, 92: 11471-11491.

SKOGSEID, J., and ELDHOLM, O., 1989. Vøring Plateau continental margin: Seismic interpretation, stratigraphy and vertical movements. *Proc. ODP, Sci. Results*, 104: 993-1030.

SONDER, L., and ENGLAND, P.C., 1989. Effects of a temperature-dependent rheology on large-scale continental extension. *J. Geophys. Res.*, 94 (B6): 7603-7619.

SRIVASTAVA, S.P., 1978. Evolution of the Labrador Sea and its bearing on the early evolution of the North Atlantic. *Geophys. J. R. Astron. Soc.*, 52: 313-357.

SRIVASTAVA, S.P., 1985. Evolution of the Eurasian Basin. *Tectonophysics*, 114: 29-53.

SRIVASTAVA, S.P., and ROEST, W.R., 1989. Seafloor spreading history. In: *East Coast Basin Atlas Series: Labrador Sea*, J.S. Bell (ed.), Atlantic Geosci. Cent. Geol. Surv. Can. Map Sheet L17.2-L17.6.

STECKLER, M.S., 1989. The role of the thermal-mechanical structure of the lithosphere in the formation of sedimentary basins. In: *Quantitative Dynamic Stratigraphy*, T.A. Cross (ed.), Prentice Hall, pp: 89-112.

STEEL, R., GJELBERG, J., HELLAND-HANSEN, W., KLEINSPEHN, K., NØTTVEDT, A., and RYE-LARSEN, M., 1985. The Tertiary strike-slip basins and orogenic belt of Spitsbergen. In: Strike-slip deformation Basin Formation and Sedimentation, *SEPM Spec. Publ.*, 37: 339-359.

STEIN, C.A., and STEIN, S., 1992. A model for the global variation in oceanic depth and heat flow with lithospheric age. *Nature*, 359: 123-129.

STOCKS, T., 1950. Die Tiefenverhaltnisse des Europaischen Nordmeeres. Dt. hydrogr. Z., 3: 93-100.

SUNDVOR, E., 1986. Heat flow measurements on the western Svalbard margin. Univ. Bergen, Seism. Observ., Sci. Rep., 11 pp.

SUNDVOR, E., and ELDHOLM, O., 1979. The western and northern margin off Svalbard. *Tectonophysics*, 59: 239-250.

SUNDVOR, E., and TORP, J.E., 1987. Measurements of heat flow and thermal conductivity in the Nansen Basin, Arctic Ocean, Univ. Bergen, Seism. Obs., *Cruise Report.*

SUNDVOR, E. and AUSTEGÅRD, A., 1990. The evolution of the Svalbard Margins: synthesis and new results. In: *Geological History of the Polar Oceans:* Arctic versus Antarctic, U. Bleil and J. Thiede (eds.), Kluwer Publ., Amsterdam. pp: 77-94.

SUNDVOR, E., ELDHOLM, O., GIDSKEHAUG, A., and MYHRE, A. M., 1977. Marine geophysical survey on the western and northern continental margin off Svalbard, Univ. Bergen, Seismol. Observ., *Sci. Rep.*, 4: 35 pp.

SUNDVOR, E., GIDSKEHAUG, A., MYHRE, A., ELDHOLM, O., 1978. Marine Geophysical Survey on the Northern Svalbard Margin, Univ. Bergen, Seis., Obs. *Sci. Rep.*, 5: 46 pp.

SUNDVOR, E., MYHRE, M. A., and ELDHOLM, O., 1979. The Svalbard continental margin. Norwegian Sea Symposium. *Norw. Petrol. Soc.*, NSS/6, 1-25.

SUNDVOR, E., MYHRE, A. M., AUSTEGÅRD, A., HAUGLAND, K., ELDHOLM, O., and GIDSKEHANG, A., 1982a. Marine Geophysical Survey on the Yermak Plateau. Univ. Bergen, Seismol. Observ., *Sci. Rep.*, 7: 26 pp.

SUNDVOR, E., LEONARD, G. J., and MYHRE, A., 1982b. Some aspects of morphology and structure of the Yermak Plateau, northwest of Spitsbergen. Univ. Bergen, Seismol. Observ., *Sci. Rep.*, 8: 29 pp.

SUNDVOR, E., VOGT, P.R., CRANE, K., CHAYES, D., JONES, C., NISHMURA, C., deMOUSTIER, C., and DOSS, H., 1990. SeaMARC-II and associated geophysical investigation of the Knipovich Ridge, Molloy Ridge/Fracture Zone and Barents/Spitsbergen continental margin: Part I, Overview. *EOS* Trans. (Abs.), 71 (17): 622.

SUNDVOR, E., CRANE, K., VOGT, P.R., MARTINEZ, F., JONES, C., deMOUSTIER, C., DOSS, H., OKAY, N., and SeaMARC-II Team, 1991. SeaMARC II and associated geophysical investigation of the Knipovich Ridge, Molloy Ridge/Fracture Zone and Barents/Spitsbergen continental margin: Part I, Overview of two year program completed. *EOS*, Trans. (Abs.), 72 (22): 232.

SYKES, L., 1965. The seismicity of the Arctic. *Bull. Seis. Soc. Ame.*, 55 (2): 501-517.

SYKES, L. R., 1967. Mechanism of earthquakes and nature of faulting on the Mid-Atlantic Ridge. *J. Geophys. Res.*, 72: 2131-2153.

SYLVESTERS, A.G., 1975. Petrology of volcanic ashes in deep-sea cores near Jan Mayen Ridge: Site 338, *Proc. DSDP-Leg 38*, pp: 101-110.

TALWANI, M., and ELDHOLM, O., 1972. The continental margin off Norway: a geophysical study. *Geol. Soc. Amer. Bull.*, 83: 3575-3608.

TALWANI, M., and ELDHOLM, O., 1973. The boundary between continental and oceanic crust at the margin of rifted continents. *Nature*, 241: 325-330.

TALWANI, M., and ELDHOLM, O., 1977. Evolution of the Norwegian-Greenland Sea. *Geol. Soc. Amer. Bull.*, 88: 969-999.

TALWANI, M., UDINSEV, Leg 38-Scientific Party, 1976. Tectonic synthesis. In: *Init. Rep. DSDP 38*, Talwani, M., and Udinsev, G., *et al.* (eds.), Washington (US Govt. Printing Office), pp:1213-1242.

TALWANI, M., MUTTER, J., HOUTZ, R., and KONIG, M., 1979. The crustal structure and evolution of the area underlying the magnetic quiet zone on the margin south of Australia. In: geological and geophysical investigations of continental margins, J. Watkins, L. Montadert, and P. Dickerson (eds.). *Am. Ass. Petrol. Geol. Mem.*, 29: 151-175.

TALWANI, M., MUTTER, J.C., and HINZ, K., 1982. Ocean-continent boundary under the Norwegian continental margin. In: Structure and Development of the Greenland-Scotland Ridge: New Methods and Concepts, M.H.P. Bott, S. Saxov, M. Talwani, and J. Thiede (eds.), Plenum Publ., NY., p: 121-132.

TANKARD, A.J., and BALKWILL, H.R., 1989. Extensional tectonics and stratigraphy of the North Atlantic Margins. *Mem. Am. Assoc. Pet. Geol.*, 46.

THIEDE, J., PFIRMAN, S., JOHNSON, G.L., MUDIE, P.J., MIENERT, J., and VORREN, T., 1989. Arctic Deep-Sea Drilling: Scientific and Technical Challenge of the next decade. In: *Oceanography 1988*, A. Ayala-Castañares, W. Wooster, and A. Yañez-Arancibia (eds.), UNAM Press, 208 p.

THIEDE, J., PFIRMAN, S., SCHENKE, H-W, and REID, W., 1990. Bathymetry of Molloy Deep: Fram Strait between Svalbard and Greenland. *Mar. Geophys. Res.*, 12: 197-214.

THURMAN, H.V., 1991. Introductory Oceanography, MacMillian Publ. Co., NY, 6th edition, 526 pp.

TORP J.E., 1988. Måling reduction og modellering av varmestrøøm anvendt på data fra Grønlandshavet/Svalbardmarginen. *Cand. Sci. Thesis*, Univ. Bergen.

TORSKE, T., and PRESTVIK, T., 1991. Mesozoic detachment faulting between Greenland and Norway: inferences from Jan Mayen Fracture Zone system and associated alkalic volcanic rocks. *Geology*, 19: 481-484.

TURCOTTE, D.L., TORRENCE, D.E., and HSUI, A.T., 1973. Convection in the earth's mantle. *Method. Comput. Phys.*, 13: 431-454.

VanANDEL, T., PHILLIPS, J.D., and Van HERZEN, R.P., 1969. Rifting origin for the Vema Fracture Zone in the North Atlantic. *Earth Planet. Sci. Lett.*, 5: 296-300.

VERHOOGEN, J., 1954. Petrological evidence on temperature distribution in the mantle of the Earth. *EOS*, Trans. (AGU), 35: 85-92.

VINE, F.J., and MATHEWS, D.H., 1963. Magnetic anomalies over oceanic ridges. Nature, Lond., 199: 947-949.

VOGT, P.R., 1986. Geophysical and geochemical signatures and plate tectonics, In: *The Nordic Seas*, B.G. Hurdle (ed.), Springer-Verlag, New York, p: 413-627.

VOGT, P.R., TAYLOR, P.T., KOVACS, L.C., and JOHNSON, G.L., 1979. Detailed aeromagnetic investigations of the Arctic Basin. *J. Geophys. Res.*, 84: 1071-1089.

VOGT, P. R., PERRY, R. K., FEDEN, R. H., FLEMING, H. S., and CHERKIS, N. Z., 1981. "The Greenland-Norwegian Sea and Iceland environment: Geology and Geophysics", In: *The Ocean Basins and Margins*, A. E. M. Nairn and M. Churkin (Eds.), 5: 493-598.

VOGT, P. R., SUNDVOR, E., CRANE, K., PFIRMAN, S., NISHMURA, C., and MAX, M., 1990. SeaMARC-II and associated geophysical investigation of the Knipovich Ridge, Molloy Ridge/Fracture Zone and Barents/Spitsbergen continental margin: Part III, Sedimentary Processes. *EOS*, Trans. (Abs.), 71 (17): 622.

VOGT, P.R., CRANE, K., and SUNDVOR, E., 1993. Glacigenic Mudflows on the Bear Island Submarine Fan. *EOS*, Trans. (AGU), 74 (40): 449.

VOGT, P.R., CRANE, K., and SUNDVOR, E., 1994. Deep Pleistocene iceberg plowmarks on the Yermak Plateau: Sidescan and 3.5 kHz evidence for thick calving ice fronts and a possible marine ice sheet in the Arctic Ocean. *Geology*, 22: 403-406.

VORREN, T.O., LEBESBYE, E., ANDREASSEN, K., and LARSEN, K.-B., 1989. Glacigenic sediments on a passive continental margin as exemplified by the Barents Sea. *Mar. Geol.*, 85: 251-272.

WERNICKE, B., 1981. Low-angle normal faults in the Basin and range Province: nappe tectonics in an extending orogen. *Nature*, 291: 645-648.

WERNICKE, B., 1985. Uniform-sense normal simple shear of the continental lithosphere. *Can. J. Earth Sci.*, 22: 108-125.

WHITE, R.S., 1988. A hot-spot model for Early Tertiary volcanism in the Atlantic. In: Early Tertiary Volcanism and the Opening of the NE Atlantic, A.C. Morton and L.M. Parson (eds.). *Geol. Soc. London Spec. Publ.*, 39: 3-13.

WHITE, R.S., and McKENZIE, D., 1989. Magmatism at rift zones: The generation of volcanic continental margins and flood basalts. *J. Geophys. Res.*, 94: 7685-7729.

WHITE, R.S., SPENCE, G.D., FOWLER, S.R., McKENZIE, D.P., WESTBROOK, G.K., and BOWEN, A.N., 1987. Magmatism at rifted continental margins. *Nature*, 330: 439-444.

WOODCOCK, N.H., 1986. The role of strike-slip fault systems at plate boundaries in major crustal lineaments and their influence on the geological history of the continental lithosphere. *Phil. Trans. Royal Soc. London*, A317: 13-30.

YMER-80, 1984. *Swedish Arctic Expedition*, cruise report for marine geology and geophysics, K. Boström, and J. Thiede (eds.). Univ. Stockholm Press, Stockhom, 260: 1-123.

YODER, H.S., 1976. *Generation of Basaltic Magma*, Washington, D.C. (National Academy of Sciences).

ZEHNDER, C.M., MUTTER, J.C., and BUHL, P., 1990. Deep seismic and geochemical constraints on the nature of rift-induced magmatism during breakup of the North Atlantic, *Tectonophysics*, 173: 545-565.

ZIEGLER, P.A., 1978. North-western Europe: tectonics and basin development. *Geol. en Mijnbouw*, 57: 589-626.

ZIELINSKI, G.W., 1979. On the thermal evolution of passive continental margins, thermal depth anomalies, and the Norwegian-Greenland Sea. *J. Geophys. Res.*, 84: 7477-7588.